arXiv:hep-lat/0407018v1 9 Jul 2004

Dense Baryonic Matter in Strong Coupling Lattice Gauge Theory

Thesis submitted towards the degree of

“Doctor of Philosophy”

by

Barak Bringoltz

This work was carried out under the supervision of
Professor Benjamin Svetitsky

July, 2004

To my parents Yehudit and Naum

Abstract

We investigate the strong coupling limit of quantum chromodynamics on a lattice (lattice QCD) for systems with high baryon density. Our starting point is the Hamiltonian of lattice QCD for quarks with N_c colors and N_f flavors at strong coupling. We regard this Hamiltonian as an effective Hamiltonian that describes QCD at large distances, and expand it in orders of the inverse coupling. In leading order one finds a Hamiltonian that looks like an antiferromagnet. It has interactions between nearest-neighbor and next-nearest-neighbor sites, and is invariant under $U(N_f)\times U(N_f)$. Physically this Hamiltonian describes meson dynamics with a fixed background of baryon density. Our goal is to extract the ground state and low lying excitations of this Hamiltonian for systems with non-zero baryon density.

We first write the partition function of the Hamiltonian with boson coherent states and take the limit of large N_c and N_f with the ratio $r = N_c/N_f$ kept fixed. In this limit we make a mean field ansatz to extract the ground state. For zero density we extend a condensed matter physics result to three dimensions, and show that above a critical value of r the ground state breaks global symmetry. Departing from zero density we show that for certain cases, where the baryon density is periodic, the critical value of r increases with increasing density. In cases where the baryon positions are random, we average over them (in a quenched calculation that is valid only for low density) and show that the mean field ansatz is misleading near the critical r. Nevertheless, following the condensed matter analog of this quenched calculation, we expect that in the presence of baryons, low lying excitations will have non-zero widths and reduced velocities.

Writing the partition function with generalized spin coherent states leads to a nonlinear sigma model, which we investigate in the rest of the thesis. We first analyze the classical counterpart of a toy sigma model with mean field theory, and find that the critical temperature, under which the symmetry of the model is spontaneously broken, decreases with increasing density.

The quantum sigma model is treated in the limit of large N_c with N_f fixed. We find that the ground state is classically degenerate. For zero density the degeneracy is discrete. In the case of non-zero uniform density the ground state is continuously and locally degenerate, like classical ground states of frustrated magnetic systems.

When we consider quantum corrections of order $1/N_c$ we find the phenomenon of "order from disorder," also present in frustrated magnetic systems. For zero density we extend an old result to the next-nearest-neighbor theory, and show that fluctuations remove the

discrete degeneracy to choose a ground state that spontaneously breaks $U(N_f) \times U(N_f)$ to $U(N_f)_V$. For non-zero density we see that fluctuations remove the local degeneracy and choose a state that spontaneously breaks $U(N_f) \times U(N_f)$ as well as discrete lattice rotations in a way that depends on N_f and the baryon density.

Finally we find a rich variety of low lying excitations that includes type I and type II Goldstone bosons. The latter emerge only for non-zero density and only when quantum fluctuations are taken into account. Their energies are of order $1/N_c$, and are quadratic in momentum. Bosons of either type can develop anisotropic dispersion relations.

Contents

1 **Introduction** **1**

2 **The effective Hamiltonian** **9**

2.1 Hamiltonian approach to lattice QCD 9

2.2 The strong coupling limit 15

2.3 Strong coupling perturbation theory 17

2.3.1 Second order: the antiferromagnet 18

2.3.2 Third order: the baryon kinetic term 24

2.4 Summary 26

3 **Mean field theory with Schwinger bosons** **29**

3.1 Schwinger bosons 30

3.2 Hubbard-Stratonovich transformation 34

3.3 Mean field theory at zero density 36

3.4 Mean field theory at non-zero density 41

3.4.1 Periodic density with baryon concentration $c = \frac{1}{8}, \frac{1}{4}$ 42

3.4.2 Random baryon positions – the quenched approximation 47

4 **Nonlinear sigma model and the classical ground state** **63**
4.1 Coherent states and sigma fields 63
4.2 Partition function and action 67
4.3 The classical counterpart of the sigma model 69
4.3.1 Mean field theory 70
4.3.2 The toy model of $U(3)$ 72
4.4 The semiclassical large N_c limit 80
4.4.1 Zero density 81
4.4.2 Non-zero density 83

5 **Quantum fluctuations in the sigma model** **89**
5.1 Removal of classical degeneracy at zero density 89
5.2 Removal of classical degeneracy at non-zero density 92
5.2.1 Zero modes at $O(1)$ 95
5.2.2 Removal of zero modes at $O(1/N_c)$ – the self energy calculation . . 100

6 **Next-nearest-neighbor interactions in the sigma model** **107**
6.1 Action and symmetries of next-nearest-neighbor interactions 108
6.2 Ground state of the next-nearest-neighbor theory 109
6.3 Excitations in the next-nearest-neighbor theory 116

7 **Summary and discussion** **125**

A **Anticommutation relations of baryon operators** **131**

B **Discretization of Euclidean time** **135**

C **Minimizing the next-nearest-neighbor term** **139**

D The function Φ for the $U(3)$ toy model at non-zero density 141

E The matrices C and D in the $O(1/N_c)$ calculations 145

F Feynman rules for the effective action of the sigma model 147

G Integral equations for the self energy of the zero modes 151

G.1 Evaluation of diagrams 152

G.2 Evaluation of frequency integrals 154

G.3 Solution of integral equations 158

H Hamiltonian approach to order from disorder 163

H.1 The ground state at $O(1)$ 166

H.2 Self energy and $O(1/N_c)$ effective Hamiltonian 167

I Effective interaction between odd sites in the sigma model 175

J Fluctuations on the odd sites at non-zero density 181

K Coefficients in the dispersions of Goldstone bosons 183

L Classification of fields according to unbroken subgroups 185

Acknowledgments 197

List of Figures

1.1 The representation of $U(4N_f)$ 5

2.1 $U(4N_f)$ representation of a baryon operator with $N_c = 3$ 21
2.2 $SU(N_c)$ representation carried of a single site state 21
2.3 S_n representation of a single site state 22
2.4 $U(4N_f)$ representation of a single site state 23

3.1 The integration measure of γ for $d = 3$. 39
3.2 $f(\eta)$ – right hand side of MF equation at zero baryon number. 40
3.3 Phase diagram of Schwinger bosons MF theory at $T = 0$ and zero density. . . 41
3.4 A unit cell with $c = \frac{1}{8}$ concentration of "magnetic" vacancies 43
3.5 The integration measures of $\gamma_{1,3,5}$ for $c = \frac{1}{8}$. 45
3.6 Right hand side of the MF equation for $c = \frac{1}{8}$. 46
3.7 The integration measures of $\gamma_{1,3,5}$ for $c = \frac{1}{4}$ 48
3.8 Right hand side of the MF equation for $c = \frac{1}{4}$. 49
3.9 The boson propagator. 51
3.10 The impurity vertex 52
3.11 Scattering of bosons off three impurities 52
3.12 The loop diagram that corresponds to the expression (3.93). 53

3.13 The loop diagrams that corresponds to $p = 4$, $q = q_e = 2$, and $s = 1, 2, 3$. . . 54

3.14 Right hand side of the MF equation with $c \neq 0$ in the quenched approximation. 58

3.15 MF action for $c = \frac{1}{8}$; quenched approximation vs. exact diagonalization . . 59

3.16 MF action for $c = \frac{1}{4}$; quenched approximation vs. exact diagonalization . . 60

3.17 Right hand side of MF equation for $c = \frac{1}{8}$; quenched approximation vs. exact diagonalization 61

3.18 Right hand side of MF equation for $c = \frac{1}{4}$; quenched approximation vs. exact diagonalization 62

4.1 The most symmetric $B = 0$ state in the $U(3)$ toy model 72

4.2 Adding a baryon in the $U(3)$ toy model. 73

4.3 Φ at zero density for $N = 3$. 76

4.4 Φ non-zero density for $N = 3$ 79

4.5 Classical phase diagram of the $U(3)$ toy model 80

4.6 A configuration with zero baryon number on all sites. 81

4.7 A configuration with alternating baryon number on adjacent sites. 81

4.8 Adding one baryon to the lattice. 83

4.9 Two sites that carry $U(N)$ representations with m_1 and m_2 rows. 84

5.1 Coupling two 7-row reps of $U(12)$. 93

5.2 Weight diagram for $N = 3$, $m = 1$, $N_c = 2$ 94

5.3 Schwinger-Dyson equation for the χ fields self energy. 101

5.4 Solution of integral equation 103

5.5 Dispersion relation of the χ fields. 104

F.1 Propagator of the π fields. 147

F.2 Propagator of the χ fields. 147

F.3 Vertices corresponding to the quartic interaction. 148

F.4 Vertices corresponding to the cubic interaction. 149

G.1 Evaluation of Σ_1. 152

G.2 Evaluation of Σ_2. 153

G.3 The first Brillouin zone (BZ) of the fcc lattice. 159

G.4 Behavior of the approximated integral equation. 160

List of Tables

4.1 Baryon number configurations in the $U(3)$ toy model. 77

5.1 Field classification under the unbroken group of the nearest-neighbor theory.100

6.1 Realization of chiral symmetry for different densities 114
6.2 Eigenvalues of $n_{e,o}$ and $m_{e,o}$ 121

K.1 The coefficients in the dispersion relations of Goldstone bosons 184

L.1 Classification of σ fields on the even sites 186
L.2 Classification of σ fields on the odd sites 187

Chapter 1

Introduction

The theoretical framework that describes the strong interactions of quarks and gluons is the theory of quantum chromodynamics (QCD). It is of fundamental interest to study what QCD predicts for nuclear matter at extreme conditions. This includes systems at very high temperatures ($\sim 10^{12}$ K) accessible in ultra-relativistic collisions of heavy ions, and systems with high nuclear densities ($\sim 10^{15}$-$10^{16}\,\mathrm{g\,cm^{-3}}$) that can be found in the cores of neutron stars. In this work we are concerned with the latter, nuclear systems of high density.

The study of quantum chromodynamics at high density is almost as old as the theory itself, and goes hand in hand with the discovery of asymptotic freedom [1, 2]. The first to approach the problem were Collins and Perry [3]. They argued that at high baryon densities of the order of ten to a hundred times nuclear density, the hadrons overlap and lose their individuality. At these densities asymptotic freedom weakens the color interactions, and in the absence of long range forces the system can be considered as a weakly interacting "quark soup", with quarks arranged in a Fermi sea.

Next, Barrois [4, 5] suggested that the Fermi quark sea is unstable, and shows some phenomenon analogous to superconductivity. He suggested that the instability is caused by gluon exchange between quarks in the antisymmetric $\underline{\bar{3}}$ channel, which is attractive. Nevertheless Barrois argued in [4] that the ground state does not break $SU(3)$ gauge symmetry, and is rather characterized by condensates of six quark operators, which are color invariants.

The next step is the work of Bailin and Love [6], that studied relativistic fermionic systems in similar lines to the study of fermions in condensed matter systems that exhibit non-perturbative phenomena. Using similar arguments to those in [3] they justify that quarks in neutron stars weakly interact and that they are the relevant degrees of freedom, rather than the neutrons themselves. They describe the superfluid, superconductor, and color superconductor ground states of this dense quark matter, generated by one-gluon exchange between quarks in the $\underline{\overline{3}}$ channel. In contrast to Barrois they treat condensates of quark-quark cooper pairs, rather than higher condensates. These condensates are not gauge invariant and spontaneously break $SU(3)_{\text{color}}$. This is the phenomenon of color superconductivity (CSC).

Although these are fascinating theoretical predictions, one finds that the the gap and critical superconducting temperature T_c are in the MeV range. This is disappointing, since it means that the color superconductive part of the QCD phase diagram is very narrow. For that reason the study of color superconductivity was at a halt for over a decade. The stimulus for the revival of the idea of CSC was the observation [7, 8] that the instanton-induced quark–quark interaction can be much stronger than that induced by simple one-gluon exchange, and can thus give a transition temperature on the order of 100 MeV. Subsequent work [9] showed that the perturbative color-magnetic interaction also gives rise to a strong pairing interaction. These and other dynamical considerations [10] underlie a picture of the ground state of high-density QCD in which the $SU(3)$ gauge symmetry is spontaneously broken by a BCS-like condensate. The details of the breaking, which include both the Higgs (or Meissner) effect and the rearrangement of global symmetries and Goldstone bosons, depend on quark masses, chemical potentials, and temperature. Prominent in the list of possibilities are those of color-flavor locking in three-flavor QCD [11] and crystalline superconductivity—with broken translation invariance—when there are two flavors with different densities [12]. For a review see [13].

As noted, CSC at high density is so far a prediction of weak-coupling analysis. One expects the coupling to become weak only at high densities, and in fact it turns out that reliable calculations demand extremely high densities [14]. The use of weak-coupling methods to make predictions for moderate densities is thus not an application of QCD, but of a model based on it. It is imperative to confirm these predictions by non-perturbative methods. Standard lattice Monte Carlo methods, unfortunately, fall afoul of well-known technical problems when the chemical potential is made non-zero, although we do note remarkable progress made recently in the small-μ regime [15, 16, 17]. For a review of these methods see for example [18].

In this work we study high-density quark matter based on lattice QCD in the strong-coupling limit, which we regard as an effective theory that describes QCD at large distances. We work in the Hamiltonian formalism, which is more amenable than the Euclidean formalism to strong-coupling perturbation theory and to qualitative study of the ensuing effective theory [19, 20, 21, 22]. The fermion kinetic Hamiltonian is a perturbation that mixes the zero-flux states that are the ground-state sector of the electric term in the gauge Hamiltonian. In second order, it moves color-singlet fermion pairs around the lattice; the effective Hamiltonian for these pairs is a generalized antiferromagnet, with spin operators constructed of fermion bilinears.

We depart from studies of the vacuum by allowing a background baryon density, which is perforce static in second order in perturbation theory. Our aim is to discover the ground state of the theory with this background. In third order (when $N_c = 3$) the baryons become dynamical; we display the effective Hamiltonian but make no attempt to treat it.

The symmetry group of the effective antiferromagnet is the same as the global symmetry group of the original gauge theory. This depends on the formulation chosen for the lattice fermions. Following [20], we begin with naive, nearest-neighbor fermions, which suffer from species doubling [23] and possess a global $U(4N_f)$ symmetry group that contains the ordinary chiral symmetries [as well as the axial $U(1)$] as subgroups. We subsequently break the too-large symmetry group with next-nearest-neighbor (NNN) couplings along the axes in the fermion hopping Hamiltonian. A glance at the menu of fermion formulations reveals the reasons for our choice. Wilson fermions [24] have no chiral symmetry and make comparison of results to continuum CSC difficult if not impossible. Staggered fermions [25] likewise possess only a reduced axial symmetry while suffering a reduced doubling problem. The overlap action [26] is non-local in time and hence possesses no Hamiltonian; attempts [27] to construct an overlap Hamiltonian directly have not borne fruit. Finally, domain-wall fermions [28, 29] have been shown [22] to lose chiral symmetry and regain doubling when the coupling is strong.

While the NNN theory still exhibits doubling in the free fermion spectrum, we are not interested in the perturbative fermion propagator but in the spectrum of the confining theory. We take it as a positive sign that the unbroken symmetry is now $U(N_f) \times U(N_f)$.[1] This symmetry is what we want for the continuum theory, except for the axial $U(1)$. The latter can still be broken by hand [32].

Our emphasis on the global symmetries is a consequence of the fact that the gauge field is not present in the ground-state sector and does not reappear in strong-coupling perturbation theory. In other words, confinement is a *kinematic* feature of the theory, leaving no possibility of seeing the Higgs-Meissner effect directly. This is but an instance of confinement-Higgs duality, typical of gauge theories with matter fields in the fundamental representation [33]. Our aim is thus to identify the pattern of spontaneous breaking of global symmetries. For various values of N_c and N_f, this can be compared to weak-coupling results [34].

---

[1] The breaking of the naive fermions' symmetry by longer-range terms is a feature [20] of SLAC fermions [30] and also occurs if naive fermions are placed on a *bcc* lattice [31].

Other groups have recently studied the strong-coupling limit of QCD in the Hamiltonian and Euclidean formalisms at non-zero chemical potential and baryon density [35, 36, 37, 38, 39, 40, 41]. We differ from most approaches in eschewing mean field theory in favor of the exact transformation to a different representations, which is amenable to semiclassical treatment. Also we base our program on NNN fermions; we also work at fixed baryon density.

The outline of this dissertation is as follows. In Chapter 2 we first give a brief introduction to Hamiltonian lattice QCD, and discuss our approach that regards the strong coupling limit of the Hamiltonian as an effective model for QCD at large distances. Next, in Section 2.3, we present the derivation of the effective Hamiltonian of lattice QCD in strong-coupling perturbation theory [20, 21]. The second-order Hamiltonian $[O(1/g^2)]$ is an antiferromagnet with $U(4N_f)$ spins; the global symmetry group is $U(4N_f)$ for the nearest-neighbor theory, broken to $U(N_f) \times U(N_f)$ by NNN terms. The baryon number at each site determines the representation of $U(4N_f)$ carried by the spin at that site. In second order, baryon number is static; it becomes mobile in the next order, where (for $N_c = 3$) the new term in the effective Hamiltonian is a baryon hopping term.

In the remainder of this thesis, we work only to $O(1/g^2)$, where the baryons are fixed in position. Motivated by the similarity of our Hamiltonian to the Heisenberg antiferromagnet, we apply condensed matter methods developed for that problem. Indeed, condensed matter physicists have generalized the $SU(2)$, spin-1/2 Heisenberg model to $SU(N)$ in many representations [42, 43, 44, 45, 46, 47, 48, 49, 50], which corresponds to adding flavor and color degrees of freedom to the electrons.[2] These are exactly the generalizations needed for our effective Hamiltonian. With N_c colors and N (single-component) flavors, a site of the lattice can be constrained to contain a color-singlet combination of mN_c particles. The flavor indices of the spin then make up a representation of $SU(N)$ whose Young diagram has N_c columns and m rows (see Fig. 1.1). We set

$$N = 4N_f \tag{1.1}$$

and the correspondence is complete (until we include NNN terms in the Hamiltonian).

---

[2] We refer the reader to the paper by Read and Sachdev [46] for a survey, including a phase diagram in the (N, N_c) plane.

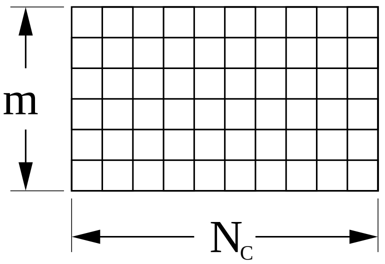

Figure 1.1: The representation of $U(N)$ carried by the spin in the effective antiferromagnet [See Chapter 2]. m is related to the baryon number B at the site according to $m = B+2N_f$, with $|B| \leq 2N_f$.

In Chapter 3 we analyze the effective Hamiltonian by following Arovas and Auerbach [45] and write it with boson operators that obey appropriate constraints to restrict quantum states to the Hilbert space represented by Fig. 1.1. After introducing the boson operators and their corresponding path integral in Section 3.1, we apply the Hubbard-Stratonovich transformation in Section 3.2 and decouple the quartic boson interaction to a quadratic interaction. The result of integrating the bosons is a path integral tractable in the limit of large N_c and N_f with a fixed ratio $r = N_c/N_f$. We take this limit in Sections 3.3–3.4 and study a mean field ansatz for the ground state of a set of baryon number configurations. In Section 3.3 we extend the zero density results of [45] from dimension $d = 2$ to $d = 3$. As for $d = 2$, one finds a Bose-Einstein condensate (BEC) above some critical value of r. This BEC corresponds to a Néel ground state which represents a spontaneous breaking of chiral symmetry, as expected. For QCD, with $N_c = 3$, the system is safely in the *ordered* phase for any reasonable number of flavors. In Section 3.4 we depart zero density by inserting non-zero baryon number on some of the sites. More precisely we fill some of the sites with the maximum allowed baryon number per site. The $U(N)$ representation on these sites then has $m = N$ rows, and is a singlet. Analyzing again a mean field ansatz we discuss how these singlets affect the free energy and critical value of r. In this chapter we mainly restrict to the disordered side of the phase transition.

In Chapter 4, and in the rest of the thesis, we treat the system deep in its ordered phase. Also the non-zero baryon number configuration we investigate are different than those of Chapter 3, and we mainly concentrate on uniform baryon configuration, with the same baryon number B on all sites. In Section 4.1–4.2 we follow Read and Sachdev [46] and employ spin coherent states [51] to write the partition function as a path integral for a nonlinear sigma model. N_f and m determine the target space of the sigma model to be the symmetric space $U(N)/[U(m) \times U(N-m)]$; the number of colors N_c becomes an overall coefficient of the action. As for the quantum Hamiltonian, the nearest-neighbor theory is symmetric under $U(N)$ while the NNN terms break the symmetry to $U(N_f) \times U(N_f)$ (while leaving the manifold unchanged).

In Section 4.3 we make a pause from the real sigma model, and treat its classical counterpart, with a variety of baryon number configurations. This analysis presumably describes the high temperature region of the system, where quantum fluctuations are not very important. It also serves as a tool to see how the symmetry realization changes as we add baryons to the lattice. Although the classical sigma model can be treated numerically (its action is real), we postpone this to future research and use mean field theory instead for a toy model that has $N = 3$. In that case calculations can be done analytically, and we extract the *classical* phase diagram in temperature-density plane.

Next we return to discuss the real quantum sigma model. The factor of N_c that multiplies the action invites a large-N_c analysis which we make in Section 4.4. We start by studying this limit for zero baryon number in Section 4.4.1. This leads us to an exercise proposed and solved by Smit [21], in generalizing the zero baryon number sector to allow baryon number $\pm B$ on alternating sites; this means specifying conjugate representations of $U(N)$ on alternating sites, with respectively m and $N-m$ rows. We find the ground state of the nearest-neighbor theory to be discretely degenerate as seen in [21]. We extend this result to the NNN theory and show how the degeneracy is removed by the NNN terms.

We turn to non-zero baryon density in Section 4.4.2. As mentioned, we study homogeneous states, in which all sites carry the same representation of $U(N)$, with $m > N/2$. We begin by studying the two-site problem, and we learn that its ground state is continuously degenerate. This degeneracy is additional to the global degeneracy of rotating the sigma fields on the two sites together. Replicating this ground state to the infinite lattice makes the lattice vacuum locally degenerate. This makes our system similar to some frustrated models of magnetic systems [52, 53, 54, 55, 56, 57]. In contrast to the zero density case this local degeneracy is not removed by the NNN terms.

In order to remove this degeneracy we consider quantum fluctuations in Chapter 5. We first treat the case of zero baryon number in Section 5.1, where we see that $1/N_c$ corrections to the free energy removes the discrete degeneracy of the nearest-neighbor theory[3]. We find that fluctuations choose the same ground state chosen by the NNN terms.

We treat fluctuations for the non-zero density system in Section 5.2. In Section 5.2.1

---

[3] This result was obtained by Smit using a Holstein-Primakoff transformation on the quantum Hamiltonian.

we first show that the local degeneracy is expressed by having zero modes in the $O(1)$ dispersion relations of excitations around the classical ground state. These have zero energy for all momenta. In Section 5.2.2, we show that these zero modes get non-zero self energy of order $1/N_c$, thus removing the classical local degeneracy. This is the phenomenon of "order from disorder" also present in the frustrated spin systems mentioned above. We also find that the energies produced are quadratic in momentum, which makes the zero modes type II Goldstone bosons.

The analysis in Chapters 3–5 is mainly concerned with the nearest-neighbor theory that is symmetric under the too large group of $U(4N_f)$. In Chapter 6 we take into account next-nearest-neighbor interactions, and treat them as a perturbation on the nearest-neighbor ground state. In Section 6.1 we introduce the action of the sigma model which is now invariant only under $U(N_f) \times U(N_f)$. In Section 6.2, we show that some of the global degeneracy of the nearest-neighbor ground state is removed, and discuss how the vacuum expectation values of the sigma fields break chiral symmetry and discrete lattice rotations. In Section 6.3 we calculate the effects of these next-nearest-neighbor interactions on the spectrum of the nearest-neighbor theory.

In Chapter 7 we summarize the thesis and point to directions of future research.

All the work presented is this dissertation, except for Section 3.4, and some of the technical appendices, has already been published. The analysis of Chapter 2 has appeared already in earlier work [19, 20, 21, 22, 30] and in [58, 59]. The results of Section 3.3 (without the analysis itself) and Chapter 4 were published in [58] and [59]. Sections 5.1 and 5.2 were also published in [59], whereas the remainder of Chapter 5 was published in [60]. Finally the treatment of NNN interactions of Chapter 6 was published in [61] and [62].

Chapter 2

The effective Hamiltonian

In this chapter we derive the effective Hamiltonian we use to investigate QCD at high densities. We begin by giving a short review on the Hamiltonian approach to lattice QCD in Section 2.1, where we stress important points relevant to this work, and fix some of the notations. Aiming to work at strong coupling, and aware of the fact that the continuum limit is at weak coupling, we take the point of view that the investigated Hamiltonian is an effective one that describes QCD at large distances. We elaborate on this formal point in Section 2.2. We then proceed to derive the effective Hamiltonian by strong coupling expansion in Section 2.3. We conclude by emphasizing the similarity of the Hamiltonian to the t–J model Hamiltonian of condensed matter physics.

2.1 Hamiltonian approach to lattice QCD

In this section we introduce the Hamiltonian formalism of lattice QCD. This formalism is more amenable to strong-coupling perturbation theory and to qualitative study of the ensuing effective theory [19, 20, 21, 22, 30] than the Euclidean formalism.

The Hamiltonian formalism was first introduced by Kogut and Susskind in 1975 [63], shortly after Wilson's Euclidean formulation [64]. This formalism defines the theory of strong interactions on a three dimensional space lattice with lattice spacing a and continuous time t. A lattice site is denoted by a three dimensional vector $\boldsymbol{n} = (n_x, n_y, n_z)$ taking integer values, and a lattice link is denoted by $(\boldsymbol{n}\hat{\boldsymbol{\mu}})$, where $\mu = \pm x, \pm y, \pm z$.

The quantum fields that describe quarks are the fermion fields $\psi_{\boldsymbol{n}}^{af\alpha}$ that live on the sites $\boldsymbol{n}$ of the lattice. They have color indices $a = 1, \dots, N_c$, Dirac indices $\alpha = 1, \dots, 4$, and flavor indices $f = 1, \ldots, N_f$. It is more convenient to group the Dirac and flavor indices to a single index α that takes values from 1 to $4N_f$. The Fermi fields obey the following anti-commutation relations

$$\left\{\psi_{\boldsymbol{n}}^{a\alpha}, \psi_{\boldsymbol{m}}^{\dagger b\beta}\right\} = \delta_{\boldsymbol{nm}}\delta_{ab}\delta_{\alpha\beta}. \tag{2.1}$$

For the gauge fields, that describe the gluons, one chooses to work in the temporal gauge that fixes $A_0 = 0$, and removes one degree of freedom (and its conjugate momentum). As a result, one is left only with the link operators $(U_{\boldsymbol{n}\hat{\boldsymbol{\mu}}})_{ab}$, and $\left(U^{\dagger}_{\boldsymbol{n}\hat{\boldsymbol{\mu}}}\right)_{ab} = (U_{\boldsymbol{n}+\hat{\boldsymbol{\mu}},-\hat{\boldsymbol{\mu}}})_{ab}$. These represent gauge fields on the link $(\boldsymbol{n}\hat{\boldsymbol{\mu}})$, whose two edges are colored with colors a and b. There are 6 links emanating from each site $\boldsymbol{n}$. On each link reside the gauge fields $(U_{\boldsymbol{n}\hat{\boldsymbol{\mu}}})_{ab}$ and their conjugate momenta $E^i_{\boldsymbol{n}\hat{\boldsymbol{\mu}}}$, $i = 1, \ldots, N_c^2 - 1$. The following are the commutation relations of this set of operators,

$$\begin{aligned} \left[E^i_{\boldsymbol{n}\hat{\boldsymbol{\mu}}}, (U_{\boldsymbol{n}\hat{\boldsymbol{\mu}}})_{ab}\right] &= \left(\lambda^i U_{\boldsymbol{n}\hat{\boldsymbol{\mu}}}\right)_{ab}, && (2.2) \\ \left[E^i_{\boldsymbol{n}\hat{\boldsymbol{\mu}}}, E^j_{\boldsymbol{n}\hat{\boldsymbol{\mu}}}\right] &= if^{ijk}E^k_{\boldsymbol{n}\hat{\boldsymbol{\mu}}}, && (2.3) \end{aligned}$$

for the set of the links $(\boldsymbol{n}\hat{\boldsymbol{\mu}})$, and

$$\begin{aligned} \left[E^i_{\boldsymbol{n},-\hat{\boldsymbol{\mu}}}, (U_{\boldsymbol{n},-\hat{\boldsymbol{\mu}}})_{ab}\right] &= -\left(U_{\boldsymbol{n},-\hat{\boldsymbol{\mu}}}\lambda^i\right)_{ab} && (2.4) \\ \left[E^i_{\boldsymbol{n},-\hat{\boldsymbol{\mu}}}, E^j_{\boldsymbol{n},-\hat{\boldsymbol{\mu}}}\right] &= -if^{ijk}E^k_{\boldsymbol{n},-\hat{\boldsymbol{\mu}}}, && (2.5) \end{aligned}$$

for the set $(\boldsymbol{n}, -\hat{\boldsymbol{\mu}})$. Here λ^i are matrices that represent the generators of $SU(N_c)$ in the fundamental representation, and f^{ijk} are the structure constants of $SU(N_c)$. For $N_c = 2$, Eqs. (2.2)–(2.5) are exactly the commutations relations that appear in the classical problem of the rotating top, where $E^i_{\boldsymbol{n}\hat{\boldsymbol{\mu}}}$, and $E^i_{\boldsymbol{n},-\hat{\boldsymbol{\mu}}}$ generate rotations of space fixed and body fixed coordinate systems. One uses this analogy to write

$$E^i_{\boldsymbol{n}+\hat{\boldsymbol{\mu}},-\hat{\boldsymbol{\mu}}} = -\left(U^{\text{Adj.}}_{\boldsymbol{n}\hat{\boldsymbol{\mu}}}\right)_{ij} E^j_{\boldsymbol{n},-\hat{\boldsymbol{\mu}}}, \tag{2.6}$$

where $U^{\text{Adj.}}_{\boldsymbol{n}\hat{\boldsymbol{\mu}}}$ is the rotation $U_{\boldsymbol{n}\hat{\boldsymbol{\mu}}}$ in the adjoint representation of $SU(N_c)$. For a more detailed discussion see [63].

We now discuss the lattice Hilbert space. A state $|\Omega\rangle$ is the direct product on all lattice sites,

$$|\Omega\rangle = |\Omega\rangle_G \otimes |\Omega\rangle_\Psi. \tag{2.7}$$

Here the first factor is the projection of the state $|\Omega\rangle$ to the gauge field sector, while the second factor describes the fermionic sector.

Any state $|\Omega\rangle_\Psi$ is the following direct product

$$|\Omega\rangle_\Psi = \prod_{\otimes \boldsymbol{n}} \left(|\Omega\rangle_\Psi\right)_{\boldsymbol{n}}. \tag{2.8}$$

We now concentrate on the Hilbert space of each site. The "lowest" state is the no-quantum "drained" state $|\mathrm{Dr}\rangle_{\boldsymbol{n}}$, defined as

$$\psi^{a\alpha}_{\boldsymbol{n}}|\mathrm{Dr}\rangle_{\boldsymbol{n}} = 0. \tag{2.9}$$

Applications of various $\psi^{\dagger a\alpha}_{\boldsymbol{n}}$ create the corresponding quarks on that site,

$$|a\alpha\rangle_{\boldsymbol{n}\Psi} = \psi^{\dagger a\alpha}_{\boldsymbol{n}}|\mathrm{Dr}\rangle_{\boldsymbol{n}}. \tag{2.10}$$

For the free theory, $\alpha = 1, \ldots, 2N_f$ correspond to creation of positive energy excitations, i.e. quarks, whereas $\alpha = 2N_f, \ldots, 4N_f$ corresponds to creation of negative energy excitations, i.e. annihilation of anti-quarks. To use the usual quark–anti-quark language we write for each site, color, and flavor,

$$\psi = \begin{pmatrix} b_\uparrow \\ b_\downarrow \\ d^\dagger_\downarrow \\ d^\dagger_\uparrow \end{pmatrix}. \tag{2.11}$$

$b^\dagger$ create a quark and $d^\dagger$ an anti-quark. From Eq. (2.9) we see that b and $d^\dagger$ annihilate the drained state, which means that this state is empty of quarks, and filled with anti-quarks. The operator of local baryon number is

$$B_{\boldsymbol{n}} = \frac{1}{N_c}\sum_{a=1}^{N_c}\sum_{s=\uparrow,\downarrow}\sum_{f=1}^{N_f}\left[b^{\dagger af}_s b^{af}_s - d^{\dagger af}_s d^{af}_s\right]_{\boldsymbol{n}} = \frac{1}{N_c}\psi^\dagger_{\boldsymbol{n}}\psi_{\boldsymbol{n}} - 2N_f. \tag{2.12}$$

According to Eq. (2.12), the baryon number of the drained state is $-2N_f$, corresponding to filling the site with anti-quarks. The vacuum $|0\rangle$ is the state with no quarks and no anti-quarks. This state is the filled Dirac sea on a single site and obeys,

$$b|0\rangle = d|0\rangle = 0. \tag{2.13}$$

The baryon number of this state is $B = 0$. Because of Pauli exclusion principle we cannot put too many fermions on a single site. The maximum number of local baryon number will be $2N_f$, and is found only in the state $|\mathrm{filled}\rangle$

$$b^\dagger|\mathrm{filled}\rangle = d|\mathrm{filled}\rangle = 0. \tag{2.14}$$

Below we will see that gauge invariance puts more restrictions on the single site Hilbert space in order that it be color neutral.

Moving to the gauge Hilbert space, we also write it as a direct product of the form

$$|\Omega\rangle_G = \prod_{\otimes \boldsymbol{n}\hat{\boldsymbol{\mu}}} \left(|\Omega\rangle_G\right)_{\boldsymbol{n}\hat{\boldsymbol{\mu}}} . \tag{2.15}$$

One denotes the state with no electric field E by $|0\rangle_G$,

$$E^i |0\rangle_G = 0, \qquad \forall i. \tag{2.16}$$

Any application of the link operators $\left(U^\dagger_{\boldsymbol{n}\hat{\boldsymbol{\mu}}}\right)_{ab}$ on $|0\rangle_G$, creates states which correspond to flux lines on the link $(\boldsymbol{n}\hat{\boldsymbol{\mu}})$. The state $|0\rangle_G$ is the only state with no flux at all. Using the fact that the electric field operators generate a $SU(N_c)$ algebra, one can distinguish between the different quantum states created by the link operators as follows. Define the quadratic Casimir operator

$$\vec{E}^2_{\boldsymbol{n}\hat{\boldsymbol{\mu}}} \equiv \sum_{i=1}^{N_c^2-1} E^{i2}_{\boldsymbol{n}\hat{\boldsymbol{\mu}}}. \tag{2.17}$$

It is clear that the fluxless state $|0\rangle_G$ is an eigenstate of this Casimir, with zero eigenvalue. Next the commutations of the Casimir with the link operators are verified from Eqs. (2.2)–(2.5) to be

$$\left[\vec{E}^2_{\boldsymbol{n}\hat{\boldsymbol{\mu}}}, \left(U^\dagger_{\boldsymbol{n}\hat{\boldsymbol{\mu}}}\right)_{ab}\right] = C_F \left(U^\dagger_{\boldsymbol{n}\hat{\boldsymbol{\mu}}}\right)_{ab}, \tag{2.18}$$

where C_F is the Casimir operator in the fundamental representation, and is

$$C_F = \frac{N_c^2 - 1}{2N_c} \tag{2.19}$$

for $SU(N_c)$.

This means that the state $\left[\left(U^\dagger_{\boldsymbol{n}\hat{\boldsymbol{\mu}}}\right)_{ab} |0\rangle_G\right]$ is also an eigenstate of (2.17), with eigenvalue equal to C_F. One can now classify the states in $|\Omega\rangle_G$ according to their $\vec{E}^2$ eigenvalue. The result is a Hilbert space with a ladder-like structure. The lowest state is $|0\rangle_G$, with zero flux, and is a singlet of $SU(N_c)$. Repeated applications of the gauge field operators $\left(U^\dagger_{\boldsymbol{n}\hat{\boldsymbol{\mu}}}\right)_{ab}$ create states with higher and higher values of flux and the operators $\vec{E}^2_{\boldsymbol{n}\hat{\boldsymbol{\mu}}}$ measures the flux on the link $(\boldsymbol{n}\hat{\boldsymbol{\mu}})$. Indeed we shall see shortly that it is proportional to the (kinetic) energy of the gauge fields.

To complete the picture we now discuss gauge invariance. First recall that the starting point of this formalism was to choose the timelike gauge. This leaves only time-independent gauge transformations as a symmetry. The fermion operators belong to the fundamental representation of the gauge symmetry and transform as

$$\psi^a_{\boldsymbol{n}} \to \left(V_{\boldsymbol{n}}\right)^{ab} \psi^b_{\boldsymbol{n}}, \tag{2.20}$$

with $V \in SU(N_c)$ given in general by

$$V = \exp\left[i \sum_{i=1}^{N_c^2-1} \theta^i_{\boldsymbol{n}} \lambda^i \right]. \tag{2.21}$$

Note that here, and in the following discussion, we suppress the Dirac-flavor indices, irrelevant to gauge invariance. Using the anticommutation relations (2.1), one can show that the quantum operator $\mathcal{V}_F$ that realizes Eq. (2.20) in Hilbert space as

$$\psi^a_{\boldsymbol{n}} \to \mathcal{V}_F \psi^a_{\boldsymbol{n}} \mathcal{V}^\dagger_F, \tag{2.22}$$

is

$$\mathcal{V}_F = \exp\left[i \sum_{\boldsymbol{n}} \sum_{i=1}^{N_c^2-1} \theta^i_{\boldsymbol{n}} \left(\psi^{\dagger a}_{\boldsymbol{n}} \lambda^i_{ab} \psi^b_{\boldsymbol{n}} \right) \right]. \tag{2.23}$$

The gauge fields transform according to

$$\left(U_{\boldsymbol{n}\hat{\boldsymbol{\mu}}}\right)_{ab} \to \left(V_{\boldsymbol{n}} U_{\boldsymbol{n}\hat{\boldsymbol{\mu}}} V^\dagger_{\boldsymbol{n}+\hat{\boldsymbol{\mu}}} \right)_{ab}. \tag{2.24}$$

Using the commutation relations (2.2)–(2.5), one shows that the quantum operator $\mathcal{V}_G$ that generates these rotations is given by

$$\mathcal{V}_G = \exp\left[i \sum_{\boldsymbol{n}} \sum_{i=1}^{N_c^2-1} \theta^i_{\boldsymbol{n}} \left(\sum_{\pm\hat{\boldsymbol{\mu}}} E^i_{\boldsymbol{n}\hat{\boldsymbol{\mu}}} \right) \right]. \tag{2.25}$$

Finally putting Eq. (2.23), and Eq. (2.25) together and using Eq. (2.6), we see that operator that induces gauge transformations is

$$\mathcal{V} = \exp\left[i \sum_{\boldsymbol{n}} \sum_{i=1}^{N_c^2-1} \theta^i_{\boldsymbol{n}} \left(\rho^i_G + \rho^i_F \right)_{\boldsymbol{n}} \right], \tag{2.26}$$

where $\rho^i_{F\boldsymbol{n}}$, and $\rho^i_{G\boldsymbol{n}}$ are the color charge densities of the fermions, and gauge fields. These two quantities are given by

$$\begin{aligned}\rho^i_{F\boldsymbol{n}} &= \psi^{\dagger a}_{\boldsymbol{n}}\lambda^i_{ab}\psi^b_{\boldsymbol{n}}, && (2.27)\\ \rho^i_{G,\boldsymbol{n}} &= \sum_\mu \left(E^i_{\boldsymbol{n},\hat{\boldsymbol{\mu}}} - \left(U^{\text{Adj.}}_{\boldsymbol{n}-\hat{\boldsymbol{\mu}},\hat{\boldsymbol{\mu}}}\right)_{ij} E^j_{\boldsymbol{n}-\hat{\boldsymbol{\mu}},\hat{\boldsymbol{\mu}}}\right). && (2.28)\end{aligned}$$

Note that Eq. (2.28) can be written as the covariant divergence of the electric field,

$$\rho^i_{G\boldsymbol{n}} = \vec{D}\cdot\vec{E}^i_{\boldsymbol{n}} \equiv \vec{\nabla}_L\cdot\vec{E}^i_{\boldsymbol{n}} + \sum_\mu \left(1 - U^{\text{Adj.}}_{\boldsymbol{n}-\hat{\boldsymbol{\mu}},\hat{\boldsymbol{\mu}}}\right)_{ij} E^j_{\boldsymbol{n}-\hat{\boldsymbol{\mu}},\hat{\boldsymbol{\mu}}}, \tag{2.29}$$

where the lattice divergence is given by

$$\vec{\nabla}_L\cdot\vec{E}^i_{\boldsymbol{n}} \equiv \sum_\mu \left(E^i_{\boldsymbol{n}\mu} - E^i_{\boldsymbol{n}-\mu,\mu}\right). \tag{2.30}$$

Since the lattice Hamiltonian is gauge invariant, we know that the generators of the gauge transformations commute with the Hamiltonian

$$\left[H, \rho^i_{G\boldsymbol{n}} + \rho^i_{F\boldsymbol{n}}\right] = 0, \qquad \forall i \quad \forall \boldsymbol{n}, \tag{2.31}$$

This means that we can choose to work with a basis that block diagonalizes $\rho^i_G + \rho^i_F$. This breaks the Hilbert space to separate sectors classified by their $\rho^i_G + \rho^i_F$ representations on the lattice. Each set of operators $\rho^i_{\text{ext},\boldsymbol{n}}$ describes a different physical case, with a different *external* distribution of color charge (that can correspond, for example, to infinitely heavy quarks etc.). To describe the physics of quarks with finite masses, and zero external gauge fields, we work with the choice $\rho^i_{\text{ext}} = 0$. Working in this subspace means that *all* physical states must be color singlets, since all gauge transformations are trivial.

Finally we describe the lattice Hamiltonian H of $SU(N_c)$ gauge theory with N_f flavors of fermions. H is given by

$$H = H_E + H_G + H_F. \tag{2.32}$$

Here H_E is the electric term, a sum over links $(\boldsymbol{n}\mu)$ of the $SU(N_c)$ Casimir operator

$$H_E = \frac{1}{2}g^2\sum_{\boldsymbol{n}\mu}\vec{E}^2_{\boldsymbol{n}\mu}. \tag{2.33}$$

Next is the magnetic term, a sum over plaquettes,

$$H_G = \frac{1}{2g^2}\sum_p \left(N_c - \operatorname{Tr} U_p\right). \tag{2.34}$$

Finally we have the fermion Hamiltonian,

$$H_F = -i \sum_{\boldsymbol{n}\mu} \psi^{\dagger af}_{\boldsymbol{n}} \alpha_\mu \sum_{j>0} D(j) \left(\prod_{k=0}^{j-1} U_{\boldsymbol{n}+k\hat{\boldsymbol{\mu}},\mu} \right)_{ab} \psi^{bf}_{\boldsymbol{n}+j\hat{\boldsymbol{\mu}}} + h.c. \tag{2.35}$$

In Eq. (2.35) we suppress Dirac and color indices, and denote explicitly the flavor index f. The function $D(j)$ is a kernel that defines the lattice fermion derivative. It should be sufficiently local, namely at least falling exponentially with distance. For example it can yield a naive, nearest-neighbor action if $D(j) = \frac{1}{2}\delta_{j,1}$; a next-nearest-neighbor kernel with $D(j \geq 3) = 0$; a long-range SLAC derivative [30] with $D(j) = -(-1)^j/j$ will however not be good enough, since it falls only algebraically.

The choice of the fermion kernel is important, since it fixes the global symmetries of the Dirac Hamiltonian (2.35), and in turn the global symmetries of the effective Hamiltonian that we derive in Section 2.3. Superficially, the Hamiltonian has only the chiral symmetry of $U(N_f)_R \times U(N_f)_L$ regardless of the kernel used. This is however not true. For a naive kernel, one can spin diagonalize the fermions, and show that the Dirac α_μ matrices disappear. This means that the Dirac $\alpha = 1, \ldots, 4$ indices become just a different kind of flavor, and the symmetry is then $U(4N_f)$. Applying the same procedure to the next-nearest-neighbor kernel, one sees that the Dirac structure does not disappear, and the symmetry is indeed only chiral symmetry $U(N_f) \times U(N_f)$. We postpone further discussion in symmetries to the level of the effective Hamiltonian calculated in Section 2.3.

2.2 The strong coupling limit

Formulating a quantum field theory on a lattice is in fact a way of regulating the theory by providing it with a cutoff in coordinate space. As in any other regularization scheme, the cutoff must be removed at the end in favor of observable quantities. On the lattice, the removal of the cutoff is basically the procedure of taking the continuum limit of the theory, i.e., taking the lattice spacing a to zero. In order to extract continuum physics, one calculates a physical observable as a function of the bare parameters of the theory (e.g. a and the bare coupling g_0), and demands that the $a \to 0$ continuum limit of the observable will be its measured value. This procedure tells us how the bare coupling g_0 behaves as a function of the cutoff a. In the case of asymptotically free theories (and in particular in the case of QCD), the bare coupling $g_0(a)$ approaches zero as $a \to 0$. This means that ideally we should examine the lattice theory at small coupling and small lattice spacings. The regime where these both are small enough is determined by the scaling behavior of physical observables one calculates. This approach has become standard, and is realized by doing Monte Carlo simulations of the lattice theory. These, performed close to the continuum limit, give us information on non-perturbative aspects of QCD.

As mentioned in Chapter 1, these Monte Carlo approaches fail when the theory is defined at finite chemical potential. In order to examine the dense system, one is forced to resort to other methods of calculation. We turn to the strong coupling regime of QCD, which is far from the continuum limit. As a result one cannot trust numerical figures that come out of strong-coupling calculations (especially since we use only the lowest order and do not perform any extrapolation to small coupling). Despite this, examining the strong-coupling regime gives insight on qualitative features of the dense nuclear system. The physical picture we have in mind is that if one would perform a block-spin transformation of the lattice theory near its continuum limit, and integrate out high momentum degrees of freedom, then one will be left with a lattice theory for large distances (of the order of hadronic scale distances of 1 fm.) The resulting effective theory will be strongly-coupled, and have the symmetries of QCD. In particular it will have an $SU(3)$ gauge group (or in general an $SU(N_c)$, where N_c is the number of colors). It will also have the global symmetry

$$SU(N_f)_L \times SU(N_f)_R \times U(1)_B. \tag{2.36}$$

Its dynamical physical features should include confinement and spontaneous chiral symmetry breaking (at zero density). All these important features are present in lattice QCD with strong bare coupling, and a suitable definition of the fermion kernel, which we take to be our starting point. In this work we show that the Hamiltonian formulation of this theory is tractable even with non-zero baryon density.

The only property that the theory explored here does not have is the anomaly of the axial $U(1)$ symmetry. In QCD, this symmetry is classically conserved, but broken in the presence of gauge fields. This is expressed in the fact that the corresponding singlet axial current has a non-zero divergence. This fact is most easily seen in perturbation theory in continuum QCD [65], and is verified experimentally by the large mass of the η' meson, which should have been as small as the pion masses in the absence of this anomaly. The same calculation can be done with weak-coupling perturbative methods of lattice QCD [66]. There, the lattice doubling of the fermions plays a crucial role and leads to conservation of the singlet axial current; the doubled fermions fall into two groups with opposite chiral charges, and the contribution of each group to the anomaly is canceled. In order to obtain the anomaly in a lattice theory, one must break chiral symmetry explicitly (for example by a Wilson term) to remove the doubling. The continuum limit is then taken carefully to restore all chiral symmetries except the axial $U(1)$.

We do not use Wilson fermions, and as mentioned also do not work in the continuum limit. Our fermion kernel leads to full species doubling in the weak-coupled continuum limit, but this fact by itself is not a real problem, since we work at strong coupling, where we do not have quark excitations. Our Hamiltonian will *not* lead to doubling of mesonic excitations, as long as it has the correct symmetry. Nevertheless, we can not avoid the absence of the anomaly; $U(1)_A$ is not anomalous, and is conserved at the quantum level as well. At this point we stress the fact that we regard our theory as an effective theory for QCD at large distances. In the process of the block-spin transformation that begins from a theory with no axial singlet symmetry, a $U(1)_A$ violating term will have to be generated. Therefore in order to have physical features related to this term, we will have to add it by hand, without knowledge of its exact strength. Note that in addition, we know neither the exact value of the coupling, nor the exact way the fermion kernel behave (we do assume that it falls fast enough).

In practice we can add the $U(1)_A$ violating term in any stage of the calculation. At the level of the effective lattice Hamiltonian introduced below, it will be a 't Hooft vertex. For two flavors it can also be expressed in terms of the color singlet objects of Section 2.3.1, and for any number of flavors it is easiest to add this term at the level of the non-linear sigma model derived in Chapter 4 [32]. This term will have some simple effects on the low energy spectrum we derive, and we discuss them in Chapter 6.

2.3 Strong coupling perturbation theory

Our starting point is therefore the Hamiltonian (2.32) with large bare coupling. For $g \gg 1$ the ground state of H is determined by H_E alone to be any state with zero gauge flux, whatever its fermion content,

$$|0\rangle = \left[\prod_{\boldsymbol{n}\mu} |E^2_{\boldsymbol{n}\mu} = 0\rangle\right]_G |\Psi\rangle. \tag{2.37}$$

These states have energy $\epsilon_0 = 0$ and are degenerate with respect to all the fermionic degrees of freedom. We consider perturbation theory in $V = H_G + H_F$. Both H_G and H_F are sums of operators that are strictly bounded, independent of g except for the explicit coefficient in H_G. We can dismiss first-order perturbations by noting that H_G and H_F are multilinear in link operators U and $U^\dagger$, which are raising/lowering operators for the electric field; thus there are no non-zero matrix elements within the zero-field sector.

We proceed to higher orders, and seek an effective Hamiltonian that acts in the zero-field sector [67]. Define P_0 to be the projector onto the subspace of all the $E = 0$ states. Then perturbation theory in V gives an effective Hamiltonian,

$$H_{\text{eff}} = P_0 V Q D V P_0 + P_0 V Q D V Q D V P_0 + \cdots . \tag{2.38}$$

Here $Q = 1 - P_0$ projects onto the subspace orthogonal to the $E = 0$ states; the operator $D \equiv (\epsilon_0 - H_E)^{-1}$ supplies energy denominators, so that

$$QD = \sum_{E \neq 0\,\text{states}} |\lambda\rangle \frac{1}{\epsilon_0 - \epsilon_\lambda} \langle\lambda|. \tag{2.39}$$

The intermediate states $|\lambda\rangle$ contain flux excitations. In second and third order the patterns of flux can only be strings of length j in the fundamental representation of the color group. Thus the energy denominators are

$$\epsilon_0 - \epsilon_\lambda = -\frac{1}{2} g^2 C_F |j|. \tag{2.40}$$

The perturbations H_G and H_F are explicitly of $O(1/g^2)$ and $O(1)$, respectively; each energy denominator gives a factor of $1/g^2$. Thus to $O(1/g^4)$ we can forget about H_G. Our result to this order is

$$H_{\text{eff}} = P_0 H_F D H_F P_0 + P_0 H_F D H_F D H_F P_0. \tag{2.41}$$

Since H_F has no non-zero matrix elements within the $E = 0$ sector, we have dispensed with Q in Eq. (2.41). The first term in Eq. (2.41) arises for any value of N_c and is $O(1/g^2)$; the case $N_c = 2$ must be treated carefully, but all cases $N_c > 2$ are generic. The second term is special to $N_c = 3$ and is $O(1/g^4)$.

2.3.1 Second order: the antiferromagnet

We calculate explicitly the first term in H_{eff}. Each term in H_F creates a string of flux of length j, which must be destroyed by the conjugate term. Thus

$$H^{(2)}_{\text{eff}} = 2 \sum_{j>0} [-K(j)] \sum_{\boldsymbol{n}\mu} \left(\psi^{\dagger af}_{\boldsymbol{n}} \alpha_\mu \psi^{bf}_{\boldsymbol{n}+j\hat{\boldsymbol{\mu}}} \right) \langle 0| \left(\prod U \right)_{ab} \left(\prod U^\dagger \right)_{cd} |0\rangle \left(\psi^{\dagger cg}_{\boldsymbol{n}+j\hat{\boldsymbol{\mu}}} \alpha_\mu \psi^{dg}_{\boldsymbol{n}} \right), \tag{2.42}$$

where we define

$$K(j)=\frac{[D(j)]^2}{\frac{1}{2}g^2C_F|j|}>0. \tag{2.43}$$

The matrix element of the gauge fields yields $\frac{1}{N_c}\delta_{ad}\delta_{bc}$, independent of j.

As they appear in Eq. (2.42), each $\psi^\dagger$ is next to a ψ on a different site. This invites a Fierz transformation on the product of fermion fields, which we write generally as

$$\left(\psi_i^\dagger\alpha_\mu\psi_j\right)\left(\psi_k^\dagger\alpha_\mu\psi_l\right)=\delta_{jk}\psi_i^\dagger\psi_l-\frac{1}{4}\sum_A s_A^\mu\left(\psi_i^\dagger\Gamma^A\psi_l\right)\left(\psi_k^\dagger\Gamma^A\psi_j\right). \tag{2.44}$$

Here i,j,k,l are combined site, flavor, and color indices, and we have assumed that k and l are always different while j and k might be equal [as in Eq. (2.42)]. The matrices Γ^A are the 16 Dirac matrices, normalized to $(\Gamma^A)^2=\mathbf{1}$, and we have defined

$$s_A^\mu=\frac{1}{4}\mathrm{Tr}\,\Gamma^A\alpha_\mu\Gamma^A\alpha_\mu=\pm1. \tag{2.45}$$

This sign factor is ±1 according to whether Γ^A commutes or anticommutes with α_μ; it will be a constant companion in our calculations. As they appear in $H_{\text{eff}}^{(2)}$, the indices i,l are the same site and color but different flavors, and likewise j,k. Leaving the flavor indices explicit, we obtain

$$H_{\text{eff}}^{(2)}=\frac{1}{4N_c}\sum_{\substack{\boldsymbol{n}\mu\\ j\neq0}}K(j)s_A^\mu\left(\psi^{\dagger f}\Gamma^A\psi^g\right)_{\boldsymbol{n}}\left(\psi^{\dagger g}\Gamma^A\psi^f\right)_{\boldsymbol{n}+j\hat{\boldsymbol{\mu}}}-d\sum_{j\neq0}K(j)\sum_{\boldsymbol{n}}\left(\psi^{\dagger f}\psi^f\right)_{\boldsymbol{n}}. \tag{2.46}$$

Each fermion bilinear in parentheses is a color singlet located at a given site. The second term contains the baryon density[1] $B'_{\boldsymbol{n}}=N_c^{-1}\psi_{\boldsymbol{n}}^\dagger\psi_{\boldsymbol{n}}$, and the sum $\sum_{\boldsymbol{n}}B'_{\boldsymbol{n}}$ is the total baryon number B'. A final important note is that one can easily verify that the effective Hamiltonian $H_{\text{eff}}^{(2)}$ commutes with the local baryon number $B_{\boldsymbol{n}}$ (and $B'_{\boldsymbol{n}}$). This is a result of the fact that each of the local operators in Eq. (2.46) does not change the fermion occupation of a site.

We now combine the Dirac indices with the flavor indices and write

$$\left(\psi^{\dagger f}\Gamma^A\psi^g\right)_{\boldsymbol{n}}\left(\psi^{\dagger g}\Gamma^A\psi^f\right)_{\boldsymbol{n}'}=8\left(\psi^\dagger M^\eta\psi\right)_{\boldsymbol{n}}\left(\psi^\dagger M^\eta\psi\right)_{\boldsymbol{n}'}. \tag{2.47}$$

---

[1] This baryon number is positive semidefinite, and is zero for the drained state. The conventional baryon number $B_{\boldsymbol{n}}$ is zero in the half-filled state, and thus $B'_{\boldsymbol{n}}=B_{\boldsymbol{n}}+2N_f$.

We have defined new matrices M^η as direct products of the 4×4 Dirac matrices and the $U(N_f)$ flavor generators,

$$M^\eta = \Gamma^A \otimes \lambda^a, \tag{2.48}$$

and we have normalized them conventionally according to

$$\operatorname{Tr} M^\eta M^{\eta'} = \frac{1}{2}\delta^{\eta\eta'}. \tag{2.49}$$

The M^η generate a $U(N)$ algebra, with $N \equiv 4N_f$.

An alternating flip

$$\psi_{\boldsymbol{n}} \to \left[\prod_\mu (\alpha_\mu)^{n_\mu}\right]\psi_{\boldsymbol{n}} \tag{2.50}$$

(spin diagonalization [20]) removes the α_μ matrices from the odd-j terms in H_F, and hence removes the sign factors s_A^μ from the odd-j terms in $H_{\text{eff}}^{(2)}$. We have finally

$$H_{\text{eff}}^{(2)} = \frac{2}{N_c}\sum_{\boldsymbol{n}\mu j} K(j)\left(s_\eta^\mu\right)_{\substack{\text{even j}\\ \text{only}}}\left(\psi^\dagger M^\eta \psi\right)_{\boldsymbol{n}}\left(\psi^\dagger M^\eta \psi\right)_{\boldsymbol{n}+j\hat{\boldsymbol{\mu}}} - \left(dN_c\sum_j K(j)\right)B'. \tag{2.51}$$

The odd-j terms are of the form $\boldsymbol{M}\cdot\boldsymbol{M}$ which can be written in any basis for the $U(4N_f)$ algebra. The even-j terms, however, contain s_η^μ which is defined only in the original basis (2.48).

We now turn to describe the zero-field sector Hilbert space in which the Hamiltonian (2.51) works. In this sector in which we work, Gauss' Law constrains the fermion state at each site to be a color singlet. The drained state $|\text{Dr}\rangle$, with $\psi_{\boldsymbol{n}}^{af\alpha}|\text{Dr}\rangle = 0$ for all $(af\alpha)$, is the unique state with $B'=0$. The other color singlet states may be generated by repeated application of the baryon creation operator,

$$b_{\alpha\beta\cdots}^\dagger = \epsilon_{ab\cdots}\psi_{\boldsymbol{n}}^{\dagger a\alpha}\psi_{\boldsymbol{n}}^{\dagger b\beta}\cdots, \tag{2.52}$$

with N_c operators ψ. (Here and henceforth, the indices $\alpha,\beta,\ldots$ combine the flavor and Dirac indices.)

At each site $\boldsymbol{n}$ the operators

$$Q_{\boldsymbol{n}}^\eta = \psi_{\boldsymbol{n}}^\dagger M^\eta \psi_{\boldsymbol{n}} = \psi_{\boldsymbol{n}}^{\dagger a\alpha} M_{\alpha\beta}^\eta \psi_{\boldsymbol{n}}^{a\beta} \tag{2.53}$$

generate a $U(N)$ algebra, with $N = 4N_f$. The drained state is obviously a singlet under this algebra. The creation operator $b_{\alpha\beta\cdots}^\dagger$ is symmetric to any exchange of its N_c Dirac-flavor indices. As a result it is in the symmetric representation of $U(N)$ with one row and N_c columns (see Fig. 2.1).

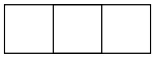

Figure 2.1: Young diagram of the representation of $U(4N_f)$ carried by the baryon operator

Repeated application of $b^\dagger_{\alpha\beta\cdots}$ to the drained state gives the state

$$b^\dagger b^\dagger \cdots |\mathrm{dr}\rangle. \tag{2.54}$$

The form (2.54) places the single site state within an irreducible representation of $SU(4N_f)$. Let us elaborate on this point. The single site state (2.54) is generated by an operator that has two sets of n indices; $SU(N_c)$ color indices, and $U(4N_f)$ Dirac-flavor indices. The number n is the number of fermions occupying the site. Gauge invariance restricts the color indices to be in an $SU(N_c)$ singlet, which means that

$$n = m \cdot N_c, \tag{2.55}$$

where m is an integer. In fact, m is the number of $b^\dagger$ applications in Eq. (2.54). More precisely, gauge invariance restricts the color indices to belong to the singlet representation $\underline{s}$ given in Fig 2.2.

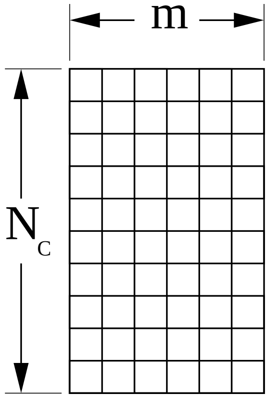

Figure 2.2: The representation of $SU(N_c)$ carried by the color indices of the singlet site state, that has mN_c fermions. The baryon number is $B = m - 2N_f$.

Next, we recall that states in an irreducible representation of any special unitary group $SU(k)$, are also an irreducible representation of the permutation group. In our case, this means that the n color indices belong also to the $\underline{\mathrm{s}}$ irreducible representation of S_n. Our aim is to determine the irreducible representation $\underline{\mathrm{r}}$ of the Dirac-flavor indices, with regard to the $SU(4N_f)$ group. Since this is also the S_n irreducible representation of the n Dirac-flavor indices, we find that the state (2.54) can belong to any possible part of the *reducible* representation $\underline{\mathrm{r}} \otimes \underline{\mathrm{s}}$ of S_n. Finally, we consider the fermionic nature of the state, and realize that the state belongs *only* to the completely antisymmetric representation $\underline{\mathrm{A}}$ of S_n included in $\bar{r} \otimes \bar{s}$ and given in Fig. (2.3).

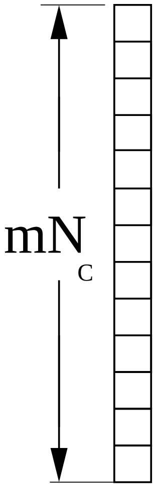

Figure 2.3: The representation of S_n carried by the complete set of indices of the singlet site state.

For given $\underline{\mathrm{s}}$ and $\underline{\mathrm{r}}$, $\underline{\mathrm{A}}$ occurs in $\underline{\mathrm{s}} \otimes \underline{\mathrm{r}}$ if and only if $\underline{\mathrm{r}}$ is the S_n conjugate representation of $\underline{\mathrm{s}}$ (which means flipping the Young tableau's rows and columns). Moreover the representation $\underline{\mathrm{A}}$ occurs only once in the decomposition of $\underline{\mathrm{s}} \otimes$ conjugate($\underline{\mathrm{s}}$). The conclusion is that the S_n (and therefore the $SU(4N_f)$) representation of the Dirac-flavor indices is given in Fig. 2.4.

We conclude by emphasizing the importance of the result of this section. Since the second-order effective Hamiltonian $H_{\text{eff}}^{(2)}$ preserves $B'_{\boldsymbol{n}}$, the baryon number on each site, then any distribution of $B'_{\boldsymbol{n}}$ defines a sector within which $H_{\text{eff}}^{(2)}$ is to be diagonalized. In other words, baryons constitute a fixed background in which to study "mesonic" dynamics. The baryon number at each site fixes the representation of $U(N)$ at that site, which is the space of states in which the charges $Q^{\eta}_{\boldsymbol{n}}$ act.

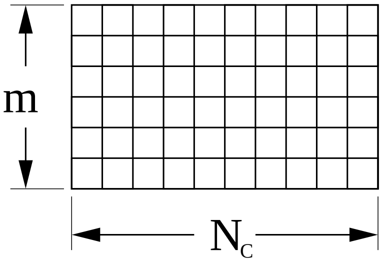

Figure 2.4: The representation of $U(4N_f)$ carried by the spin in the effective antiferromagnet. m is related to the baryon number at the site according to $m = B + 2N_f$, with $|B| \leq 2N_f$.

We now describe the global symmetries of the Hamiltonian. The $j = 1$ terms in Eq. (2.51) are of the form $Q^\eta_{\boldsymbol{n}} Q^\eta_{\boldsymbol{n}+\hat{\boldsymbol{\mu}}}$, and they commute with the generators

$$Q^\eta = \sum_{\boldsymbol{n}} Q^\eta_{\boldsymbol{n}} \tag{2.56}$$

of a global $U(N)$ symmetry group. This symmetry is in fact familiar from the lattice Hamiltonian of naive, nearest-neighbor fermions: Spin diagonalization of N_f naive Dirac fermions transforms the Hamiltonian into that of $4N_f$ staggered fermions. In the weak coupling limit, there are in fact $8N_f$ fermion flavors—the doubling problem. This doubling is partially reflected in the accidental $U(4N_f)$ symmetry, which is intact in the $g \to \infty$ limit and is respected by the effective Hamiltonian. Retaining terms in the fermion Hamiltonian (and thus in $H^{(2)}_{\text{eff}}$) that involve odd separations j does not break this symmetry.

The Nielsen-Ninomiya theorem [23] guarantees that any fermion Hamiltonian of finite range will possess the full doubling problem. This is a statement, however, about weak coupling only, since the dispersion relation of free fermions is irrelevant if the coupling is strong and the fermions are confined. It is interesting that the accidental $U(4N_f)$ symmetry nonetheless survives into strong coupling as a vestige of doubling.

The terms in Eq. (2.51) with *even* j, on the other hand, break the $U(N)$ symmetry, as do even-j terms in the original fermion Hamiltonian. It is easy to see via spin diagonalization, which leaves the even-j terms unchanged, that the only generators left unbroken are the Q^η corresponding to

$$M^\eta = \mathbf{1} \otimes \lambda^a \quad \text{and} \quad \gamma_5 \otimes \lambda^{\mathrm{a}}, \tag{2.57}$$

which form the $U(N_f)_L \times U(N_f)_R$ chiral algebra. This of course makes no difference to the Nielsen-Ninomiya theorem, which will enforce 8-fold doubling in the perturbative propagator even without the $U(4N_f)$ symmetry. If we are interested in the realization of the global symmetries of the continuum theory, though, we can study this lattice theory which has the same symmetry. The simplest theory one may study is thus one containing nearest-neighbor and next-nearest-neighbor terms. We shall proceed to discard terms with longer range; we shall begin with the nearest-neighbor theory, with its accidental doubling symmetry, and later break this symmetry to $U(N_f)_L \times U(N_f)_R$ with the next-nearest-neighbor terms.

Two essential differences will always remain between this lattice theory and the continuum theory. One is the presence of the axial $U(1)$ symmetry on the lattice. This symmetry is exact, broken by no anomaly, and may make the drawing of conclusions for the continuum theory less than straightforward unless it is broken by hand. The other difference is the fact that the effective Hamiltonian for baryons (see below) is also a short-ranged hopping Hamiltonian. If the baryons were almost free, we would say that they are surely doubled like the original quarks. The fact that the simplicity of the hopping terms is only apparent, and that the baryons are still coupled strongly to mesonic excitations, offers the possibility that doubling may not return.

2.3.2 Third order: the baryon kinetic term

Finally we show here the form of the third-order contribution to H_{eff}, which only exists in the case of $N_c = 3$. This term is calculated via

$$H_{\text{eff}}^{(3)} = P_0 V_F D V_F D V_F P_0. \tag{2.58}$$

For a single link, we have

$$\langle 0 | U_{ab} U_{a'b'} U_{\dot{a}\dot{b}} | 0 \rangle = \frac{1}{6} \epsilon_{aa'\dot{a}} \epsilon_{bb'\dot{b}}, \tag{2.59}$$

and the same can be proved for a chain of links,

$$\langle 0 | \left(\prod U \right)_{ab} \left(\prod U \right)_{a'b'} \left(\prod U \right)_{\dot{a}\dot{b}} | 0 \rangle = \frac{1}{6} \epsilon_{aa'\dot{a}} \epsilon_{bb'\dot{b}}. \tag{2.60}$$

Thus [$f, g, h, \ldots$ are here flavor indices],

$$H_{\text{eff}}^{(3)} = -i \sum_{j>0} \tilde{K}(j) \sum_{\boldsymbol{n}\mu} \left(\psi_{\boldsymbol{n}}^{\dagger af} \alpha_\mu \psi_{\boldsymbol{n}+j\hat{\boldsymbol{\mu}}}^{bf} \right) \left(\psi_{\boldsymbol{n}}^{\dagger a'g} \alpha_\mu \psi_{\boldsymbol{n}+j\hat{\boldsymbol{\mu}}}^{b'g} \right) \left(\psi_{\boldsymbol{n}}^{\dagger \dot{a}h} \alpha_\mu \psi_{\boldsymbol{n}+j\hat{\boldsymbol{\mu}}}^{\dot{b}h} \right) \epsilon_{aa'\dot{a}} \epsilon_{bb'\dot{b}} + h.c. \tag{2.61}$$

The kernel is

$$\tilde{K}(j) = \frac{(D(j))^3}{6\left(\frac{1}{2}g^2 C_F|j|\right)^2}. \tag{2.62}$$

Again, spin diagonalization simplifies the odd-j terms, but not the even-j terms. The result is

$$H^{(3)}_{\text{eff}} = H^{(3)}_{\text{odd}} + H^{(3)}_{\text{even}}, \tag{2.63}$$

with

$$H^{(3)}_{\text{odd}} = -i \sum_{\substack{j>0 \\ j\text{odd}}} \tilde{K}(j) \sum_{\boldsymbol{n}\mu} b^{\dagger I}_{\boldsymbol{n}} b^{I}_{\boldsymbol{n}+j\hat{\boldsymbol{\mu}}} \eta_\mu(\boldsymbol{n}) + h.c., \tag{2.64}$$

where $\eta_\mu(\boldsymbol{n})$ is the usual staggered-fermion sign factor, and

$$H^{(3)}_{\text{even}} = -i \sum_{\substack{j>0 \\ j\text{even}}} \tilde{K}(j) \sum_{\boldsymbol{n}\mu} b^{\dagger I}_{\boldsymbol{n}} \left[\alpha_\mu \otimes \alpha_\mu \otimes \alpha_\mu\right]_{II'} b^{I'}_{\boldsymbol{n}+j\hat{\boldsymbol{\mu}}} \zeta_\mu(\boldsymbol{n}) + h.c., \tag{2.65}$$

where $\zeta_\mu(\boldsymbol{n}) = (-1)^{\sum_{\nu\neq\mu} n_\nu}$. The baryon operators are

$$b^I = \epsilon_{abc} \psi^{a\alpha} \psi^{b\beta} \psi^{c\gamma}, \tag{2.66}$$

where we have written I to represent the compound index $\{\alpha\beta\gamma\}$, taking values in the symmetric three-index representation of $U(N)$ in Fig. 2.1. More precisely,

$$b^I = \begin{cases} \psi^1_\alpha \psi^2_\alpha \psi^3_\alpha & I = (\alpha, \alpha, \alpha) \\ \frac{1}{\sqrt{3}}(\psi^1_{(\alpha} \psi^2_\alpha \psi^3_{\beta)}) & I = (\alpha, \alpha, \beta) \\ \frac{1}{\sqrt{3!}}(\psi^1_{(\alpha} \psi^2_\beta \psi^3_{\gamma)}) & I = (\alpha, \beta, \gamma) \end{cases}$$

α, β and γ are indices of the fundamental representation of $U(4N_f)$, and the numbers are color indices. Note that these baryonic operators do not obey the canonical anticommutation relations of fundamental fermions [68, 69, 70, 71, 72, 73], but rather obey

$$\left\{b^I_{\boldsymbol{n}}, b^{\dagger I'}_{\boldsymbol{n}'}\right\} = \Delta_{II'} \delta_{\boldsymbol{n}\boldsymbol{n}'} \neq \delta_{II'} \delta_{\boldsymbol{n}\boldsymbol{n}'}. \tag{2.67}$$

The operator $\Delta_{II'}$ has a complex index structure and is given in Appendix A.

The odd-j part of $H^{(3)}_{\text{eff}}$, like that of $H^{(2)}_{\text{eff}}$, is symmetric under the $U(N)$ doubling symmetry. The even-j part breaks $U(N)$ to $U(N_f)_L \times U(N_f)_R$. $H^{(3)}_{\text{eff}}$ is a baryon hopping term. As mentioned in the introduction, however, its simplicity is deceptive.

The separation of $H_{\text{eff}}^{(3)}$ into a canonical kinetic energy and an interaction term is a challenge for the future.

The baryon operators responsible for the hopping are composite operators that do not obey canonical anti-commutation relations. If this were not the case, then the effective Hamiltonian in third order would strongly resemble that of the t–J model of condensed matter physics [50],

$$H_{t-J} = -t \sum_{\substack{\langle ij \rangle \\ s}} c_{is}^{\dagger} c_{js} + J \sum_{\langle ij \rangle} \left(\boldsymbol{S}_i \cdot \boldsymbol{S}_j - \frac{n_i n_j}{4} \right) + \mathcal{J}'. \tag{2.68}$$

Here c_{js} is an annihilation operator for an electron at site j with spin s, and the number operators $n_i = c_i^{\dagger} c_i$ and spin operators $\boldsymbol{S}_i = \frac{1}{2} c_i^{\dagger} \boldsymbol{\sigma} c_i$ are constructed from it. The added term $\mathcal{J}'$ is a more complicated hopping and interaction term. The t–J model describes a doped antiferromagnet; it arises as the strong-binding limit of Hubbard model, a popular model for itinerant magnetism and possibly for high-T_c superconductivity. The model is not particularly tractable and, absent new theoretical developments, does not offer much hope for progress in our finite-density problem. It is nonetheless worth pondering the fact that a model connected, however tentatively, with superconductivity appears in a study of high-density nuclear matter.

A first step will be to replace these baryon operators with simpler operators that mimic only some of their features. Reintroducing all the properties of the real baryons can be done using methods of Hilbert space mapping (see for example [69]). These methods have been introduced in the context of atomic and nuclear physics to treat quantum fields that are composite operators and therefore do not obey canonical commutation relations. One adds to the physical, original Hilbert space an auxiliary Hilbert space that is occupied by canonical operators, that replace the composite (non-canonical) operators. The price for this replacement is mainly very complicated interactions between the composite operators (baryons in our case), that has up to six-dimension operators. One can simplify these interactions by solving a non-Hermitian effective Hamiltonian, whose spectrum can provide us with insight on the real spectrum only if its projection on the physical spectrum is clustered at low energies.

2.4 Summary

To conclude we gather the results of the previous sections and present the effective Hamiltonian derived from the strong coupling limit of lattice QCD. We restrict to the second order contribution to the effective Hamiltonian. At this order the *local* baryon number operator commutes with the Hamiltonian. As a result, the baryon number on each of the sites is fixed, and the Hamiltonian acting on the degenerate subspace of fluxless states takes a block diagonal form, in which each block corresponds to a certain distribution of baryon number on the lattice. This also means that the last term in Eq. (2.46) is just a constant and can be dropped. One must now diagonalize $H^{(2)}_{\rm eff}$ within each of the blocks, i.e., for a certain distribution of baryon number, and therefore a certain distribution of representations of the $Q_{\boldsymbol{n}}$ operators.

The effective Hamiltonian has the structure of an antiferromagnet with interactions that connect sites over j lattice links, with $j = 1, 2, 3, \ldots$. It has the following form (we drop a constant proportional to B').

$$H = \sum_{\substack{\boldsymbol{n}\mu,\eta \\ j=1,2,3,\ldots}} \left(s^\eta_\mu\right)^{j+1} J_j\, Q^\eta_{\boldsymbol{n}} Q^\eta_{\boldsymbol{n}+j\hat{\boldsymbol{\mu}}}. \tag{2.69}$$

Here $Q^\eta_{\boldsymbol{n}}$ are $U(N)$ charges at site $\boldsymbol{n}$, with $\eta = 1, \ldots, N^2$. This Hamiltonian moves mesonic excitations around the lattice, leaving the baryon density fixed. The states at $\boldsymbol{n}$ comprise a $U(N)$ representation whose Young tableau has N_c columns. The number of rows m depends on the baryon number B at $\boldsymbol{n}$ according to

$$m = B_{\boldsymbol{n}} + 2N_f. \tag{2.70}$$

The sign factors s^η_μ are given by

$$s^\eta_\mu = 2\,\mathrm{Tr}\, M^\eta \alpha_\mu M^\eta \alpha_\mu. \tag{2.71}$$

Here $M^\eta = \Gamma^A \otimes \lambda^i$, where Γ^A are the 16 Dirac matrices, and λ^i are the N_f^2 flavor generators. This makes M^η; $\eta = 1, \ldots, 16N_f^2$, the generators of $U(N)$ in the fundamental representation. We fix their normalization by, $\mathrm{Tr}\, M^\eta M^{\eta'} = \frac{1}{2}\delta_{\eta\eta'}$. The matrices α_μ are the 4×4 Dirac matrices times the unit matrix in flavor space.

In terms of the fermion kernel $D(j)$ the effective couplings J_j are

$$J_j = \frac{4|D(j)|^2}{g^2 C_F N_c \cdot j} = \frac{8|D(j)|^2}{g^2(N_c^2-1)\cdot j} > 0. \tag{2.72}$$

Recalling that we regard the strong coupling Hamiltonian as an effective Hamiltonian that describes QCD at large distances, then a physical fermion kernel must fall with j at least exponentially. In view of the symmetry structure of the even and odd terms in $H_{\rm eff}$ it is sufficient to take into account only nearest-neighbor and next-nearest-neighbor terms, and fix $D(j > 2) = 0$. The real values of the exchange coupling should be determined by the block-spin transformation discussed in Section 2.2.

Chapter 3

Mean field theory with Schwinger bosons

In this chapter we follow Arovas and Auerbach [45] and express the nearest-neighbor Hamiltonian derived in Chapter 2 in terms of Schwinger bosons[1]. We write the partition function as a path integral whose action is quartic in the bosons. Using a Hubbard-Stratonovich (HS) transformation, the interaction is decoupled, and the action becomes a quadratic form. After integrating the bosons we get an effective action for the HS fields. This action is proportional to the number $N = 4N_f$ of boson flavors, and can be approached in the large N limit. (To be precise the number N_c of colors is also large in this limit, and N_c/N is kept fixed.) We restrict to uniform and time-independent configurations of the HS fields, and replace the action by the mean field (MF) action S_{MF}. The latter depends on the MF values of the HS fields, and its minimization yields the ground state, which we analyze.

We first extend the analysis of [45] to three dimensions and show that at zero density and for large enough values of N_c/N the ground state spontaneously breaks the global $U(N)$ symmetry. The ordered phase is the Néel phase of the antiferromagnet and in terms of chiral symmetry respects only vector rotations.[2]

Next we examine how the MF approach changes when we insert a non-zero concentration c of baryons into the lattice. The baryons cannot move, and are represented by sites filled completely with baryon number. On such a site there is only one state, which is an $SU(N)$ singlet. This means that the generalized "spin" operators defined in Eq. (3.3) obey $Q^\eta = 0$, and that there are missing links in the nearest-neighbor antiferromagnetic Hamiltonian (2.69). Therefore the system becomes similar to an antiferromagnet with magnetic vacancies. We calculate the MF action to this system by two methods. For concentrations $c = \frac{1}{8}$ and $\frac{1}{4}$ we exactly minimize the MF action and see that the Néel phase shrinks as c increases. For other values of $c \ll 1$ we disorder the baryon background and use a quenched approximation [74].

---

[1] This paper is concerned with $SU(N)$ antiferromagnets, in order to understand the $SU(2)$ antiferromagnet. For more work in that context see [43, 44, 46, 47, 48, 49, 50].

[2] This is a subtle point, since the initial global symmetry $U(N)$ is much larger than chiral symmetry. We discuss this point in chapters 4 and 6.

3.1 Schwinger bosons

Our starting point is the effective nearest-neighbor Hamiltonian derived in Chapter 2,

$$H = \frac{\tilde{J}_1}{N} \sum_{\boldsymbol{n}} \sum_{\mu > 0} \vec{Q}_{\boldsymbol{n}} \cdot \vec{Q}_{\boldsymbol{n}+\hat{\boldsymbol{\mu}}}, \tag{3.1}$$

with $\tilde{J}_1/N = J_1$ from Chapter 2. For brevity we drop the tilde sign in the rest of the chapter. The operators Q^η generate the $U(N)$ algebra

$$[Q^\eta_{\boldsymbol{n}}, Q^\rho_{\boldsymbol{m}}] = i f^{\eta\rho\sigma} Q^\sigma_{\boldsymbol{n}} \delta_{\boldsymbol{nm}}, \tag{3.2}$$

and are defined as

$$Q^\eta_{\boldsymbol{n}} = \sum_{\alpha\beta, a} \psi^{\dagger a\alpha}_{\boldsymbol{n}} M^\eta_{\alpha\beta} \psi^{a\beta}_{\boldsymbol{n}}. \tag{3.3}$$

Here α and β are Dirac-flavor indices that range from 1 to N, while a is a color index that ranges from 1 to N_c. The matrices M^η are the generators of $U(N)$ in the fundamental representation. The Hilbert space on site $\boldsymbol{n}$, occupied by B baryons, is an irreducible representation of $U(N)$ that corresponds to a rectangular Young tableau of the form of Fig. 2.4. It has N_c columns, and its number of rows m obeys $m = B + N/2$. Following [45, 46] we first restrict to configurations with zero average baryon number. In particular we examine configurations with baryon number B on the even sites and $-B$ on the odd sites. This means we put conjugate $U(N)$ representations on adjacent sites, represented by Young tableaux with m rows on the even sites, and with $(N - m)$ on the odd sites. The case of exactly zero baryon number on each site is the case of $m = N/2$.

We now show how to construct the Hilbert spaces using bosons. On an even site $\boldsymbol{n}$, we define a boson operator $b_{\alpha p, \boldsymbol{n}}$. α is again a Dirac-flavor index that ranges from 1 to N, but the index p is now an auxiliary "color" index that ranges from 1 to m. The bosons belong to the fundamental representations of both $SU(N)$ and $SU(m)$, and obey

$$\left[b_{\alpha p\boldsymbol{n}}, b^{\dagger}_{\beta q\boldsymbol{m}}\right] = \delta_{\alpha\beta}\delta_{pq}\delta_{\boldsymbol{nm}}. \tag{3.4}$$

The Hilbert space on this site is constructed by mN_c applications of the operators $b^{\dagger}_{\boldsymbol{n}}$ on the no-quantum state $|0\rangle$

$$|\alpha\beta\cdots;pq\cdots\rangle \sim b^{\dagger}_{\alpha p,\boldsymbol{n}}b^{\dagger}_{\beta q,\boldsymbol{n}}\cdots|0\rangle. \tag{3.5}$$

We denote the $SU(N)$ representation of the Dirac-flavor indices $(\alpha, \beta, \ldots)$ as $\underline{\mathrm{r}}$, and the $SU(m)$ representation of the color indices $(p, q, \ldots)$ as $\underline{\mathrm{r}}'$. This means that the state (3.5) belongs to a representation $\underline{\mathrm{r}}'' \in \underline{\mathrm{r}} \times \underline{\mathrm{r}}'$ of the permutation group S_{mN_c}. In particular, since the state $|\alpha\beta\cdots;pq\cdots\rangle$ is created with bosons, $\underline{\mathrm{r}}''$ is the completely symmetric representation of S_{mN_c}. This means that $\underline{\mathrm{r}}'$ must obey $\underline{\mathrm{r}} = \underline{\mathrm{r}}'$. As a result we find that in order to constraint the $SU(N)$ indices of Eq. (3.5) to belong to Fig. 2.4, it suffices to restrict its $SU(m)$ indices to a representation with the same tableau. This is easy. Because Fig. 2.4 has m rows, it is a singlet of $SU(m)$, so any state $|\Omega\rangle$ must obey

$$\sum_{\alpha=1}^{N} b^{\dagger}_{\alpha p,\boldsymbol{n}}b_{\alpha q,\boldsymbol{n}}|\Omega\rangle = N_c\delta_{pq}|\Omega\rangle. \tag{3.6}$$

On the odd sites we choose the bosons to be in the conjugate-to-fundamental representations of $SU(N)$ and $SU(m)$, and consider them as hole operators. The commutation relations (3.4) are the same, and so is the restriction (3.6), which is now interpreted as counting the number of holes created by applying the hole operators $b^{\dagger}$ to the filled singlet state with N rows in its Young tableaux.

In term of the bosons, the operators $Q^{\eta}_{\boldsymbol{n}}$ are given by

$$Q^{\eta}_{\boldsymbol{n}} = \begin{cases} b^{\dagger}_{\boldsymbol{n}} \cdot M^{\eta} \cdot b_{\boldsymbol{n}} & \boldsymbol{n} \in \text{even}, \\ b^{\dagger}_{\boldsymbol{n}} \cdot (-M^{\eta})^{*} \cdot b_{\boldsymbol{n}} & \boldsymbol{n} \in \text{odd}. \end{cases} \tag{3.7}$$

Here we have suppressed all indices. The difference between the even and odd definitions of $Q^{\eta}_{\boldsymbol{n}}$ above is inserted in order that on both sublattices the operators $Q^{\eta}_{\boldsymbol{n}}$ belong to the adjoint representation of $SU(N)$; the fact that b transforms in the fundamental representation on the even sites and in the conjugate-to-fundamental representation on the odd sites is compensated by the fact that while M^{η} generates the fundamental, $-M^{\eta *}$

generates its conjugate. Using these definitions, the Hamiltonian becomes the following normal ordered quartic form,

$$\begin{aligned} H &= -\frac{J_1}{2N}\sum_{\boldsymbol{n}\mu}\mathrm{Tr}\left[\mathcal{A}^{\dagger}_{\boldsymbol{n}\hat{\boldsymbol{\mu}}}\mathcal{A}_{\boldsymbol{n}\hat{\boldsymbol{\mu}}}\right], && (3.8)\\ \left(\mathcal{A}_{\boldsymbol{n}\hat{\boldsymbol{\mu}}}\right)_{pq} &\equiv \sum_{\alpha=1}^{N} b_{\alpha p,\boldsymbol{n}} b_{\alpha q,\boldsymbol{n}+\hat{\boldsymbol{\mu}}}. && (3.9)\end{aligned}$$

Here we have used the hermiticity of M^{η} and the relation

$$\sum_{\eta} M^{\eta}_{\alpha\beta} M^{\eta}_{\alpha'\beta'} = \frac{1}{2}\delta_{\alpha\beta'}\delta_{\beta\alpha'}. \tag{3.10}$$

We now introduce bosonic coherent states (see for example [50]). This enables us to write the partition function as a path integral.

For each bosonic operator b (we suppress all site, Dirac-flavor and color indices), one defines the bosonic coherent state $|z\rangle$ as

$$|z\rangle = e^{z b^{\dagger}}|0\rangle. \tag{3.11}$$

Here $|0\rangle$ is the state annihilated by b, and z is a complex number. This state obeys

$$\begin{aligned} b|z\rangle &= z|z\rangle, && (3.12)\\ \langle z_1|z_2\rangle &= e^{z_1^* z_2}, && (3.13)\\ \mathbf{1} &= \int d^2 z\, e^{-|z|^2}|z\rangle\langle z|, && (3.14)\\ \mathrm{Tr}\left(\hat{O}\right) &= \int d^2 z\, e^{-|z|^2}\langle z|\hat{O}|z\rangle. && (3.15)\end{aligned}$$

Here $\hat{O}$ is an operator that depends on b and $b^{\dagger}$. We use Eq. (3.15) to write the partition function

$$Z = \mathrm{Tr}\,' e^{-\beta H}, \tag{3.16}$$

where $\beta = 1/T$, as

$$Z = \int' d^2 z_0\, \langle z_0|e^{-\beta H}|z_0\rangle\, e^{-|z_0|^2}. \tag{3.17}$$

Here the trace in Eq. (3.16) and integral of Eq. (3.17) are constrained to contain bosonic states that obey Eq. (3.6) only.

Next, we regard the inverse temperature β as Euclidean time and slice it N_τ times,

$$\langle z_0|e^{-\beta H}|z_0\rangle = \langle z_0|e^{-\epsilon H}e^{-\epsilon H}e^{-\epsilon H}\cdots e^{-\epsilon H}|z_0\rangle. \tag{3.18}$$

Here $\epsilon = \beta/N_\tau$ and is small enough to write

$$e^{-\epsilon H} = (1-\epsilon H)\,. \tag{3.19}$$

Inserting the unity (3.14) in between each of the $1-\epsilon H$ factors in Eq. (3.18) we have

$$Z = \prod_{\tau=0}^{N_\tau-1}\int d^2 z_\tau e^{-z^*_\tau z_\tau}\langle z_\tau|1-\epsilon H|z_{\tau+1}\rangle, \tag{3.20}$$

where $z_{N_\tau} = z_0$. Each of the unities inserted is denoted by a different Euclidean time index $\tau = 0,\ldots,N_\tau-1$, hence the notations. Next we evaluate the matrix elements of Eq. (3.19) to $O(\epsilon)$ using Eqs. (3.12)–(3.13). The result is

$$\langle z_\tau|1-\epsilon H|z_{\tau+1}\rangle = e^{z^*_\tau z_{\tau+1}-\epsilon H(z^*_\tau,z_{\tau+1})}. \tag{3.21}$$

Here $H(z^*_\tau, z_{\tau+1})$ is given by replacing all $b^\dagger$ with z^* and all b with z in the quantum Hamiltonian. This procedure gives in the following path integral.

$$\begin{aligned}
Z &= \int_{z_0=z_{N_\tau}} DzDz^*\, e^{-S}\prod_{\boldsymbol{n}pq}\delta\left(\sum_\alpha z^*_{\alpha p,\boldsymbol{n}}z_{\alpha q,\boldsymbol{n}} - N_c\delta_{pq}\right), && (3.22)\\
S &= \epsilon\sum_{\tau=1}^{N_\tau-1} -z^*_\tau\partial_\tau z_\tau + H(z^*_\tau, z_\tau), && (3.23)\\
H &= -\frac{J_1}{2N}\sum_{\boldsymbol{n}\mu}\mathrm{Tr}\left[\mathcal{A}^\dagger_{\boldsymbol{n}\mu}(\tau)\mathcal{A}_{\boldsymbol{n}\mu}(\tau)\right], && (3.24)\\
\left(\mathcal{A}_{\boldsymbol{n}\mu}(\tau)\right)_{pq} &= \sum_{\alpha=1}^{N} z_{\alpha p,\boldsymbol{n}}z_{\alpha q,\boldsymbol{n}+\hat{\boldsymbol{\mu}}}. && (3.25)
\end{aligned}$$

Here one assumes smooth Euclidean time configurations of the fields, and we have suppressed site, Dirac-flavor and color indices in the first term of Eq. (3.23). A note is needed regarding the definition of the temporal derivative of Eq. (3.23). To be unambiguous we write

$$\epsilon\,\partial_\tau f(\tau) \equiv f_{\tau+1} - f_\tau. \tag{3.26}$$

In appendix B we show that ignoring this slicing procedure, and taking the continuum limit of the derivative, leads to slightly different results for energies. The difference is usually ignored, but in our context it remains important.

Finally let us note the δ function in Eq. (3.22). This constrains the boson fields and keeps the Hilbert space explored by the path integration within the quantum constraint (3.6).

3.2 Hubbard-Stratonovich transformation

We proceed to implement a Hubbard-Stratonovich (HS) transformation to decouple the quartic interaction Eq. (3.23) into quadratic forms. We use the identity

$$\int DQDQ^\dagger \, \exp\left(-\mathrm{Tr}\int_0^\beta d\tau \, (Q_{\boldsymbol{n}\mu} - (J_1/2N)\mathcal{A}_{\boldsymbol{n}\mu})^\dagger \, \frac{2N}{J_1} \, (Q_{\boldsymbol{n}\mu} - (J_1/2N)\mathcal{A}_{\boldsymbol{n}\mu})\right) = 1, \tag{3.27}$$

where we suppress all auxiliary color indices, and symbolically write the temporal sums as an integration over the variable τ. The HS fields $Q^{pq}_{\boldsymbol{n}\mu}$ are complex matrices in the color indices p and q, and live on links of the lattice. Eq. (3.27) leads to

$$\begin{aligned}\exp\left(\frac{J_1}{2N}\mathrm{Tr}\int d\tau \, \mathcal{A}^\dagger_{\boldsymbol{n}\mu}(\tau)\mathcal{A}_{\boldsymbol{n}\mu}(\tau)\right) &= \int DQDQ^\dagger \exp\left[\mathrm{Tr}\left(-\frac{2N}{J_1}Q^\dagger_{\boldsymbol{n}\mu}Q_{\boldsymbol{n}\mu}\right.\right. \\ &\qquad \left.\left. + Q^\dagger_{\boldsymbol{n}\mu}\mathcal{A}_{\boldsymbol{n}\mu} + \mathcal{A}^\dagger_{\boldsymbol{n}\mu}Q_{\boldsymbol{n}\mu}\right)\right].\end{aligned} \tag{3.28}$$

We also write the constraint in Eq. (3.22) as

$$\int D\lambda \exp\left[i\sum_{pq}\lambda^{pq}_{\boldsymbol{n}}(\tau)\left(\sum_\alpha z^*_{\alpha p,\boldsymbol{n}} z_{\alpha q,\boldsymbol{n}} - N_c\delta_{pq}\right)\right], \tag{3.29}$$

where $\lambda^{pq}_{\boldsymbol{n}}(\tau)$ is a real valued matrix field. Using Eq. (3.28) and Eq. (3.29) the partition function becomes

$$Z = \int DzDz^* DQDQ^\dagger D\lambda \, e^{-S}, \tag{3.30}$$

$$\begin{aligned} S &= \int d\tau \, \mathrm{Tr}\left\{\sum_{\boldsymbol{n}\mu}\frac{2N}{J_1}Q^\dagger_{\boldsymbol{n}\mu}Q_{\boldsymbol{n}\mu} + i\sum_{\boldsymbol{n}} N_c\lambda_{\boldsymbol{n}} - \sum_{\boldsymbol{n}} z^\dagger_{\boldsymbol{n}}\left[\partial_\tau + i\lambda_{\boldsymbol{n}}\right] z_{\boldsymbol{n}}\right. \\ &\qquad \left. - \sum_{\boldsymbol{n}\mu}\left[Q^\dagger_{\boldsymbol{n}\mu}\mathcal{A}_{\boldsymbol{n}\mu} + \mathcal{A}^\dagger_{\boldsymbol{n}\mu}Q_{\boldsymbol{n}\mu}\right]\right\}.\end{aligned} \tag{3.31}$$

The action is now quadratic in the bosons, and they can be integrated. This gives the following effective action for the Q and λ.

$$S = N\int d\tau \, \mathrm{Tr}\left\{\sum_{\boldsymbol{n}\mu}\frac{2}{J_1}Q^\dagger_{\boldsymbol{n}\mu}Q_{\boldsymbol{n}\mu} + i\sum_{\boldsymbol{n}}\kappa\lambda_{\boldsymbol{n}} + \log G^{-1}\right\}. \tag{3.32}$$

Here G^{-1} is the propagator of a *single* boson in the presence of Q and λ, while the general propagator is proportional to unity in the Dirac-flavor indices. Therefore the boson integration gives an overall factor of N, and $\log G^{-1}$ is of $O(1)$. Also note that we have introduced $\kappa \equiv N_c/N$. [3] This will be useful in the following sections when we take the large N limit and keep κ fixed.

Let us make a final remark on the HS transformation. This exact transformation is based on Eq. (3.27), which is always true for $J_1 > 0$. As a result we see that we can perform a HS transformation only if the interaction term in Eq. (3.23) can be written in the form (3.8). The latter was received with the aid of Eq. (3.7), which is true only for the special baryon number configuration of conjugate representations on adjacent sites (that has zero total baryon number). There are two additional simple cases in which one can write the magnetic interaction in the form of Eq. (3.8) [45]. The first is the ferromagnet with identical representations on all sites, and the second is the antiferromagnet, written with *fermions* and zero baryon number on all the sites. The HS transformation for the fermions was examined in the large N limit by many authors (for example [46]), and seems to lead to a disordered phase. This limit is of no interest to us, since we expect that at zero density, our Hamiltonian describes an ordered phase with spontaneously broken chiral symmetry.

Antiferromagnetic interactions for other baryon distributions can also be written in the form of Eq. (3.8). The key point is that for each link one must have a representation of the generators analogous to Eq. (3.7). This however makes calculations more difficult. For example let us take uniform baryon density, with the same baryon number B on all sites. This distribution is realized by having the same $U(N)$ representations on all sites, and therefore the same number of rows m in the Young tableaux of all sites. We now build the Hilbert space on even and odd sites differently, making the boson operators on the even and odd sites belong to the fundamental and conjugate-to-fundemental representation of $SU(m)$ and $SU(N-m)$ respectively. This choice of bosons indeed leads to a relation similar to Eq. (3.7). This means that while the bosons on the even sites have an auxiliary color index p that takes values in $[1, m]$, the auxiliary color index q on the odd sites will take values in $[1, N-m]$. The bosons on the two sublattices are of a different kind and calculations become more difficult. For example, the HS field will now be rectangular matrices with m rows and $N-m$ columns.

---

[3] κ is equal to $r/4$, where r is the ratio N_c/N_f mentioned in Chapter 1, and in the abstract and summary of the thesis.

3.3 Mean field theory at zero density

Taking the large N limit with κ fixed allows a stationary approximation for the path integral. We therefore proceed to work with the following ansatz,

$$Q^{pq}_{\boldsymbol{n}\mu}(\tau) = Q\,\delta^{pq}, \tag{3.33}$$

$$\lambda^{pq}_{\boldsymbol{n}}(\tau) = i\lambda\,\delta^{pq}, \tag{3.34}$$

where we take Q and λ to be real. Using this ansatz we find that the MF action S_{MF} defined by

$$S_{\mathrm{MF}} = (Nm\beta N_s)^{-1}\log Z_{\mathrm{MF}}, \tag{3.35}$$

becomes

$$S_{\mathrm{MF}}(Q,\lambda) = \frac{2dQ^2}{J_1} - \kappa\lambda + \frac{1}{\beta N_s}\mathrm{Tr}\,\log G^{-1}(Q,\lambda). \tag{3.36}$$

To evaluate the last term, we perform the integration over the bosons with the constraint and HS fields replaced by their MF values. (Here we have a single flavor and "color" field.)

$$\det G(Q,\lambda) = \int DzDz^\dagger \exp\left\{\int d\tau \sum_{\boldsymbol{n}}\left[z^*_{\boldsymbol{n}}\left(\partial_\tau - \lambda\right)z_{\boldsymbol{n}} + Q\sum_{\mu=1}^{d}\left(z_{\boldsymbol{n}}z_{\boldsymbol{n}+\hat{\boldsymbol{\mu}}} + z^*_{\boldsymbol{n}}z^*_{\boldsymbol{n}+\hat{\boldsymbol{\mu}}}\right)\right]\right\}. \tag{3.37}$$

We redefine the bosons on the even and odd sites as $z^{e,o}_{\boldsymbol{N}}$, where $\boldsymbol{N}$ is an index denoting sites on the even sublattice, which is an fcc. We now have two degrees of freedom on each site of the fcc. The first is the original boson z^e on $\boldsymbol{N}$, and we use the convention that the second is the boson residing on the odd site $\boldsymbol{N}+\hat{z}/2$, one link above the even site occupied by $z^e_{\boldsymbol{N}}$.[4] We now apply the Fourier transform,

$$z^a_{\boldsymbol{N}}(\tau) = \sqrt{\frac{2}{N_s\beta}}\sum_{\boldsymbol{k},n} z_{\boldsymbol{k},n}e^{i(\boldsymbol{k}\cdot\boldsymbol{N}-\omega_n\tau)} \times \left\{\begin{array}{ll} 1 & a=e \\ e^{-ik_z/2} & a=o \end{array}\right., \tag{3.38}$$

where $\omega_n = 2\pi n/T$ are Matsubara frequencies, and $\boldsymbol{k}$ belongs to the first Brillouin zone of an fcc (i.e. to the unit cell of a bcc lattice.) In momentum space the inverse propagator is

$$G^{-1}_{\boldsymbol{k}}(\omega_n) = \begin{pmatrix} \lambda + i\omega_n & -2dQ\gamma_{\boldsymbol{k}} \\ -2dQ\gamma_{\boldsymbol{k}} & \lambda - i\omega_n \end{pmatrix}, \tag{3.39}$$

---

[4] We use the convention that the lattice spacing of the fcc lattice is 1.

with the 2×2 internal space defined by

$$f_{\boldsymbol{k},n} \equiv \left(\begin{array}{c} z^{a}_{\boldsymbol{k},n} \\ \\ z^{*o}_{-\boldsymbol{k},-n} \end{array} \right), \tag{3.40}$$

and $\gamma_{\boldsymbol{k}} = \frac{1}{d}\sum_{\mu=1}^{d}\cos(k_\mu/2)$. The spectrum of this mean field theory is given by the poles of the propagator,

$$\omega_n^2 + \lambda^2 - 4d^2Q^2\gamma_{\boldsymbol{k}}^2 = 0. \tag{3.41}$$

Near $\boldsymbol{k} = 0$, the energy described in Eq. (3.41) is $E_{\boldsymbol{k}}^2 = \Delta^2 + c^2\boldsymbol{k}^2$, with the squared mass $\Delta^2 = \lambda^2 - 4d^2Q^2$, and the velocity $c^2 = dQ^2$. This spectrum becomes massless for $\lambda^2 = 4d^2Q^2$. Evaluating the determinant of G we get

$$S_{\text{MF}} = \frac{2dQ^2}{J_1} - \lambda\left(\kappa + \frac{1}{2}\right) + \frac{2}{N_s\beta}\sum_{\boldsymbol{k}}\log 2\sinh\left(\frac{\beta\omega_{\boldsymbol{k}}}{2}\right). \tag{3.42}$$

Here $\omega_{\boldsymbol{k}} = \sqrt{\lambda^2 - 4d^2Q^2\gamma_{\boldsymbol{k}}^2}$, and λ is assumed to be positive. Note that the transition from Eq. (3.36) and Eq. (3.39) to Eq. (3.42) included performing a Matsubara sum. We stress that a naive summation will *not* lead to the $+\frac{1}{2}$ in the second term of Eq. (3.42). This factor is received only by performing the determinant of the inverse propagator exactly, with the correct discretization of Euclidean time given in Eq. (3.21). We give a detailed explanation in Appendix B, where we derive the following rule of thumb for evaluations of a two-sublattice determinants of the form (3.37): Evaluate the determinant "naively" by replacing the partial derivative ∂_τ with its simple continuum form $-i\omega_n$, and multiply the result by a factor of $e^{\beta\lambda/2}$ for each degree of freedom. For example, in the case considered, the number of degrees of freedom is NmN_s, hence the factor $\frac{1}{2}$ in Eq. (3.42).

We proceed to write the mean field equations for the action (3.42),[5]

$$\frac{\partial S_{\text{MF}}}{\partial\lambda} = \frac{\partial S_{\text{MF}}}{\partial Q} = 0, \tag{3.43}$$

that become

$$\frac{Q}{2dJ_1} = \frac{2}{N_s}\sum_{\boldsymbol{k}}\frac{Q\gamma_{\boldsymbol{k}}^2}{\omega_{\boldsymbol{k}}}\left(n(\omega_{\boldsymbol{k}}) + \frac{1}{2}\right), \tag{3.44}$$

$$\kappa + \frac{1}{2} = \frac{2}{N_s}\sum_{\boldsymbol{k}}\frac{\lambda}{\omega_{\boldsymbol{k}}}\left(n(\omega_{\boldsymbol{k}}) + \frac{1}{2}\right). \tag{3.45}$$

---

[5] Note that in principle one should also check whether the point $(Q_{\text{MF}}, \lambda_{\text{MF}})$ is a minimum. If it is not, however, one can take some of the variables (in this case Q or λ) to be imaginary, and make all curvatures positive. This is actually the reason for the ansatz (3.34)

Here $n(\omega)$ is the Bose function $(e^{\beta\omega}-1)^{-1}$. From this point on we restrict to $T=0$. The first solution (solution A) to Eqs. (3.44)–(3.45) is

$$\begin{aligned} Q_A &= 0, && (3.46)\\ \lambda_A &= \frac{2}{\beta}\coth^{-1}(2\kappa+1). && (3.47)\end{aligned}$$

This gives $Q_A=\lambda_A=0$ at $T=0$, and a value of $S_{\rm MF}=-\beta^{-1}\log\frac{(\kappa+1)^{\kappa+1}}{\kappa^{\kappa}}\to 0^-$.

The second solution has $Q\neq 0$ and Eq. (3.45) becomes

$$\begin{aligned} \kappa &= f(\eta)+\frac{n(\Delta)}{N_s/2}\frac{\lambda}{\Delta}, && (3.48)\\ f(\eta) &= \int d\gamma\, D(\gamma)\,\frac{1}{2}\left[\frac{1}{\sqrt{1-\eta^2\gamma^2}}-1\right], && (3.49)\end{aligned}$$

with $\eta\equiv\lambda/(2dQ)$. Here the momentum integration was replaced by an integration over the function $\gamma_{\boldsymbol{k}}$, provided with a integration measure $D(\gamma)$ given in Fig. 3.1, normalized to $\int d\gamma D(\gamma)=1$.

Note that we have separated the $\boldsymbol{k}=0$ $(\gamma=1)$ mode from the others, to allow a Bose-Einstein condensate (BEC). The second term in Eq. (3.48) will be non-zero at the thermodynamic limit only if $n(\Delta)/\sqrt{1-\eta^2}\sim O(N_s)$, which in turn means that $\eta\to 1$. Note that since $\gamma^2\leq 1$, the range of η is $[0,1]$. The function $f(\eta)$ is given in Fig. 3.2. It is monotonically increasing, and at $\eta=1$ takes the following values:

$$f(1)=\left[\begin{array}{ll}\infty & d=1,\\ 0.19 & d=2,\\ 0.0787 & d=3.\end{array}\right. \qquad (3.50)$$

We divide the solution of Eq. (3.48) into two cases.

Disordered phase (solution B)

Here one assumes that $\Delta\neq 0$ at the thermodynamic limit and drops the second term in the right hand side of Eq. (3.48). The solution then reduces to

$$\begin{aligned} \kappa &= f(\eta_B), && (3.51)\\ \lambda_B/dJ_1 &= \int d\gamma\, D(\gamma)\,\frac{\gamma^2}{\sqrt{1-\eta^2\gamma^2}}, && (3.52)\\ Q_B &= \eta_B\lambda_B/2d. && (3.53)\end{aligned}$$

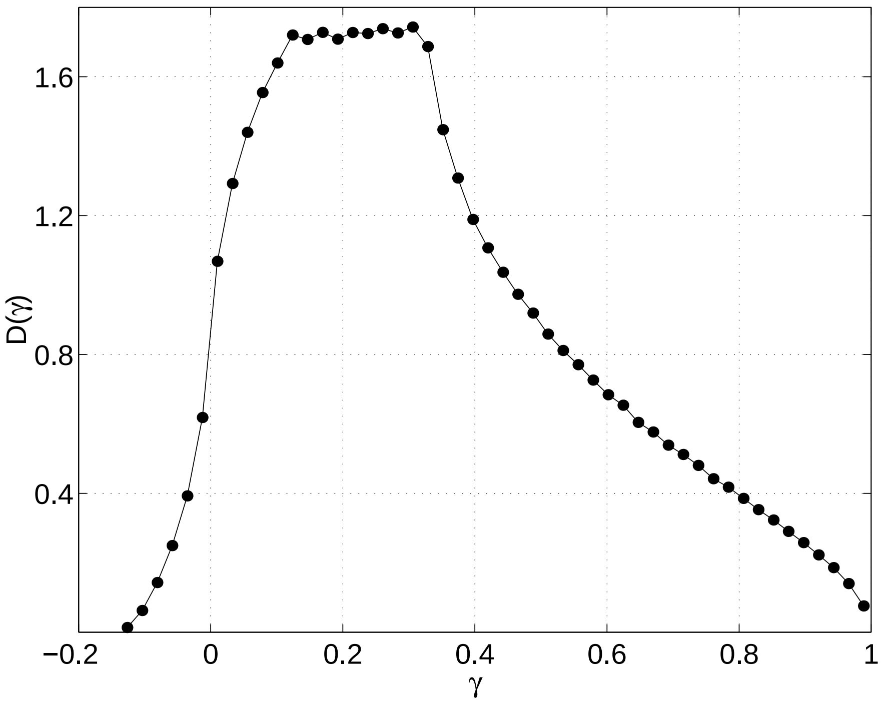

Figure 3.1: The integration measure of γ for $d = 3$.

This solution is guaranteed as long as $\kappa \leq f(1)$. Recalling Eq. (3.50), this solution exists always for $d = 1$, but only for $\kappa \leq \kappa_c$, with $\kappa_c \simeq 0.19$ for $d = 2$, and $\kappa_c \simeq 0.0787$ for $d = 3$. The MF action of this solution is $-4dQ_B^2/J_1 < 0$.

Ordered phase (solution C)

For $\kappa > \kappa_c$, Eq. (3.48) cannot be solved without the extra condensation term. A consistent solution will be

$$\lambda_C = \lambda_B(1) + dJ_1(\kappa - \kappa_c), \tag{3.54}$$

$$Q_C = \lambda_C/2d, \tag{3.55}$$

$$\eta_C = \sqrt{1 - \frac{T}{N_s \lambda_C(\kappa - \kappa_c)}} \simeq 1. \tag{3.56}$$

Here $\lambda_B(1)$ means the value of Eq. (3.52) at $\eta = 1$. The action of this solution is $-4dQ_C^2/J_1$, so solutions B and C have lower action than solution A, and are continu-

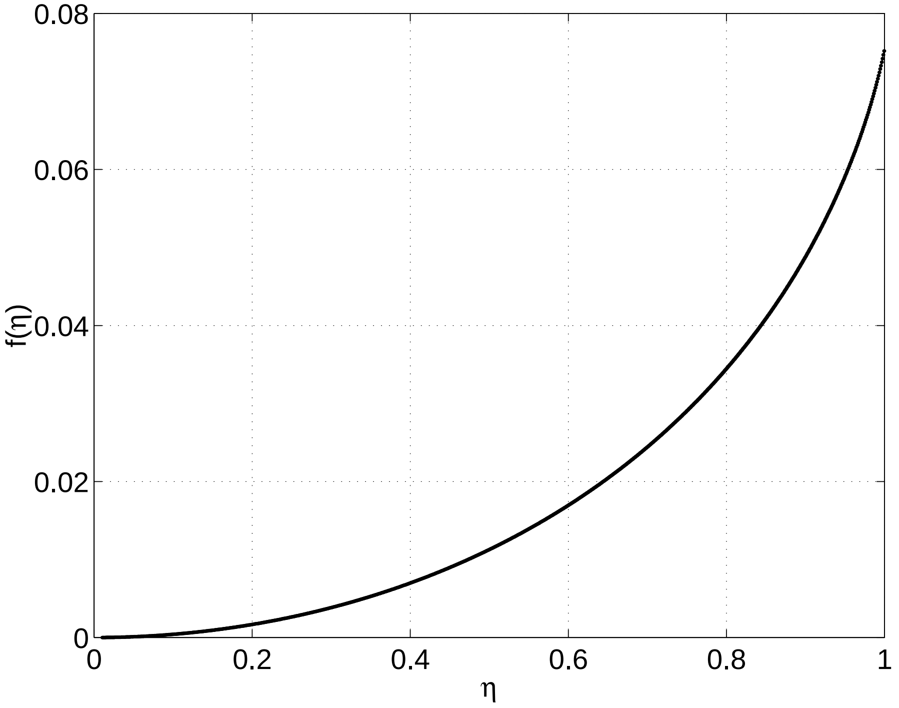

Figure 3.2: The right hand side of Eq. (3.48) excluding the condensation term for $d = 3$.

ous at $\kappa = \kappa_c$. Nevertheless, the derivative of the mass Δ at $\kappa = \kappa_c$ is not continuous. Recalling that $\kappa \equiv N_c/4N_f$, one finds that for $d = 3$, and at $T = 0$ there is a Néel phase for $\frac{N_c}{N_f} > 0.31$. This means that for $N_c = 3$, and $N_f \leq 9.6$ the $U(4N_f)$ is spontaneously broken (for calculations of the staggered magnetization that show that the BEC indeed corresponds to a Néel phase [45, 50]).

We summarize the zero density problem in the schematic phase diagram in plane N_c–N_f in Fig. 3.3, borrowed from [45]. The large-N_f phase is disordered, and will not concern us. The location of the phase boundary is a line of constant slope, which turns out to be the line $N_c/N_f = 0.31$; this means that QCD is safely in the *ordered* phase for any reasonable number of flavors.

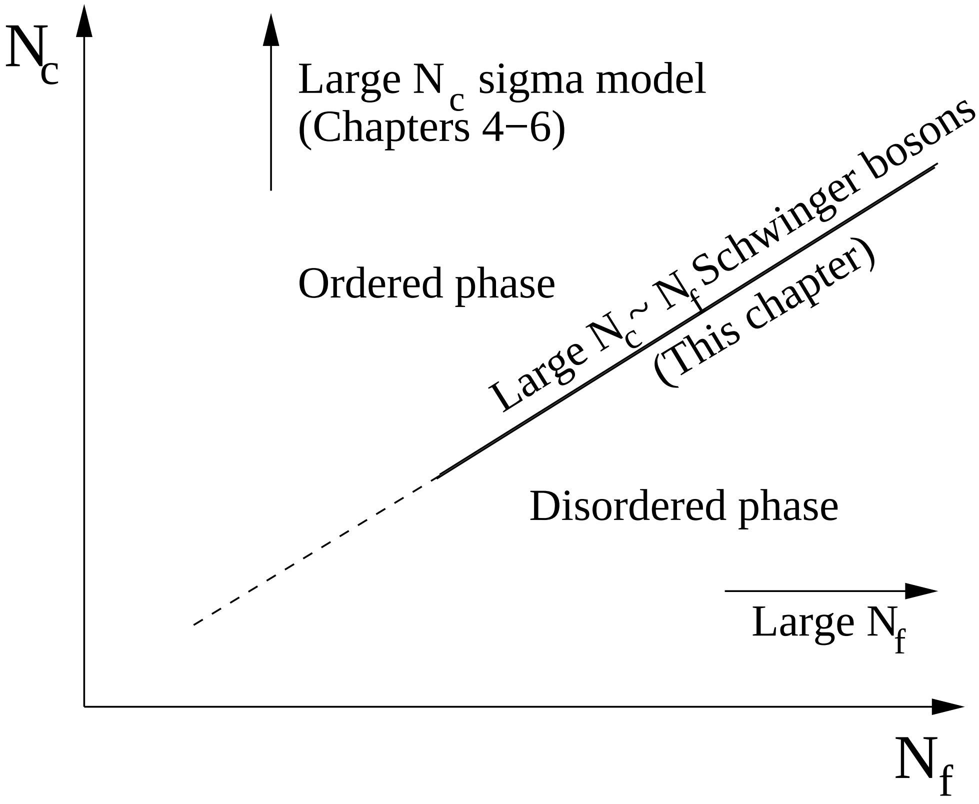

Figure 3.3: Phase diagram for the nearest-neighbor antiferromagnet at $T = 0$, and zero density in N_c–N_f plane, for MF theory with Schwinger bosons.

3.4 Mean field theory at non-zero density

In this section we investigate how a non-zero density of baryons influences the MF equations and changes the boundary of the Néel phase in the N_c–N_f plane. The MF approach discussed above can be used to investigate the following configuration of non-zero baryon number. On M of the N_s lattice sites we replace the $U(N)$ representations with the singlet of $SU(N)$, that has $B = 2N_f$. This means that the $Q^{\eta}_{\boldsymbol{n}}$ operators in these sites are zero (except Q^0 which corresponds to baryon number). The density ρ of these configurations is $\rho = mc$, where

$$c = \frac{M}{N_s}, \tag{3.57}$$

is the concentration of the singlet representations. In the presence of the "impurities", the effective Hamiltonian (3.1) suffers from a set of missing links and becomes

$$H = \frac{J_1}{2N} \sum_{\boldsymbol{n},\boldsymbol{n}+\hat{\boldsymbol{\mu}} \notin \{\boldsymbol{r}\}} \vec{Q}_{\boldsymbol{n}} \vec{Q}_{\boldsymbol{n}+\hat{\boldsymbol{\mu}}}. \tag{3.58}$$

$\{\boldsymbol{r}\}$ denotes the locations of the M impurities. We again make the MF ansatz (3.33)–(3.34) and turn to calculate the MF action and MF equations. First note that cN_s sites do not participate in the Hamiltonian. Also if there are no neighboring impurities, then there are $2c\,dN_s$ missing links. This means that the first two terms in Eq. (3.36) are now multiplied by $(1-c)$ and $(1-2c)$.

$$\begin{aligned} Q^2 &\rightarrow (1-c)\,Q^2, \\ \kappa\lambda &\rightarrow (1-2c)\,\kappa\lambda. \end{aligned} \tag{3.59}$$

Also, the evaluation of the functional determinant is different. We have analyzed this problem using two techniques. The first is an analysis of certain configurations of impurities, in which the system does not lose translation invariance. We solve only the simplest cases of $c = \frac{1}{8}, \frac{1}{4}$ in section 3.4.1. In section 3.4.2 we make a quenched average of the impurities' positions which restores translation invariance. In this method we find that the corrections to the MF action for low values of c can be written as a power series in c, and we the present results of the first order.

3.4.1 Periodic density with baryon concentration $c = \frac{1}{8}, \frac{1}{4}$

In general a random distribution of baryon impurities destroys translation invariance found at zero baryon number, and makes the methods used in the previous section inapplicable. In particular, a Fourier transform does not diagonalize the propagator of the bosons, making the evaluation of the determinant very difficult. There are however densities that can be realized with a translation invariant configuration of impurities. In three dimensions the simplest configurations have $c = \frac{1}{8}$, and $c = \frac{1}{4}$. In this section we calculate the MF action of these configurations, and proceed to solve the corresponding MF equations.

Concentration $c = \frac{1}{8}$

We divide the lattice into unit cells of the form shown in Fig. 3.4. Each includes seven

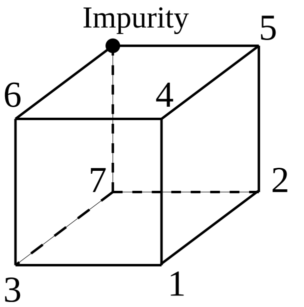

Figure 3.4: A unit cell for impurity concentration of $c = \frac{1}{8}$.

ordinary sites and one impurity. We place the latter on the upper-left-back corner of the cell, and denote the bosons on the other sites by $z_{\boldsymbol{n},\rho}$. Here $\boldsymbol{n}$ is the location of the cell in a simple cubic lattice of spacing 2. The index $\rho = 1, \ldots, 7$, is an internal index denoting the sites in each cell, corresponding to the numbering in Fig. 3.4. Using these notations, the MF action is

$$\begin{aligned} S_{\mathrm{MF}} &= \frac{9Q^2}{2J_1} - \frac{7}{8}\lambda\kappa + \frac{1}{N_s\beta}\mathrm{Tr}\,\log G^{-1}, && (3.60)\\ \det G &= \int DzDz^* \exp\left[-\int d\tau \sum_{\boldsymbol{n}\rho} z^*_{\boldsymbol{n}\rho}\left(-\partial_\tau + \lambda\right) z_{\boldsymbol{n}\rho} - S'(Q)\right], && (3.61)\\ S'(Q) &= -Q\int d\tau \sum_{\boldsymbol{n}} [z_{\boldsymbol{n},2}(z_{\boldsymbol{n},1} + z_{\boldsymbol{n}-\hat{x},1}) + z_{\boldsymbol{n},3}(z_{\boldsymbol{n},1} + z_{\boldsymbol{n}-\hat{y},1}) \\ &\quad + z_{\boldsymbol{n},4}(z_{\boldsymbol{n},1} + z_{\boldsymbol{n}-\hat{z},1}) + z_{\boldsymbol{n},5}(z_{\boldsymbol{n},2} + z_{\boldsymbol{n}-\hat{z},2}) \\ &\quad + z_{\boldsymbol{n},6}(z_{\boldsymbol{n},3} + z_{\boldsymbol{n}-\hat{z},3}) + z_{\boldsymbol{n},7}(z_{\boldsymbol{n},2} + z_{\boldsymbol{n}-\hat{y},2}) \\ &\quad + z_{\boldsymbol{n},7}(z_{\boldsymbol{n},3} + z_{\boldsymbol{n}-\hat{x},3}) + z_{\boldsymbol{n},5}(z_{\boldsymbol{n},4} + z_{\boldsymbol{n}-\hat{x},4}) \\ &\quad + z_{\boldsymbol{n},6}(z_{\boldsymbol{n},4} + z_{\boldsymbol{n}-\hat{y},4})] + c.c. && (3.62) \end{aligned}$$

Next we introduce the Fourier transform

$$z_{\boldsymbol{n},\rho} = \sqrt{\frac{8}{N_s}} \sum_{\boldsymbol{k},n} z_{\boldsymbol{k}n,\rho} e^{i(\boldsymbol{n}\cdot\boldsymbol{k} - \omega_n\tau)}, \tag{3.63}$$

where $\boldsymbol{k}$ belongs to the first Brillouin zone of the simple cubic lattice. In momentum space $S'(Q)$ becomes

$$S'(Q) = -\frac{1}{2}\left(6Q\, z^T_{\boldsymbol{k}}\, \Gamma_{\boldsymbol{k}}\, z_{-\boldsymbol{k}} + c.c.\right), \tag{3.64}$$

where z and Γ are

$$z_{\boldsymbol{k}} \equiv \begin{pmatrix} z_{\boldsymbol{k},1} \\ \vdots \\ z_{\boldsymbol{k},7} \end{pmatrix}, \qquad \Gamma_{\boldsymbol{k}} = \begin{pmatrix} 0 & X & Y & Z & 0 & 0 & 0 \\ X^* & 0 & 0 & 0 & Z & 0 & Y \\ Y^* & 0 & 0 & 0 & 0 & Z & X \\ Z^* & 0 & 0 & 0 & X & Y & 0 \\ 0 & Z^* & 0 & X^* & 0 & 0 & 0 \\ 0 & 0 & Z^* & Y^* & 0 & 0 & 0 \\ 0 & Y^* & X^* & 0 & 0 & 0 & 0 \end{pmatrix}, \tag{3.65}$$

and $X_i = \frac{1}{6}(1 + e^{-ik_i})$. We find that the eigenvalues γ_ρ of $\Gamma_{\boldsymbol{k}}$ obey

$$0 = \gamma\left[\gamma^6 + a_2\gamma^4 + a_1\gamma^2 + a_0\right], \tag{3.66}$$

$$a_2 = -3\sum_i \rho_i^2, \tag{3.67}$$

$$a_1 = 3\sum_i \rho_i^4 + 4\sum_{i>j}\rho_i^2\rho_j^2 - 2\,\mathrm{Re}\left((XY^*)^2 + \rho_3^2\,(X^2+Y^2)\right), \tag{3.68}$$

$$\begin{aligned} a_0 = {} & \sum_{i\neq j}\rho_i^4\rho_j^2 - \sum_i \rho_i^6 - 4\rho_x^2\rho_y^2\rho_z^2 + 2\,\mathrm{Re}\Big[(XY^*)^2(\rho_x^2+\rho_y^2-\rho_z^2) \\ & +(X^2-Y^2)(\rho_z^2\rho_x^2 - \rho_z^2\rho_y^2) + (X^2+Y^2)\rho_z^4\Big], \end{aligned} \tag{3.69}$$

with $\rho_i^2 = |X_i|^2$. We have verified that the solutions to Eq. (3.66) are real and obey $\gamma_0 = 0$, $\gamma_2 = -\gamma_3$, $\gamma_4 = -\gamma_5$, and $\gamma_6 = -\gamma_7$, and are all even in the momentum $\boldsymbol{k}$. Since the first term in the action of Eq. (3.61) is unity in the 7-dimensional internal space, we write

$$\det G = \int DzDz^*\exp\left\{-\sum_{\substack{k_z>0 \\ \rho}}\int d\tau \begin{pmatrix} z_{\boldsymbol{k}\rho}^* & z_{-\boldsymbol{k},\rho}\end{pmatrix}\begin{pmatrix} \partial_\tau + \lambda & -6Q\gamma_{\boldsymbol{k}\rho} \\ -6Q\gamma_{\boldsymbol{k}\rho} & -\partial_\tau + \lambda \end{pmatrix}\begin{pmatrix} z_{\boldsymbol{k}\rho} \\ z_{-\boldsymbol{k}\rho}^* \end{pmatrix}\right\}. \tag{3.70}$$

Here the factor 1/2 of Eq. (3.64) is replaced by summing over only half of the Brillouin zone (the remainder of the Brillouin zone gives the same contribution due to the coupling of $z_{\boldsymbol{k}}$ and $z_{-\boldsymbol{k}}$). As Eq. (3.70) stands, all the fields are independent and can be integrated over. This gives

$$S_{\mathrm{MF}} = \frac{9Q^2}{2J_1} - \frac{7}{8}\lambda\left(\kappa + \frac{1}{2}\right) + \frac{1}{8}\sum_\rho \frac{1}{\beta}\int_\rho d\gamma D_\rho(\gamma)\log 2\sinh\left(\frac{\beta\omega(\gamma)}{2}\right), \tag{3.71}$$

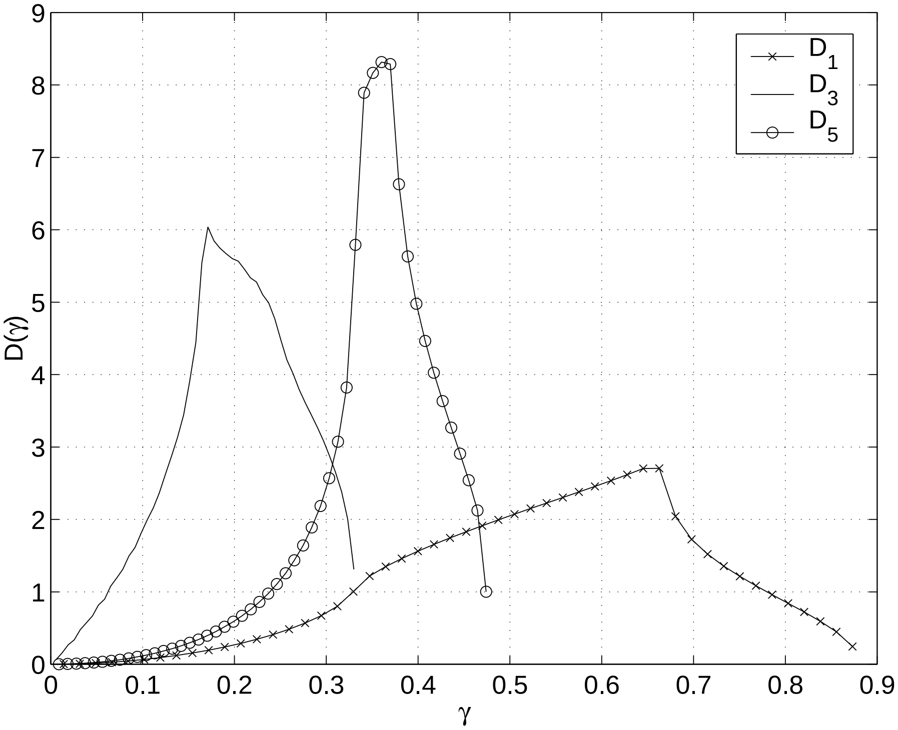

Figure 3.5: The integration measures for $c = \frac{1}{8}$.

where $\omega(\gamma) \equiv \sqrt{\lambda^2 - 36Q^2\gamma^2}$, and $D_\rho(\gamma)$ is the integration measure of $\gamma_{\boldsymbol{k},\rho}$ given in Fig. 3.5, normalized to $\int d\gamma D_\rho(\gamma) = 1$. The factor $\frac{1}{8}$ accounts for the $N_s/8$ sites found in the simple cubic lattice. Also note that the third term, $-\frac{7}{8}\lambda\frac{1}{2}$, is added according to the rule of thumb prescription of Appendix B.

We proceed to concentrate on the MF equation

$$\frac{\partial S_{\mathrm{MF}}}{\partial \lambda} = 0, \tag{3.72}$$

which, excluding BEC, becomes

$$\frac{7}{8}(\kappa + \frac{1}{2}) = \frac{1}{8}\left(n(\lambda) + \frac{1}{2}\right) + \frac{1}{4}\sum_{\rho=1,3,5}\int d\gamma D_\rho(\gamma)\frac{1}{\sqrt{1-\eta^2\gamma^2}}\left(n(\omega) + \frac{1}{2}\right). \tag{3.73}$$

At $T = 0$ this simplifies to

$$\kappa = \frac{1}{7} \sum_{\rho=1,3,5} \int d\gamma D_\rho(\gamma) \left[\frac{1}{\sqrt{1-\eta^2\gamma^2}} - 1 \right] . \tag{3.74}$$

In Fig. 3.6 we show the right hand side of the MF equations (3.51) and (3.74) for comparison. First note that for $c = \frac{1}{8}$, η takes values up to 1.14. This is because the maximum value γ can have is 0.877, and not 1 as for $c = 0$. Next we find that the right hand side has a maximum of 0.0881 at $\eta = 1.14$. This is the point where BEC occurs. The physical result is therefore that the Néel phase at $c = \frac{1}{8}$ shrinks, and symmetry restoration occurs above $\kappa_c = 0.0881$. For QCD with $N_c = 3$ this means that the symmetry is restored already at $N_f \simeq 8.5$ instead at $N_f \simeq 9.6$ at $c = 0$.

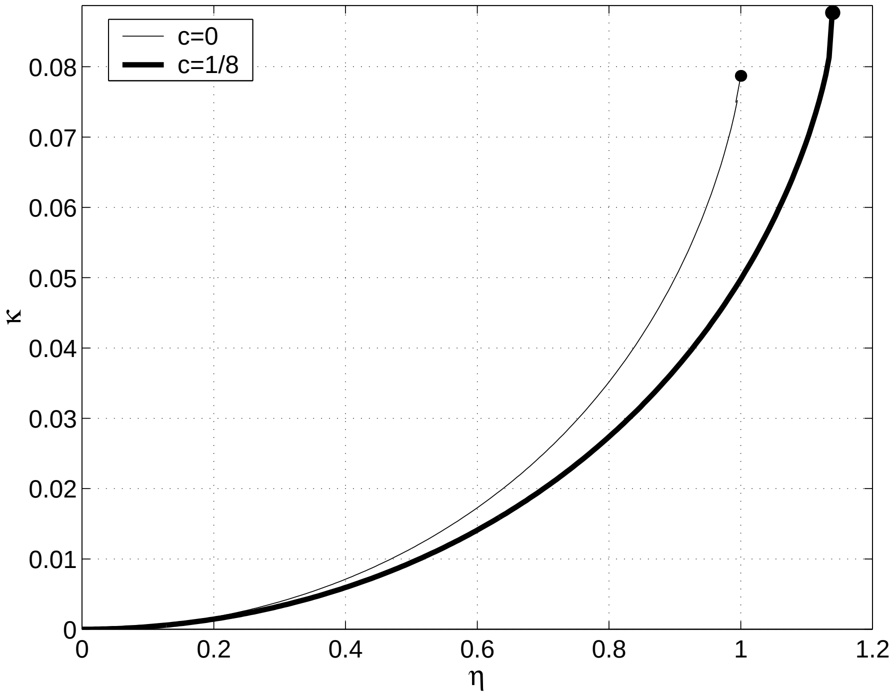

Figure 3.6: Right hand side of the MF equations Eq. (3.51) and Eq. (3.74), with $c = 0$ and $c = \frac{1}{8}$. The solution $\eta(\kappa)$ is given by intersection of the curves with horizontal lines. Note that the curves have an end at $\eta = 1$ and $\eta = 1.14$, marked by the full circles there.

Concentration $c = \frac{1}{4}$

In this case we put an impurity on site no. 1 in Fig. 3.4 as well. This means that $c = \frac{1}{4}$, and Eq. (3.60) is changed to

$$S_{\mathrm{MF}} = \frac{3Q^2}{J_1} - \frac{3}{4}\lambda\kappa + \frac{1}{N_s\beta}\mathrm{Tr}\,\log G^{-1}, \tag{3.75}$$

In evaluating the last term, we again use Eq. (3.61), but with the boson field $z_{\boldsymbol{n},1}$ omitted. This means that the matrix $\Gamma_{\boldsymbol{k}}$ in Eq. (3.65) has lost its first row and column and is now 6-dimensional. We find that its eigenvalues obey

$$\gamma^6 + a_2\gamma^4 + a_1\gamma^2 + a_0 = 0, \tag{3.76}$$

with

$$a_2 = -2\sum_i \rho_i^2, \qquad a_1 = \left(\sum_i \rho_i^2\right)^2, \qquad a_0 = -4\rho_x^2\rho_y^2\rho_z^2. \tag{3.77}$$

Again we find that the solutions γ_ρ are real and obey $\gamma_1 = -\gamma_2$, $\gamma_3 = -\gamma_4$, and $\gamma_5 = -\gamma_6$. At $T = 0$, the MF equation becomes

$$\kappa = \frac{1}{6}\sum_{\rho=1,3,5}\int d\gamma D_\rho(\gamma)\left[\frac{1}{\sqrt{1-\eta^2\gamma^2}} - 1\right], \tag{3.78}$$

with the measures given in Fig. 3.7.

In Fig. 3.8 we show the right hand side of the MF equations (3.51) and (3.78) for comparison. In this case, because the maximum value of γ is 0.66, η takes values up to 1.5. We find that the right hand side at the BEC point $\eta = 1.5$ is 0.117. The physical result is therefore that the Néel phase at $c = \frac{1}{4}$ shrinks even more than in $c = \frac{1}{8}$, and symmetry restoration occurs above $\kappa_c = 0.117$, or for QCD with $N_c = 3$ already above $N_f \simeq 6.4$.

3.4.2 Random baryon positions – the quenched approximation

In this section we solve the MF equation of a quenched random distribution of baryon impurities. We adopt the formalism of [74] developed to treat the affect of magnetic impurities on an $SU(2)$ magnet. Here the analog to the impurities are sites with $SU(4N_f)$ singlet representations. We denote the number of of singlet representations on the even and odd sites as M_e and M_o, and present calculations to first order in the concentration M_e/N_s, and

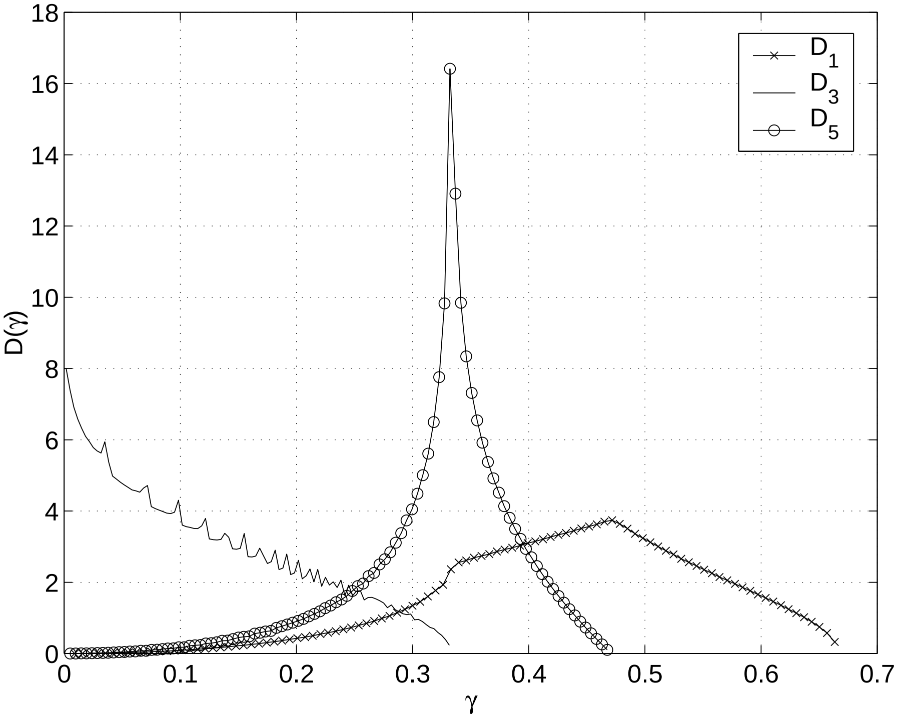

Figure 3.7: The integration measures $D_\rho(\gamma)$. The oscillations in D_3 are an artifact of the resolution of the momentum mesh.

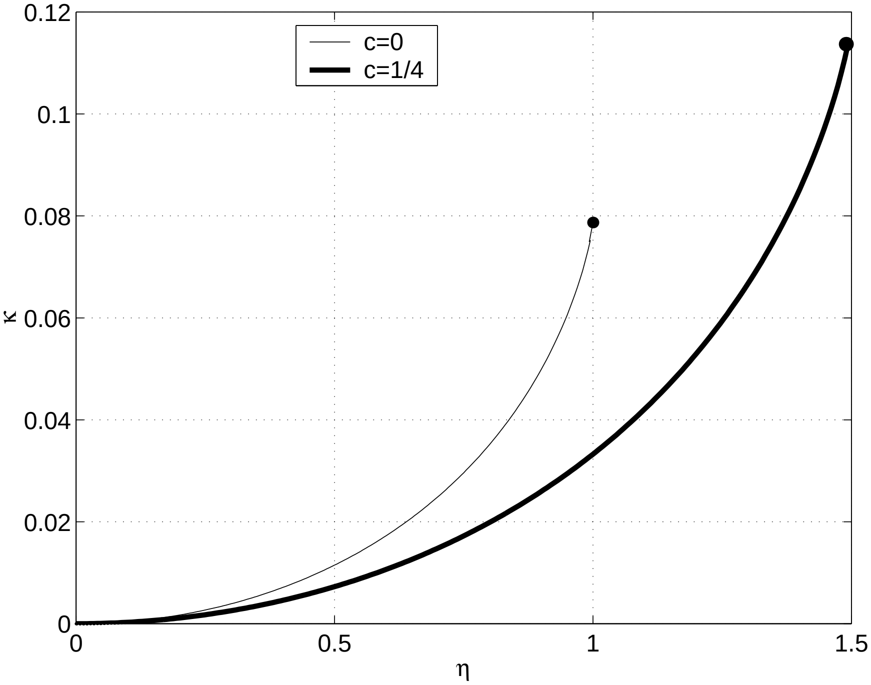

Figure 3.8: The right hand side of the MF equations Eq. (3.51) and Eq. (3.78), with $c = 0$ and $c = \frac{1}{4}$. Note that the curves have an end at $\eta = 1$ and $\eta = 1.5$, marked by the full circles there.

M_o/N_s. Again the tricky part is to calculate the functional determinant (3.37), because now the boson propagator is no longer diagonal in momentum space.

We begin by modifying Eq. (3.37) as follows,

$$\det G(Q,\lambda)\left[\int (DzDz^*)_{\boldsymbol{n}\in\{\boldsymbol{r}\}}\, e^{-S'}\right] = \int DzDz^\dagger \exp\{-S_0 - S_{\mathrm{Imp}}\}\,, \tag{3.79}$$

where S_0 is the 'pure' action of Eq. (3.37)

$$S_0 = \int d\tau \sum_{\boldsymbol{n}}\left[z^*_{\boldsymbol{n}}\left(-\partial_\tau + \lambda\right) z_{\boldsymbol{n}} - Q\sum_{\mu>0}\left(z_{\boldsymbol{n}} z_{\boldsymbol{n}+\hat{\boldsymbol{\mu}}} + z^*_{\boldsymbol{n}} z^*_{\boldsymbol{n}+\hat{\boldsymbol{\mu}}}\right)\right]. \tag{3.80}$$

The auxiliary action S' is

$$S' = \int d\tau \sum_{\boldsymbol{n}\in\{\boldsymbol{r}\}} z^*_{\boldsymbol{n}}\left(-\partial_\tau + \lambda + \lambda'\right) z_{\boldsymbol{n}}, \tag{3.81}$$

where λ' is real and obeys $\lambda + \lambda' > 0$ for stability. Also we choose the action S' to be defined in the continuum temporal limit, i.e. with the "naive" definition of ∂_τ (in Matsubara space it is just $-i\omega_n$). This means that the expression in the square brackets in the left hand side of Eq. (3.79) is given by

$$\log Z' = -c\, N_s \log 2 \sinh \frac{\beta(\lambda + \lambda')}{2}. \tag{3.82}$$

The λ' term was inserted in order that S_{Imp} will have the following form,

$$S_{\text{Imp}} = \int d\tau \sum_{\boldsymbol{n}\in\{\boldsymbol{r}\}} \left[\lambda' z^*_{\boldsymbol{n}} z_{\boldsymbol{n}} + Q \sum_{\mu=\pm 1}^{\pm d} \left(z_{\boldsymbol{n}} z_{\boldsymbol{n}+\hat{\boldsymbol{\mu}}} + z^*_{\boldsymbol{n}} z^*_{\boldsymbol{n}+\hat{\boldsymbol{\mu}}} \right) \right] \equiv \int d\tau \sum_{\boldsymbol{n},\boldsymbol{m}} z^*_{\boldsymbol{n}} V_{\boldsymbol{n}\boldsymbol{m}} z_{\boldsymbol{m}}. \tag{3.83}$$

We now write the MF action for the Hamiltonian (3.58) as

$$\begin{aligned} S_{\text{MF}} &= (1-2c)\frac{2dQ^2}{J_1} - c\,\lambda(\kappa + \frac{1}{2}) - c \log\left(1 - e^{-\beta(\lambda+\lambda')}\right) && (3.84)\\ &\quad + \frac{1}{N_s\beta} \text{Tr } \log G^{-1} + \Delta S, && (3.85)\\ \Delta S &= \frac{1}{N_s\beta} \text{Tr } \log\left(\mathbf{1} + GV\right). && (3.86) \end{aligned}$$

Here $G^{-1}(Q,\lambda)$ is the same inverse propagator that appears in the zero density problem in section 3.3, and we proceed to evaluate ΔS. Using the Fourier transform (3.38) we write V in momentum space as

$$\begin{aligned} S_{\text{Imp}} &= \sum_{\omega_n} \sum_{\boldsymbol{k},\boldsymbol{k}'} f^\dagger_{\boldsymbol{k},n} V_{\boldsymbol{k},\boldsymbol{k}'} f_{\boldsymbol{k}',n}, && (3.87)\\ V_{\boldsymbol{k},\boldsymbol{k}'} &= 2dQ\, \frac{2}{N_s} \left[\sum_{\boldsymbol{m}\in\{\boldsymbol{r}_e\}} e^{i(\boldsymbol{k}'-\boldsymbol{k})\boldsymbol{m}} \begin{pmatrix} b^2 & \gamma_{\boldsymbol{k}'} \\ \gamma_{\boldsymbol{k}} & 0 \end{pmatrix} + \sum_{\boldsymbol{m}\in\{\boldsymbol{r}_o\}} e^{i(\boldsymbol{k}'-\boldsymbol{k})\boldsymbol{m}} \begin{pmatrix} 0 & \gamma_{\boldsymbol{k}} \\ \gamma'_{\boldsymbol{k}} & b^2 \end{pmatrix} \right]. && (3.88) \end{aligned}$$

Here $f_{\boldsymbol{k},n}$ is given in Eq. (3.40), $\boldsymbol{m}$ are the positions of the impurity sites in terms of the original simple cubic lattice, $\{\boldsymbol{r}_e\}$ and $\{\boldsymbol{r}_o\}$ denote the impurities on even and odd sublattices, and $b^2 \equiv \lambda'/2dQ$. Fortunately, the vertex $V_{\boldsymbol{k},\boldsymbol{k}'}$ is reducible to the form [6]

$$V_{\boldsymbol{k},\boldsymbol{k}'} = \frac{1}{N_s} \sum_{\boldsymbol{m}\in\{\boldsymbol{r}\}_e} \mathcal{I}^e_{\boldsymbol{k}} \mathcal{J}^e_{\boldsymbol{k}'} e^{i(\boldsymbol{k}'-\boldsymbol{k})\boldsymbol{m}} + \frac{1}{N_s} \sum_{\boldsymbol{m}\in\{\boldsymbol{r}\}_o} \mathcal{I}^o_{\boldsymbol{k}} \mathcal{J}^o_{\boldsymbol{k}'} e^{i(\boldsymbol{k}'-\boldsymbol{k})\boldsymbol{m}}, \tag{3.89}$$

---

[6] This reducibility is achieved only for $b \neq 0$, and is in fact the reason we introduced λ'.

$$\mathcal{I}^e_{\boldsymbol{k}} = \sqrt{4dQ}\begin{pmatrix} b & 0 \\ \gamma_{\boldsymbol{k}}/b & -\gamma_{\boldsymbol{k}}/b \end{pmatrix}, \qquad \mathcal{J}^e_{\boldsymbol{k}'} = \sqrt{4dQ}\begin{pmatrix} b & \gamma_{\boldsymbol{k}'}/b \\ 0 & \gamma'_{\boldsymbol{k}}/b \end{pmatrix}, \tag{3.90}$$

$$\mathcal{I}^o_{\boldsymbol{k}} = \sqrt{4dQ}\begin{pmatrix} -\gamma_{\boldsymbol{k}}/b & \gamma_{\boldsymbol{k}}/b \\ 0 & b \end{pmatrix}, \qquad \mathcal{J}^o_{\boldsymbol{k}'} = \sqrt{4dQ}\begin{pmatrix} \gamma_{\boldsymbol{k}'}/b & 0 \\ \gamma'_{\boldsymbol{k}}/b & b \end{pmatrix}. \tag{3.91}$$

With the above definitions the evaluation of ΔS becomes tractable, and takes the form of a power series in the impurity concentration. We proceed to write

$$N_s\beta\Delta S = \sum_{p=1}^{\infty} \frac{(-1)^{p+1}}{p}\,\mathrm{Tr}\,(GV)^p, \tag{3.92}$$

where we implicitly assume that the sum (3.92) is convergent. The trace is over the momentum and internal even-odd indices. Using Eqs. (3.90)–(3.91) and Eq. (3.39) we find that Eq. (3.92) contains contributions of the form

$$\mathrm{Tr} \sum_{\substack{\boldsymbol{k}_1,\ldots,\boldsymbol{k}_p \\ \boldsymbol{m}_1,\ldots,\boldsymbol{m}_p \in \{\boldsymbol{r}\}}} \mathcal{A}^1_{\boldsymbol{k}_1}\mathcal{A}^2_{\boldsymbol{k}_1}\cdots\mathcal{A}^p_{\boldsymbol{k}_p} e^{i[(\boldsymbol{k}_1-\boldsymbol{k}_2)\boldsymbol{m}_1+\ldots+(\boldsymbol{k}_p-\boldsymbol{k}_1)\boldsymbol{m}_p]}. \tag{3.93}$$

Here $\mathcal{A}^i_{\boldsymbol{k}}$ can be any one of the four matrices

$$\mathcal{A}^{ee} = \frac{1}{N_s}\mathcal{J}^e_{\boldsymbol{k}} G_{\boldsymbol{k}} \mathcal{I}^e_{\boldsymbol{k}}, \qquad \mathcal{A}^{oo} = \frac{1}{N_s}\mathcal{J}^o_{\boldsymbol{k}} G_{\boldsymbol{k}} \mathcal{I}^o_{\boldsymbol{k}}, \tag{3.94}$$

$$\mathcal{A}^{eo} = \frac{1}{N_s}\mathcal{J}^e_{\boldsymbol{k}} G_{\boldsymbol{k}} \mathcal{I}^o_{\boldsymbol{k}}, \qquad \mathcal{A}^{oe} = \frac{1}{N_s}\mathcal{J}^e_{\boldsymbol{k}} G_{\boldsymbol{k}} \mathcal{I}^e_{\boldsymbol{k}}. \tag{3.95}$$

A diagrammatic method is useful to treat the evaluation of Eq. (3.93), and we define the following Feynman rules.

1. The propagator G given by Eq. (3.39) is represented by Fig. 3.9. It is diagonal in momentum and Matsubara frequency. $a, b = e, o$ are the even-odd indices.

$$\left(G_{\boldsymbol{k}}(\omega_n)\right)_{ab} =$$

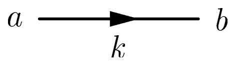

Figure 3.9: The boson propagator.

2. The interaction are given in Eq. (3.89) is a sum of $M_e + M_o$ vertices, one for each of the impurities. The vertex that corresponds to the impurity on site $\boldsymbol{r}$ is given in Fig. 3.10.

$$\left(V^{\boldsymbol{r}}_{\boldsymbol{k},\boldsymbol{k}'}\right)_{ab} =$$

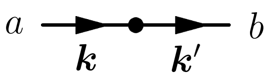

$$= \frac{2}{N_s}e^{i(\boldsymbol{k}'-\boldsymbol{k})\boldsymbol{r}}\left(\mathcal{I}_{\boldsymbol{k}}\mathcal{J}_{\boldsymbol{k}'}\right)_{ab}$$

Figure 3.10: The vertex of the impurity that resides on the site $\boldsymbol{r}$. Here $\mathcal{I}, \mathcal{J}$ are defined by either Eq. (3.90) or Eq. (3.91).

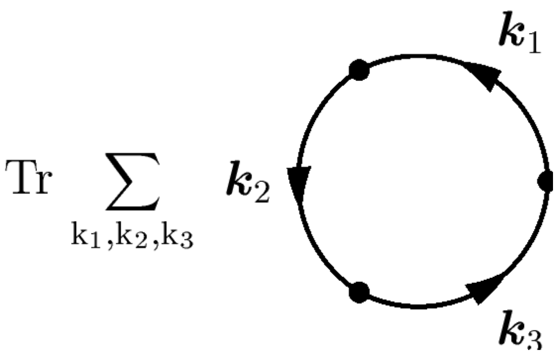

Figure 3.11: The loop diagram that corresponds to the expression in Eq. (3.93) with $p = 3$.

3. The expression (3.93) is represented by the diagram in Fig. 3.11, which describes the scattering of the bosons off three impurities. Note that this diagram stands for all possible ways to scatter three times off $M_e + M_o$ available impurities.

4. We adopt the notations in [74], and write the diagram in Fig. 3.11 as the sum in Fig. 3.12. A diagram with q external points (each denoted by an $\times$) corresponds to a process in which the bosons scatter off q *different* impurities. The lines connecting the external points with the vertices denote which of the impurities was hit in a given vertex. For example in the leftmost diagram, the boson collides three times off the same impurity, while in the rightmost diagram, it collides three times off three different impurities. Finally note that each of the diagrams in Fig. 3.12 stands for all possibilities to choose the impurities that the bosons scatter off.

The next step is to use the quenched approximation, and average Eq. (3.93) over the position of each impurity. This assumes that the impurities cannot move on the time scale that the bosons move, and is exact in the order we work to within the strong coupling expansion. We define the averaging procedure over the locations of the set $\{\boldsymbol{r}\}$

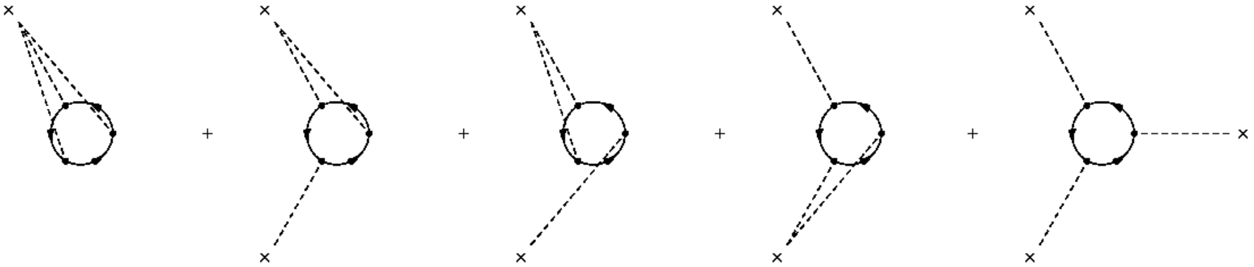

Figure 3.12: The loop diagram that corresponds to the expression (3.93) with $p = 3$. The leftmost diagram describes a boson scatters three times off the same impurity, while the rightmost diagram describes a boson that scatters three times off three different impurities.

as

$$\langle \mathcal{O} \rangle \equiv \left(\frac{2}{N_s} \right)^{M_e+M_o} \sum_{\{\boldsymbol{r}_{e,o}\}=1}^{N_s/2} \mathcal{O}((\{\boldsymbol{r}_e\}; \{\boldsymbol{r}_o\}). \tag{3.96}$$

This relies on the assumption that the concentration of impurities is sufficiently small that there are no links between any two impurities. This assumption is invalid at high c.

Applying the averaging procedure to each of the diagrams in Fig. 3.12 results in the following power series for expression (3.93),

$$N_s \sum_{q=1}^{\mathrm{Min[p,M]}} \sum_{q_e=0}^{q} c_e^{q_e} c_o^{q-q_e} \mathcal{B}_p^{(q,q_e)}. \tag{3.97}$$

Here q_e and $q - q_e$ are, respectively, the number of external points that correspond to an impurity residing on an even or odd site, and $c_{e,o}$ are defined as

$$c_a = M_a/N_s, \qquad a = e, o. \tag{3.98}$$

We proceed to prove this point. First we denote a diagram with p vertices and a total of q external points, out of which q_e represent impurities on even sites, by $\mathcal{D}^{(s)}_{p,q,q_e}$. s is an additional index that denotes the different diagrams that have the same values of p, q, and q_e. For example for $p = 4$, and $q = q_e = 2$, s takes the values $1, 2$, and 3, and corresponds to the three diagrams in Fig. 3.13.

Looking at the structure of the exponentials in Eq. (3.93) we see that when we evaluate $\mathcal{D}^{(s)}_{p,q,q_e}$, where $\boldsymbol{m}_i$ take q different values, the exponential turn into

$$e^{i(\boldsymbol{k}'_1\boldsymbol{r}_1+\boldsymbol{k}'_2\boldsymbol{r}_2+\ldots+\boldsymbol{k}'_{q-1}\boldsymbol{r}_{q-1})}. \tag{3.99}$$

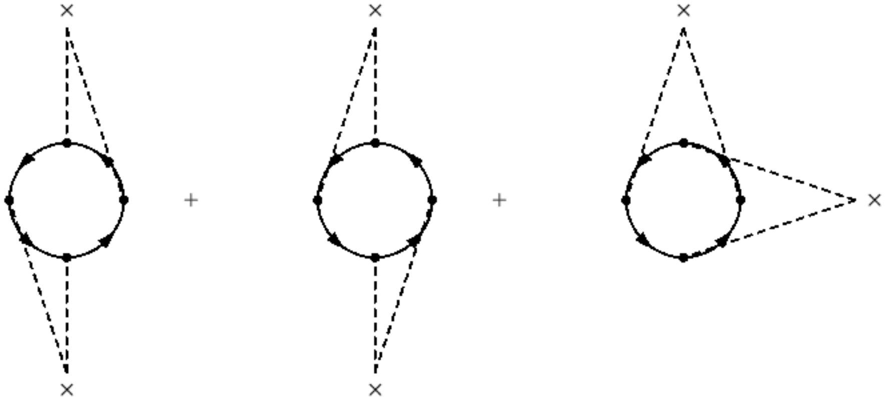

Figure 3.13: The loop diagrams that corresponds to $p = 4$, $q = q_e = 2$, and $s = 1, 2, 3$.

Here $\{\boldsymbol{k}'_i\}$ are linear combinations of the momenta that flow in the diagram. The averaging procedure is in fact applied only to the exponentials (3.99), and results in $q-1$ momenta conservation rules,

$$\langle e^{i(\boldsymbol{k}'_1\boldsymbol{r}_1+\boldsymbol{k}'_2\boldsymbol{r}_2+\ldots+\boldsymbol{k}'_{q-1}\boldsymbol{r}_{q-1})}\rangle = \delta_{\boldsymbol{k}'_1}\delta_{\boldsymbol{k}'_2}\cdots\delta_{\boldsymbol{k}'_{q-1}}. \tag{3.100}$$

Substituting Eq. (3.100) into Eq. (3.93), and taking into account of the number of possibilities to choose which impurities are represented by the external points in $D^{(s)}_{p,q,q_e}$ we have

$$\langle\mathcal{D}^{(s)}_{p,q,q_e}\rangle = \left(\begin{array}{c} M_e \\ q_e \end{array}\right)\left(\begin{array}{c} M_o \\ q-q_e \end{array}\right)\mathrm{Tr}\sum_{\boldsymbol{k}_1,\ldots,\boldsymbol{k}_p}\mathcal{A}^1_{\boldsymbol{k}_1}\cdots\mathcal{A}^p_{\boldsymbol{k}_p}\delta_{\boldsymbol{k}'_1}\delta_{\boldsymbol{k}'_2}\cdots\delta_{\boldsymbol{k}'_{q-1}}. \tag{3.101}$$

The next step is to assume that the terms in Eq. (3.92) with $p > M_{e,o}$ are negligible. ($M_{e,o}$ are of the order of N_s) Recalling that $\mathcal{A}^i_{\boldsymbol{k}} \propto N_s^{-1}$, we find the following continuum limit of Eq. (3.101) for $p, q_e, q-q_e \ll M_{e,o}$.

$$\begin{aligned}\langle\mathcal{D}^{(s)}_{p,q,q_e}\rangle &= \frac{M_e^{q_e}}{q_e!}\frac{M_o^{q-q_e}}{(q-q_e)!}N_s^{-p}\left(N_s\int d\boldsymbol{k}\right)^{p-q+1}F^{(s)}_{p,q,q_e}(\{\boldsymbol{k}\}) \\ &= N_s\frac{(c_e)^{q_e}(c_o)^{q_o}}{q_e!(q-q_e)!}\left(\int d\boldsymbol{k}\right)^{p-q+1}F^{(s)}_{p,q,q_e}(\{\boldsymbol{k}\}), \end{aligned} \tag{3.102}$$

where the $(p-q+1)$ momentum integrals are over the Brillouin zone and are finite. We can now identify that

$$\mathcal{B}^{(q,q_e)}_p = \frac{(c_e)^{q_e}(c_o)^{q-q_e}}{q_e!(q-q_e)!}\sum_s\left(\int d\boldsymbol{k}\right)^{p-q+1}F^{(s)}_{p,q,q_e}(\{\boldsymbol{k}\}), \tag{3.103}$$

for $p \ll M_{e,o}$. Q.E.D

MF action to $O(c)$

We now evaluate ΔS to first order in the concentration c. We therefore take into account diagrams with $q = 1$ only. In that case $q_e = 0, 1$, and $s = 1$ (there is only one possible diagram for each value of q_e). In this case the diagrams that contribute to the p-th term in Eq. (3.92) correspond to p scatterings off the same impurity, which resides on either sublattice. The structure of Eq. (3.92) is now simple. For $q_e = 1$ all $\mathcal{A}^i = \mathcal{A}^{ee}$, and for $q_e = 0$ all $\mathcal{A}^i = \mathcal{A}^{oo}$. The result is

$$\begin{aligned} N_s\beta\Delta S &\simeq N_s \sum_{\omega_n} \mathrm{Tr} \sum_{p \ll M_{e,o}} \frac{(-1)^{p+1}}{p} \left[c_e \mathcal{B}_p^{(1,1)} + c_o \mathcal{B}_p^{(1,0)}\right] \\ &= N_s \sum_{\omega_n} \sum_{a=e,o} c_a \mathrm{Tr} \sum_{p \ll M_{e,o}} \frac{(-1)^{p+1}}{p} \left[\int \left(\frac{d\boldsymbol{k}}{2\pi}\right)^d \mathcal{J}_{\boldsymbol{k}}^a G_{\boldsymbol{k}}(\omega_n) \mathcal{I}_{\boldsymbol{k}}^a\right]^p \\ &\simeq N_s \sum_n \sum_a c_a \mathrm{Tr} \log \left[\mathbf{1} + \int \left(\frac{d\boldsymbol{k}}{2\pi}\right)^d \mathcal{J}_{\boldsymbol{k}}^a G_{\boldsymbol{k}}(\omega_n) \mathcal{I}_{\boldsymbol{k}}^a\right]. \end{aligned} \tag{3.104}$$

We have verified that the contribution of the Tr is independent of a, so ΔS becomes

$$\begin{aligned} \beta\Delta S(\lambda, \eta; b) = c \sum_{\epsilon_n} \log \Bigg\{ \det \Bigg[\mathbf{1} + \int d\gamma\, D(\gamma)\, \frac{\eta}{1 + \epsilon_n^2 - \eta^2\gamma^2} \times \\ \begin{pmatrix} b^2(1 - i\epsilon) + 2\eta\gamma^2 + \gamma^2(1 + i\epsilon_n)/b^2 & -\gamma^2(\eta + (1 + i\epsilon_n)/b^2) \\ \gamma^2(\eta + (1 + i\epsilon_n)/b^2) & -(1 + i\epsilon_n)\gamma^2/b^2 \end{pmatrix} \Bigg] \Bigg\}. \end{aligned} \tag{3.105}$$

Here the overall concentration $c = c_e + c_o = M/N_s$, $\epsilon_n \equiv \omega_n/\lambda$, and the momentum integration was again replaced by an integration over the variable γ with the measure shown in Fig. 3.1. We have calculated $\Delta S(\lambda, \eta; b)$ and confirmed that for $|\eta| \leq 1$ it is real. Substituting Eq. (3.105) into Eq. (3.86) we have

$$\begin{aligned} S_{\mathrm{MF}} &= \frac{2d(1 - 2c)}{J_1} Q^2 - (1 - c)\lambda\kappa \\ &\quad + \frac{1}{\beta} \int d\gamma D(\gamma) \log 2 \sinh \frac{\beta\omega(\gamma)}{2} - \frac{1}{2}\lambda(1 - c) \\ &\quad + \frac{c}{\beta} \left(- \log 2 \sinh \frac{\beta\lambda(1 + \eta b^2)}{2} + \Delta S(\lambda, \eta; b)\right). \end{aligned} \tag{3.106}$$

The first row of Eq. (3.106) is the result of (3.59). The second row is Tr $\log G^{-1}$ for the pure system. (Note the term proportional to $(1-c)$ is exactly the rule of thumb prescription from Appendix B) The contributions to the third row are the continuum evaluation of ΔS and $-\log Z'$, evaluated in the continuum limit of Euclidean time. We have verified that the contributions in the third row do not depend on the value of the unphysical constant b.

MF equations to $O(c)$

We concentrate here on the $T=0$ case. There we have

$$\begin{aligned}\frac{1}{N_s N m\beta} S_{\mathrm{MF}} &= \frac{2d(1-2c)}{J_1} Q^2 - \lambda\left(\kappa(1-c)+\frac{1}{2}\right) + \lambda\mathcal{F}(\eta), && (3.107)\\ \mathcal{F}(\eta) &\equiv \frac{1}{2}\int d\gamma D(\gamma)\sqrt{1-\eta^2\gamma^2} + c\left(\lim_{\beta\lambda\to\infty}\left[\frac{1}{\beta\lambda}\Delta S(\lambda,\eta;b)\right] - \frac{1}{2}\eta b^2\right). && (3.108)\end{aligned}$$

Where we have evaluated the $\beta\lambda\to\infty$ limit of the second term in $\mathcal{F}(\eta)$ as an integral over ϵ. In order to investigate the boundary of the Neél phase with non-zero value of c, we concentrate on the equation

$$\frac{\partial S_{\mathrm{MF}}}{\partial\lambda} = 0, \tag{3.109}$$

and assume no condensates. This becomes

$$\kappa = \frac{1}{1-c}\left[f(\eta) + c\,\mathcal{G}_{\mathrm{loop}}\right]. \tag{3.110}$$

Here $f(\eta)$ is the right hand side of the MF equation for $c=0$, Eq. (3.48), as plotted in Fig. 3.2. $\mathcal{G}_{\mathrm{loop}}$ includes all other loop contributions.

We plot the right hand side of Eq. (3.110) in Fig. 3.14 and see that as the concentration c increases, the maximum value of κ *decreases*. This means that the Néel phase is expanding, which appears to contradict the results of Section 3.4.1.

In order to resolve this problem we compare the results of the quenched calculation for $c=\frac{1}{8}$ and $c=\frac{1}{4}$ with the exact diagonalization in Section 3.4.1. We present the results of the two calculations in Figs. 3.15–3.18. The results are very similar. We see that the errors of the quenched results are larger for $c=\frac{1}{4}$ than for $c=\frac{1}{8}$. This is presumably because of the restriction to first order in c. Also we note that the quenched perturbative approximation is inapplicable for $\eta > 1$, since the unperturbed ground state does not admit such values of η. Nevertheless, the result of Section 3.4.1 lets η be larger than 1, and in fact it is in this extra interval that the right hand side of the MF equation continues to grow, and the Néel phase shrinks. For both $c = \frac{1}{8}$ and $c = \frac{1}{4}$, there is a value of $\eta_{\max} > 1$ at which BEC occurs. This regime of MF parameters is unfortunately not accessible in the quenched approach.

To conclude we see that the MF quenched approximation in first order in c does not reproduce the MF theory near the phase transition. The deviation between the quenched approximation and the exact diagonalization grows as one approaches the BEC. This approach is not applicable to extract information about the phase transition, simply because it is a perturbative approach whose starting point is the $c = 0$ system. One can use this approach to extract quantitative properties of the disordered phase, and to see how these change when baryons are included. For example, the propagators of bosons will then obtain a self-energy contribution also calculable via the diagrammatic tools described above. It is expected that this will show that the baryon impurities slow down the bosons, and even make them decay. This is in analogy to what happens in condensed matter magnetic systems with lattice vacancies [74, 75, 76].

Finally we note that although this MF analysis was devoted to the regime $\kappa < \kappa_c$ and explored the disordered phase (while emphasizing the location of the phase transition), it is also possible to investigate the ordered phase. This can be done in the large N_c limit by using a Holstein-Primakoff representation of the Q^η operators (which is presented for $m = 1$ in Appendix H). The quenched approach can be also applied in this limit, and in analogy to [74] we expect that the Goldstone bosons in this phase (the pions and kaons in our system) will have a smaller velocity, and will obtain finite decay widths.

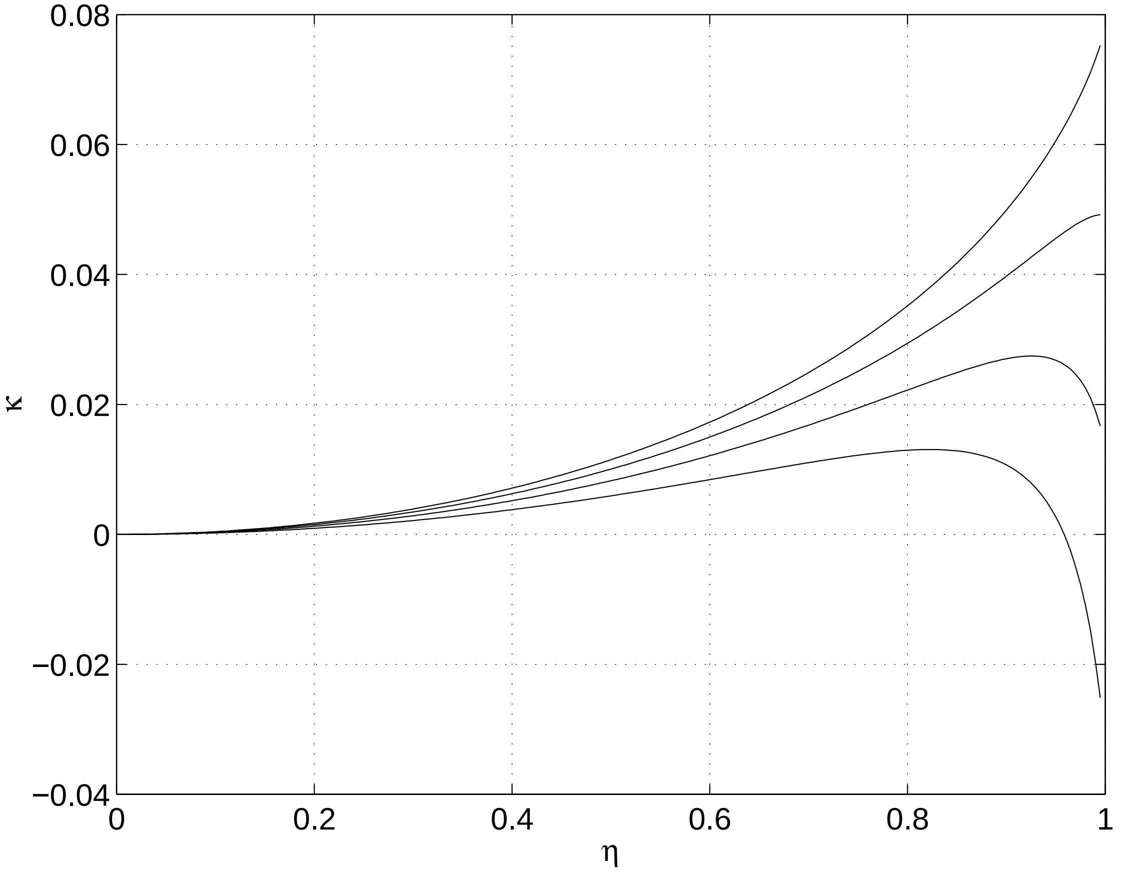

Figure 3.14: The right hand side of Eq. (3.110) for $c = 0$ (highest curve), 0.1, 0.2, and 0.3 (lowest curve).

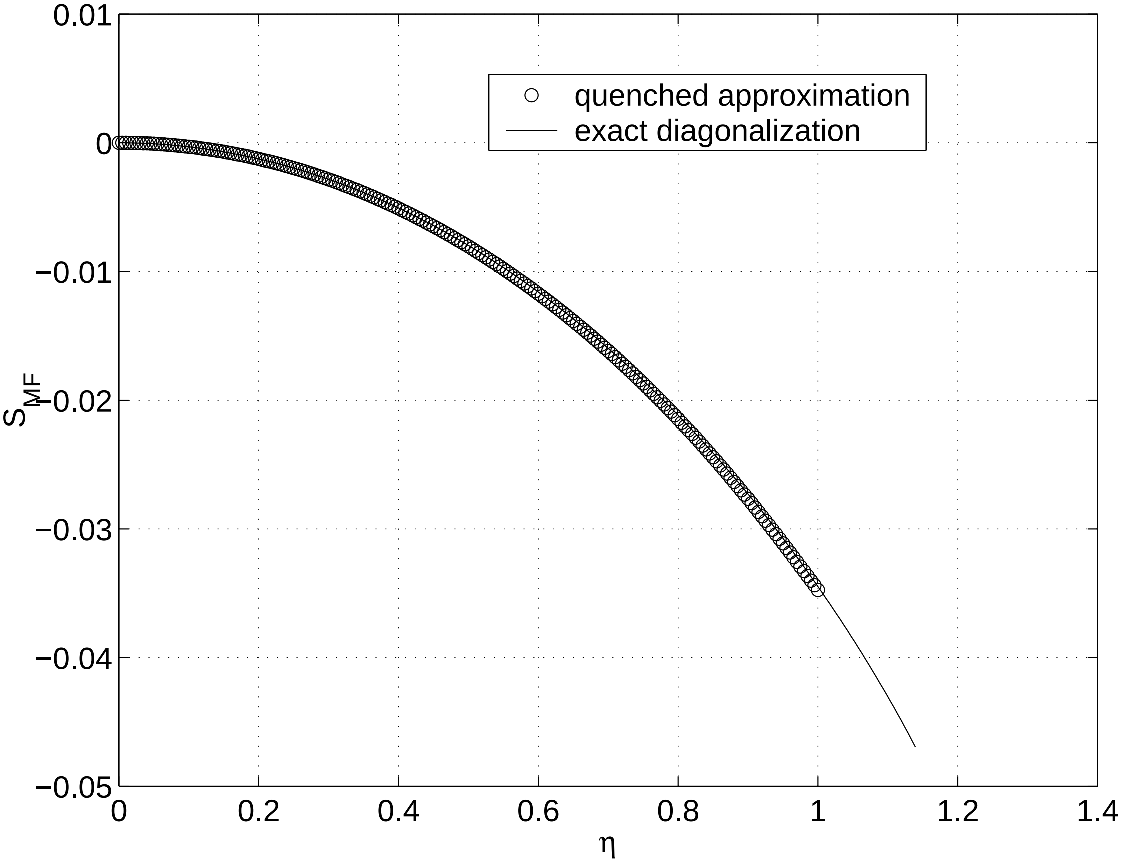

Figure 3.15: The MF effective action for $c = \frac{1}{8}$ in the quenched approximation, and the exact diagonalization.

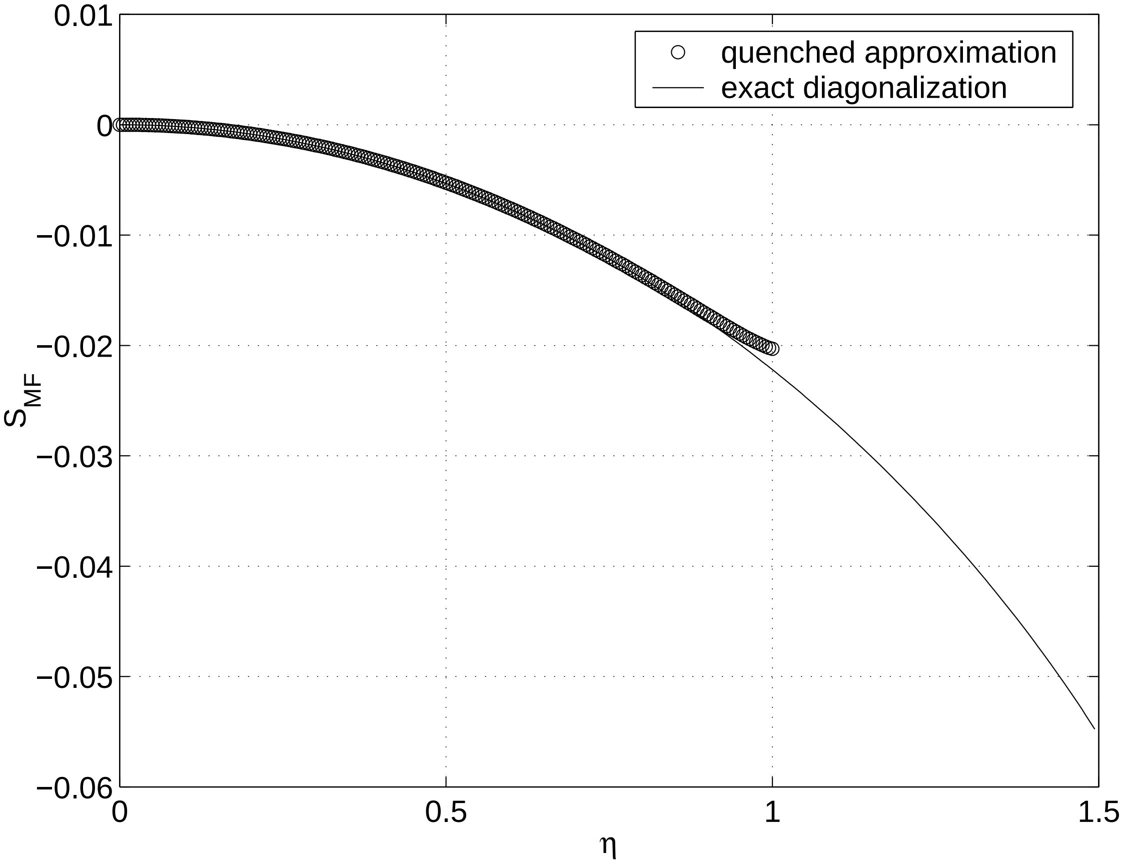

Figure 3.16: The MF effective action for $c = \frac{1}{4}$ in the quenched approximation, and the exact diagonalization.

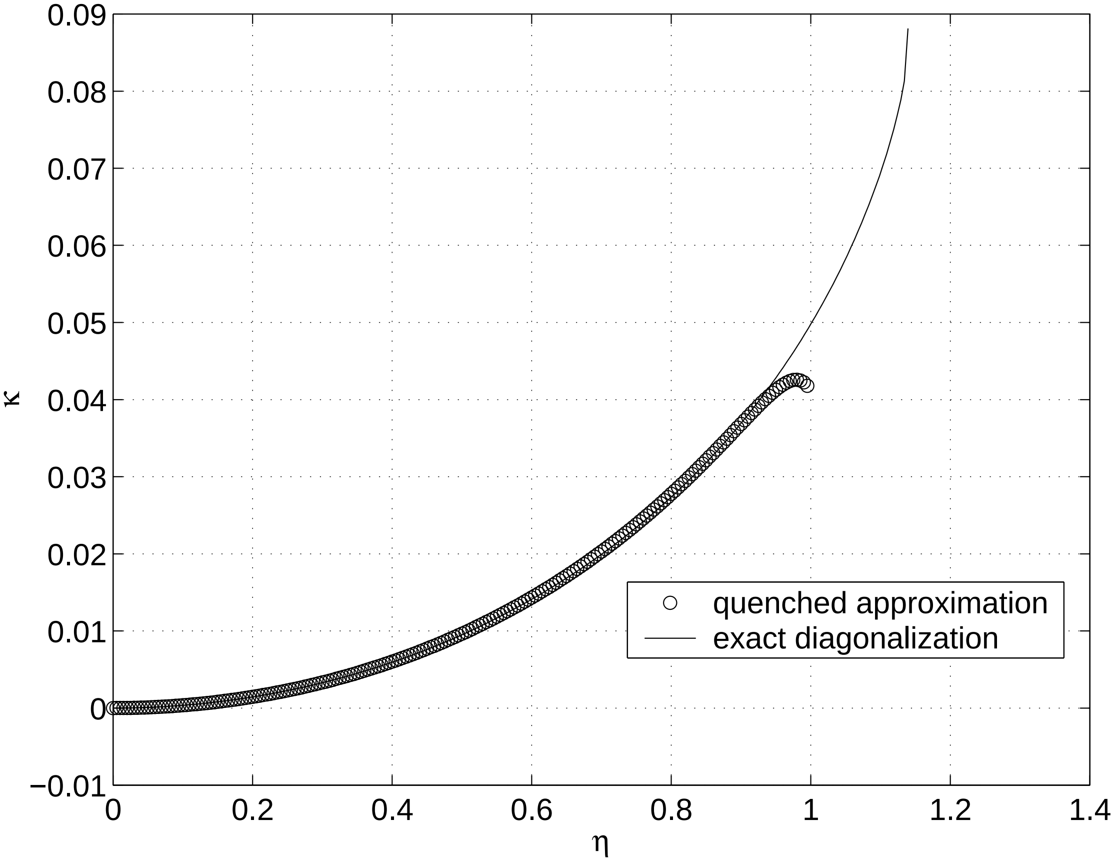

Figure 3.17: The right hand side of the MF equation for $c = \frac{1}{8}$ in the quenched approximation, and the exact diagonalization.

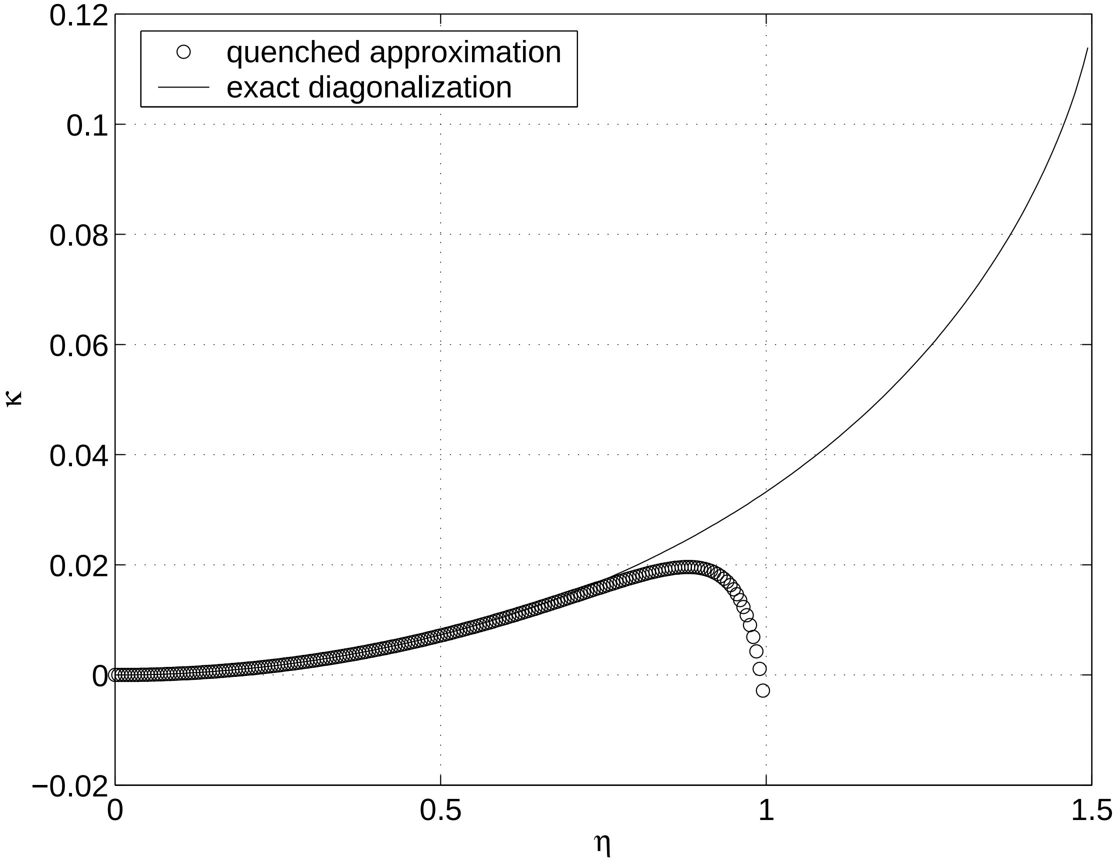

Figure 3.18: The right hand side of the MF equation for $c = \frac{1}{4}$ in the quenched approximation, and the exact diagonalization.

Chapter 4

Nonlinear sigma model and the classical ground state

In this chapter we use a coherent state basis to write the partition function of the Hamiltonian (2.69) as a path integral. The result is a nonlinear sigma model. We first analyze the properties of the classical counterpart of a toy sigma model that has $N = 3$. We use mean field theory to find its ground state as a function of temperature for a set of baryon number configurations. Next we approach the full quantum sigma model. The action of the model has an overall factor of N_c, and is tractable in the large N_c limit. We take this limit and examine the classical ground state for a set of uniform baryon number configurations.

4.1 Coherent states and sigma fields

We employ a generalization of spin coherent states [51] to derive a path integral for the spin model of $H^{(2)}_{\text{eff}}$. We recall that a given site carries generators $Q^{\eta}_{\boldsymbol{n}}$ of $U(N)$ in a representation with N_c columns and m rows, with $B_{\boldsymbol{n}} = m - 2N_f$.

First we choose a basis for the Lie algebra of $U(N)$. This consists of the generators S^{α}_{β}, with $\alpha, \beta = 1, \ldots, N$, whose matrix elements in the fundamental representation are

$$(S^{\alpha}_{\beta})_{\gamma\delta} = \delta_{\alpha\gamma}\delta_{\beta\delta}. \tag{4.1}$$

The corresponding charges are

$$\begin{aligned} Q^\alpha_\beta &= \sum_a \psi^\dagger_a S^\alpha_\beta \psi_a - \frac{1}{2} N_c \delta^\alpha_\beta \\ &= \sum_\alpha \psi^\dagger_{a\alpha} \psi_{a\beta} - \frac{1}{2} N_c \delta^\alpha_\beta, \end{aligned} \tag{4.2}$$

where we have subtracted a constant for convenience. The Cartan subalgebra consists of the operators

$$H_\alpha = Q^\alpha_\alpha. \tag{4.3}$$

We build the coherent states from the state of highest weight $|\Psi_0\rangle$

$$|\Psi_0\rangle = \prod_{\alpha=1}^{m} \left(\psi^\dagger_{\alpha,1} \psi^\dagger_{\alpha,2} \cdots \psi^\dagger_{\alpha,N_c} \right) |\mathrm{Dr}\rangle, \tag{4.4}$$

where the numbers are the color indices. This state is an eigenstate of the Cartan generators,

$$H_\alpha |\Psi_0\rangle = \begin{cases} (N_c/2)|\Psi_0\rangle & \text{for } \alpha = 1, \ldots, m, \\ -(N_c/2)|\Psi_0\rangle & \text{for } \alpha = m+1, \ldots, N. \end{cases} \tag{4.5}$$

The expectation values of the generators in this state obey

$$\langle \Psi_0 | Q^\alpha_\beta | \Psi_0 \rangle = \frac{1}{2} N_c \Lambda_{\alpha\beta}, \tag{4.6}$$

with

$$\Lambda = \begin{pmatrix} \mathbf{1}_m & 0 \\ 0 & -\mathbf{1}_{N-m} \end{pmatrix}. \tag{4.7}$$

In order to obtain the other states in the rep, we perform the following $U(N)$ rotations on $|\Psi_0\rangle$,

$$|a\rangle = \exp\left(\sum_{\lambda=1}^{m} \sum_{\mu=m+1}^{N} (a^\lambda_\mu Q^\mu_\lambda - a^{*\lambda}_\mu Q^\lambda_\mu) \right) |\Psi_0\rangle. \tag{4.8}$$

The only generators Q^μ_λ that appear in Eq. (4.8) are those that lower an H_α that starts from $N_c/2$ in Eq. (4.5) while raising another H_α that starts from $-N_c/2$. Any other generator would annihilate $|\Psi_0\rangle$ and thus give no effect in the exponential.

The coherent states are normalized,

$$\langle a|a\rangle = 1, \tag{4.9}$$

and over-complete,

$$\int d\mu(a)\,|a\rangle\langle a| = \mathbf{1}. \tag{4.10}$$

In Eq. (4.10) the integral is over the coset space $U(N)/[U(m)\times U(N-m)]$ (see below). Matrix elements of the generators are given by

$$\langle a|Q^{\alpha}_{\beta}|a\rangle = \frac{1}{2}N_c\sigma_{\alpha\beta}, \tag{4.11}$$

where the matrix $\sigma_{\alpha\beta}$ is given by a unitary rotation from Λ,

$$\sigma = U(a)\Lambda U(a)^{\dagger}. \tag{4.12}$$

The matrix $U(a)$ is built out of the $m\times(N-m)$ matrix a^{λ}_{μ},

$$U = e^{A} = \exp\left[\begin{pmatrix} 0 & a \\ -a^{\dagger} & 0 \end{pmatrix}\right]. \tag{4.13}$$

σ is both Hermitian and unitary.

The manifold of matrices σ is the coset space $U(N)/[U(m)\times U(N-m)]$, a sub-manifold of $U(N)$. This is because for any matrix $U(a)$, one can generate an orbit $U(a)V$ by multiplying with a matrix

$$V = \begin{pmatrix} X & 0 \\ 0 & Y \end{pmatrix}, \tag{4.14}$$

where $X\in U(m)$ and $Y\in U(N-m)$. All matrices in the orbit will give the same matrix σ when inserted into Eq. (4.12), and thus in integrating over the configuration space of σ one must choose only a single representative of each orbit. This set of representatives, the coset space $U(N)/[U(m)\times U(N-m)]$, is the quotient space of the non-invariant subgroup $U(m)\times U(N-m)$. Basically the origin of this manifold is the fact that the quantum state $|\Psi_0\rangle$ is invariant (up to a phase) to $U(N)$ rotations that belong to the subgroup $U(m)\times U(N-m)$. This can be understood by the form of the Young tableau in Fig. 2.4. This representation of $SU(N)$ is a singlet of a certain $SU(m)\times SU(N-m)$ subgroup, more precisely, of the rotations that do not involve indices from the $[m+1,N]$ range and that leave the $[1,m]$ indices of the state invariant.

The measure over the coset space must be invariant under unitary rotations,

$$|a\rangle \to R(V)|a\rangle, \tag{4.15}$$

where $R(V)$ represents the rotation V in Hilbert space. Equation (4.11) shows that this is a rotation

$$\sigma \to V\sigma V^\dagger \tag{4.16}$$

and by Eq. (4.12), this means that a measure in U must be invariant under $U \to VU$. This fixes the measure uniquely to be the Haar measure in $U(N)$, and thus one can integrate over the coset space by integrating with respect to U over $U(N)$ and using Eq. (4.12).

A representation whose Young diagram has $N-m$ rows is the conjugate to the representation with m rows. Its coherent state space can be constructed to look the same, with only a sign difference. To do this we start with the *lowest*-weight state, which satisfies [cf. Eq. (4.5)]

$$H_\alpha|\Psi_0\rangle = \begin{cases} -(N_c/2)|\Psi_0\rangle & \text{for } \alpha = 1,\ldots,m \\ (N_c/2)|\Psi_0\rangle & \text{for } \alpha = m+1,\ldots,N. \end{cases} \tag{4.17}$$

This introduces a minus sign into Eq. (4.6). The subsequent steps are identical, with only the replacement of Eq. (4.11) by

$$\langle a|Q^\alpha_\beta|a\rangle = -\frac{1}{2}N_c\sigma_{\alpha\beta}. \tag{4.18}$$

Here, too, σ is given in terms of Λ and U by Eq. (4.12).

Using the Taylor expansion of the exponentials in Eq. (4.13) and noting that the exponential argument A anticommutes with Λ we have [1]

$$\sigma(a) = \begin{pmatrix} \cos\left(2\sqrt{aa^\dagger}\right) & -a\dfrac{\sin\left(2\sqrt{a^\dagger a}\right)}{\sqrt{a^\dagger a}} \\ -\dfrac{\sin\left(2\sqrt{a^\dagger a}\right)}{\sqrt{aa^\dagger}}\,a^\dagger & -\cos\left(2\sqrt{a^\dagger a}\right) \end{pmatrix}. \tag{4.19}$$

Here $a^\dagger a$ is a square matrix of dimension $N-m$ and $aa^\dagger$ is a square matrix of dimension m. Using the notation

$$\phi = a\frac{\sin\left(\sqrt{a^\dagger a}\right)}{\sqrt{a^\dagger a}}, \tag{4.20}$$

we have

$$U(\phi) = \begin{pmatrix} \sqrt{1-\phi\phi^\dagger} & -\phi \\ \phi^\dagger & \sqrt{1-\phi^\dagger\phi} \end{pmatrix}, \tag{4.21}$$

$$\sigma(\phi) = \begin{pmatrix} 1-2\phi\phi^\dagger & -2\phi\sqrt{1-\phi^\dagger\phi} \\ -2\sqrt{1-\phi^\dagger\phi}\phi^\dagger & -1+2\phi^\dagger\phi \end{pmatrix}. \tag{4.22}$$

---

[1] This generalizes a parametrization found in [77].

The representation given in Eqs. (4.21)–(4.22) is useful to treat fluctuations of order $1/N_c$, as will be seen in next chapter. Also for $m = N-1$ it coincides with the form given in [49], which in turn can be used to infer a generalized Holstein-Primakoff realization of the $U(N)$ generators (the ϕ operators then become the Holstein-Primakoff bosons). We note in passing that another useful representation given in [78] is related to Eqs. (4.21)–(4.22) ϕ by identifying $Z^\dagger = a \tan \sqrt{a^\dagger a}/\sqrt{a^\dagger a} = \phi/\sqrt{1-\phi^\dagger \phi}$.

4.2 Partition function and action

The partition function $Z = \mathrm{Tr}\, e^{-\beta H}$ with $\beta = 1/T$, can be written as a path integral by inserting the completeness relation (4.10) at every slice of imaginary time. This gives

$$Z = \int D\sigma \, \exp -S, \tag{4.23}$$

where the the action is

$$S = \int_0^\beta d\tau \left[\frac{1 - \langle a(\tau) | a(\tau + d\tau) \rangle}{d\tau} + H(\sigma(\tau)) \right]. \tag{4.24}$$

The Hamiltonian $H(\sigma)$ is a transcription of the quantum Hamiltonian to the classical σ matrices. Starting with the quantum operator $Q^\eta_{\boldsymbol{n}}$, we have

$$\begin{aligned} Q^\eta_{\boldsymbol{n}} &= \psi^\dagger_{\boldsymbol{n}} M^\eta \psi_{\boldsymbol{n}} = M^\eta_{\alpha\beta} \psi^\dagger_{\boldsymbol{n}} S^\alpha_\beta \psi_{\boldsymbol{n}} \\ &= M^\eta_{\alpha\beta} Q^\alpha_\beta(\boldsymbol{n}) + \frac{1}{2} N_c \mathrm{Tr}\, M^\eta. \end{aligned} \tag{4.25}$$

Expressed in these variables, the quantum Hamiltonian is[2]

$$H^{(2)}_{\mathrm{eff}} = \sum_{\substack{\boldsymbol{n}\mu \\ j \neq 0}} J_j Q^\eta_{\boldsymbol{n}} Q^\eta_{\boldsymbol{n}+j\hat{\boldsymbol{\mu}}} \left(s^\mu_\eta \right)^{j+1}. \tag{4.26}$$

where $J_j = (2/N_c) K(j)$. We transcribe this according to Eq. (4.11) to obtain the classical Hamiltonian,

$$H(\sigma) = \left(\frac{N_c}{2} \right)^2 \sum_{\substack{\boldsymbol{n}\mu \\ j \neq 0}} J_j \sigma^\eta_{\boldsymbol{n}} \sigma^\eta_{\boldsymbol{n}+j\hat{\boldsymbol{\mu}}} \left(s^\mu_\eta \right)^{j+1}, \tag{4.27}$$

---

[2] The B' term from Eq. (2.51) indeed disappears. We have dropped an additive constant that is independent of B'.

where

$$\sigma^{\eta}_{\boldsymbol{n}} = \mathrm{Tr}\, M^{\eta T} \sigma_{\boldsymbol{n}}. \tag{4.28}$$

Recall that each $\sigma_{\boldsymbol{n}}$ is an $N \times N$ matrix ranging over the coset space appropriate to site $\boldsymbol{n}$. We find it useful to write the interaction as

$$H(\sigma) = \frac{1}{2}\left(\frac{N_c}{2}\right)^2 \sum_{\boldsymbol{n},\mu} \left[\sum_{j \in \mathrm{odd}} J_j \,\mathrm{Tr}\, \sigma_{\boldsymbol{n}} \sigma_{\boldsymbol{n}+j\hat{\boldsymbol{\mu}}} + \sum_{j \in \mathrm{even}} J_j \,\mathrm{Tr}\, \sigma_{\boldsymbol{n}} \alpha_\mu \sigma_{\boldsymbol{n}+j\hat{\boldsymbol{\mu}}} \alpha_\mu \right], \tag{4.29}$$

where the three Dirac matrices α_μ have replaced the sign factors s^{η}_{μ}.

The time-derivative term in S is a Berry phase [46]. It can be expressed as follows

$$S_B = -\frac{N_c}{4} \int_0^\beta d\tau \int_0^1 du \,\mathrm{Tr}\, \left[\sigma(\tau,u)\, \partial_u \sigma(\tau,u)\, \partial_\tau \sigma(\tau,u) \right]. \tag{4.30}$$

Here $\sigma(\tau,u) = U(\tau,u)\Lambda\, U^\dagger(\tau,u)$ with

$$U(\tau,u) = e^{uA(\tau)}, \tag{4.31}$$

and obeys

$$\begin{aligned} \sigma(\tau,0) &= \sigma(\tau',0), && \forall \tau,\tau', && (4.32)\\ \sigma(\tau,1) &= \sigma(\tau), && \forall \tau, && (4.33)\\ \sigma(0,u) &= \sigma(\beta,u). && \forall u, && (4.34) \end{aligned}$$

This means that the τ–u plane is a disk with unit radius. τ plays the role of an angular variable, while u is the radial coordinate. Using Stokes theorem Eq. (4.30) is brought to the form

$$S_B(U) = -\frac{N_c}{2} \int_0^\beta d\tau \mathrm{Tr}\, \left(\Lambda U^\dagger(\tau)\, \partial_\tau U(\tau) \right). \tag{4.35}$$

It is interesting that Eq. (4.35) gives the same result even if U is a general $U(N)$ matrix, not restricted to the form of Eq. (4.13). To see that we write $U'(\tau,u) = U(\tau,u)V(\tau,u)$. Here $U' \in U(N)$, U is given by Eq. (4.31), and $V \in U(m) \times U(N-m)$,

$$V = \begin{pmatrix} \exp\left(uA_0^{(1)}(\tau)\right) & 0 \\ 0 & \exp\left(uA_0^{(2)}(\tau)\right) \end{pmatrix}. \tag{4.36}$$

U' and therefore V are continuous functions on the disk. Substituting U' into Eq. (4.35) one finds that

$$\Delta S_B = S_B(U') - S_B(U) = \frac{N_c}{2} \int \partial_\tau \left(\mathrm{Tr}\, \left(A_0^{(1)}\right) - \mathrm{Tr}\, \left(A_0^{(2)}\right) \right), \tag{4.37}$$

This means that ΔS_B is a an integer multiple of $i\pi N_c$. A non-zero value of ΔS_B is a result of winding the $U(1)$ factors of V on the disk boundary $u=1$. Such winding is however forbidden, since it means that V must have a discontinuity inside the disk. In fact the continuity of V means that $\det(V)$ must also be continuous, so $\forall u \in [0,1]$ one has

$$0=\int d\tau\,\partial_\tau\ \det V(\tau,u)=\int d\tau\,\partial_\tau\left(\log\det\exp\left(uA_0^{(1)}\right)+\log\det\exp\left(uA_0^{(2)}\right)\right). \tag{4.38}$$

Substituting Eq. (4.38) with $u=1$ into Eq. (4.37) we find that ΔS_B is an integer multiple of $i2\pi N_c$. Since N_c is an integer, $\exp\Delta S_B=1$, and $\exp S_B(U)=\exp S_B(U')$.[3]

Finally the lattice action is

$$S=\frac{N_c}{2}\int_0^\beta d\tau\left[-\sum_{\boldsymbol{n}}\operatorname{Tr}\Lambda_{\boldsymbol{n}}U_{\boldsymbol{n}}^\dagger\partial_\tau U_{\boldsymbol{n}}+\frac{2}{N_c}H(\sigma(\tau))\right]. \tag{4.39}$$

$\Lambda_{\boldsymbol{n}}$ will vary from site to site if m does. If one takes the route of Eq. (4.18) for a representation with $N-m$ rows, then the kinetic term for that site acquires a minus sign (see below).

The number of colors has largely dropped out of the problem, since σ is just an $N\times N$ unitary matrix field. The explicit factor of $N_c/2$ that multiplies the action invites a semiclassical approximation in the large-N_c limit which we do in Section 4.4. This of course neglects the N_c-dependence of the interaction term, but we recall that for $N_c\gg 1$, the couplings of the quantum Hamiltonian in Chapter 2 are $J_j\sim 1/\left(g^2N_c^2\right)$. This means that the couplings of the classical Hamiltonian in Eq. (4.29), multiplied by $2/N_c$ in Eq. (4.39) scale like $1/g^2N_c$, which we then fix when taking $N_c\to\infty$.

We conclude this section by noting that the form of the Berry phase of Eq. (4.39) is exactly the reason why the representation of σ and U in term of the variable ϕ given in Eq. (4.21) becomes useful. In terms of this variable the kinetic term becomes

$$S_B=\frac{N_c}{2}\int d\tau\sum_{\boldsymbol{n}}\operatorname{Tr}\left[\phi_{\boldsymbol{n}}^\dagger\cdot\partial_\tau\phi_{\boldsymbol{n}}-\partial_\tau\phi_{\boldsymbol{n}}^\dagger\cdot\phi_{\boldsymbol{n}}\right]. \tag{4.40}$$

This simple *quadratic* form is not obtained by expanding U in terms of a or Z.

4.3 The classical counterpart of the sigma model

In this section we make a pause from the discussion on the real quantum sigma model and investigate its classical counterpart by ignoring the Berry phase S_B. The classical sigma model provides us insight about the way the system behaves at high temperatures, where S_B should not be very important. Also, thermal fluctuations may partly replace the quantum fluctuations of the real system which, as discussed in Chapter 5, are very important.

---

[3] Nevertheless we will concentrate on U that has the form given in Eq. (4.13).

The classical model is much more accessible than the real quantum one because its action is real, and relying on convexity arguments, we can look for a mean field theory that mimics its dynamics. This classical action is also amenable to Monte Carlo simulations, but we defer any progress in that direction to future research.

The partition function of this classical model is given by

$$Z_{\text{classical}} = \int D\sigma \, e^{-\beta \, S_{\text{classical}}}, \tag{4.41}$$

in $d = 3$, with $S_{\text{classical}} = H(\sigma)$ defined by Eq. (4.29). In particular we concentrate on the nearest-neighbor (NN) theory only, and have

$$S_{\text{classical}} = \frac{J_1}{2} \left(\frac{N_c}{2} \right)^2 \sum_{\boldsymbol{n},\mu} \operatorname{Tr} \sigma_{\boldsymbol{n}} \sigma_{\boldsymbol{n}+\hat{\boldsymbol{\mu}}}. \tag{4.42}$$

Using mean field (MF) theory, we analyze a toy sigma model that has $N = 3$. We restrict to a set of configurations with different values of baryon number density n_B, and derive the classical MF phase diagram in the temperature-density plane. We will show that the MF ground states at zero temperature break the $U(3)$ symmetry, and that as we increase the temperature, thermal fluctuations melt the condensate and restore the symmetry above a certain temperature T_c. We will show that T_c decreases with increasing n_B.

4.3.1 Mean field theory

Our starting point to mean field theory is the partition function Eq. (4.41) that we rewrite

$$Z = \int D\sigma \; e^{-S_0(\sigma)} \times e^{-[S_{\text{classical}}(\sigma) - S_0(\sigma)]} \equiv Z_0 \cdot \langle \, e^{-[S_{\text{classical}}(\sigma) - S_0(\sigma)]} \, \rangle_0. \tag{4.43}$$

Here S_0 is a trial MF action, and Z_0 is its partition function. Also the brackets $\langle , \rangle_0$ denote the MF average of any functional A that depends on the sigma fields.

$$\langle \, A\left(\{\sigma_{\boldsymbol{n}}\}\right) \, \rangle_0 \equiv Z_0^{-1} \int D\sigma \; e^{-S_0(\sigma)} A\left(\{\sigma_{\boldsymbol{n}}\}\right). \tag{4.44}$$

Using standard convexity arguments one has

$$\langle\, e^{-[S_{\rm classical}-S_0]}\,\rangle \leq e^{-\langle\,[S_{\rm classical}-S_0]\,\rangle}. \tag{4.45}$$

This means that the free energy $F=-\log Z$ has a upper bound, and obeys the Bogoliubov inequality,

$$F \leq F_0 + \langle\, S_{\rm classical} - S_0\,\rangle_0 \equiv \Phi. \tag{4.46}$$

This bound is useful since we can now guess a MF action S_0, minimize it with respect to its parameters and obtain an evaluation for the real free energy of the system. The value of the upper bound Φ determines how close the MF guess is to capture the dynamics of the system.

In our case we choose the simplest possible MF action that corresponds to decoupling all the nearest-neighbor interactions in $S_{\rm classical}$. We first choose to proceed in the basis of $U(N)$ generators M^η that obey

$$\mathrm{Tr}\, M^\eta M^{\eta'} = \frac{1}{2}\delta_{\eta,\eta'}, \qquad \sum_\eta \left(M^\eta\right)_{ij}\left(M^\eta\right)_{kl} = \frac{1}{2}\delta_{il}\delta_{jk}. \tag{4.47}$$

In this basis the sigma field is given by its N^2 components σ^η,

$$\sigma = 2\sum_\eta \sigma^\eta M^{\eta T}, \tag{4.48}$$

and we write the MF action as

$$S_{\rm MF} = \beta J_1 \left(\frac{N_c}{2}\right)^2 \sum_{\mathbf{n}} \vec{\sigma}_{\mathbf{n}}\cdot\vec{h}_{\mathbf{n}}, \tag{4.49}$$

parametrized by the set $\vec{h}_{\mathbf{n}}$. The function Φ is then

$$\Phi = -\sum_{\mathbf{n}} \log\left\{\int d\sigma_{\mathbf{n}}\, e^{-K\vec{\sigma}_{\mathbf{n}}\cdot\vec{h}_{\mathbf{n}}}\right\} + K\sum_{\langle\mathbf{nm}\rangle}\vec{\mu}_{\mathbf{n}}\cdot\vec{\mu}_{\mathbf{n}} - K\sum_{\mathbf{n}}\vec{\mu}_{\mathbf{n}}\cdot\vec{h}_{\mathbf{n}}, \tag{4.50}$$

where the first contribution is F_0, and the next two terms correspond to $\langle\, S_{\rm classical}\,\rangle_0$ and $\langle\, S_0\,\rangle_0$. $K=\beta J_1\left(\frac{N_c}{2}\right)^2$ and $\vec{\mu}$ is the magnetization

$$\vec{\mu}_{\mathbf{n}} \equiv \frac{\int d\sigma_{\mathbf{n}} e^{-K\vec{\sigma}_{\mathbf{n}}\cdot\vec{h}_{\mathbf{n}}}\vec{\sigma}_{\mathbf{n}}}{\int d\sigma_{\mathbf{n}} e^{-K\vec{\sigma}_{\mathbf{n}}\cdot\vec{h}_{\mathbf{n}}}}. \tag{4.51}$$

Note that the integration measure $d\sigma_{\mathbf{n}}$ depends on the $U(N)$ representation chosen on site $\boldsymbol{n}$. We minimize Φ with respect to $\{\vec{h}_{\mathbf{n}}\}$ to obtain the MF equations,

$$\vec{\mu}_{\mathbf{n}} = \frac{\int d\sigma_{\mathbf{n}} e^{-K\vec{\sigma}_{\mathbf{n}}\cdot\sum_{\mathbf{m}(\mathbf{n})}\vec{\mu}_{\mathbf{m}}}\vec{\sigma}_{\mathbf{n}}}{\int d\sigma_{\mathbf{n}} e^{-K\vec{\sigma}_{bfn}\cdot\sum_{\mathbf{m}(\mathbf{n})}\vec{\mu}_{\mathbf{m}}}}, \tag{4.52}$$

which are extrema (in $\vec{\mu}$ space) of Φ. This allows us to write Φ as a function of $\vec{\mu}$ only,

$$\Phi = -\sum_{\mathbf{n}} \log\left\{\int d\sigma\, e^{-K\vec{\sigma}_{\mathbf{n}}\cdot\sum_{\mathbf{m}(\mathbf{n})}\vec{\mu}_{\mathbf{m}}}\right\} - K\sum_{\langle\mathbf{nm}\rangle}\vec{\mu}_{\mathbf{n}}\cdot\vec{\mu}_{\mathbf{m}}. \tag{4.53}$$

The MF equations Eq. (4.52) and the function Φ in Eq. (4.53) constitute our classical MF theory. For each value of $K \sim 1/T$, Φ has a set of extrema points that obey the MF equations. A subset of these are minima that correspond to classical ground states of the MF theory. The magnetizations, $m_{\mathbf{n}} = 2\vec{\mu}_{\mathbf{n}}\cdot\vec{M}^T$, of each minimum determine the symmetry properties of the corresponding ground state.

4.3.2 The toy model of $U(3)$

The $N_f = 1$ theory is a $U(4)$ antiferromagnet and contains many degrees of freedom in which to do mean field theory. We treat the *simplest* non-trivial model which is a toy model with $U(3)$ symmetry. It does not correspond to an actual value of N_f, but allows for analytical evaluation of the MF quantities. The most symmetric $B = 0$ state in this model cannot have $B = 0$ on every site, but must alternate between the representations corresponding to $B = \pm 1/2$ (see Fig. 4.1). Increasing B is done by replacing some of the $B = -1/2$ representations with $B = +1/2$ representations as in Fig. 4.3.2. Another option is to replace either $B = -1/2$ representations or $B = +1/2$ representations by $U(3)$ singlets with $B = +3/2$ and three rows.

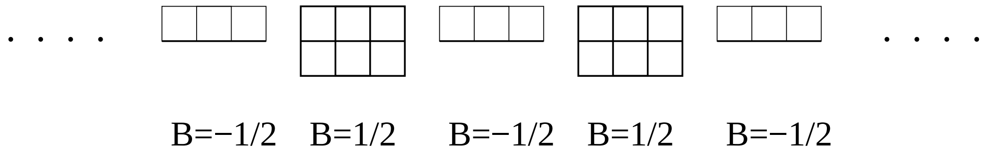

Figure 4.1: The most symmetric $B = 0$ state in the $U(3)$ toy model

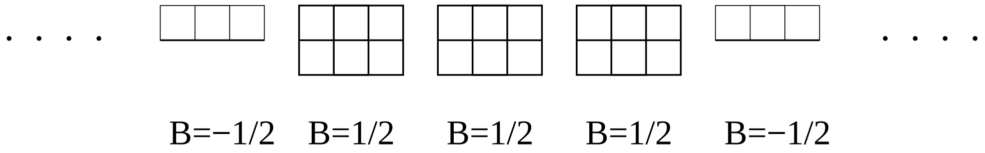

Figure 4.2: Adding a baryon in the $U(3)$ toy model.

As mentioned, several MF theory quantities such as Φ can be calculated analytically for this toy model. The reason is that for $N = 3$, and $m = 2$, Eq. (4.13) takes the simple form

$$U_{\boldsymbol{n}} = \exp\begin{pmatrix} 0 & 0 & a_1 \\ 0 & 0 & a_2 \\ -a_1^* & -a_2^* & 0 \end{pmatrix}. \tag{4.54}$$

We use the definitions

$$\begin{aligned} a_1 &= \rho\cos(\theta/2)e^{i\alpha_1}, \\ a_2 &= \rho\sin(\theta/2)e^{i\alpha_2}, \end{aligned} \tag{4.55}$$

with $0 < \rho < \pi$, $0 < \theta < \pi$ and $0 < \alpha_{1,2} < 2\pi$, and get

$$\vec{\sigma} = -2\begin{pmatrix} -\frac{1}{\sqrt{6}} \\ \sin^2\rho\,\sin\theta\,\cos\phi \\ -\sin^2\rho\,\sin\theta\,\sin\phi \\ \sin^2\rho\,\cos\theta \\ \sin2\rho\,\cos\theta/2\,\cos(\frac{1}{2}(\psi+\phi)) \\ -\sin2\rho\,\cos\theta/2\,\sin(\frac{1}{2}(\psi+\phi)) \\ \sin2\rho\,\sin\theta/2\,\cos(\frac{1}{2}(\psi-\phi)) \\ -\sin2\rho\,\sin\theta/2\,\sin(\frac{1}{2}(\psi-\phi)) \\ -\sqrt{3}(\cos^2\rho-\frac{1}{3}) \end{pmatrix}, \tag{4.56}$$

here $\phi \equiv \alpha_1 - \alpha_2$ and $\psi = \alpha_1 + \alpha_2$, with $0 < \psi < 4\pi$ and $0 < \phi < 2\pi$.

At zero density we assume that the magnetizations on even and odd sites are $\vec{\mu}_1$ and $\vec{\mu}_2$ respectively. This results in the following MF equations

$$\vec{\mu}_1 = \frac{\int d\sigma e^{-6K\vec{\sigma}\cdot\vec{\mu}_2}\vec{\sigma}}{\int d\sigma e^{-6K\vec{\sigma}\cdot\vec{\mu}_2}}, \tag{4.57}$$

$$\vec{\mu}_2 = -\frac{\int d\sigma e^{+6K\vec{\sigma}\cdot\vec{\mu}_1}\vec{\sigma}}{\int d\sigma e^{+6K\vec{\sigma}\cdot\vec{\mu}_1}}. \tag{4.58}$$

The measure of the manifold $U(3)/U(2) \times U(1)$ is the measure of the manifold of 3×3 hermitian matrices $d\vec{\sigma}$ modified to account for the dependence (4.56) of $\vec{\sigma}$ on the manifold coordinates. The induced metric of the space is

$$g_{\alpha\beta}^{\text{induced}} = \sum_{\mu,\nu} g_{\mu\nu} \cdot \frac{\partial \sigma_\mu}{\partial \theta_\alpha} \frac{\partial \sigma_\nu}{\partial \theta_\beta}, \tag{4.59}$$

where $g_{\mu\nu} = \delta_{\mu\nu}$, and the coordinates θ_α are the coset coordinates that appear in σ^μ. The measure of integration is thus

$$d\sigma = d\vec{\theta} \sqrt{\det(g_{\text{induced}})}. \tag{4.60}$$

For $U(3)/U(2) \times U(1)$, we find that

$$d\sigma = d(\sin^4\rho)\, d(\cos\theta)\, \frac{d\phi}{2\pi} \frac{d\Psi}{4\pi}. \tag{4.61}$$

In order to solve the MF equations we choose a basis that diagonalizes $m_1 \equiv 2 \sum_\eta \mu_1^\eta M^{\eta T}$. Since the measure in the angles Ψ and ϕ is flat, $m_2 \equiv 2 \sum_\eta \mu_2^\eta M^{\eta T}$ is diagonal as well, and only μ_2^0, μ_2^3, and μ_2^8 are non-zero. Since μ^0 is fixed [see Eq. (4.56)], one is left with the following MF equations for $\vec{\mu}_i = (\mu_i^3, \mu_i^8)$ with $i = 1, 2$,

$$\mu_1^3 = f_3(6K\mu_2^3, 6K\mu_2^8), \qquad \mu_1^8 = f_8(6K\mu_2^3, 6K\mu_2^8), \tag{4.62}$$

$$\mu_2^3 = -f_3(-6K\mu_1^3, -6K\mu_1^8), \qquad \mu_2^8 = -f_8(-6K\mu_1^3, -6K\mu_1^8). \tag{4.63}$$

Here

$$\begin{aligned} f_3(x,y) &= \left[\frac{e^{x_+}}{x_+} + \frac{e^{x_-}}{x_-} - \frac{e^{x_-} - 1}{x_-}\left(\frac{1}{x^3} - \frac{1}{x_-}\right) - \frac{e^{x_+} - 1)}{x_+}\left(\frac{1}{x^3} + \frac{1}{x_+}\right)\right] \times \\ &\qquad \left[\frac{e^{x_-} - 1}{x_-} - \frac{e^{x_+} - 1}{x_+}\right]^{-1}, \end{aligned} \tag{4.64}$$

$$\begin{aligned} f_8(x,y) &= \frac{2}{\sqrt{3}} + \sqrt{3}\left[\frac{e^{x_+}}{x_+} - \frac{e^{x_-}}{x_-} - \frac{e^{x_+} - 1}{x_+^2} + \frac{e^{x_-} - 1)}{x_-^2}\right] \times \\ &\qquad \left[\frac{e^{x_-} - 1}{x_-} - \frac{e^{x_+} - 1}{x_+}\right]^{-1}, \end{aligned} \tag{4.65}$$

with $x_\pm = \sqrt{3}y \pm x$.

We use Eq. (4.62) to evaluate $\Phi(\vec{\mu}_i)$ as a function of $\vec{\mu}_2$,

$$\begin{aligned} \Phi(\vec{\mu}_i)/N_s &= -3K\ \vec{\mu}_1 \cdot \vec{\mu}_2 - 2K\sqrt{3}(\mu_1^8 - \mu_2^8) - \varphi(6K\ \vec{\mu}_i), \quad (4.66) \\ \varphi(\vec{x}_i) &= \frac{1}{2}\left[\log\left(\frac{e^{-x_{+,1}}-1}{x_{+,1}x_1^3} - \frac{e^{-x_{-,1}}-1}{x_{-,1}x_1^3}\right) - \log\left(\frac{e^{x_{+,2}}-1}{x_{+,2}x_2^3} - \frac{e^{x_{+,2}}-1}{x_{+,2}x_2^3}\right)\right]. \quad (4.67) \end{aligned}$$

Here N_s is the number of sites and $x_{\pm,i} = \sqrt{3}\mu_i^8 \pm \mu_i^3$. It is easy to check that the MF equations have a symmetric solution with $\vec{\mu}_2 = 0$ (and hence $\vec{\mu}_1 = 0$) for all values of K. The magnetizations of this solution are

$$m_1 = -m_2 \sim \mathbf{1}, \tag{4.68}$$

and are invariant under $U(3)$. As we increase K, three additional nontrivial minima appear. In the μ^3–μ^8 plane, the solutions are found on the following three lines.

$$\begin{aligned} \mu_i^3 &= 0, && (4.69) \\ \mu_i^3 &= +\sqrt{3}\mu_i^8, && (4.70) \\ \mu_i^3 &= -\sqrt{3}\mu_i^8, && (4.71) \end{aligned}$$

They have the same Φ. The magnetizations of each solutions are invariant under a certain $U(2) \times U(1)$ subgroup of $U(3)$. For example the solution with $\mu^3 = 0$ has

$$m_1 \sim -m_2 \sim \begin{pmatrix} 1 & 0 & 0 \\ 0 & 1 & 0 \\ 0 & 0 & -2 \end{pmatrix}. \tag{4.72}$$

For $K > K_c$ these solutions have lower free energy than the symmetric solution (4.68) and $U(3)$ is spontaneously broken to $U(2) \times U(1)$. In Fig. 4.3 we present Φ on the line $\mu_2^3 = 0$ for $K/K_c = 0.98, 1, 1.02$. We find that there exists a first order phase transition at $K_c = 0.9$.

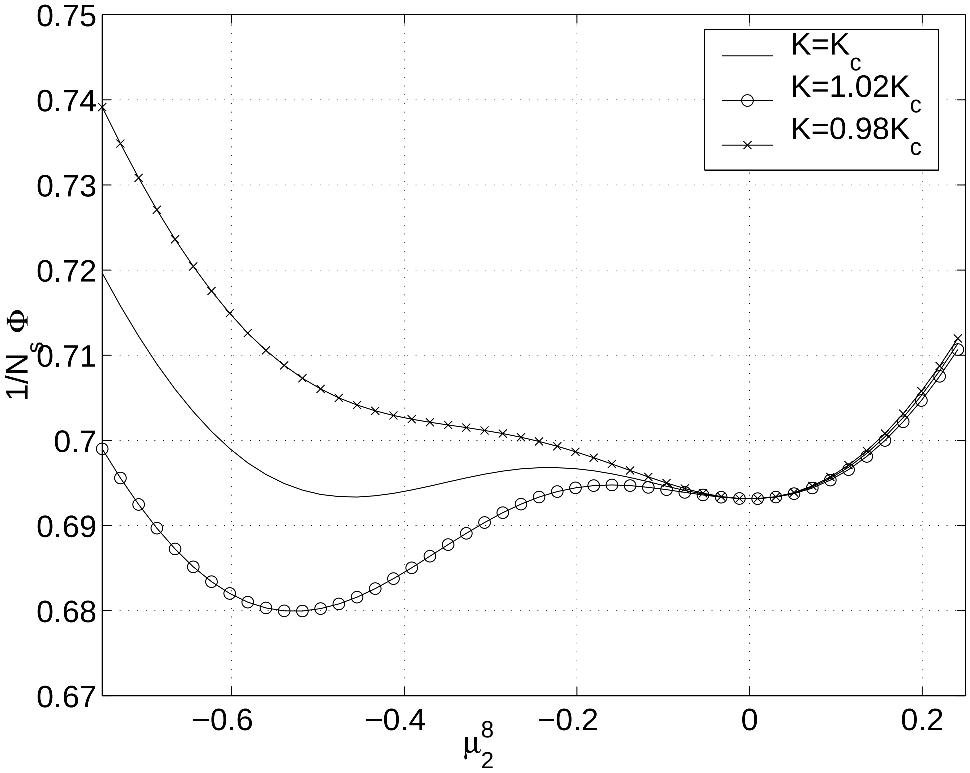

Figure 4.3: Φ for zero density near the first order phase transition.

Next we performed the MF analysis for a set of configurations that have non-zero baryon number. We construct these by putting net baryon number on the sites of 2 × 2 × 2 unit cells. This set is listed in Table 4.1, where we give a pictorial description of the unit cells of each configuration.

Table 4.1: The set of configurations with different baryon number density for the $U(3)$ toy model. Here $\rho_{\max} = 3/2$. A ± represents $B = \pm 1/2$, and a • represents $B = +3/2$ with $\sigma = \mathbf{1}$.

Configuration	$\rho/\rho_{\max}$	Unit cell	K_c
1	0	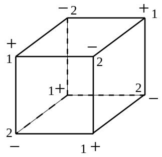	0.9
2	$\frac{1}{12}$	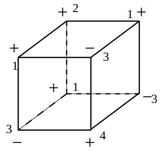	0.94
3	$\frac{1}{6}$	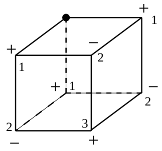	1.03
4	$\frac{1}{3}$	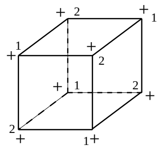	1
5	$\frac{5}{12}$	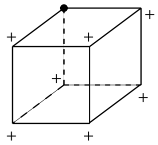	1.14

Table 4.1: (continued)

Configuration	$\rho/\rho_{\max}$	Unit cell	K_c
6	$\frac{7}{12}$	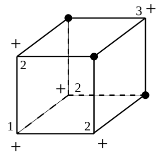	1.72
7	$\frac{2}{3}$	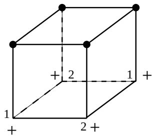	1.5
8	$\frac{5}{6}$	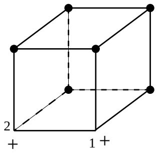	3

The numbering of the sites in the unit cells denotes the magnetization distribution of the ansatz used for each configuration. For example, in configuration no. 1 the ansatz consists of having two magnetizations denoted by m_1 and m_2 on the even and odd sites denoted by 1 and 2. We present the MF equations and corresponding Φ's for all configurations in Appendix D.

Except for configuration no. 2, the MF equations are consistent with the assumption that all magnetizations commute and are diagonalized simultaneously. Therefore as for zero baryon number, the MF equations and Φ's can be written for μ^3, and μ^8 only. Also, in all these configurations Φ becomes a function of two variables, allowing a simple graphical minimization of Φ. For configuration no. 2 Φ is a function of four variables, and we make an ansatz that only μ^8 is non-zero in order to treat this case graphically as well.

Except for the symmetric solution that exists for all values of K, nontrivial minima of Φ appear on the lines (4.69)–(4.71). In configurations 3, 5, 6 one has three equivalent minima that have the same symmetry and Φ. As for zero baryon number $U(3)$ is spontaneously broken to $U(2) \times U(1)$ above a certain value of K, and the phase transition is first order. We give the values of K_c in Table 4.1. In configurations 4, 7, 8 we find six minima.

Four of these correspond to breaking $U(3)$ into $U(2) \times U(1)$, and the remaining two correspond to breaking $U(3)$ to $U(1) \times U(1) \times U(1)^4$. All six solutions have the same Φ, and become preferable over the symmetric solution above the same value of K_c. Here the phase transition is second order, and we illustrate it in Fig. 4.4 where we plot Φ on the line (4.32) for $K/K_c = 0.8, 1, 1.16$ (for configuration 4).

As mentioned, for configuration no. 2 we take an ansatz that $\mu^3 = 0$, and find similar behavior to that of the zero density system. In view of what happens in the other cases, we believe that there are at least two more equivalent minima with the same free energy and the same symmetry properties. There is also a possibility that there are other nonequivalent minima, with different symmetries as in configurations 4, 7, 8.

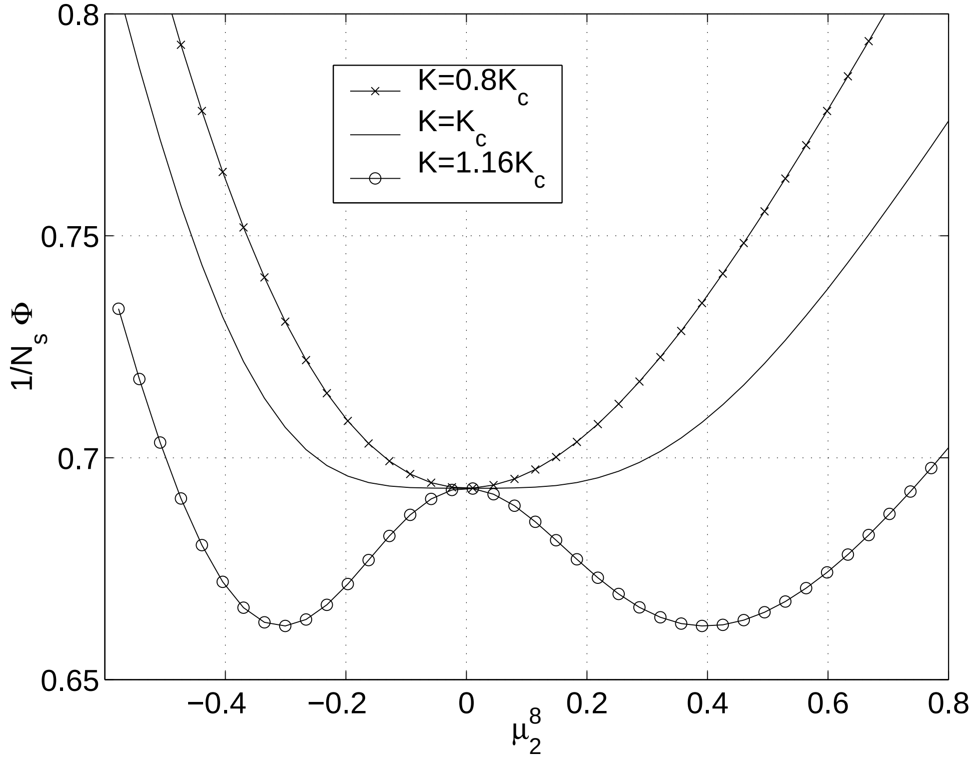

Figure 4.4: Φ for non-zero density near the second order phase transition.

We give the results of these MF calculation in the phase diagram of Fig. 4.5. Increasing

---

[4] This is the symmetry of the ground state of the *quantum* sigma model at these configurations, as predicted in the large N_c limit. See Chapter 5.

the baryon number density decreases the transition temperature. Note however that we do not find a restoration of the symmetry at zero temperature for any density since this is a MF theory which always breaks the symmetry at $T = 0$, even at one dimension.

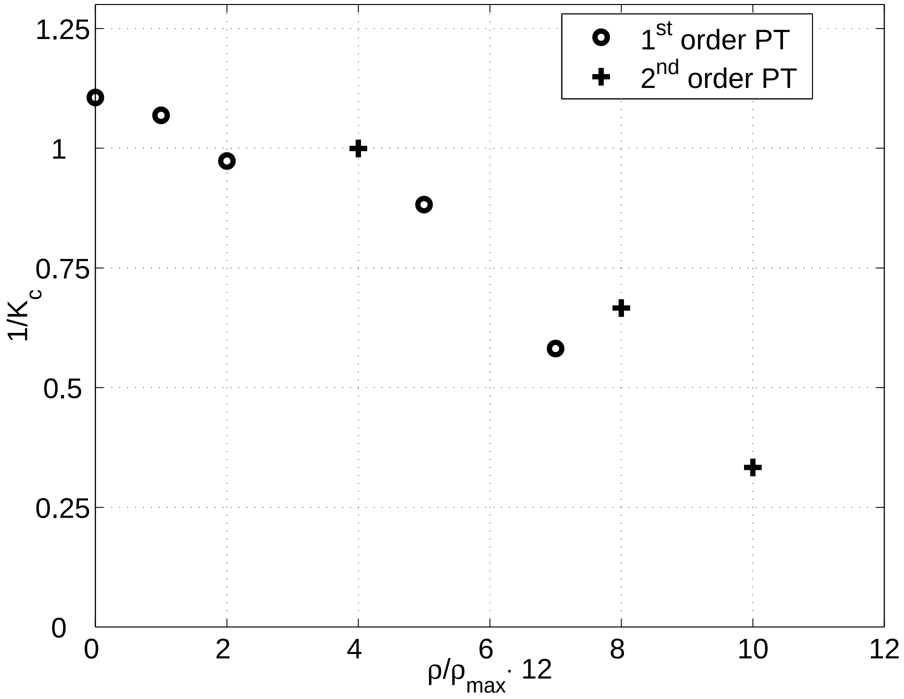

Figure 4.5: Classical phase diagram of the $U(3)$ antiferromagnet at finite temperature and density. We find that when the phase transition is second order, $U(3)$ is spontaneously broken either to $U(2) \times U(1)$ or $U(1) \times U(1) \times U(1)$. In all other cases $U(3)$ is broken to $U(2) \times U(1)$.

4.4 The semiclassical large N_c limit

We now treat the full quantum sigma model in the large N_c limit by performing a saddle point evaluation of the ground state of the system. We will see that the ground state is degenerate. For $B = 0$ this degeneracy is discrete, while for $B > 0$ the ground state has a huge continuous degeneracy, exponential in the lattice volume. In general these degeneracies are removed only by $1/N_c$ corrections that we calculate in the next chapter.

4.4.1 Zero density

The simplest way to set the baryon density to zero is just to choose $B_{\boldsymbol{n}} = 0$ on each site, meaning $m = N/2 = 2N_f$ (see Fig. 4.6). It turns out to be just as easy to consider a slightly generalized case [21], in which $B_{\boldsymbol{n}}$ is chosen to alternate, $B_{\boldsymbol{n}} = \pm b$, on even and odd sublattices (see Fig .4.7). This means to choose a representation with $m = N/2 + b$ rows on even sites and $N - m = N/2 - b$ rows on odd sites, which gives a pair of conjugate representations of $U(N)$. In view of Eq. (4.18), we can substitute $\sigma \to -\sigma$ on the odd sites and thus have identical manifolds on all sites. The Hamiltonian is then

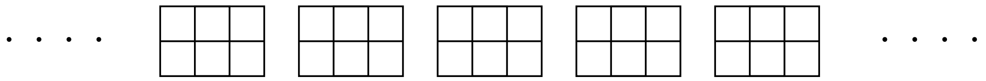

Figure 4.6: $B = 0$ configuration, for the case of $N_f = 1$.

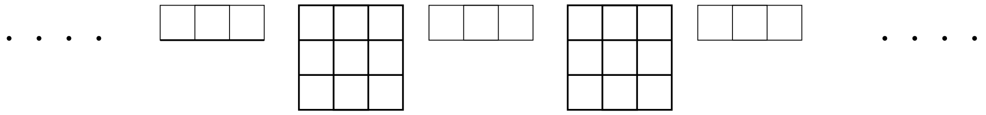

Figure 4.7: $B = 0$ state, for the case of $N_f = 1$, and $b = \pm 1$.

$$H(\sigma) = \left(\frac{N_c}{2}\right)^2 \sum_{\substack{\boldsymbol{n}\mu \\ j\neq 0}} J_j (-1)^j \sigma^\eta_{\boldsymbol{n}} \sigma^\eta_{\boldsymbol{n}+j\hat{\boldsymbol{\mu}}} \left(s^\mu_\eta\right)^{j+1}. \tag{4.73}$$

m is a new parameter in the theory, and we can ask what value of m gives the lowest energy for the ground state.

In the large-N_c limit, we seek the classical saddle point[5] of S. We assume the saddle is at a configuration $\sigma_{\boldsymbol{n}}(\tau)$ that is independent of time, and so we drop the time derivative. We begin with the nearest-neighbor Hamiltonian,[6]

$$\begin{aligned} H &= -J_1 \left(\frac{N_c}{2}\right)^2 \sum \sigma^\eta_{\boldsymbol{n}} \sigma^\eta_{\boldsymbol{n}+\hat{\boldsymbol{\mu}}} \\ &= -\frac{J_1}{2} \left(\frac{N_c}{2}\right)^2 \sum \operatorname{Tr} \sigma_{\boldsymbol{n}} \sigma_{\boldsymbol{n}+\hat{\boldsymbol{\mu}}}. \end{aligned} \tag{4.74}$$

---

[5] Note that the kinetic term is pure imaginary.

[6] This classical Hamiltonian is ferromagnetic; the antiferromagnetic nature of the quantum Hamiltonian (4.26) is preserved by the alternating signs in the time-derivative term.

Again, the matrices $\sigma_{\boldsymbol{n}}$ are Hermitian and unitary, and the expansion coefficients $\sigma^\eta_{\boldsymbol{n}}$ are real and satisfy $\sum(\sigma^\eta)^2 = N/2$. The minimum of H is clearly at a constant field, $\sigma_{\boldsymbol{n}} = \sigma_0$, which can be diagonalized to $\sigma_{\boldsymbol{n}} = \Lambda$ by a $U(N)$ rotation. This is a Néel state in the original variables. The $U(N)$ symmetry is broken to $U(m) \times U(N-m)$ and there are $2m(N-m)$ Goldstone bosons.

The classical energy density (per link) is $\epsilon_0 = -J_1 N_c^2 N/8$, independent of m. Thus at leading order in $1/N_c$, the optimal value of m is undetermined, and any alternating background of baryon number is equally good.

Since it turns out that the $1/N_c$ corrections select $m = N/2$ [see Section 5.1 let us consider the effect of the next-nearest-neighbor (NNN) term in H for this case only. The perturbation is

$$H' = J_2 \left(\frac{N_c}{2}\right)^2 \sum_{\boldsymbol{n}\mu} \sigma^\eta_{\boldsymbol{n}} \sigma^\eta_{\boldsymbol{n}+2\hat{\boldsymbol{\mu}}} s^\mu_\eta. \tag{4.75}$$

It breaks the $U(N)$ symmetry to $SU(N_f)_L \times SU(N_f)_R \times U(1)_A \times U(1)_B$. Assuming that $J_2 \ll J_1$, we again seek the minimum energy configuration in the form of a constant field; we minimize

$$\epsilon_2 = \sum_{\mu\eta} \sigma^\eta \sigma^\eta s^\mu_\eta \tag{4.76}$$

among the $U(N)$-equivalent $\sigma = \sigma_0$ states that minimize the nearest-neighbor action. It is not hard to show (see Appendix C) that ϵ_2 is minimized for $\sigma = \gamma_0 \otimes \mathbf{1}$. This is a condensate that is symmetric under the vector generators $M^\eta = \mathbf{1} \otimes \lambda^a$ but not under the axial generators $\gamma_5 \otimes \lambda^a$, and thus it breaks the chiral symmetry to the vector subgroup, $SU(N_f)_V \times U(1)_B$.

It is interesting to note that the discrete degeneracy in the number m can be removed at $O(1/N_c^0)$ as well by the NNN terms themselves. To see this we calculate the NNN energy Eq. (4.76) for the configurations that minimize the NN enegry Eq. (4.74). It is easiest to do the calculation by writing the NNN energy in terms of the Dirac matrices α_μ as

$$\epsilon_2 = \frac{1}{2} \sum_\mu \mathrm{Tr}\, [\sigma \alpha_\mu \sigma \alpha_\mu]. \tag{4.77}$$

We show in Chapter 6 [Eq. (6.13)] that Eq. (4.77) has a lower bound

$$\epsilon_2 \geq \frac{3}{2}(4m - 3N), \tag{4.78}$$

which means that the energy from NN and NNN interactions is bounded by

$$E(m) \geq \frac{3N_c^2}{8} \left[-J_1 N + \frac{J_2}{2}(4m - 3N)\right]. \tag{4.79}$$

Since $m \geq N/2$ then $E(m) \geq E(N/2)$. In Appendix C we show that the ground state for $m = N/2$ saturates $E(N/2) = -3N/2$. This means that the ground state of $m = N/2$, is also the overall ground state (out of values of m). As a result we find that the discrete degeneracy of the classical NN energy in the number m is removed by NNN as well as by $1/N_c$ corrections.

4.4.2 Non-zero density

The zero-density theories considered in the preceding section were defined by selecting representations with m and $N - m$ rows on alternating sites. For any m, this led to a σ model with identical degrees of freedom on all sites—after redefinition of the spins on the odd sublattice—and ferromagnetic couplings.[7] We eventually settled on $m = N/2$ as the background that gives the ground state of lowest energy.

Introducing non-zero baryon density means changing m on some sites of the lattice. Choosing a different representation adds (or subtracts) baryons on a site-by-site basis. For instance, we can add a single baryon by adding a row to the Young tableau as in Fig. 4.8. Since in general there will be representations on different sites that are not mutually conjugate, different sites will carry σ variables that do not live in the same submanifold of $U(N)$. We here limit ourselves to the simpler case of uniform m, where adjacent sites carry identical spins—but the coupling is *antiferromagnetic.*

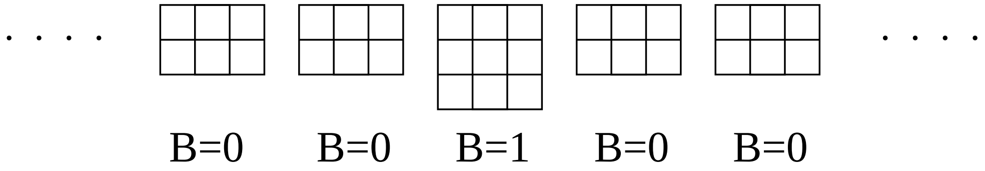

Figure 4.8: Adding one baryon to a site in the $N_f = 1$ theory [a $U(4)$ antiferromagnet]

In order to learn how to work with such a theory, we begin by studying the two-site problem. The results of this study will lead directly to an *ansatz* for the ground state of a lattice with a fixed density of baryons.

---

[7] The $(-1)^n$ factor in the kinetic energy retained information about the antiferromagnetic nature of the quantum problem; it did not affect the classical analysis.

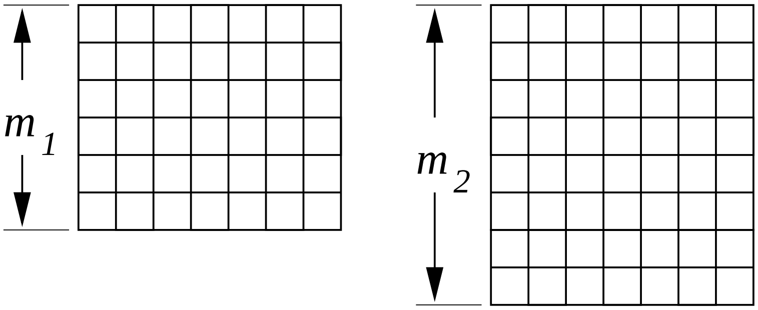

Figure 4.9: Two sites that carry $U(N)$ representations with m_1 and m_2 rows.

Two site problem

Consider, therefore, two sites with quantum spins Q_1 and Q_2 that carry representations of $U(N)$ with m_1 and m_2 rows, and N_c columns (see Fig. 4.9).

The quantum Hamiltonian is

$$H = J_1 \sum_\eta Q_1^\eta Q_2^\eta, \tag{4.80}$$

an antiferromagnetic coupling. The corresponding classical σ model has the interaction Hamiltonian

$$H(\sigma) = \frac{J_1}{2} \left(\frac{N_c}{2}\right)^2 \operatorname{Tr} \sigma_1 \sigma_2, \tag{4.81}$$

where

$$\sigma_i = U_i \Lambda_i U_i^\dagger. \tag{4.82}$$

The two Λ matrices reflect the different values of m_i according to

$$\Lambda_i = \begin{pmatrix} \mathbf{1}_{m_i} & 0 \\ 0 & -\mathbf{1}_{N-m_i} \end{pmatrix}. \tag{4.83}$$

The $N_c \to \infty$ limit is the classical limit, in which we seek values of $\sigma_{1,2}$ that minimize $H(\sigma)$. A global $U(N)$ rotation, *viz.*,

$$\sigma_i \to V \sigma_i V^\dagger, \tag{4.84}$$

can be used to diagonalize σ_1 so that $\sigma_1 = \Lambda_1$. Now we have to minimize $\operatorname{Tr} \Lambda_1 \sigma_2$. The case of conjugate representations, $m_2 = N - m_1$, is easy: σ_2 is a unitary rotation of Λ_2, which (in this case) can be rotated into $-\Lambda_1$. This is the unique antiferromagnetic ground state. σ_1 and σ_2 can be copied to the odd and even sublattices of an infinite lattice to give the classical Néel state considered in the preceding section.

The case $m_1 = m_2 = m$ is more complex. We consider $m > N/2$ for definiteness; the other case is similarly handled. We write explicitly

$$\sigma_2 = \begin{pmatrix} \cos\left(2\sqrt{aa^\dagger}\right) & -a\dfrac{\sin\left(2\sqrt{a^\dagger a}\right)}{\sqrt{a^\dagger a}} \\ -\dfrac{\sin\left(2\sqrt{a^\dagger a}\right)}{\sqrt{aa^\dagger}}\, a^\dagger & -\cos\left(2\sqrt{a^\dagger a}\right) \end{pmatrix}. \tag{4.85}$$

Since σ_2 is a rotation of Λ,

$$2m - N = \mathrm{Tr}\,\sigma_2 = \mathrm{Tr}\,\cos\left(2\sqrt{aa^\dagger}\right) - \mathrm{Tr}\,\cos\left(2\sqrt{a^\dagger a}\right), \tag{4.86}$$

and hence the energy is

$$E = \frac{J_1}{2}\left(\frac{N_c}{2}\right)^2 \mathrm{Tr}\,\Lambda\sigma_2 \tag{4.87}$$

$$= J_1\left(\frac{N_c}{2}\right)^2 \left[\mathrm{Tr}\,\cos\left(2\sqrt{a^\dagger a}\right) + m - N/2\right]. \tag{4.88}$$

E is minimized when all the eigenvalues of $a^\dagger a$ are equal to $\pi^2/4$. This means that the $N-m$ column vectors $\boldsymbol{a}_i$ form an orthogonal set in m dimensions, with

$$\boldsymbol{a}_i^\dagger \cdot \boldsymbol{a}_j = \left(\frac{\pi}{2}\right)^2 \delta_{ij}. \tag{4.89}$$

Since $m > N - m$ by assumption, such a set of vectors can always be found.

Since $a^\dagger a = (\pi^2/4)\mathbf{1}_{N-m}$, we have $\sin\left(2\sqrt{a^\dagger a}\right) = 0$ and so the off-diagonal blocks of Eq. (4.85) vanish. The lower-right block of σ_2 is the unit matrix $\mathbf{1}_{N-m}$. We know that $(\sigma_2)^2 = 1$ since $\Lambda^2 = 1$ and thus the upper-left block must have eigenvalues ± 1. Equating traces of σ_2 and Λ, we find that the upper-left $m \times m$ block must take the form

$$\sigma^{(m)} = U^{(m)}\Lambda^{(m)}U^{(m)\dagger}, \tag{4.90}$$

where

$$\Lambda^{(m)} = \begin{pmatrix} \mathbf{1}_{2m-N} & 0 \\ 0 & -\mathbf{1}_{N-m} \end{pmatrix} \tag{4.91}$$

and $U^{(m)} \in U(m)$. $\sigma^{(m)}$ represents the coset $U(m)/[U(2m-N) \times U(N-m)]$.

We conclude that the classical ground state of this $B \neq 0$ two-site problem is degenerate, even beyond breaking the overall $U(N)$ symmetry. The solutions can be written as

$$\begin{aligned} \sigma_1 &= \Lambda_1 = \begin{pmatrix} \mathbf{1}_m & 0 \\ 0 & -\mathbf{1}_{N-m} \end{pmatrix}, \\ \sigma_2 &= \begin{pmatrix} \sigma^{(m)} & 0 \\ 0 & \mathbf{1}_{N-m} \end{pmatrix} \end{aligned} \tag{4.92}$$

(to which a global $U(N)$ rotation can be applied). A particular instance of $\sigma^{(m)}$ is $\Lambda^{(m)}$, given by Eq. (4.91). The symmetry of the vacuum is the set of rotations that leaves both σ_1 and σ_2 invariant, namely, $U(2m-N) \times U(N-m) \times U(N-m)$.

Infinite lattice

At $N_c = \infty$ we seek the saddle point of the action, which we assume to be a time-independent configuration. The classical Hamiltonian of the σ model is

$$H = \frac{J_1}{2} \left(\frac{N_c}{2} \right)^2 \sum_{\boldsymbol{n},\mu} \operatorname{Tr} \sigma_{\boldsymbol{n}} \sigma_{\boldsymbol{n}+\hat{\boldsymbol{\mu}}}. \tag{4.93}$$

Seeking an antiferromagnetic ground state, we set $\sigma_{\boldsymbol{n}} = \Lambda$ on the sublattice of even sites. The odd sites are then governed by

$$H^{\text{odd}} = J_1 d \left(\frac{N_c}{2} \right)^2 \sum_{\boldsymbol{n} \text{ odd}} \operatorname{Tr} \Lambda \sigma_{\boldsymbol{n}}. \tag{4.94}$$

This is just the two-site problem studied above, replicated over the lattice. As we saw above, the ground state energy is degenerate with respect to the configuration at each odd site,

$$\sigma_{\boldsymbol{n}} = \begin{pmatrix} \sigma^{(m)}_{\boldsymbol{n}} & 0 \\ 0 & \mathbf{1}_{N-m} \end{pmatrix}, \tag{4.95}$$

and we find that at $N_c = \infty$ there is a large number of ground state configurations with the same classical energy, that differ in the choice $\sigma^{(m)}_{\boldsymbol{n}}$ on each of the odd sites. These ground states are continuously connected by the coordinates of $\sigma^{(m)}_{\boldsymbol{n}}$ that furnish $U(m)/[U(2m-N) \times U(N-m)]$. They have different realizations of the global symmetry of $U(N)$; A uniform choice for the odd sites, $\sigma^{(m)}_{\boldsymbol{n}} = \Lambda^{(m)}$ for instance, breaks the $U(N)$

symmetry to $U(2m-N)\times U(N-m)\times U(N-m)$; a non-uniform choice can break the symmetry all the way to $U(N-m)$. Furthermore, one can contemplate making a non-uniform *ansatz* for the *even* spins as well. The entropy of this classical ground state is evidently proportional to the volume.

The situation is reminiscent of that in the antiferromagnetic Potts model [79]. The crucial difference is, however, that here the degeneracy is continuous, and the sigma fields are allowed to oscillate around the classical ground state, even at zero temperature. In fact this makes the problem more similar to problems encountered in condensed matter physics in the context of frustrated magnetic systems. These systems are known to experience the phenomenon of "order from disorder", [52, 53, 54, 55, 56, 57] where fluctuations remove a classical degeneracy and choose a ground state. We discuss how order from disorder happens in our problem in Chapter 5. There we show that when $N_c=\infty$, and one keeps $\sigma_{\boldsymbol{n}}$ on the even sites fixed to be Λ, it costs no energy to change $\sigma_{\boldsymbol{n}}$ on an odd site by changing its direction within $U(m)/[U(2m-N)\times U(N-m)]$. Fluctuations in these directions are "zero modes" and have zero energy for any momentum. In principle they can lead to instabilities of the classical ground state, but as we will show, order from disorder gives the zero modes non-zero energy of $O(1/N_c)$, removes the classical degeneracy, and stabilizes a canted ground state in which all the even sites point to Λ, and *all* the odd sites align uniformly to have the same $\sigma^{(m)}$.

A final note here is that different from the zero baryon case, the NNN interactions do not remove the degeneracy of the NN theory. In particular the zero modes are not removed when one takes a non-zero value for J_2. This can be seen in Section 6.3 that gives the dispersion relations of excitations in the sigma model with NN and NNN interaction. Taking $N_c=\infty$ and keeping $J_2\neq 0$ still results in zero modes.

Chapter 5

Quantum fluctuations in the nonlinear sigma model

In this chapter we investigate the effects that quantum fluctuations of $O(1/N_c)$ have on the classical ground state of the NLSM introduced in Chapter 4. We restrict ourselves to nearest-neighbor interactions only and show that the degeneracies present in the classical $N_c = \infty$ limit are removed at this order. We first show that for zero baryon density fluctuations remove the discrete degeneracy in the parameter m [See Section 4.4.1] and choose the configuration that has zero baryon number on each site. We proceed to perform a similar calculation for non-zero density and see that in that case fluctuations remove the infinite continuous degeneracy present in the classical ground state. This degeneracy is represented by the fact that in the classical level, the sigma fields on the odd sites can move freely independent of each other in certain flat directions. Fluctuations in these directions have zero energy at $O(1)$ for all momentum and are zero modes. We find that quantum fluctuations give these modes non-zero energy of $O(1/N_c)$, and stabilized the classical ground state. Furthermore we find that these energies are quadratic in momentum, which makes them type II Goldstone bosons.

5.1 Removal of classical degeneracy at zero density

At zero density we consider fluctuations around the $\sigma_{\boldsymbol{n}} = \Lambda$ minimum of S.

$$S = \frac{N_c}{2} \int_0^\beta d\tau \left[-\sum_{\boldsymbol{n}} (-1)^{\boldsymbol{n}} \mathrm{Tr}\, \Lambda U_{\boldsymbol{n}}^\dagger \partial_\tau U_{\boldsymbol{n}} - \frac{J_1'}{2} \sum_{\boldsymbol{n}\mu} \mathrm{Tr}\, \sigma_{\boldsymbol{n}} \sigma_{\boldsymbol{n}+\hat{\boldsymbol{\mu}}} \right]. \tag{5.1}$$

with $J_1' = 2J_1/N_c \sim 1/g^2 N_c$. (From here on we drop the prime) Recalling Eq. (4.13), we write

$$U_{\boldsymbol{n}} = e^{A_{\boldsymbol{n}}}, \tag{5.2}$$

where $A_{\boldsymbol{n}}$ is anti-Hermitian and anticommutes with Λ. It is more convenient to work with the Hermitian matrix

$$L_{\boldsymbol{n}} = 2A_{\boldsymbol{n}}\Lambda, \tag{5.3}$$

in terms of which we expand

$$\sigma_{\boldsymbol{n}} = \Lambda + L_{\boldsymbol{n}} - \frac{1}{2}L^2\Lambda. \tag{5.4}$$

If we further expand $L_{\boldsymbol{n}}$ in the basis of generators of $U(N)$,

$$L_{\boldsymbol{n}} = \sum_{\eta} l^{\eta} M^{\eta}, \tag{5.5}$$

we find that the l^{η} corresponding to generators of $U(m) \times U(N-m)$ vanish; this is the subgroup under which the vacuum is symmetric. The field $L_{\boldsymbol{n}}$ thus contains $2m(N-m)$ real degrees of freedom, corresponding to the Goldstone bosons.

We expand $U_{\boldsymbol{n}}$ and $\sigma_{\boldsymbol{n}}$ in powers of $L_{\boldsymbol{n}}$; using Eq. (5.5), we obtain to second order

$$S = S_0 + \frac{N_c}{2}\int d\tau \sum_{\boldsymbol{n}} \left[\frac{(-1)^{\boldsymbol{n}}}{8} C^{\eta\eta'} l^{\eta}_{\boldsymbol{n}} \partial_\tau l^{\eta'}_{\boldsymbol{n}} + \frac{J_1}{8}\sum_{\mu} \left(l_{\boldsymbol{n}+\hat{\boldsymbol{\mu}}} - l_{\boldsymbol{n}}\right)^2 \right]. \tag{5.6}$$

The coefficient matrix is

$$C^{\eta\eta'} = \mathrm{Tr}\,(\Lambda[M^{\eta}, M^{\eta'}]), \tag{5.7}$$

and the classical energy is $S_0 = -\frac{J_1}{2}\left(\frac{N_c}{2}\right)^2 N N_s d\beta$. C is antisymmetric and purely imaginary; we show in Appendix E that C has eigenvalues ± 1, each with degeneracy $m(N-m)$. We change basis so as to diagonalize C, and write the index η as the compound $(\alpha, \pm)$ with $\alpha = 1, \ldots, m(N-m)$ and the $\pm$ corresponding to the eigenvalue of C. Since the original l^{η} are real, we have

$$(l^{\alpha+})^* = l^{\alpha-}. \tag{5.8}$$

Thus we eliminate $l^{\alpha-}$ and write

$$S = S_0 + \frac{N_c}{8}\int d\tau \sum_{\boldsymbol{n}} \left[(-1)^{\boldsymbol{n}} i\,\mathrm{Im}\, l^{\alpha+*}_{\boldsymbol{n}} \partial_\tau l^{\alpha+}_{\boldsymbol{n}} + \frac{J_1}{2}\sum_{\mu} \left| l^{\alpha+}_{\boldsymbol{n}+\hat{\boldsymbol{\mu}}} - l^{\alpha+}_{\boldsymbol{n}} \right|^2 \right]. \tag{5.9}$$

The alternating sign in Eq. (5.9) is what makes the theory antiferromagnetic. It forces us to differentiate between even and odd sites, and we transform to momentum space as follows (dropping the + superscript):

$$l^\alpha_{\boldsymbol{n}} = \sqrt{\frac{2}{N_s}} \sum_{\boldsymbol{k}} \begin{cases} l^\alpha_{1,\boldsymbol{k}} e^{i\boldsymbol{k}\cdot\boldsymbol{n}} & \boldsymbol{n} \text{ even,} \\ l^\alpha_{2,\boldsymbol{k}} e^{i\boldsymbol{k}\cdot(\boldsymbol{n}-\hat{z})} & \boldsymbol{n} \text{ odd.} \end{cases} \tag{5.10}$$

The even sites comprise an *fcc* lattice with lattice constant 2, and the momenta $\boldsymbol{k}$ take values in its Brillouin zone. We obtain

$$S = S_0 + \frac{N_c}{8} \sum_{\boldsymbol{k}} \int d\tau \, (l_1^* \quad l_2^*)^\alpha_{\boldsymbol{k}} \mathcal{M}(\boldsymbol{k}) \begin{pmatrix} l_1 \\ l_2 \end{pmatrix}^\alpha_{\boldsymbol{k}} . \tag{5.11}$$

Here

$$\mathcal{M}(\boldsymbol{k}) = \begin{pmatrix} -\partial_\tau + J_1 d & -J_1 d \gamma(\boldsymbol{k}) \\ -J_1 d \gamma(\boldsymbol{k}) & +\partial_\tau + J_1 d \end{pmatrix} \tag{5.12}$$

and $\gamma(\boldsymbol{k}) = \frac{1}{d} \sum_\mu \cos k_\mu$.

The Gaussian path integral over the l field is very similar to the path integrations that appear in Chapter 3 and gives the free energy,

$$F = F_0 + m(N-m) \frac{N_c}{2} \sum_{\boldsymbol{k}} \left[\frac{1}{\beta} \log \left(2 \sinh \frac{\beta \omega(\boldsymbol{k})}{2} \right) - \frac{J_1 d}{2} \right], \tag{5.13}$$

where $\omega(\boldsymbol{k}) = d J_1 N_c \sqrt{1 - \gamma^2(\boldsymbol{k})}$ and $F_0 = -\frac{1}{2} J_1 d N N_s (N_c/2)^2$. For the ground state energy, we take $\beta \to \infty$ and obtain (restoring all constants)

$$E_0 = -J_1 N_s N d \left(\frac{N_c}{2} \right)^2 \left[1 + \frac{1}{N_c} \frac{m(N-m)}{N} \int_{\mathrm{BZ}} \left(\frac{dk}{2\pi} \right)^d \left(1 - \sqrt{1 - \gamma^2(\boldsymbol{k})} \right) \right] . \tag{5.14}$$

This is exactly the result of Smit [21]. The $O(1/N_c)$ corrections lift the degeneracy of the ground states with different values of m. The integral in Eq. (5.14) is positive and its coefficient contains the number of Goldstone bosons. Thus the state of lowest energy is that with $m = N/2 = 2N_f$, and the symmetry breaking scheme is $U(4N_f) \to U(2N_f) \times U(2N_f)$. Further breaking by the next-nearest-neighbor terms was discussed in Chapter 4 where we extended this result to the next-nearest-neighbor theory and found that its $U(N_f) \times U(N_f)$ chiral symmetry is broken to the vector $U(N_f)$ flavor subgroup.

5.2 Removal of classical degeneracy at non-zero density

Recall the classical solution of the nonzero-density two-site problem, given in Chapter 4. We found that the sigma fields are

$$\begin{aligned}\sigma_1 &= \Lambda_1 = \begin{pmatrix} \mathbf{1}_m & 0 \\ 0 & -\mathbf{1}_{N-m} \end{pmatrix}, \\ \sigma_2 &= \begin{pmatrix} \sigma^{(m)} & 0 \\ 0 & \mathbf{1}_{N-m} \end{pmatrix}, \end{aligned} \tag{5.15}$$

and σ^m is given in Eq. (4.90). The symmetry of the vacuum is the set of rotations that leaves both σ_1 and σ_2 invariant, namely, $U(2m-N)\times U(N-m)\times U(N-m)$. There are two kinds of degeneracy in this two-site problem: that which results from breaking the global $U(N)$ to $U(m)\times U(N-m)$, and that which comes of breaking the $U(m)$ subgroup to $U(2m-N)\times U(N-m)$. The latter degeneracy is connected with freedom in choosing the orientation of σ_2 *relative to* σ_1. It is instructive to see how quantum mechanical fluctuations lift the classical degeneracies.

The quantum two-site problem is easy to solve. We rewrite the Hamiltonian (4.80) as

$$H = \frac{J_1}{2}\left[(Q_1+Q_2)^2 - Q_1^2 - Q_2^2\right]. \tag{5.16}$$

Q_1^2 and Q_2^2 are constants, the quadratic Casimir operator in the m-row, N_c-column representation of $U(N)$. The first term in Eq. (5.16) is minimized by coupling Q_1 and Q_2 to the representation that minimizes the Casimir, which is the representation with $2m-N$ rows and N_c columns (see Fig. 5.1). The ground state has discrete degeneracy equal to the dimension of this representation.

The exact quantum solution naturally shows no sign of spontaneous symmetry breaking and hence it is not of much relevance to the infinite volume problem. More interesting is the problem where the state of Q_1 is *fixed* and Q_2 is allowed to vary. This breaks by hand the global $U(N)$ while allowing quantum fluctuations to lift any remaining degeneracy in the relative orientation of the two spins, so it can be regarded as quantization in the presence of spontaneous symmetry breaking. In effect, this is mean field theory.

We replace the Hamiltonian (4.80) by

$$H^{MF} = J_1 \sum_{\eta=1}^{N^2} \langle Q_1^\eta \rangle Q_2^\eta. \tag{5.17}$$

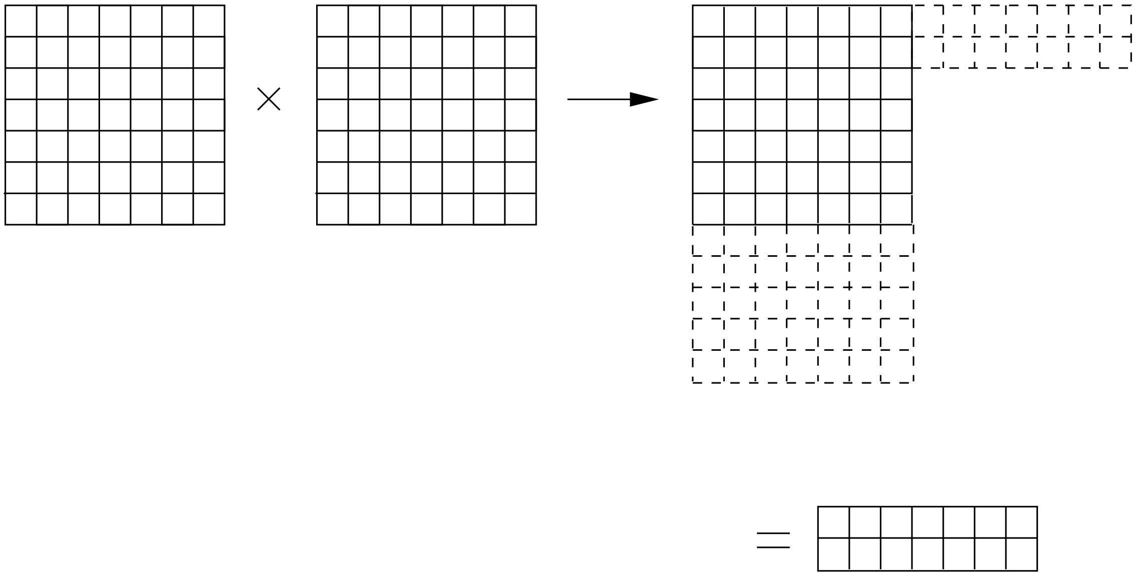

Figure 5.1: Coupling two spins in a 7-row representation of $U(12)$ to the representation with minimal Casimir operator

To minimize the energy we maximize the mean field by choosing the state of Q_1 to be the highest-weight state. This state diagonalizes the generators H_α of the Cartan subalgebra while other generators of $U(N)$ have expectation value zero. Thus

$$H^{MF} = J_1 \sum_{\alpha=1}^{N} \langle H_{1\alpha} \rangle H_{2\alpha}. \tag{5.18}$$

The operators H_α all commute, and their eigenvalues make up the weight diagram of the representation.[1] H^{MF} is a dot product of the weight vectors of the two spins. The energy is minimized by choosing for Q_2 a state that lies opposite the highest-weight state in the weight diagram. As shown in the example of Fig. 5.2, this still leaves a degeneracy, albeit a discrete one. We stress that this degeneracy comes from freedom in the relative orientation of Q_1 and Q_2.

In the $N_c \to \infty$ limit, the discrete degeneracy becomes infinite and presumably it is well described by the continuous degeneracy of the classical problem. As mentioned this is

---

[1] More precisely, the weight diagram shows eigenvalues of the $N-1$ traceless diagonal generators of $SU(N)$. These can be obtained by isolating the $U(1)$ member of the set H_α and taking linear combinations of the rest.

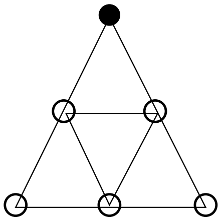

Figure 5.2: Weight diagram for $N=3$, $m=1$, $N_c=2$ [the sextet of $SU(3)$]. The highest-weight state lies at the top of the triangle; all states at the base minimize H^{MF}. All values of N_c give the same triangular shape, with multiplicity of one along the boundary. There are N_c+1 states at the base. For $N=4$ the triangle becomes a tetrahedron, and there are $(N_c+1)(N_c+2)/2$ states at its base.

similar to problems of frustrated magnetic systems, where a local group of spins will have a degenerate ground state, with a continuous degeneracy.

This degeneracy, however, is an artifact of the mean-field approach that, like the classical *ansatz*, assumes a fixed state for the spins on the even sites. In fact the sigma fields will fluctuate as soon as they are allowed to do so, i.e., when $N_c < \infty$. A given odd spin will *not* be surrounded by a uniform fixed background; the neighboring even spins will be influenced by *all* their odd neighbors, and will induce an interaction among the odd spins. This should reduce the entropy of the ground state to zero.

The systematic way to see this effect is to carry out an expansion in $1/N_c$ and verify the stability of the classical *ansatz*. We do that for the canted ground state, which is the solution to the two-site problem, replicated *uniformly* over the lattice:

$$\begin{aligned} \sigma_{\boldsymbol{n}} &= \Lambda, && \boldsymbol{n} \text{ even}, \\ \sigma_{\boldsymbol{n}} &= \begin{pmatrix} \sigma^{(m)} & 0 \\ 0 & \mathbf{1}_{N-m} \end{pmatrix}, && \boldsymbol{n} \text{ odd}, \end{aligned} \tag{5.19}$$

where $\sigma^{(m)} = U^{(m)}\Lambda^{(m)}U^{(m)\dagger}$ is now a *global* degree of freedom.

The meaning of the classical local degeneracy is that at $O(1)$ there is a set of directions in which one can move from one classical vacuum to another without cost of energy. Fluctuations in these directions are zero modes, that have zero energy for all momentum, and we discuss them in Section 5.2.1. The sign for stability must therefore be the removal of these zero modes at $O(1/N_c)$, which we demonstrate in Section 5.2.2 along the lines of the phenomenon of “order from disorder” [52, 53, 54, 55, 56, 57] in frustrated magnetic systems.

The essence of order from disorder is that fluctuations of quantum, thermal or even quenched nature can lift a classical degeneracy. A famous example is the Kagomé antiferromagnet [55] whose classical ground state energy is invariant under correlated rotations of local groups of spins, leading to a degeneracy exponential in the volume. This system also has modes with zero energy for all momentum. These zero modes obtain non-zero energy due to quantum fluctuations. Most discussions of order from disorder work in a Hamiltonian framework (but see [56, 57]). We employ instead the Euclidean path integral. In Appendix H we also present a Hamiltonian calculation using a generalized Holstein-Primakoff transformation. The latter can only be constructed easily for a subset of the cases we consider [21, 49]. The Euclidean calculations are less restrictive in their applicability.

Finally, as an exercise, we present a derivation of the effective ferromagnetic interaction among the $\sigma_{\boldsymbol{n}}$ on the odd sites in Appendix I, which in fact motivated us to investigate the canted ground state in particular.

5.2.1 Zero modes at $O(1)$

We begin to investigate the stability of the canted ansatz, where the vacuum expectation values (vevs) of the σ fields on the odd sites point in the same direction (a ferromagnetic alignment). Without loss of generality the ground state can be chosen to have

$$\begin{aligned} \langle\sigma_{\text{even}}\rangle &\propto \Lambda, \\ \langle\sigma_{\text{odd}}\rangle &\propto \Lambda_2 \equiv \begin{pmatrix} 1_{2m-N} & 0 & 0 \\ 0 & -1_{N-m} & 0 \\ 0 & 0 & 1_{N-m} \end{pmatrix} = V\Lambda V^{\dagger}, \end{aligned} \tag{5.20}$$

with

$$V = \begin{pmatrix} 1 & 0 & 0 \\ 0 & 0 & 1 \\ 0 & -1 & 0 \end{pmatrix}. \tag{5.21}$$

These vevs break $U(N)$ to $U(2m-N)\times U(N-m)\times U(N-m)$, with $n_G = 2(3m-N)(N-m)$ broken generators. Here we write an effective action for the fluctuations around the up to $O(1/N_c)$. Working at $O(1)$ first, we identify the zero modes that correspond to the classical degeneracy. We then show how quantum fluctuations give them non-zero energy.

In this and next sections we choose to work with the parametrization of the coset space $U(N)/[U(m)\times U(N-m)]$ [49] of Eqs. (4.21)–(4.22), in terms of the $m\times(N-m)$ complex matrix ϕ. As mentioned, the main advantage of this ϕ parameterization is that the kinetic part of the action is quadratic in ϕ [see (4.40)].

The fields ϕ, suitably shifted, can be identified with Goldstone bosons around the ground state (5.19). For the even sites, $\phi=0$ indeed gives $\sigma=\Lambda$. For the odd sites, the vacuum is at

$$\phi=\begin{pmatrix} 0 \\ 1_{N-m} \end{pmatrix},$$

where the upper part of ϕ is a $(2m-N)\times(N-m)$ matrix. We therefore shift ϕ on the odd sites according to

$$\begin{aligned} U' &\equiv VU, \\ \sigma'(\phi) &\equiv V\sigma(\phi)V^\dagger. \end{aligned} \tag{5.22}$$

This gives $\sigma'(0)=\Lambda_2$. We drop the primes henceforth. For later convenience we write ϕ as

$$\phi=\begin{pmatrix} \chi \\ \pi \end{pmatrix}. \tag{5.23}$$

Here π is an $(N-m)-$ dimensional square matrix while χ has $(2m-N)$ rows and $(N-m)$ columns. Both are complex. Thus

$$\sigma_{\text{even}}=\begin{pmatrix} 1-2\chi\chi^\dagger & -2\chi\pi^\dagger & -2\chi\sqrt{1-\phi^\dagger\phi} \\ -2\pi\chi^\dagger & 1-2\pi\pi^\dagger & -2\pi\sqrt{1-\phi^\dagger\phi} \\ -2\sqrt{1-\phi^\dagger\phi}\chi^\dagger & -2\sqrt{1-\phi^\dagger\phi}\pi^\dagger & -1+2\phi^\dagger\phi \end{pmatrix}, \tag{5.24}$$

and

$$\sigma_{\text{odd}}=\begin{pmatrix} 1-2\chi\chi^\dagger & -2\chi\sqrt{1-\phi^\dagger\phi} & 2\chi\pi^\dagger \\ -2\sqrt{1-\phi^\dagger\phi}\chi^\dagger & -1+2\phi^\dagger\phi & 2\sqrt{1-\phi^\dagger\phi}\pi^\dagger \\ 2\pi\chi^\dagger & 2\pi\sqrt{1-\phi^\dagger\phi} & 1-2\pi\pi^\dagger \end{pmatrix}. \tag{5.25}$$

Each submatrix in Eqs. (5.24)–(5.25) has dimensions as indicated in (5.19).

After scaling $\phi \to \phi/\sqrt{N_c}$ the action takes the form

$$\begin{aligned} S &= \mathrm{Tr} \int d\tau \sum_{\boldsymbol{n}} \left[\chi^\dagger_{\boldsymbol{n}} \partial_\tau \chi_{\boldsymbol{n}} + \pi^\dagger_{\boldsymbol{n}} \partial_\tau \pi_{\boldsymbol{n}} \right] \\ &\quad + J_1 \sum_{\boldsymbol{n}\hat{\boldsymbol{\mu}}} \left[\pi_{\boldsymbol{n}} \pi^\dagger_{\boldsymbol{n}} + \pi_{\boldsymbol{n}+\hat{\boldsymbol{\mu}}} \pi^\dagger_{\boldsymbol{n}+\hat{\boldsymbol{\mu}}} - \pi_{\boldsymbol{n}} \pi_{\boldsymbol{n}+\hat{\boldsymbol{\mu}}} - \pi^\dagger_{\boldsymbol{n}} \pi^\dagger_{\boldsymbol{n}+\hat{\boldsymbol{\mu}}} \right] \\ &\quad + \frac{J_1}{\sqrt{N_c}} \sum_{\boldsymbol{n}\hat{\boldsymbol{\mu}}} \left[\chi^\dagger_{\boldsymbol{n}} \chi_{\boldsymbol{n}+\hat{\boldsymbol{\mu}}} \pi_{\boldsymbol{n}} - \chi^\dagger_{\boldsymbol{n}+\hat{\boldsymbol{\mu}}} \chi_{\boldsymbol{n}} \pi_{\boldsymbol{n}+\hat{\boldsymbol{\mu}}} + h.c. \right] \qquad (5.26) \\ &\quad + \frac{J_1}{N_c} \sum_{\boldsymbol{n}\hat{\boldsymbol{\mu}}} \Big[\chi_{\boldsymbol{n}} \chi^\dagger_{\boldsymbol{n}} \chi_{\boldsymbol{n}+\hat{\boldsymbol{\mu}}} \chi^\dagger_{\boldsymbol{n}+\hat{\boldsymbol{\mu}}} - \pi_{\boldsymbol{n}} \pi^\dagger_{\boldsymbol{n}+\hat{\boldsymbol{\mu}}} \pi^\dagger_{\boldsymbol{n}+\hat{\boldsymbol{\mu}}} \pi_{\boldsymbol{n}+\hat{\boldsymbol{\mu}}} - \pi_{\boldsymbol{n}+\hat{\boldsymbol{\mu}}} \pi^\dagger_{\boldsymbol{n}+\hat{\boldsymbol{\mu}}} \pi^\dagger_{\boldsymbol{n}} \pi_{\boldsymbol{n}} \\ &\qquad\qquad - \pi_{\boldsymbol{n}} \pi^\dagger_{\boldsymbol{n}} \chi^\dagger_{\boldsymbol{n}+\hat{\boldsymbol{\mu}}} \chi_{\boldsymbol{n}+\hat{\boldsymbol{\mu}}} - \pi_{\boldsymbol{n}+\hat{\boldsymbol{\mu}}} \pi^\dagger_{\boldsymbol{n}+\hat{\boldsymbol{\mu}}} \chi^\dagger_{\boldsymbol{n}} \chi_{\boldsymbol{n}} \\ &\qquad\qquad + \frac{1}{2} \Big(\pi_{\boldsymbol{n}+\hat{\boldsymbol{\mu}}} \pi^\dagger_{\boldsymbol{n}+\hat{\boldsymbol{\mu}}} \pi_{\boldsymbol{n}+\hat{\boldsymbol{\mu}}} \pi_{\boldsymbol{n}} + \pi_{\boldsymbol{n}+\hat{\boldsymbol{\mu}}} \pi_{\boldsymbol{n}} \pi^\dagger_{\boldsymbol{n}} \pi_{\boldsymbol{n}} \\ &\qquad\qquad\qquad + \pi_{\boldsymbol{n}+\hat{\boldsymbol{\mu}}} \chi^\dagger_{\boldsymbol{n}+\hat{\boldsymbol{\mu}}} \chi_{\boldsymbol{n}+\hat{\boldsymbol{\mu}}} \pi_{\boldsymbol{n}} + \pi_{\boldsymbol{n}+\hat{\boldsymbol{\mu}}} \pi_{\boldsymbol{n}} \chi^\dagger_{\boldsymbol{n}} \chi_{\boldsymbol{n}} + h.c. \Big) \Big] \\ &\quad + O(1/N_c^{3/2}). \end{aligned}$$

The AF structure of the action demands the introduction of an fcc lattice. We write the fields $\phi_{\boldsymbol{n}} \equiv \phi^A_{\boldsymbol{N}}$ with $A = (\mathrm{even}, \mathrm{odd})$ and $\boldsymbol{N}$ belonging to an fcc lattice. We Fourier transform according to

$$\phi^A_{\boldsymbol{N}}(\tau) = \sqrt{\frac{2}{N_s}} \sqrt{\frac{1}{\beta}} \sum_{\boldsymbol{k},\omega} \phi^A_k e^{i(\boldsymbol{k}\cdot\boldsymbol{N} - \omega\tau)} \times \left\{ \begin{array}{ll} 1 & A = \mathrm{even} \\ e^{-ik_z/2} & A = \mathrm{odd} \end{array} \right. . \qquad (5.27)$$

Here $k \equiv (\boldsymbol{k}, \omega)$. In momentum space the action is given by $S = S_2 + S_3 + S_4$ with (discarding *Umklapp* terms)

$$\begin{aligned} S_2 &= \mathrm{Tr} \sum_k \begin{pmatrix} \pi^{\mathrm{e}\dagger}_k & \pi^{\mathrm{o}}_{-k} \end{pmatrix} \begin{pmatrix} -i\omega + 2dJ_1 & -2J_1 d\gamma_{\boldsymbol{k}} \\ -2J_1 d\gamma_{\boldsymbol{k}} & i\omega + 2J_1 d \end{pmatrix} \begin{pmatrix} \pi^{\mathrm{e}}_k \\ \pi^{\mathrm{o}\dagger}_{-k} \end{pmatrix} \\ &\qquad + \begin{pmatrix} \chi^{\mathrm{e}\dagger}_k & \left(\chi^{\mathrm{o}}_{-k}\right)^T \end{pmatrix} \begin{pmatrix} -i\omega & 0 \\ 0 & i\omega \end{pmatrix} \begin{pmatrix} \chi^{\mathrm{e}}_k \\ \left(\chi^{\mathrm{o}*}_{-k}\right) \end{pmatrix}, \qquad (5.28) \\ S_3 &= 2J_1 d \sqrt{\frac{2}{N_s N_c \beta}} \mathrm{Tr} \sum_{kp} \left(\chi^{\mathrm{o}\dagger}_p \chi^{\mathrm{e}}_k \pi^{\mathrm{o}}_{p-k} \gamma_{\boldsymbol{k}} - \chi^{\mathrm{e}\dagger}_k \chi^{\mathrm{o}}_{k-p} \pi^{\mathrm{e}}_p \gamma_{\boldsymbol{k}-\boldsymbol{p}} + h.c. \right), \qquad (5.29) \\ S_4 &= 2J_1 d \frac{2}{N_s N_c \beta} \mathrm{Tr} \sum_{kpq} \Big(\chi^{\mathrm{e}}_k \chi^{\mathrm{e}\dagger}_p \chi^{\mathrm{o}}_q \chi^{\mathrm{o}\dagger}_{q+k-p} - \pi^{\mathrm{e}}_k \pi^{\mathrm{e}\dagger}_p \pi^{\mathrm{o}\dagger}_q \pi^{\mathrm{o}}_{q-k+p} - \pi^{\mathrm{e}\dagger}_k \pi^{\mathrm{e}}_p \pi^{\mathrm{o}}_q \pi^{\mathrm{o}\dagger}_{q-k+p} \\ &\qquad\qquad - \chi^{\mathrm{e}\dagger}_k \chi^{\mathrm{e}}_p \pi^{\mathrm{o}}_q \pi^{\mathrm{o}\dagger}_{q+k-p} - \pi^{\mathrm{e}}_k \pi^{\mathrm{e}\dagger}_p \chi^{\mathrm{o}\dagger}_q \chi^{\mathrm{o}}_{q-k+p} \Big) \gamma_{\boldsymbol{k}-\boldsymbol{p}} \qquad (5.30) \end{aligned}$$

$$+\frac{1}{2}\left(\left(\pi_k^{\mathrm{e}\dagger}\pi_p^{\mathrm{e}}+\chi_k^{\mathrm{e}\dagger}\chi_p^{\mathrm{e}}\right)\left(\pi_{k-p-q}^{\mathrm{o}}\pi_q^{\mathrm{e}}+\pi_{-q}^{\mathrm{e}\dagger}\pi_{-(k-p-q)}^{\mathrm{o}\dagger}\right)\right.$$
$$\left.\left(\pi_k^{\mathrm{o}\dagger}\pi_p^{\mathrm{o}}+\chi_k^{\mathrm{o}\dagger}\chi_p^{\mathrm{o}}\right)\left(\pi_{k-p-q}^{\mathrm{e}}\pi_q^{\mathrm{o}}+\pi_{-q}^{\mathrm{o}\dagger}\pi_{-(k-p-q)}^{\mathrm{e}\dagger}\right)\right)\gamma_{\boldsymbol{k}-\boldsymbol{p}-\boldsymbol{q}}.$$

$\gamma_{\boldsymbol{k}}$ is given by

$$\gamma_{\boldsymbol{k}}=\frac{1}{d}\sum_{\mu=1}^{d}\cos k_\mu/2. \tag{5.31}$$

At large N_c, S_3 and S_4 are small perturbations. The bare propagators can be read from S_2,

$$(G_k^\pi)_{AB} = \frac{1}{\omega^2+4J_1^2d^2E_{\boldsymbol{k}}^2}\begin{pmatrix} i\omega+2J_1d & 2J_1d\gamma_{\boldsymbol{k}} \\ 2J_1d\gamma_{\boldsymbol{k}} & -i\omega+2J_1d \end{pmatrix}_{AB}, \tag{5.32}$$

$$(G_k^\chi)_{AB} = \begin{pmatrix} -1/i\omega & 0 \\ 0 & 1/i\omega \end{pmatrix}_{AB}. \tag{5.33}$$

(The propagators are diagonal in the internal group indices.) Here $E_{\boldsymbol{k}}=\sqrt{1-\gamma_{\boldsymbol{k}}^2}$. The poles of the propagators give the dispersion relations of the various bosons at $O(1)$. The result is

$$\omega^2+(2J_1dE_{\boldsymbol{k}})^2=0 \qquad \text{for } \pi, \tag{5.34}$$

and

$$\omega=0 \qquad \text{for } \chi. \tag{5.35}$$

There are $4(N-m)^2$ real fields per momentum of the π kind on the even and odd sites, and the propagator (5.32) has $4(N-m)^2$ poles that obey (5.34). We pair these into $2(N-m)^2$ physical massless excitations with

$$i\omega=\pm 2J_1dE_{\boldsymbol{k}}, \tag{5.36}$$

which are $2(N-m)^2$ spin waves. It is easy to verify that the Euclidean dispersion relation is $\omega^2\sim-|\boldsymbol{k}|^2$ at low momentum. We note that at $B=0$ they are the only excitations.

Let us pause to see how the above discussion would change if the interaction between the π fields were ferromagnetic. First the propagator (5.32) would be replaced by

$$G_{\mathrm{FM}}^{-1}=i\omega-2J_1d(1-\gamma_{\boldsymbol{k}}), \tag{5.37}$$

where $\boldsymbol{k}$ is now a momentum in the first BZ of a simple cubic lattice (the fcc structure is redundant for a ferromagnet). Here one has $2(N-m)^2$ fields per momentum, all of them are massless and obey $i\omega \sim J_1|\boldsymbol{k}|^2$. Pairing negative and positive frequencies together, one has $(N-m)^2$ massless excitations only. To see the connection to the antiferromagnetic case write the ferromagnetic action and propagator in terms of fcc degrees of freedom as

$$\begin{aligned} S_{\mathrm{FM}} &\sim \sum_{\boldsymbol{k}} \left(\begin{array}{cc} \pi_k^{\dagger e} & \pi_k^{\dagger o} \end{array} \right) G_{\mathrm{FM}}^{-1} \left(\begin{array}{c} \pi_k^e \\ \pi_k^o \end{array} \right), && (5.38) \\ G_{\mathrm{FM}}^{-1} &= \left(\begin{array}{cc} i\omega - 2J_1 d & 2J_1 d\gamma_{\boldsymbol{k}} \\ 2J_1 d\gamma_{\boldsymbol{k}} & i\omega - 2J_1 d \end{array} \right). && (5.39) \end{aligned}$$

Here the zeros obey $(i\omega - 2J_1 d)^2 = (2J_1 d\gamma_{\boldsymbol{k}})^2$, or

$$i\omega = 2J_1 d(1 \pm \gamma_{\boldsymbol{k}}). \tag{5.40}$$

So one has again $4(N-m)^2$ fields per momentum, but half of them have a mass equal to $4J_1 d$. Next we pair positive and negative frequencies together and find that half of the remaining $2(N-m)^2$ massless real fields describe $(N-m)^2$ massless particles. The difference between the two cases is that while the number of broken real fields is the same $n_G = 2(N-m)^2$, the number of physical excitations is different. It is n_G for the antiferromagnet, and $n_G/2$ for the ferromagnet.

The χ fields are $4(N-m)(2m-N)$ zero modes ("soft" modes). Their energy is zero for all momentum, a sign of the local degeneracy of the classical ground state discussed above.

We conclude this subsection by classifying the different fields according to their $U(2m-N) \times U(N-m) \times U(N-m)$ representations. We denote a representation by

$$(r_1, r_2, r_3)^{(q_1,q_2,q_3)}. \tag{5.41}$$

Here r_1 denotes the representation of $SU(2m-N)$, and $r_{2,3}$ denote the representations of the two $SU(N-m)$ subgroups. q_i are the charges of the excitations under the remaining $U(1)$ factors of the unbroken subgroup. These are generated by the following diagonal matrices.

$$1_N, \qquad \left(\begin{array}{ccc} 1_{2m-N} & 0 & 0 \\ 0 & 0 & 0 \\ 0 & 0 & 0 \end{array} \right), \quad \text{and} \quad \left(\begin{array}{ccc} 0 & 0 & 0 \\ 0 & 1_{N-m} & 0 \\ 0 & 0 & -1_{N-m} \end{array} \right). \tag{5.42}$$

We give the different representations in Table 5.1. The crucial point is that the AF spin waves and the zero modes reside in completely different representations. This means that the separation between these excitations in the $O(1)$ spectrum will survive at higher orders

Field	Representation	Dimension
π	$\left(1, N-m, \overline{N-m}\right)^{(0,0,+2)}$	$(N-m)^2$
χ_{even}	$\left(2m-N, 1, \overline{N-m}\right)^{(0,+1,+1)}$	$(2m-N)(N-m)$
χ_{odd}	$\left(2m-N, \overline{N-m}, 1\right)^{(0,+1,-1)}$	$(2m-N)(N-m)$

Table 5.1: $U(2m-N) \times U(N-m) \times U(N-m)$ representations of the excitations. The conjugate fields belong to the conjugate representations. $n(\overline{n})$ stands for the fundamental (its conjugate) representation of $SU(n)$ and 1 stands for a singlet.

and that mixing can not occur (unless there is further spontaneous symmetry breakdown in higher orders).

To be precise we give the transformation laws of each of the fields with respect to a $U(2m-N) \times U(N-m) \times U(N-m)$ element given by

$$U = \begin{pmatrix} u_1 & 0 & 0 \\ 0 & u_2 & 0 \\ 0 & 0 & u_3 \end{pmatrix}. \tag{5.43}$$

Here $u_{2,3} \in U(N-m)$, and $u_1 \in U(2m-N)$. The fields π^e and $\pi^{\dagger o}$ transform as

$$\pi^e \rightarrow u_2 \pi^e u_3^\dagger, \qquad \pi^{\dagger o} \rightarrow u_2 \pi^{\dagger o} u_3^\dagger, \tag{5.44}$$

while the χ fields transform as

$$\chi^e \rightarrow u_1 \chi^e u_3^\dagger, \qquad \chi^o \rightarrow u_1 \chi^o u_2^\dagger. \tag{5.45}$$

From Eq. (5.26) we see that the action is invariant under these transformations.

5.2.2 Removal of zero modes at $O(1/N_c)$ – the self energy calculation

In this section we calculate the self energy of the χ fields to first order in $1/N_c$. We shall see that the poles in the soft modes propagators move away from zero energy in this order. The Feynman rules for this problem are presented in Appendix F. We treat S_3

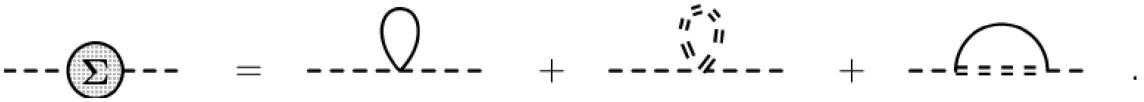

Figure 5.3: Schwinger-Dyson equation for the self energy of the χ fields in one loop. Solid lines correspond to the π propagators, and double dashed lines represent the *full* χ propagator. Single dashed lines are amputated external legs.

and S_4 as perturbations to S_2 and present the contributions to the self energy in one loop in Fig. 5.3.

Since the bare χ propagator is divergent at $\omega = 0$ for all $\boldsymbol{k}$, we insert its self energy self-consistently, making the replacement

$$(G^{\chi}_{k})^{-1} = (G^{\chi}_{0\,k})^{-1} - \Sigma_k. \tag{5.46}$$

G_0 is the bare propagator given in Eq. (5.33) and Σ is a matrix coupling odd and even degrees of freedom according[2] to

$$\Sigma = \begin{pmatrix} \Sigma_1 & \Sigma_2 \\ \Sigma_2^* & \Sigma_1^* \end{pmatrix}. \tag{5.47}$$

Thus the full χ propagator is

$$G^{\chi}_{k} = \frac{1}{(-i\omega - \Sigma_{1,k})(i\omega - \Sigma^*_{1,k}) - |\Sigma_{2,k}|^2} \begin{pmatrix} i\omega - \Sigma^*_{1,k} & \Sigma_{2,k} \\ \Sigma^*_{2,k} & -i\omega - \Sigma_{1,k} \end{pmatrix}. \tag{5.48}$$

Here we assume that both matrices $\Sigma_{1,k}$ and $\Sigma_{2,k}$ are diagonal in group space and that

$$\operatorname{Re}\Sigma_{1,k} < 0 \tag{5.49}$$

for the stability of the path integral.

At this point we note that the ansatz (5.47) is invariant under (5.45) only for $\Sigma_2 = 0$. A non-zero Σ_2 leads to the following non-zero vev

$$\langle \chi^e(k)_{\alpha i} \chi^o(-k)_{\beta j} \rangle \sim \Delta_2(k) \delta_{\alpha\beta} \delta_{ij}, \tag{5.50}$$

which is of $O(1/N_c)$. This vev is invariant under Eq. (5.45) only for $u_1 = u_1^T$ and $u_2 = u_3^*$. This in turn means that when the Schwinger-Dyson equation has a solution with $\Sigma_2 \neq 0$, then the stationary subgroup $U(2m-N)\times U(N-m)\times U(N-m)$ of the vevs in (5.19) is broken by the $O(1/N_c)$ correlation function (5.50) to

---

[2] We assume that the χ propagator has a similar structure as Eq. (5.32).

$$O(2m-N)\times U(N-m). \tag{5.51}$$

A different ansatz can lead to a different symmetry. For example, a self-energy structure that couples $\chi^{\dagger e}$ to χ^{o} leaves the $U(2m-N)$ subgroup intact. In principle one should compare the free energy of these two ground states. We do not investigate in this direction any further since the only difference will be in the symmetry structure of condensates of $O(1/N_c)$. The symmetry structure at $O(1)$ will be the same.

In fact because the additional condensates here are of $O(1/N_c)$, the physics related to it (Goldstone modes corresponding to the generators it breaks) is weakly coupled to the $O(1)$ physics related to the vevs in (5.19), and we ignore it in this work.

In Appendix G we derive self-consistent equations for $\Sigma_{1,k}$ and $\Sigma_{2,k}$. Defining $\tanh\theta_{\boldsymbol{k}} = -\mathrm{Re}\,\Sigma_{2,(0,\boldsymbol{k})}/\mathrm{Re}\,\Sigma_{1,(0,\boldsymbol{k})}$, we write these equations in the form of a single integral equation,

$$(N-m)\tanh\theta_{\boldsymbol{k}} = \frac{\displaystyle\int_{\mathrm{BZ}}\left(\frac{dq}{4\pi}\right)^{d} I_2(\boldsymbol{q},\boldsymbol{k})\sinh\theta_{\boldsymbol{q}}}{\displaystyle\int_{\mathrm{BZ}}\left(\frac{dq}{4\pi}\right)^{d} I_1(\boldsymbol{q},\boldsymbol{k})\cosh\theta_{\boldsymbol{q}} - \eta(\boldsymbol{k})} \equiv \frac{\beta_{\boldsymbol{k}}}{\alpha_{\boldsymbol{k}}}. \tag{5.52}$$

$\eta(\boldsymbol{k})$ and $I_{1,2}(\boldsymbol{q},\boldsymbol{k})$ are defined in appendix G. The poles of the propagators may then be obtained from Eq. (5.48) [see Eq. (G.15)]. The dispersion relations turn out to be

$$\begin{aligned}\pm i\omega &= \frac{2J_1 d}{N_c}\sqrt{(N-m)^2\alpha_{\boldsymbol{k}}^2-\beta_{\boldsymbol{k}}^2}\\ &= \frac{2J_1 d(N-m)}{N_c}\alpha_{\boldsymbol{k}}\sqrt{1-\tanh^2\theta_{\boldsymbol{k}}}\\ &\equiv \frac{2J_1 d(N-m)}{N_c}\epsilon_{\boldsymbol{k}}.\end{aligned} \tag{5.53}$$

The solution of Eq. (5.52) for $d=3$ can be obtained numerically by assuming that the function $\theta_{\boldsymbol{k}}$ depends only on $|\boldsymbol{k}|$. We plot the solution in Fig. 5.4 for $N-m=1,2,3,4,5$ (for details see Appendix G). Recall that the baryon density is given by $B=m-N/2$. Thus for $N_f\le 3$ we cover all baryon density short of saturation.

The form of $\epsilon_{\boldsymbol{k}}$ is shown in Fig. 5.5. It is easy to check that the bosons are massless, since $\eta(0)=I_{1,2}(\boldsymbol{q},0)=0$ implies that $\alpha_{\boldsymbol{k}}$ and $\beta_{\boldsymbol{k}}$ vanish at $\boldsymbol{k}=0$. This is a direct result of

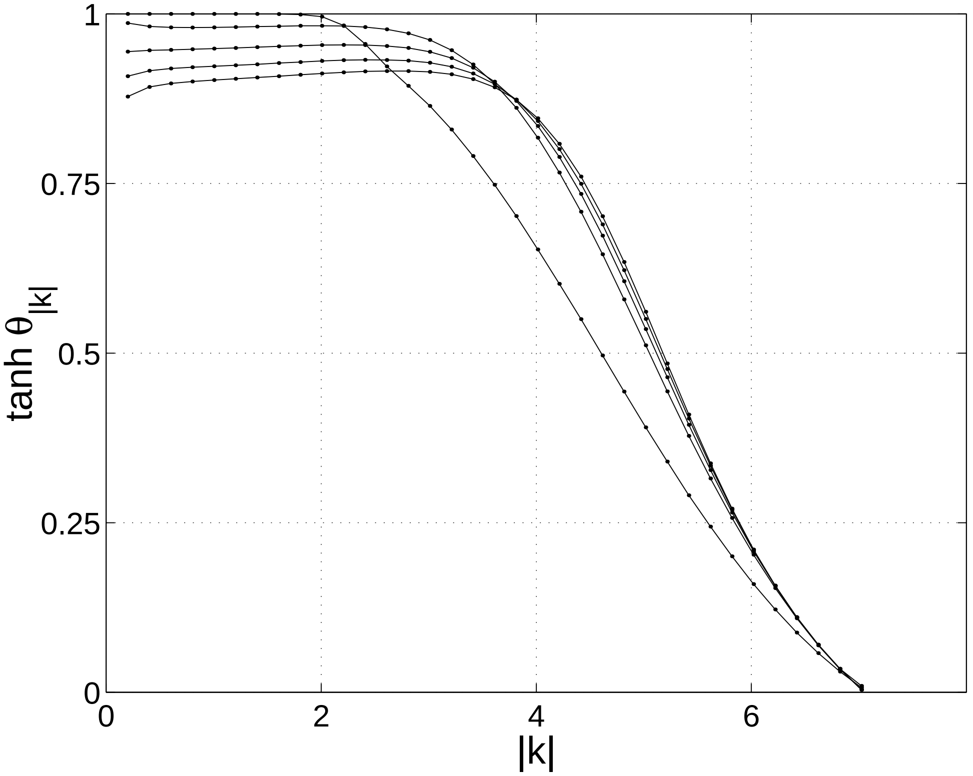

Figure 5.4: Solution of Eq. (5.52) for $N-m=1,2,3,4,5$. The value of $\tanh\theta$ for $|\boldsymbol{k}|\to 0$ drops with increasing $(N-m)$.

the Ward identities concerning the global $U(N)$ symmetry. Moreover, near $\boldsymbol{k}=0$ both α and β have a quadratic dependence on $|\boldsymbol{k}|$. This means that at low momenta $\epsilon_{\boldsymbol{k}} \sim |\boldsymbol{k}|^2$, characteristic of ferromagnetic magnons. A possible exception is the case $N-m=1$. There we see that at low momenta, $\tanh\theta_{\boldsymbol{k}} \to 1$ and thus it is possible that $\epsilon_{\boldsymbol{k}} \sim |\boldsymbol{k}|^{2+p}$ with p a positive integer[3].

Finally we recall that the relation between the number of χ fields and the number of physical excitations depends on the dispersion relation. Since these soft modes obey $\epsilon_{\boldsymbol{k}} \sim |\boldsymbol{k}|^2$, the $4(N-m)(2m-N)$ fields describe only half that many ferromagnetic magnons. The case of $N-m=1$ might be different depending on whether p is odd or even. In order to determine p it is necessary to improve the resolution of the momentum mesh. (This may explain the different behavior of $\tanh\theta$ in Fig. (5.4) and of the resulting $\epsilon_{\boldsymbol{k}}$ for this case)

---

[3] $\epsilon_{\boldsymbol{k}}$ cannot be nonanalytic at $\boldsymbol{k}=0$ since the integrals in Eq. (5.52) are regular there.

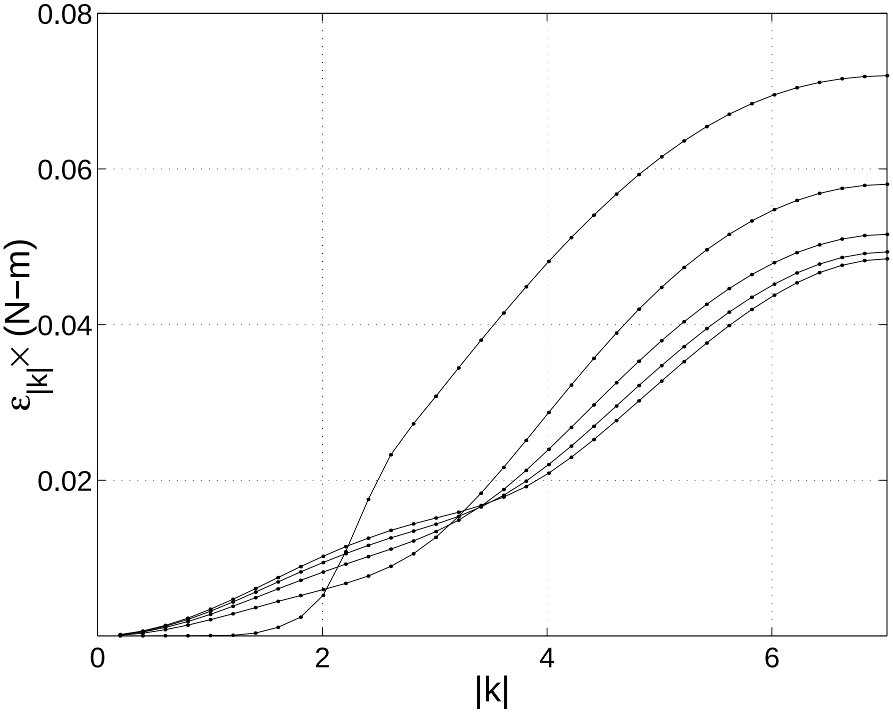

Figure 5.5: Rescaled energy of the χ bosons for for $N-m = 1,2,3,4,5$. The value of $(N-m) \times \epsilon_{\boldsymbol{k}}$ at the boundary $|\boldsymbol{k}| = \sqrt{5}\pi$ of the Brillouin zone increases with $N-m$.

The ϕ fields become two kinds of Goldstone boson. The π fields are antiferromagnetic spin waves with a linear dispersion relation. The χ fields are ferromagnetic magnons with a quadratic dispersion relation. This is consistent with the loss of Lorentz invariance due to finite density. This set of excitations falls into the pattern described by Chadha and Nielsen [80] and by Leutwyler [81] in their studies of nonrelativistic field theories.

In general, a nonrelativistic system that undergoes spontaneous symmetry breakdown can posses two types of Goldstone boson. The energy of type I bosons is an odd power of their momentum. Their effective field theory has a second time derivative which means that each excitation is described by one real field as in the case of a relativistic scalar field. Type II bosons have a dispersion relation that contains an even power of the momentum. They can appear only in nonrelativistic theories having properties similar to a Schrödinger field theory, namely theories whose action has only a first time derivative. As in the Schrödinger case, each excitation is described by a complex field, or two real fields. The number of the ϕ Goldstone fields is of course equal to the number n_G of generators broken by Eq. (5.51). The counting of these massless excitations is summarized by the Chadha–Nielsen counting rule,

$$n_I + 2n_{II} \geq n_G, \tag{5.54}$$

where $n_I(n_{II})$ are the number of type I and II Goldstone bosons. A well-known example is the $SU(2)$ spin system with a collinear ground state, where $n_G = 2$. The antiferromagnet has two spin waves with a linear dispersion relation ($n_I = 2, n_{II} = 0$) while the ferromagnet has one magnon with a quadratic dispersion relation ($n_I = 0, n_{II} = 1$). As mentioned above in our case both n_I and n_{II} are non-zero.

In addition to these massless fields there exist another set of massless fields. These are the Goldstone bosons that correspond to the breakdown of $U(2m-N)$ to $O(2m-N)$, and of $U(N-m) \times U(N-m)$ to $U(N-m)$, by the $O(1/N_c)$ condensate (5.50). In this case the Goldstone bosons are not represented by any of the fundamental χ or π fields. Similar to the BCS case, they are collective excitations that correspond to poles in two-particle propagators of the generic form $\langle \chi^{*e}\chi^{*o}\chi^{e}\chi^{o}\rangle$. These poles describe zero mass particles which are bound states of two χ particles. We do not pursue their properties (symmetry structure, dispersion relations, etc.) in this work since as mentioned they are weakly coupled to the excitations we treat.

The energy scale of the type II Goldstone bosons χ is smaller by a factor of $1/N_c$ compared to that of the type I bosons π. This points to a possible hierarchy of phase transitions at finite temperature which can be described by a classical model that has the Hamiltonian

$$H = J_1 \operatorname{Tr} \sum_{\boldsymbol{n}\hat{\boldsymbol{\mu}}} \left[\sigma_{\boldsymbol{n}}\sigma_{\boldsymbol{n}+\hat{\boldsymbol{\mu}}}\right] - J_2 \operatorname{Tr} \sum_{\boldsymbol{n}\hat{\boldsymbol{\mu}}} \left[\sigma_{\boldsymbol{n}}\sigma_{\boldsymbol{n}+2\hat{\boldsymbol{\mu}}}\right]. \tag{5.55}$$

For $J_2 = 0$, the ground state will be highly degenerate as above. A small positive value of J_2 removes this degeneracy and picks out a ferromagnetic alignment of the next-nearest-neighbor σ fields. Thus for $T \ll J_1, J_2$ the ground state is invariant only under[4]

$$U(N-m) \times U(N-m) \times U(2m-N). \tag{5.56}$$

This symmetry pattern will persists until some finite temperature $T_c^{\mathrm{FM}} \sim J_2$. For $T > T_c^{\mathrm{FM}}$ the ferromagnetic magnons melt the magnetization and restore some of the symmetry.

---

[4] We note here that order from disorder is not necessary here, and therefore there is no condensate analogous to (5.50). This means that the physics described by this classical model is *different* than the real model.

This situation will persists until a second temperature $T_c^{\mathrm{AFM}} \sim J_1$ where the symmetry will be restored completely. As long as $J_1 \gg J_2$ (which corresponds to $N_c \gg 1$ in our system), the hierarchy of phase transitions is well defined.

Finally we mention that recent work [82] on effective field theories for dense QCD also predicts the existence of type II Goldstone bosons. It is tempting to identify these with our ferromagnetic magnons. First, however, one must reduce the artificial $U(4N_f)$ symmetry of the action to the physical chiral symmetry. This important issue is discussed in the next chapter.

Chapter 6

Next-nearest-neighbor interactions in the nonlinear sigma model

The previous chapters are all mainly restricted to nearest-neighbor (NN) interactions only, which were symmetric under the global group of $U(4N_f)$. In this chapter we add the sigma model next-nearest-neighbor (NNN) interactions that reduce this symmetry to the chiral symmetry $U(N_f) \times U(N_f)$, thus completing our picture of the lattice theory that has the symmetry of continuum QCD. Taking the NNN coupling to be much smaller than the NN one, we perturb the NN ground state and its excitations, found in Chapters 4 and 5 with these NNN terms. These interactions reduce some of the global degeneracy of the NN vacuum, and leave only a part of chiral symmetry intact. We find that the global symmetry of the ground state varies with N_f and with the background baryon density. In all cases the condensate breaks the discrete rotational symmetry of the lattice as well as part of the chiral symmetry group. We also find two types of massless excitations: type I Goldstone bosons with linear dispersion relations and type II Goldstone bosons with quadratic dispersion relations. Some of the type I bosons exist also at zero density. The others were originally type II bosons that received energy contributions, linear in momentum, from the NNN terms, and became type I bosons as well. Both kinds of bosons can have anisotropic dispersion relations.

6.1 Action and symmetries of next-nearest-neighbor interactions

The NN effective Hamiltonian and sigma model discussed up to now in Chapters 3–5 correspond to an underlying kernel of naive fermions. Although these fermions suffer from species doubling in weak coupling, this doubling is not seen directly in strong coupling. The reason is that their we do not have fermion excitations, but rather only gauge invariant degrees of freedom, i.e., the mesonic $Q^{\eta}_{\boldsymbol{n}}$ operators and the baryonic $b^{I}_{\boldsymbol{n}}$ operators (see Chapter 2). Doubling of species can therefore reflect itself only in the number of excitations that correspond to these color singlet field, and is therefore determined by the global symmetry of the effective Hamiltonian.

The global symmetry group of the σ model depends on the underlying fermion kernel of the Hamiltonian. For N_f flavors of naive fermions we get an interaction between nearest-neighbor (NN) sites that is invariant under $U(N)$ with

$$N = 4N_f. \tag{6.1}$$

This symmetry is too large and is indeed indicative of species doubling. This symmetry is also present in the original Hamiltonian, as can be seen by spin-diagonalizing the interaction. In order to extract physical consequences from our model, it is imperative that it has the same global symmetry as QCD. We achieve this goal by taking a different underlying fermion kernel in Eq. (2.35) with the reduced, correct symmetry. We add next-nearest-neighbor (NNN) interactions to the kernel and reduce the symmetry to

$$U(N_f)_L \times U(N_f)_R, \tag{6.2}$$

which is almost the symmetry of the continuum theory. The additional $U(1)_A$ is inevitable if one starts with a local, chirally symmetric, underlying theory [23]. It can be easily removed by hand in the σ model by adding $U(1)_A$-breaking terms [32], and we ignore it.

The action of the σ model with nearest-neighbor next-nearest neighbor interactions is [See Chapter 4]

$$S = \frac{N_c}{2}\int d\tau \left[-\sum_{\boldsymbol{n}} \mathrm{Tr}\,\Lambda U^{\dagger}_{\boldsymbol{n}}\partial_\tau U_{\boldsymbol{n}} + \frac{J_1'}{2}\sum_{\boldsymbol{n}i} \mathrm{Tr}\,(\sigma_{\boldsymbol{n}}\sigma_{\boldsymbol{n}+\hat{\boldsymbol{\mu}}}) + \frac{J_2'}{2}\sum_{\boldsymbol{n}\mu} \mathrm{Tr}\,(\sigma_{\boldsymbol{n}}\alpha_\mu\sigma_{\boldsymbol{n}+2\hat{\boldsymbol{\mu}}}\alpha_\mu)\right]. \tag{6.3}$$

Here J_1' and J_2' are the couplings of the classical Hamiltonian Eq. (4.29), multiplied by $2/N_c$. They scale as $1/g^2N_c$ [recall the discussion in at the end of Section 4.2]. For brevity we drop the primes henceforth. If one derives the fermion Hamiltonian by truncating the SLAC Hamiltonian [30], then the couplings J_1 and J_2 obey $J_2 = J_1/8$. If we argue, however, that the strong-coupling Hamiltonian is derived by block-spin transformations applied to a short-distance Hamiltonian, then we cannot say much about the couplings that appear in it. We will assume that couplings in the effective Hamiltonian fall off strongly with distance, that is $0 < J_2 \ll J_1$.

The NN term is invariant under the global $U(N)$ transformation $U \to VU$, or $\sigma \to V\sigma V^\dagger$. The NNN term is only invariant if $V^\dagger \alpha_\mu V = \alpha_\mu$ for all μ. This restricts V to the form

$$V = \exp\left[i\left(\theta_V^a + \gamma_5 \theta_A^a\right)\lambda^a\right], \tag{6.4}$$

where λ^a are flavor generators. This is a chiral transformation in $U(N_f) \times U(N_f)$. The NNN term couples (discrete) rotational symmetry to the internal symmetry, *viz.*

$$\sigma_{\boldsymbol{n}} \to R^\dagger \sigma_{\boldsymbol{n}'} R, \qquad \boldsymbol{n}' = \mathcal{R}\boldsymbol{n}. \tag{6.5}$$

Here $\mathcal{R}$ is a 90^o lattice rotation and R represents it according to

$$R = \exp\left[i\frac{\pi}{4}\begin{pmatrix} \sigma_\mu & 0 \\ 0 & \sigma_\mu \end{pmatrix}\right] \otimes \mathbf{1}_{N_f}. \tag{6.6}$$

6.2 Ground state of the next-nearest-neighbor theory

The overall $N_c/2$ factor in Eq. (6.3) allows a systematic treatment in orders of $1/N_c$. In leading order, the ground state is found by minimizing the action, which gives field configurations that are τ independent and that minimize the interaction terms. For the NN theory, minimizing the single link interaction

$$E = \frac{J_1}{2}\mathrm{Tr}\,\sigma_1\sigma_2 \tag{6.7}$$

allows us to construct the vacuum by placing σ_1 and σ_2 on the even and odd sites.

We impose a uniform baryon density, $B_{\boldsymbol{n}} = B > 0$, on the effective Hamiltonian by setting a fixed value of $m > 2N_f$ on every site. To minimize the single-link energy (6.7) we first choose a basis where

$$\sigma_1 = \Lambda = \begin{pmatrix} \mathbf{1}_m & 0 \\ 0 & -\mathbf{1}_{N-m} \end{pmatrix}. \tag{6.8}$$

The analysis in chapter 5 shows that at the classical level the ground state is locally degenerate, but taking into consideration $O(1/N_c)$ fluctuations lifts this degeneracy. As a result we can choose the the value of σ_2 with out loss of generality to be

$$\sigma_2 = \begin{pmatrix} \mathbf{1}_{2m-N} & 0 & 0 \\ 0 & -\mathbf{1}_{N-m} & 0 \\ 0 & 0 & \mathbf{1}_{N-m} \end{pmatrix}. \tag{6.9}$$

This is a Néel structure, with two sublattices. The vacuum expectation values (vevs) of the even sigma fields break $U(N)$ to $U(m) \times U(N-m)$ and then the vevs of the odd sigma fields break the symmetry further to $U(2m-N) \times U(N-m) \times U(N-m)$.

Now we add the NNN interactions to the effective action. At the classical level, they do not by themselves remove the classical degeneracy of the NN theory (for nonzero density). We have to introduce the $O(1/N_c)$ fluctuations *first* in order to stabilize the Néel ground state of the NN Hamiltonian. More precisely we assume that

$$0 < J_2 \ll J_1/N_c. \tag{6.10}$$

This means that we take as our starting point the (globally degenerate) vacuum determined in Chapter 5 for the NN theory with $O(1/N_c)$ corrections. The NNN interaction is a perturbation on this vacuum and its excitations.

We begin, then, by assuming a Néel ansatz that minimizes the NN term in the action (6.3). The NNN term acts within each of the two sublattices. Writing $\sigma_{e,o}$ for the sublattice fields, the NNN contribution to the energy per $2 \times 2 \times 2$ lattice cell is

$$E_{NNN} = \frac{J_2}{2} \sum_{a=e,o} \sum_{\mu} \mathrm{Tr}\left[\sigma_a \alpha_\mu \sigma_a \alpha_\mu\right]. \tag{6.11}$$

Here σ_a is a global unitary rotation of the solution to the NN theory given by Eqs. (6.8)–(6.9).

We can find a lower bound for E_{NNN}. Writing in each term $\Sigma_1^a = \sigma_a$ and $\Sigma_2^{a\mu} = \alpha_{a\mu}\sigma_a\alpha_{a\mu}^\dagger$, we have

$$E_{NNN} = \frac{J_2}{2} \sum_{a\mu} \mathrm{Tr}\, \Sigma_1^a \Sigma_2^{a\mu}. \tag{6.12}$$

Note that $\Sigma_{1,2}$ are unitary rotations of the reference matrix Λ. Each term in Eq. (6.12) may be bounded from below by allowing these unitary rotations to vary independently over the entire $U(N)$ group. This is just the minimization problem posed in Eq. (6.7) above. The solution is given by Eqs. (6.8)–(6.9), whence the bound

$$E_{NNN} \geq 3J_2(4m - 3N). \tag{6.13}$$

We minimize E_{NNN} by writing an ansatz for σ_a that saturates the lower bound. At this point we choose to work in a basis where γ_5 is diagonal,

$$\gamma_5 = \begin{pmatrix} \mathbf{1}_{N/2} & 0 \\ 0 & -\mathbf{1}_{N/2} \end{pmatrix}. \tag{6.14}$$

Our ansatz is

$$\begin{aligned} \sigma_e &= U\Lambda_e U^\dagger = U \begin{pmatrix} \mathbf{1}_m & 0 \\ 0 & -\mathbf{1}_{N-m} \end{pmatrix} U^\dagger, \\ \sigma_o &= U\Lambda_o U^\dagger = U \begin{pmatrix} \mathbf{1}_{2m-N} & 0 & 0 \\ 0 & -\mathbf{1}_{N-m} & 0 \\ 0 & 0 & \mathbf{1}_{N-m} \end{pmatrix} U^\dagger. \end{aligned} \tag{6.15}$$

(Note that Λ_o is a rotation of Λ_e.) This is a global rotation (via U) of a particular configuration that minimizes the NN energy, as seen above. We further suppose that U takes the form

$$U = \frac{1}{\sqrt{2}} \begin{pmatrix} u & u \\ -u & u \end{pmatrix}, \tag{6.16}$$

with $u \in U(N/2)$.

The minimization of the energy via the ansatz is a problem of vacuum alignment [83]. We begin with the unperturbed NN problem, where the symmetry group $G \equiv U(N)$ is broken to $H \equiv U(2m - N) \times U(N - m) \times U(N - m)$. Our reference vacuum is given by $\sigma_{e,o} = \Lambda_{e,o}$, giving a specific alignment of H as the invariance group of this vacuum. We determine the rotation matrix U [within the ansatz (6.16)] that minimizes the energy of the perturbation E_{NNN}, which we write as

$$E_{NNN} = \frac{J_2}{2} \sum_{a\mu} \operatorname{Tr} \Lambda_a \bar{\alpha}_\mu \Lambda_a \bar{\alpha}_\mu^\dagger, \tag{6.17}$$

where $\bar{\alpha}_\mu = U^\dagger \alpha_\mu U = \bar{\alpha}_\mu^\dagger$.

We denote the generators of H collectively as T and the remaining generators of G as X. The T matrices commute with both Λ_e and Λ_o, while the X matrices do not. The symmetry-breaking term in the energy is E_{NNN}, given by Eq. (6.17) in terms of the rotated Hermitian matrices $\bar{\alpha}_\mu$. We project each $\bar{\alpha}_\mu$ onto the T and X subspaces, giving the decomposition

$$\bar{\alpha}_\mu = \bar{\alpha}_\mu^T + \bar{\alpha}_\mu^X. \tag{6.18}$$

Using the invariance of $\Lambda_{e,o}$ under T,

$$\left[\Lambda_a, \bar{\alpha}_\mu^T\right] = 0, \tag{6.19}$$

and the orthogonality of the T and X subspaces,

$$\mathrm{Tr}\left[\bar{\alpha}_\mu^T \bar{\alpha}_\mu^X\right] = 0, \tag{6.20}$$

we have

$$E_{NNN} = \frac{J_2}{2}\sum_{i,a} \mathrm{Tr}\left[\left(\bar{\alpha}_\mu^T\right)^2 + \Lambda_a \bar{\alpha}_\mu^X \Lambda_a \bar{\alpha}_\mu^X\right] \tag{6.21}$$

Following the block form of $\Lambda_{e,o}$, we divide the broken generators X into 3 sets, denoting them as X_a with $a = 1, 2, 3$. Their structures are respectively

$$\begin{pmatrix} 0 & \tilde{X}_1 & 0 \\ \tilde{X}_1^\dagger & 0 & 0 \\ 0 & 0 & 0 \end{pmatrix}, \quad \begin{pmatrix} 0 & 0 & \tilde{X}_2 \\ 0 & 0 & 0 \\ \tilde{X}_2^\dagger & 0 & 0 \end{pmatrix}, \quad \text{and} \begin{pmatrix} 0 & 0 & 0 \\ 0 & 0 & \tilde{X}_3 \\ 0 & \tilde{X}_3^\dagger & 0 \end{pmatrix}. \tag{6.22}$$

Writing $\bar{\alpha}_\mu^X = \sum_a \bar{\alpha}_\mu^{X_a}$, the following relations can be proved easily:

$$\begin{aligned} \left[\Lambda_1, \bar{\alpha}_\mu^{X_1}\right] &= 0 \qquad & \left\{\Lambda_2, \bar{\alpha}_\mu^{X_1}\right\} &= 0 \\ \left\{\Lambda_1, \bar{\alpha}_\mu^{X_2}\right\} &= 0 \qquad & \left[\Lambda_2, \bar{\alpha}_\mu^{X_2}\right] &= 0 \\ \left\{\Lambda_1, \bar{\alpha}_\mu^{X_3}\right\} &= 0 \qquad & \left\{\Lambda_2, \bar{\alpha}_\mu^{X_3}\right\} &= 0. \end{aligned} \tag{6.23}$$

Using these together with the further orthogonality conditions,

$$\mathrm{Tr}\left[\bar{\alpha}_\mu^{X_a} \bar{\alpha}_\mu^{X_b}\right] = 0, \qquad a \neq b, \tag{6.24}$$

we bring Eq. (6.21) to the form

$$E_{NNN} = J_2 \sum_\mu \mathrm{Tr}\left[\left(\bar{\alpha}_\mu^T\right)^2 - \left(\bar{\alpha}_\mu^{X_3}\right)^2\right]. \tag{6.25}$$

The rotation U given in Eq. (6.16) saturates the lower bound for the energy. We will proceed to prove this for the case $m \geq 3N/4$. In view of Eq. (6.16) we can write $\bar{\alpha}_\mu$ in the form

$$\bar{\alpha}_\mu = \begin{pmatrix} 0 & \bar{\sigma}_\mu \\ \bar{\sigma}_\mu & 0 \end{pmatrix}, \tag{6.26}$$

where $\bar{\sigma}_\mu \equiv u^\dagger \sigma_\mu u$. It is straightforward to check that for $m \geq 3N/4$ we have

$$\begin{aligned} \bar{\alpha}_\mu^{X_3} &= 0, & (6.27)\\ \bar{\alpha}_\mu^{T} &= \begin{pmatrix} 0 & \bar{\sigma}'_\mu \\ \bar{\sigma}'^\dagger_\mu & 0 \end{pmatrix}, & (6.28) \end{aligned}$$

with $\bar{\sigma}'_\mu$ composed of the first $(2m - 3N/2)$ columns of $\bar{\sigma}_\mu$,

$$\left(\bar{\sigma}'_\mu\right)_{pq} = \begin{cases} \left(\bar{\sigma}_\mu\right)_{pq} & \text{for} \quad q = 1, \ldots, 2m - 3N/2, \\ 0 & \text{else.} \end{cases} \tag{6.29}$$

The energy is

$$E_{NNN} = 2J_2 \sum_{i,pq} |(\bar{\sigma}'_\mu)_{pq}|^2 = 2J_2 \sum_i \sum_{q=1}^{2m-3N/2} \left(\bar{\sigma}^\dagger_\mu \bar{\sigma}_\mu\right)_{qq} = 3J_2(4m - 3N), \tag{6.30}$$

which is exactly the lower bound. Note that according to Eq. (6.30), any value u within $U(N/2)$ saturates the lower bound. Nevertheless, some values of u give the same vacuum as does $u = \mathbf{1}$. More precisely, all the elements $u \in U(2m - 3N/2) \times U(N - m) \times U(N - m)$ act trivially in Eq. (6.15). Vacua that are associated with different nontrivial choices of u are in general inequivalent, and give different realizations of the $U(N_f) \times U(N_f)$ symmetry of the theory. Since these vacua are not related by symmetry transformations, there is nothing to prevent lifting of the degeneracy in higher orders in $1/N_c$. In the sequel, we set $u = \mathbf{1}_{N/2}$. This gives the vacuum with the largest symmetry accessible via the ansatz (6.16).[1]

The simplicity of this calculation depends on the assumption $m \geq 3N/4$. For $m < 3N/4$, both $\bar{\alpha}_\mu^{X_3}$ and $\bar{\alpha}_\mu^{T}$ are non-zero. Moreover the index structure of the projections is more complex.[2] Therefore in these cases we resort to numerical minimization of Eq. (6.17) over $u \in U(N/2)$. In each case we find that the ansatz (6.15)–(6.16) yields a minimum that saturates the lower bound (6.13). In view of what happens for $m \geq 3N/4$ this may be only one point in a degenerate manifold of ground states. We emphasize that the degeneracy of these vacua is not related to the global $U(N_f) \times U(N_f)$ chiral symmetry. It is an accidental global degeneracy of the ground state.

---

[1] We have found, however, one exception where another ansatz, with different symmetries, gives larger symmetry than that of Eq. (6.15) for the case of $B = 2$ and $N_f = 3$.

[2] An exception is the $m = N/2$ case ($B = 0$), which was solved in Chapter 5.

Upon calculating the σ fields using Eqs. (6.15)–(6.16), it is straightforward to ascertain the symmetry of the vacuum. The $U(N_f) \times U(N_f)$ generators that commute with both σ_e and σ_o form the unbroken subgroup of the NNN theory. The rest are broken generators that correspond to Goldstone bosons.

The symmetry of these ground states is summarized in Table 6.1. In general, both chiral symmetry and discrete lattice rotations are broken; in some cases a symmetry under rotations around the z axis survives. Note that if we remove the unphysical axial $U(1)$ symmetry from the σ model, all its realizations will also drop from Table 6.1, namely, there will be no axial $U(1)$ unbroken symmetries (third column) and no Goldstone bosons corresponding to a broken axial $U(1)$ (fourth column). Anticipating these simple modifications we see no reason to proceed in this direction.

Table 6.1: Breaking of $SU(N_f)_L \times SU(N_f)_R \times U(1)_A$ for all baryon densities (per site) accessible for $N_f \leq 3$. Results for $B = 0$ are from Chapter 5.

N_f	$\lvert B\rvert$	Unbroken symmetry	Broken charges
1	0	$-$	1
	1	$-$	1
	2	$U(1)_A$	0
2	0	$SU(2)_V$	4
	1	$U(1)_{I_3}$	6
	2	$SU(2)_V$	4
	3	$U(1)_{I_3}$	6
	4	$SU(2)_L \times SU(2)_R \times U(1)_A$	0
3	0	$SU(3)_V$	9
	1	$U(1)_Y \times SU(2)_V$	13
	2	$U(1)_Y$	16
	3	$SU(3)_V$	9
	4	$U(1)_{I_3} \times U(1)_Y$	15
	5	$U(1)_{I_3} \times U(1)_Y \times U(1)_{A'}$	14
	6	$SU(3)_L \times SU(3)_R \times U(1)_A$	0

In addition we note the following:

- Since the baryon background is fixed, we cannot tell whether the $U(1)$ corresponding to baryon number is broken. [The $U(1)_B$ group acts trivially on $Q^{\eta}_{\boldsymbol{n}}$ and on $\sigma_{\boldsymbol{n}}$.]
- For each value of N_f, the case $B = 2N_f$ is a completely saturated lattice. Each site is in a singlet under the chiral group, and there is no spontaneous symmetry breaking.
- The axial $U(1)$ is not a symmetry of the continuum, and must be broken by hand. Wherever it appears in Table 6.1 it should be neglected, whether as an unbroken symmetry or as a broken charge.
- The $U(1)_{A'}$ appearing in the table for $N_f = 3$ is not the original $U(1)_A$ group but rather is generated by $\gamma_5 \otimes \lambda'$ with

  $$\lambda' = \begin{pmatrix} 1 & 0 & 0 \\ 0 & 0 & 0 \\ 0 & 0 & 0 \end{pmatrix}. \tag{6.31}$$

  This is the only case where an axial symmetry survives spontaneous symmetry breaking. If $U(1)_A$ is broken by hand, so is $U(1)_{A'}$.

For all non-zero densities short of saturation the vacuum breaks rotational invariance. This is easily checked for $m \geq 3N/4$ by noting that the ansatz for $\sigma_{e,o}$ fails to commute with the rotation operator (6.6). For the other cases this is easily checked numerically. (In some cases a discrete symmetry around the z axis remains unbroken.) Since this is not a continuous symmetry it will not give rise to additional Goldstone bosons. The broken rotational invariance will of course affect the excitation spectrum. In particular, whereas the NN theory possesses excitations with linear and quadratic dispersion relations [60], the NNN theory will produce anisotropic dispersion relations, like those seen in [84] and Section 6.3 below.

In comparing our results to those of continuum CSC calculations, one must keep in mind that we study systems with large, fixed, and discrete values of B, rather than with large, continuous μ. Moreover, we use large-N_c approximations which necessarily ignore the discrete properties of the $SU(N_c)$ group that are essential to baryons. Quantum effects at finite N_c, treated correctly, should yield effects that are not accessible through the $1/N_c$ expansion.

The values of (N_c, N_f) that are of interest for CSC are $N_c = 3$ and $N_f = 2$ or 3. In the two-flavor case the favored qq condensate is a flavor singlet and a color triplet, so that while color is partially broken, chiral symmetry is unbroken. We do not see this for any density at $N_f = 2$. Plainly our results are due to a $\bar{q}q$ condensate; whether there is a qq condensate as well cannot be ascertained.

For $N_f > 2$ the situation is similar. Schäfer [34] has considered the color–flavor structure of the condensates that arise for $N_c = 3$ and $N_f \geq 3$, and he has found that both color and flavor are partially broken, with a condensate that locks one or more subgroups of the flavor group to the color group. Since we work at large N_c, we should stand the argument on its head. A plausible qq condensate would lock successive subgroups of the *color* group to the flavor group and hence to each other, leaving unbroken the diagonal $SU(N_f)_{L+R+C}$ and some leftover color symmetry. Judging by the global symmetry of the vacuum, perhaps we see this for $(N_f = 3, B = 3)$. The other cases could conceivably arise from a combination of $\bar{q}q$ and qq condensates, but whether the latter actually occur is an open question.

Finally we note that according to diagrammatic power-counting arguments [85, 86], CSC is suppressed in the 't Hooft limit, where $N_c \to \infty$ and $g^2 N_c$ is kept fixed. Deryagin, Grigoriev, and Rubakov showed that in the perturbative regime of small $g^2 N_c$, a Fermi sea is unstable towards formation of a chiral density wave with momentum $|\boldsymbol{p}| = 2p_F$, where p_F is the fermi momentum [85]. Our ansatz does not permit this possibility.

6.3 Excitations in the next-nearest-neighbor theory

The Goldstone bosons of the NN theory were discussed in above. There are $2(N-m)^2$ bosons of type I with $\omega \sim J_1|\boldsymbol{k}|$ at low momenta; these are generalized antiferromagnetic spin waves (and are the only excitations at zero density). There are also $2(2m-N)(N-m)$ bosons of type II, that derive their energy from quantum fluctuations in $O(1/N_c)$. These are generalized *ferromagnetic* magnons with $\omega \sim (J_1/N_c)|\boldsymbol{k}|^2$.

Now we calculate the effects of the NNN interactions on the spectrum. In view of Eq. (6.10), the NN contributions to the propagators, found in above, remain unchanged. In particular we can take over the self-consistent determination of the self-energy of the type II bosons. We need consider the NNN contributions to the propagators in tree level only. We proceed to calculate these for $m \geq 3N/4$. In these cases, the calculations simplify and we perform them analytically.[3] We believe that the spectra of the other cases have similar features.

---

[3] An exception is $(N = 12, m = 10)$, where we have no analytic solution. See below.

In the NN theory the σ fields represent fluctuations around the vacuum (6.15) with $U = 1$. We parametrize them as in Eqs. (5.24)–(5.25). If $\phi = 0$, we have $\sigma_{\text{even,odd}} = \Lambda_{\text{even,odd}}$, which is the ground state of the NN theory. We adapt Eqs. (5.24)–(5.25) to the NNN theory by rotating them,

$$\sigma \to U\sigma U^\dagger, \tag{6.32}$$

with U as given in Eq. (6.16). Now $\phi = 0$ corresponds to the ground state of the NNN theory.

We substitute Eqs. (5.24)–(5.25) into the action (6.3). The rotation U disappears from the kinetic term and from the NN interaction—they are both $U(N)$ invariant. This means that the bare spectra found in Chapter 5, when U was absent, remain intact.

We write the NNN energy as

$$E_{\text{nnn}} = \frac{N_c J_2}{4} \sum_{a\boldsymbol{N}\mu} \text{Tr}\, \alpha_\mu \sigma_{a,\boldsymbol{N}} \alpha_\mu \sigma_{a,\boldsymbol{N}+2\hat{\boldsymbol{\mu}}}, \tag{6.33}$$

where $a = (\text{even}, \text{odd})$ and $\boldsymbol{N}$ denotes a site on the corresponding fcc sublattice. We rescale $\phi \to \phi/\sqrt{N_c}$ and expand Eq. (6.33) to second order,

$$\begin{aligned} E_{\text{nnn}} &= N_c E_0 + \frac{J_2}{4}\sqrt{N_c} \sum_{a\boldsymbol{N}\mu} \text{Tr}\, \bar{\alpha}_\mu \Lambda_a \bar{\alpha}_\mu \left(\Delta^{(1)}_{a\boldsymbol{N}} + \Delta^{(1)}_{a,\boldsymbol{N}+2\hat{\boldsymbol{\mu}}}\right) \\ &\quad + \frac{J_2}{4} \sum_{a\boldsymbol{N}\mu} \text{Tr}\, \bar{\alpha}_\mu \Delta^{(1)}_{a\boldsymbol{N}} \bar{\alpha}_\mu \Delta^{(1)}_{a,\boldsymbol{N}+2\hat{\boldsymbol{\mu}}} + \frac{J_2}{4} \sum_{a\boldsymbol{N}\mu} \text{Tr}\, \bar{\alpha}_\mu \Lambda_a \bar{\alpha}_\mu \left(\Delta^{(2)}_{a\boldsymbol{N}} + \Delta^{(2)}_{a,\boldsymbol{N}+2\hat{\boldsymbol{\mu}}}\right) \\ &\quad + O\left(\frac{1}{\sqrt{N_c}}\right). \end{aligned} \tag{6.34}$$

We have defined $\bar{\alpha}_\mu = U^\dagger \alpha_\mu U$, and $\Delta^{(1,2)}$ correspond to the linear and quadratic deviations of the σ fields from their ground state values. The latter are given by

$$\Delta^{(1)}_e = \begin{pmatrix} 0 & 0 & -2\chi \\ 0 & 0 & -2\pi \\ -2\chi^\dagger & -2\pi^\dagger & 0 \end{pmatrix}, \qquad \Delta^{(2)}_e = \begin{pmatrix} -2\chi\chi^\dagger & -2\chi\pi^\dagger & 0 \\ -2\pi\chi^\dagger & -2\pi\pi^\dagger & 0 \\ 0 & 0 & +2\phi^\dagger\phi \end{pmatrix} \tag{6.35}$$

on the even sites, and

$$\Delta^{(1)}_o = V \begin{pmatrix} 0 & 0 & -2\chi \\ 0 & 0 & -2\pi \\ -2\chi^\dagger & -2\pi^\dagger & 0 \end{pmatrix} V^\dagger, \qquad \Delta^{(2)}_o = V \begin{pmatrix} -2\chi\chi^\dagger & -2\chi\pi^\dagger & 0 \\ -2\pi\chi^\dagger & -2\pi\pi^\dagger & 0 \\ 0 & 0 & +2\phi^\dagger\phi \end{pmatrix} V^\dagger \tag{6.36}$$

on the odd sites. Here

$$V = \begin{pmatrix} 1 & 0 & 0 \\ 0 & 0 & 1 \\ 0 & -1 & 0 \end{pmatrix} \tag{6.37}$$

is the matrix that rotates Λ_{even} to Λ_{odd}. It is easy to show that the terms linear in $\Delta^{(1)}$ vanish.

In view of the block structure of $\Lambda_{\text{even,odd}}$ and of U, as given in Eqs. (6.15)–(6.16), and of α_μ, it is convenient to decompose χ for $m \geq 3N/4$ as

$$\chi = \begin{pmatrix} \chi_1 \\ \chi_2 \end{pmatrix} \tag{6.38}$$

Here χ_1 has $N/2$ rows, and χ_2 has $2m - 3N/2$ rows. Both have $N - m$ columns. Substituting into Eq. (6.34) and omitting the ground state energy we find that the $O(1)$ contribution of the NNN energy depends only on χ_1. The π and χ_2 fields do not enter the NNN energy at this order and remain of type I and of type II, respectively.

We now define a new $N \times N$ matrix $\hat{\chi}$ that contains only χ_1,

$$\hat{\chi} = \begin{pmatrix} 0 & 0 & \chi_1 \\ 0 & 0 & 0 \\ \chi_1^\dagger & 0 & 0 \end{pmatrix}, \tag{6.39}$$

and use it to write

$$\begin{aligned} E_{\text{nnn}} &= \frac{J_2}{4} \sum_{\substack{\boldsymbol{N} \in \text{fcc} \\ \mu}} \Big\{ 4\text{Tr} \left[\bar{\alpha}_\mu \hat{\chi}^e_{\boldsymbol{N}} \bar{\alpha}_\mu \hat{\chi}^e_{\boldsymbol{N}+2\hat{\mu}} + \bar{\alpha}_\mu \left(V \hat{\chi}^o_{\boldsymbol{N}} V^\dagger \right) \bar{\alpha}_\mu \left(V \hat{\chi}^o_{\boldsymbol{N}+2\hat{\mu}} V^\dagger \right) \right] \\ &\qquad -4\text{Tr} \left[\bar{\alpha}_\mu \Lambda_e \bar{\alpha}_\mu \Lambda_e \left(\hat{\chi}^e_{\boldsymbol{N}} \right)^2 + \bar{\alpha}_\mu \Lambda_o \bar{\alpha}_\mu \Lambda_o \left(V \hat{\chi}^o_{\boldsymbol{N}} V^\dagger \right)^2 \right] \Big\}. \end{aligned} \tag{6.40}$$

Next we expand $\hat{\chi} = \chi^\eta \Gamma^\eta$, where χ^η are real and Γ^η are the hermitian generators of $U(N)$, normalized to

$$\text{tr} \left[\Gamma^\eta \Gamma^{\eta'} \right] = \delta^{\eta\eta'}. \tag{6.41}$$

The form (6.39) of $\hat{\chi}$ implies that $\chi^\eta \neq 0$ for those generators whose elements $\left(\Gamma^\eta\right)_{\alpha\beta}$ are non-zero for $\alpha \in [1, N/2]$ and $\beta \in [m+1, N]$ or vice versa. Thus

$$E_{\text{nnn}} = \sum_{a\boldsymbol{N}} \sum_{\eta,\eta'} \left[\chi^{a\eta}_{\boldsymbol{N}} \left(N_a\right)^{\eta\eta'} \chi^{a\eta'}_{\boldsymbol{N}} + \sum_\mu \chi^{a\eta}_{\boldsymbol{N}} \left(M_{a\mu}\right)^{\eta\eta'} \chi^{a\eta'}_{\boldsymbol{N}+2\hat{\mu}} \right], \tag{6.42}$$

where

$$
\begin{aligned}
(N_e)^{\eta\eta'} &= -J_2 \sum_\mu \mathrm{Tr}\left[\Gamma^\eta \Gamma^{\eta'} \bar{\alpha}_\mu \Lambda_a \bar{\alpha}_\mu \Lambda_a\right], &(6.43)\\
(N_o)^{\eta\eta'} &= -J_2 \sum_\mu \mathrm{Tr}\left[V\Gamma^\eta \Gamma^{\eta'} V^\dagger \bar{\alpha}_\mu \Lambda_a \bar{\alpha}_\mu \Lambda_a\right], &(6.44)\\
(M_{e\mu})^{\eta\eta'} &= J_2 \mathrm{Tr}\left[\Gamma^\eta \bar{\alpha}_\mu \Gamma^{\eta'} \bar{\alpha}_\mu\right], &(6.45)\\
(M_{o\mu})^{\eta\eta'} &= J_2 \mathrm{Tr}\left[V\Gamma^\eta V^\dagger \bar{\alpha}_\mu V\Gamma^{\eta'} V^\dagger \bar{\alpha}_\mu\right]. &(6.46)
\end{aligned}
$$

With a Fourier transform,

$$\chi^{a\eta}_{\boldsymbol{N}} = \sqrt{\frac{2}{N_s\beta}} \sum_{\substack{\boldsymbol{k}\in BZ\\ \omega}} \chi^{a\eta}_k e^{i\boldsymbol{k}\cdot\boldsymbol{N}+i\omega\tau}, \tag{6.47}$$

we write the energy in momentum space as

$$
\begin{aligned}
E_{\mathrm{nnn}} = \sum_{\substack{\boldsymbol{k}\in BZ\\ \omega>0}} & \chi^{e\dagger}_k \left[N_e + N_e^T + M_e(\boldsymbol{k}) + M_e^\dagger(\boldsymbol{k})\right]\chi^e_k \\
& + \chi^{o\dagger}_{-k}\left[N_o + N_o^T + M_o(-\boldsymbol{k}) + M_o^\dagger(-\boldsymbol{k})\right]\chi^o_{-k}. \qquad (6.48)
\end{aligned}
$$

Here $M_a(\boldsymbol{k}) = \sum_\mu M_{a\mu} e^{ik_\mu}$.

The NN action, including the time derivative and $O(1/N_c)$ self-energy, was written down in Chapter 5 in terms of the Fourier transform $\tilde{\chi}$ of the $(2m-N)\times(N-m)$ matrix field χ [Eq. (6.38)]:

$$
\begin{aligned}
S_{\mathrm{nn}} = \sum_{\omega,\boldsymbol{k}} \mathrm{Tr} \Big[& (i\omega - \Sigma_{1,\boldsymbol{k}})\,\tilde{\chi}^{e\dagger}_k \tilde{\chi}^e_k + (-i\omega - \Sigma_{1,\boldsymbol{k}})\,\tilde{\chi}^{o\dagger}_{-k}\tilde{\chi}^o_{-k} \\
& -\Sigma_{2,\boldsymbol{k}}\left(\tilde{\chi}^e_k \tilde{\chi}^{oT}_{-k} + c.c.\right)\Big]. \qquad (6.49)
\end{aligned}
$$

The self-energies Σ_a are of order J_1/N_c and depend on N and m. We set $\chi_2 = 0$ and repeat the steps leading to Eq. (6.48) to write S_{nn} in terms of χ^η_k,

$$S_{\mathrm{nn}} = \sum_k \chi^{e\dagger}_k K_{ee}\chi^e_k + \chi^{o\dagger}_{-k}K_{oo}\chi^o_{-k} + \chi^{eT}_k K_{eo}\chi^o_{-k}, \tag{6.50}$$

with the matrices K_{ee}, K_{oo}, and K_{eo} given by

$$
\begin{aligned}
(K_{ee})^{\eta\eta'} &= \frac{i\omega}{2}\mathrm{Tr}\left[\Lambda_e \Gamma^\eta\Gamma^{\eta'}\right] - \frac{1}{2}\Sigma_{1,\boldsymbol{k}}\delta^{\eta\eta'}, &(6.51)\\
(K_{oo})^{\eta\eta'} &= -\frac{i\omega}{2}\mathrm{Tr}\left[\Lambda_e \Gamma^\eta\Gamma^{\eta'}\right] - \frac{1}{2}\Sigma_{1,\boldsymbol{k}}\delta^{\eta\eta'}, &(6.52)\\
(K_{eo})^{\eta\eta'} &= -\Sigma_{2,\boldsymbol{k}}\mathrm{Tr}\left[\Gamma^\eta\Gamma^{\eta' T}\right]. &(6.53)
\end{aligned}
$$

Equation (6.50) is to be added to Eq. (6.48) to give the quadratic action of the type II Goldstone bosons χ_1.

Diagonalizing the quadratic form is straightforward but tedious. As noted above, only a subset of the generators Γ^η of $U(N)$ appear in the expansion of Eq. (6.39). Since χ_1 has dimensions $N/2 \times (N-m)$, there are $N(N-m)/2$ pairs of generators in the sum, which we write (similar to the Pauli matrices σ_x, σ_y) as $\tilde{\Gamma}^\eta_x, \tilde{\Gamma}^\eta_y$, with $\eta = 1, \ldots, N(N-m)/2$. Their coefficients are similarly written as χ^η_x, χ^η_y. Thus for each k, η we have

$$\chi^\eta_k = \begin{pmatrix} \chi^{e\eta}_{xk} \\ \chi^{e\eta}_{yk} \\ \chi^{o\eta *}_{x,-k} \\ \chi^{o\eta *}_{y,-k} \end{pmatrix}, \tag{6.54}$$

and the action is

$$S = \sum_{\omega>0} \sum_{\boldsymbol{k}} \chi^\dagger_k \, G^{-1}_k \, \chi_k, \tag{6.55}$$

The inverse propagator is

$$G^{-1}_k = \begin{pmatrix} -\Sigma_{1,\boldsymbol{k}} + n_e + m_e & -\omega & -\Sigma_{2,\boldsymbol{k}} & 0 \\ \omega & -\Sigma_{1,\boldsymbol{k}} + n_e - m_e & 0 & \Sigma_{2,\boldsymbol{k}} \\ -\Sigma_{2,\boldsymbol{k}} & 0 & -\Sigma_{1,\boldsymbol{k}} + n_o + m_o & -\omega \\ 0 & \Sigma_{2,\boldsymbol{k}} & \omega & -\Sigma_{1,\boldsymbol{k}} + n_o - m_o \end{pmatrix}, \tag{6.56}$$

where

$$(n_a)^{\eta\eta'} = -2J_2 \sum_\mu \mathrm{tr}\left[(\Gamma^\eta_x)^2 \bar{\alpha}_\mu \Lambda_a \bar{\alpha}_\mu \Lambda_a\right] \delta^{\eta\eta'}, \tag{6.57}$$

$$(m_a)^{\eta\eta'} = 2J_2 \sum_\mu \mathrm{tr}\left[\Gamma^\eta_x \bar{\alpha}_\mu \Gamma^{\eta'}_x \bar{\alpha}_\mu\right] \cos k_\mu. \tag{6.58}$$

$\Sigma_{1,2}$ and ω contain a factor of $\delta_{\eta,\eta'}$. If we write the 4×4 matrix G^{-1}_k in terms of 2×2 blocks,

$$G^{-1}_k = \begin{pmatrix} A & B \\ C & D \end{pmatrix}, \tag{6.59}$$

then its determinant is easily calculated via

$$|G^{-1}_k| = |C| \, |B - AC^{-1}D| \tag{6.60}$$

that gives the following determinant.

$$\begin{vmatrix} \omega^2 + (n_e + m_e - \Sigma_1)(n_o + m_o - \Sigma_1) - \Sigma_2^2 & \omega(n_e + m_e - n_o + m_o) \\ \omega(n_o + m_o - n_e + m_e) & \omega^2 + (n_e - m_e - \Sigma_1)(n_o - m_o - \Sigma_1) - \Sigma_2^2 \end{vmatrix} . \tag{6.61}$$

For $N = 4N_f \leq 12$ (and $m \geq 3N/4$), the matrices n_e, n_o, m_e, m_o all commute, except for the case ($N = 12$, $m = 10$). Dropping this last from consideration, we are left with the values of (N_f, B) listed in Table 6.2. For each case, the simultaneous diagonalization of $n_{e,o}$ and $m_{e,o}$ gives the eigenvalues shown.

Table 6.2: Simultaneous eigenvalues of $n_{e,o}$ and $m_{e,o}$ (in units of $2J_2$) for all values of N_f and B considered. The resulting spectra fall into four classes. Here $v_z = \cos k_z$ and $v_\perp = 2\sin\left(\frac{k_x+k_y}{2}\right)\sin\left(\frac{k_x-k_y}{2}\right)$

N_f	B	n_e	n_o	m_e	m_o	degeneracy	class
1	1	1	2	v_z	$v_\perp$		4
		2	1	$v_\perp$	v_z		4
2	2	1	2	v_z	$v_\perp$	×3	4
		2	1	$v_\perp$	v_z	×3	4
		1	2	$-v_z$	$-v_\perp$		4
		2	1	$-v_\perp$	$-v_z$		4
2	3	0	1	0	v_z		2
		1	0	v_z	0		2
		0	2	0	$v_\perp$		3
		2	0	$v_\perp$	0		3
3	3	1	2	v_z	$v_\perp$	×6	4
		2	1	$v_\perp$	v_z	×6	4
		1	2	$-v_z$	$-v_\perp$	×3	4
		2	1	$-v_\perp$	$-v_z$	×3	4
3	5	0	0	0	0	×2	1
		0	1	0	v_z		2
		1	0	v_z	0		2
		0	2	0	$v_\perp$		3
		2	0	$v_\perp$	0		3

The zeros of the determinant (6.61) determine the spectrum $\omega(\boldsymbol{k})$, giving (after $\omega \to i\omega$)

$$\begin{aligned}\omega^2 &= {\Sigma_1}^2 - {\Sigma_2}^2 + \frac{1}{2}\left(n_e^2 - m_e^2 + n_o^2 - m_o^2\right) - \Sigma_1(n_e + n_o) \\ &\pm\Bigg\{\left[\Sigma_1(n_o - n_e) + \frac{1}{2}(n_e^2 - m_e^2 - n_o^2 + m_o^2)\right]^2 \\ &\qquad + {\Sigma_2}^2\left[(m_e + m_o)^2 - (n_e - n_o)^2\right]\Bigg\}^{1/2}. \qquad (6.62)\end{aligned}$$

Because of the symmetries of Eq. (6.62), the spectra of the various cases shown in Table 6.2 fall into four classes. We examine each class in turn.

Class 1: Here there is no contribution at all from the NNN interaction. As shown in [60], $\Sigma_{1,2}$ are proportional to J_1/N_c and for small momenta they are quadratic in $|\boldsymbol{k}|$; the same holds for the NN energy $\sqrt{{\Sigma_1}^2 - {\Sigma_2}^2}$. These fields remain isotropic type II Goldstone bosons as in the NN theory.

Class 2: Fields that correspond to the minus sign in Eq. (6.62) remain type II, but with anisotropic dispersion laws of the form

$$\omega^2 = c^2\boldsymbol{k}^4\left(1 + a\delta\frac{k_z^2}{k^2}\right). \qquad (6.63)$$

The plus sign in Eq. (6.62) gives a linear dispersion law, again anisotropic,

$$\omega^2 = 4c_1J_2\left[k_x^2 + k_y^2 + (1 + b\delta)k_z^2\right] \qquad (6.64)$$

The anisotropy in both cases is proportional to the ratio $\delta \equiv J_2/(12J_1/N_c)$ of NNN to NN couplings. The coefficients c and c_1 are defined as

$$c = \left(\frac{d}{d\boldsymbol{k}^2}\sqrt{{\Sigma_1}^2 - {\Sigma_2}^2}\right)_{\boldsymbol{k}=0}, \qquad (6.65)$$

$$c_1 = -\left(\frac{d\Sigma_1}{d\boldsymbol{k}^2}\right)_{\boldsymbol{k}=0} > 0. \qquad (6.66)$$

They are of order J_1/N_c. The coefficients

$$a = \frac{N_c}{6J_1}\frac{c_1^2 - c^2}{2c_1c^2} \quad \text{and} \quad b = \frac{N_c}{6J_1}\frac{2}{c_1} \qquad (6.67)$$

are of order 10^2 for most cases at hand. These coefficients as well as c and c_1 are given in Appendix K.

Classes 3 and 4: Taking $\boldsymbol{k} = 0$ in Eq. (6.62) we find that the fields that correspond to the plus sign get a mass equal to $2J_2$. This is a result of the explicit breaking of the $U(4N_f)$ symmetry by the NNN interaction terms; these particles are no longer Goldstone bosons. The massless bosons in Class 3, corresponding to the minus sign, are type II bosons described by

$$\omega^2 = c_1^2 \boldsymbol{k}^4. \tag{6.68}$$

(This is different from Class 1 where $\omega^2 = c^2 \boldsymbol{k}^4$.) The massless bosons in Class 4 are again anisotropic, obeying Eq. (6.64), and are of type I.

These dispersion relations are correct to $O(\delta)$ for momenta of $O(\delta)$ or smaller. In all cases the dispersion relation to $O(1)$ for $\boldsymbol{k}^2 \gg \delta$ is quadratic and isotropic, unchanged from the NN result presented in Chapter 5. Since δ is a small parameter, this means that in most of the Brillouin zone the propagator maintains its NN form. This is the reason why the self consistent calculations in Chapter 5 that yield $\Sigma_{1,2}$ do not change when we add the NNN interactions.

Chapter 7

Summary and discussion

In this work we have studied the strong coupling limit of lattice QCD with non-zero baryon density. We used the Hamiltonian formalism with nearest-neighbor (NN) fermions and next-nearest-neighbor (NNN) fermions. Also we do not take the continuum limit, but rather we regard this Hamiltonian as an effective Hamiltonian that describes QCD at large distances.

Expanding in powers of the inverse coupling one obtains an effective Hamiltonian for color singlet objects. In this work we restrict ourselves to second order in the expansion, where the effective Hamiltonian is a generalized antiferromagnet for $U(4N_f)$ spins. It has NN and NNN interactions, which are invariant under $U(4N_f)$ and $U(N_f) \times U(N_f)$ respectively. Also at this order the *local* baryon number $B_{\boldsymbol{n}}$ is conserved and one diagonalizes the antiferromagnet for a fixed background of baryon number, which fixes the representations of the $U(4N_f)$ spins.

When we write the partition function of the effective Hamiltonian with boson coherent states, it becomes tractable in the limit of large N_c and N_f, with the ratio $r = N_c/N_f$ kept fixed. In this limit we extend Arovas and Auerbach's result for zero density and dimension $d = 2$ to three dimensions. We find that for $r > r_c$, the antiferromagnet is in a Néel ordered phase, which corresponds to a phase with spontaneous broken chiral symmetry. The value of r_c in three dimensions is found to be 0.31. When we analyze this limit for a periodic configuration of baryon number, where a concentration $c = \frac{1}{8}$ and $c = \frac{1}{4}$ of the lattice sites is saturated with baryons, we find that r_c is 0.35 and 0.47 respectively. This means that the Néel phase is shrinking with increasing density.

For a random distribution of sites saturated with baryons, we average over the sites' positions in a quenched approximation. This is valid only if the concentration c of these sites obeys $c \ll 1$, and we calculate the free energy to first order in the concentration. Comparing this to the unquenched calculations at $c = \frac{1}{8}, \frac{1}{4}$, we find that the two calculations deviate near the phase transition point $r = r_c$. In fact, in the quenched calculation, r_c decreases with increasing density.

Despite this deviation, we note that the two approaches are in good agreement far from r_c. This opens the way to the systematic investigation of the system's properties with the quenched approach. For example, relying on the condensed matter analog of magnetic impurities, low lying excitations should develop non-zero decay widths and decreased velocities for non-zero density. Note that in Section 3.4.2 we were concerned with the disordered phase, where the excitations are massive. In certain cases, however, there exists a Holstein-Primakoff transformation for the generalized spins in terms of bosons (see Appendix H). Using this transformation and taking the limit of large N_c and fixed N_f, one can perform the quenched calculation in the ordered phase, on lines similar to Section 3.4.2. It will be interesting therefore to see how the Goldstone bosons decay and slow down in the presence of baryons.

Next we wrote the partition function using generalized spin coherent states to obtain a nonlinear sigma model. In Section 4.3 we analyzed the classical counterpart of the sigma model by dropping the Berry phase term. This analysis presumably describes the high temperature region of the system, where quantum fluctuations are not very important. It also serves as a tool to see how the symmetry realization changes as we add baryons to the lattice. Although the classical sigma model can be treated numerically (its action is real), we postponed this to future research and used mean field theory instead for a toy model that has $N = 3$. In that case we extracted the *classical* phase diagram in temperature-density plane. We found that $U(3)$ can be broken either to $U(2) \times U(1)$ or to $U(1) \times U(1) \times U(1)$, depending on the density. The order of the phase transition also depends on the density, as does the critical temperature, which decreases with increasing density.

We studied the full quantum sigma model in its semiclassical limit of large N_c and finite N_f. In the vacuum sector, we rederived Smit's result for the lowest-energy configuration of alternating $B_{\boldsymbol{n}} = \pm(m - N/2)$ sites. The classical degeneracy in the number m is removed by quantum fluctuations of $O(1/N_c)$, and the ground state indeed has $B_{\boldsymbol{n}} = 0$; the $U(4N_f)$ symmetry of the nearest-neighbor theory is spontaneously broken to $U(2N_f) \times U(2N_f)$. We extended this result to the NNN theory and found that its $U(N_f) \times U(N_f)$ chiral symmetry is broken to the vector $U(N_f)$ flavor subgroup. We also found that the classical degeneracy of the nearest-neighbor interactions can be removed by the NNN terms themselves, with no quantum corrections. These two procedures for lifting the degeneracy led to the same ground state.

Adding net baryon number to the system, we examined the case of uniform baryon density, $B_{\boldsymbol{n}} = B = m - 2N_f > 0$. When we limit ourselves to the nearest-neighbor theory, we find a Néel-like ground state that breaks $U(N)$ to $U(2m-N) \times U(N-m) \times U(N-m)$. The number of broken generators n_G thus depends on the baryon number B as

$$n_G = 2(2N_f - B)(2N_f + 3B). \tag{7.1}$$

When we calculate the low energy excitations of the NN theory, we find two types of Goldstone bosons [80, 81]. The type I bosons are $n_I = 2(2N_f - B)^2$ antiferromagnetic spin waves that have a linear dispersion relation. We also have $n_{II} = 4B(2N_f - B)$ type II bosons[1]. The numbers n_I, n_{II}, and n_G obey the Nielsen-Chadha counting rule

$$n_I + 2n_{II} \geq n_G. \tag{7.2}$$

We call the type II bosons ferromagnetic magnons since they emerge due to a ferromagnetic alignment of NNNspins. As typical for magnons, their energy is quadratic in momentum[2] and of $O(J_1/N_c)$, where J_1 is the coupling of the nearest-neighbor interactions.

The mechanism that removed the classical degeneracy at zero and non-zero density, and gave rise to type II Goldstone bosons in the latter case, is known in the condensed matter literature as order from disorder. It takes place in systems that possess a classically degenerate ground state. For example we mention the double exchange model [54] and the Kagomé antiferromagnet [55]. There, the classical ground state energy is invariant under a rotation of local groups of spins, making it exponentially degenerate as in our problem.

Finally when we perturb the nearest-neighbor ground state with the NNN interactions, we find that some of the global degeneracy of the nearest-neighbor ground state is removed, and that the vacuum expectation values of the sigma fields break chiral symmetry in a way that depends on N_f and the baryon number. In all cases with non-zero B, discrete lattice rotations are spontaneously broken as well. We summarize the patterns of spontaneous symmetry breaking in Table 6.1.

---

[1] Recall that the local baryon number B ranges from 0 to $2N_f$ with unit increments.

[2] A possible exception is for $N - m = 1$, where the energy may depend on a different power of the momentum. Correspondingly, the number of excitations will be different.

In comparing Table 6.1 to results of continuum CSC calculations, one must keep in mind that we study systems with large, fixed, and discrete values of B, rather than with large, continuous μ. Moreover, we use large-N_c approximations which necessarily ignore the discrete properties of the $SU(N_c)$ group that are essential to baryons.

The values of (N_c, N_f) that are of interest for CSC are $N_c = 3$ and $N_f = 2$ or 3. In the two-flavor the ground state does not break chiral symmetry. We do not see this for any density at $N_f = 2$. Our results are due to a $\bar{q}q$ condensate; whether there is a qq condensate as well cannot be ascertained.

For $N_f > 2$ the situation is similar. The CSC ground state for $N_c = 3$ and $N_f \geq 3$ partially breaks color and flavor, with a condensate that locks one or more subgroups of the flavor group to the color group [34]. Since we work at large N_c, we should stand the argument on its head. A plausible qq condensate would lock successive subgroups of the *color* group to the flavor group and hence to each other, leaving unbroken the diagonal $SU(N_f)_{L+R+C}$ and some leftover color symmetry. Judging by the global symmetry of the vacuum, perhaps we see this for $(N_f = 3, B = 3)$. The other cases could conceivably arise from a combination of $\bar{q}q$ and qq condensates, but whether the latter actually occur is an open question.

Finally we note that according to diagrammatic power-counting arguments [85, 86], CSC is suppressed in the 't Hooft limit, where $N_c \to \infty$ and $g^2 N_c$ is kept fixed. In the perturbative regime of small $g^2 N_c$, a Fermi sea prefers pairing of particle and holes that gives a chiral density wave with momentum $|\boldsymbol{p}| \simeq 2\mu$, where μ is the chemical potential. Our ansatz for the ground state does not permit this possibility.

When we determined how the NNN terms change the dispersion relations for the Goldstone bosons we found that the physics of the NN theory is mostly undisturbed by the NNN interaction. At leading order, the properties of the type I bosons (π) and of some of the type II bosons (χ_2) do not change. The type II bosons grouped in the χ_1 field suffer a variety of fates, falling into four classes that appear for different values of N_f and m. Class 1 bosons are unaffected by the NNN perturbation. Class 2 bosons split into type I and type II, and all gain anisotropic contributions of $O(J_2/(J_1/N_c))$ to their energies. Here J_2 is the coupling of the NNN interactions in the antiferromagnet. Some of the Class 3 bosons become massive while other remain unaffected. In Class 4, some become massive while the others become anisotropic type I bosons.

The symmetry of the theory, in all cases, is severely broken by the NNN terms—from $SU(4N_f)$ to $SU(N_f) \times SU(N_f) \times U(1)_A$. Not surprisingly, a simple count shows that the total number of massless real fields is far greater than the number of spontaneously broken generators of $SU(N_f) \times SU(N_f) \times U(1)_A$, as shown in Table 6.1. The particular NNN interaction we use is simply unable to generate masses *in lowest order* for many of the particles unprotected by Goldstone's Theorem. This is partly reflected in the accidental degeneracy of the ground state, which we mentioned below Eq. (6.16). Just as this degeneracy should be lifted in higher orders in $1/N_c$ [beginning with $O(J_2/N_c)$], the corresponding massless excitations should develop masses. The only particles protected from mass generation are the minimal number needed to satisfy Goldstone's theorem (or the Nielsen-Chadha variant).

Another effect that is missing is the mixing of type I and type II Goldstone bosons, which is certainly permitted when the NNN interaction is turned on. In the NN case we proved that such a mixing is forbidden, since the two types of boson belong to different representations of the unbroken subgroup. We present the classification in the NNN theory in Appendix L, where it is easy to see that it is less restrictive, and permits mixing of the bosons. Whether mixing occurs is a dynamical issue that can be settled only by calculating to higher order in $1/N_c$.

To conclude we note that other recent work [82, 84] on the high density regime of QCD—in the continuum—also predicts type II Goldstone bosons and anisotropic dispersion. There, the starting point is an effective field theory that describes the low energy dynamics of QCD with non-zero chemical potential μ. For $\mu \neq 0$, Lorentz invariance is broken, and the field equations become nonrelativistic. This leads to the emergence of type II Goldstone bosons. In addition, the ground state in [84] can support a non-zero expectation value of vector fields. This breaks rotational symmetry and makes some of the dispersion relations anisotropic.

Possible directions of future research begin with gaining more freedom in fixing the baryon configurations. In this work we restricted ourselves to either having sites saturated with baryons (in the boson coherent states approach) or with having the same baryon number on all sites (in the nonlinear sigma model approach). It is interesting to see what is the ground state of the antiferromagnet for other baryon configurations, that have $2N_f > B_{\boldsymbol{n}} > 0$ only on a sparse sublattice, along the lines of Section 4.3. This can be easily investigated for the classical counterpart of the sigma model, whose action is real, by Monte Carlo simulations. A general baryon distribution has a classical degeneracy which may be removed by order from disorder. This can be seen by calculating $1/N_c$ corrections that correspond to quantum order from disorder, as in Chapter 5. Another way to lift the degeneracy is with thermal fluctuations. These can be studied in the classical counterpart of the sigma model as well.

Another interesting direction is to fix the chemical potential μ instead of the baryon number. This requires calculating the grand canonical partition function $Z_{GC}(\mu)$, which is related to the canonical partition function $Z(\{B_{\boldsymbol{n}}\})$, treated in this work, by

$$Z_{GC} = \sum_{\{B_{\boldsymbol{n}}\}} e^{\beta\mu \sum_{\boldsymbol{n}} B_{\boldsymbol{n}}} Z(\{B_{\boldsymbol{n}}\}). \tag{7.3}$$

This will make the comparison to results of continuum and other strong coupling calculations more straightforward. Again a first step can be to calculate Z_{GC} for the classical sigma model. Also it will be interesting to see how order from disorder manifests itself in the grand canonical ensemble.

An ultimate goal is the incorporation of the third-order term in the effective Hamiltonian in order to have a theory with dynamical baryons. This Hamiltonian looks like the t–J model of condensed matter physics, but is in fact more complicated since the baryon operators do not obey canonical commutation relations. An instructive half-measure would be to study the antiferromagnet in the presence of a disordered baryon background.

One can also replace the baryon operators with simpler operators that mimic only some of the baryons' features. Reintroducing all the properties of the real operators can be done using methods of Hilbert space mapping (see for example [69]), which were introduced in the context of atomic and nuclear physics to treat quantum fields that do not obey canonical commutation relations.

Appendix A

Anticommutation relations of baryon operators

In this appendix we present the calculation of the anticommutation relations of the baryon composite operators introduced in Chapter 2. For simplicity we slightly deviate from the notations of Chapter 2 and denote color indices by $a, b, c, \ldots = 1, 2, 3$ and Dirac-flavor indices by $i, j, k, \ldots = 1, \ldots, 4N_f$. The baryon operators are given by

$$b_{ijk} = \epsilon_{abc}\psi_i^a\psi_j^b\psi_k^c, \tag{A.1}$$

where ψ_i^a are fermion operators obeying

$$\left\{\psi_i^a, \psi_j^{\dagger b}\right\} = \delta_{ab}\delta_{ij}. \tag{A.2}$$

We wish to calculate the following anticommutation relations of the baryon operators. Note that we are only interested in operators residing on the same site, and only in the anticommutators between b and $b^\dagger$. All other relations are trivial.

We wish to calculate

$$\left\{b_{ijk}^\dagger, b_{mnl}\right\} \;=\; \epsilon_{abc}\epsilon_{a'b'c'}\left(\psi_k^{\dagger c}\psi_j^{\dagger b}\psi_i^{\dagger a}\psi_m^{a'}\psi_n^{b'}\psi_l^{c'} + \psi_m^{a'}\psi_n^{b'}\psi_l^{c'}\psi_k^{\dagger c}\psi_j^{\dagger b}\psi_i^{\dagger a}\right). \tag{A.3}$$

We now concentrate on the second term, which we want to bring to a form similar to the first term, with a minus sign. The two will then cancel, and leave the expression we are after. We do that by moving the $\psi^\dagger$'s in the second term of Eq. (A.3) to the left, and have

$$
\begin{aligned}
\psi^{a'}_{m'}\psi^{b'}_{n'}\psi^{c'}_{l'}\psi^{\dagger c}_{k}\psi^{\dagger b}_{j}\psi^{\dagger a}_{i} &= \left(\psi^{a'}_{m}\psi^{\dagger c}_{k}\psi^{\dagger b}_{j}\psi^{b'}_{n}\psi^{c'}_{l}\psi^{\dagger a}_{i} + \psi^{a'}_{m}\left[\psi^{b'}_{n}\psi^{c'}_{l}, \psi^{\dagger c}_{k}\psi^{\dagger b}_{j}\right]\psi^{\dagger a}_{i}\right) \\
&= \left(-\psi^{\dagger c}_{k}\psi^{a'}_{m} + \delta_{km}\delta_{a'c}\right)\psi^{\dagger b}_{j}\psi^{b'}_{n}\left(-\psi^{\dagger a}_{i}\psi^{c'}_{l} + \delta_{il}\delta_{ac'}\right) \\
&\quad +\psi^{a'}_{m}\left(\psi^{b'}_{n}\left[\psi^{c'}_{l}, \psi^{\dagger c}_{k}\psi^{\dagger b}_{j}\right] + \left[\psi^{b'}_{n}, \psi^{\dagger c}_{k}\psi^{\dagger b}_{j}\right]\psi^{c'}_{l}\right)\psi^{\dagger a}_{i} \\
&= \psi^{\dagger c}_{k}\left(-\psi^{\dagger b}_{j}\psi^{a'}_{m} + \delta_{mj}\delta_{a'b}\right)\left(-\psi^{\dagger a}_{i}\psi^{b'}_{n} + \delta_{ni}\delta_{b'a}\right)\psi^{c'}_{l} \\
&\quad -\delta_{km}\delta a'c\psi^{\dagger b}_{j}\psi^{b'}_{n}\psi^{\dagger a}_{i}\psi^{c'}_{l} - \psi^{\dagger c}_{k}\psi^{a'}_{m}\psi^{\dagger b}_{j}\psi^{b'}_{n}\delta_{il}\delta_{ac'} \\
&\quad +\delta_{a'c}\delta_{km}\delta_{il}\delta_{ac'}\psi^{\dagger b}_{j}\psi^{b'}_{n} + \psi^{a'}_{m}\left[\psi^{b'}_{n}\left(\delta_{kl}\delta_{cc'}\psi^{\dagger b}_{j} - \delta_{lj}\delta_{c'b}\psi^{\dagger c}_{k}\right)\right. \\
&\quad \left. + \left(\delta_{nk}\delta_{b'c}\psi^{\dagger b}_{j} - \delta_{nj}\delta_{b'b}\psi^{\dagger c}_{k}\right)\psi^{c'}_{l}\right]\psi^{\dagger a}_{i}. \qquad \text{(A.4)}
\end{aligned}
$$

Moving $\psi^{\dagger a}_{i}$ in the first term of Eq. (A.4) leftward, we cancel the first term in Eq. (A.3) and obtain

$$
\begin{aligned}
\left\{b^{\dagger}_{ijk}, b_{mnl}\right\} &= \epsilon_{abc}\epsilon_{a'b'c'}\left[\psi^{\dagger c}_{k}\psi^{\dagger b}_{j}\psi^{b'}_{n}\psi^{c'}_{l}\delta_{im}\delta_{aa'} - \psi^{\dagger c}_{k}\psi^{\dagger b}_{j}\psi^{a'}_{m}\psi^{c'}_{l}\delta_{in}\delta_{b'a}\right. \\
&\quad -\psi^{\dagger c}_{k}\psi^{\dagger a}_{i}\psi^{b'}_{n}\psi^{c'}_{l}\delta_{jm}\delta_{ba'} + \psi^{\dagger c}_{k}\psi^{c'}_{l}\delta_{in}\delta_{jm}\delta_{ab'}\delta_{a'b} \\
&\quad -\psi^{\dagger b}_{j}\psi^{b'}_{n}\psi^{\dagger a}_{i}\psi^{c'}_{l}\delta_{km}\delta_{ca'} - \psi^{\dagger c}_{k}\psi^{a'}_{m}\psi^{\dagger b}_{j}\psi^{b'}_{n}\delta_{il}\delta_{ac'} \\
&\quad +\psi^{\dagger b}_{j}\psi^{b'}_{n}\delta_{a'c}\delta_{km}\delta_{il}\delta_{ac'} + \psi^{a'}_{m}\psi^{b'}_{n}\psi^{\dagger b}_{j}\psi^{daga}_{i}\delta_{kl}\delta_{cc'} \\
&\quad -\psi^{a'}_{m}\psi^{b'}_{n}\psi^{\dagger c}_{k}\psi^{daga}_{i}\delta_{jl}\delta_{bc'} + \psi^{a'}_{m}\psi^{b}_{j}\psi^{c'}_{l}\psi^{\dagger a}_{i}\delta_{nk}\delta_{b'c} \\
&\quad \left.-\psi^{a'}_{m}\psi^{\dagger c}_{k}\psi^{c'}_{l}\psi^{\dagger a}_{i}\delta_{nj}\delta_{bb'}\right]. \qquad \text{(A.5)}
\end{aligned}
$$

Using the δ functions and the two ϵ's in front of the brackets in Eq. (A.5), we have the following result for the anti-commutation relations,

$$
\begin{aligned}
\left\{b^{\dagger}_{ijk}, b_{mnl}\right\} &= 6\delta_{(ijk,lnm)} - 2\left(\delta_{kl}\delta_{im}Q_{jn} + \delta_{kl}\delta_{jm}Q_{in} + \delta_{jl}\delta_{km}Q_{in}\right) \\
&\quad -3\left(\delta_{km}\delta_{il}Q_{jn} + \delta_{km}\delta_{in}Q_{jl} + \delta_{km}\delta_{in}Q_{jl} + \delta_{kl}\delta_{jn}Q_{im}\right. \\
&\quad \left.+\delta_{kl}\delta_{in}Q_{jm} + \delta_{jl}\delta_{kn}Q_{im} + \delta_{nk}\delta_{il}Q_{jm} + \delta_{nk}\delta_{im}Q_{jl} + \delta_{jl}\delta_{im}Q_{kn}\right) \\
&\quad -4\left(\delta_{im}\delta_{jn}Q_{kl} + \delta_{in}\delta_{jl}Q_{km} + \delta_{in}\delta_{jm}Q_{kl} + \delta_{jm}\delta_{il}Q_{kn}\right. \\
&\quad \left.+\delta_{il}\delta_{jn}Q_{km} + \delta_{nk}\delta_{jm}Q_{il} + \delta_{nj}\delta_{km}Q_{il}\right) \\
&\quad +\delta_{im}\left(Q_{kl}Q_{jn} + Q_{kn}Q_{jl}\right) + \delta_{in}\left(Q_{kl}Q_{jm} + Q_{km}Q_{jl}\right) \\
&\quad +\delta_{il}\left(Q_{km}Q_{jn} + Q_{kn}Q_{jm}\right) + \delta_{jm}\left(Q_{kl}Q_{in} + Q_{kn}Q_{il}\right) \\
&\quad +\delta_{jn}\left(Q_{km}Q_{il} + Q_{kl}Q_{im}\right) + \delta_{jl}\left(Q_{kn}Q_{im} + Q_{in}Q_{km}\right) \\
&\quad +\delta_{kn}\left(Q_{jm}Q_{il} + Q_{jl}Q_{im}\right) + \delta_{km}\left(Q_{jn}Q_{il} + Q_{jl}Q_{in}\right) \\
&\quad +\delta_{kl}\left(Q_{jn}Q_{im} + Q_{in}Q_{jm}\right). \qquad \text{(A.6)}
\end{aligned}
$$

Here we define

$$\begin{aligned}
\delta_{(ijk,mnl)} &= \delta_{kl}\delta_{jm}\delta_{in}+\delta_{kl}\delta_{jn}\delta_{im}+\delta_{jl}\delta_{km}\delta_{in}+\delta_{jl}\delta_{kn}\delta_{im}+\delta_{kn}\delta_{jm}\delta_{il}+\delta_{nj}\delta_{km}\delta_{il}, \\
Q_{ij} &= \sum_{a=1}^{3}\psi_i^{\dagger a}\psi_j^a. \qquad \text{(A.7)}
\end{aligned}$$

We note in passing that in order to get Eq. (A.6) we used the following relations

$$\begin{aligned}
\psi_i^a\psi_j^{\dagger a} &= -\psi_j^{\dagger a}\psi_i^a+3\delta_{ij}, && \text{(A.8)} \\
[Q_{ij},\psi_k^a] &= -\delta_{ik}\psi_j^a, && \text{(A.9)} \\
\psi_k^{\dagger c}Q_{ij}\psi_l^c &= Q_{kl}Q_{ij}-\delta_{il}Q_{kj}, && \text{(A.10)} \\
\psi_k^c Q_{ij}\psi_l^{\dagger c} &= -Q_{ij}Q_{lk}+3\delta_{lk}Q_{ij}+3\delta_{ik}\delta_{lj}-\delta_{ik}Q_{lj} && \text{(A.11)}
\end{aligned}$$

As mentioned in Chapter 2, the baryon operators are *not* canonical anticommuting operators, and their anti-commutation relations obey $\left\{b_I, b_{I'}^\dagger\right\}=\Delta_{II'}\neq\delta_{II'}$.

Appendix B

Discretization of Euclidean time

In this section we stress the importance of the slicing prescription one uses for Euclidean time. In particular we work with a nearest-neighbor action defined on a bipartite lattice. We show the difference between using the exact prescription that results from the coherent state formalism of Section 3.1, and a naive prescription.

The coherent state formalism results in an action of the form

$$\begin{aligned} S &= \sum_{\tau=1}^{N_\tau} \Bigg\{ \sum_{\boldsymbol{n}} z^{e*}_{\tau,\boldsymbol{n}} \left(z^{e}_{\tau,\boldsymbol{n}} - z^{e}_{\tau+1,\boldsymbol{n}} \right) + \epsilon\lambda z^{e*}_{\tau,\boldsymbol{n}} z^{e}_{\tau+1,\boldsymbol{n}} \\ &\qquad + \sum_{\boldsymbol{m}} z^{o*}_{\tau,\boldsymbol{m}} \left(z^{o}_{\tau,\boldsymbol{m}} - z^{o}_{\tau+1,\boldsymbol{m}} \right) + \epsilon\lambda z^{o*}_{\tau,\boldsymbol{m}} z^{o}_{\tau+1,\boldsymbol{m}} \\ &\qquad - \epsilon \sum_{\boldsymbol{n},\boldsymbol{m}} z^{e}_{\tau,\boldsymbol{n}} Q_{\boldsymbol{n}\boldsymbol{m}} z^{o}_{\tau,\boldsymbol{m}} + z^{o*}_{\tau,\boldsymbol{m}} Q^*_{\boldsymbol{m}\boldsymbol{n}} z^{e*}_{\tau,\boldsymbol{n}} \Bigg\} \\ &\equiv f^* G^{-1} f. \end{aligned} \tag{B.1}$$

Here the index $\boldsymbol{n}(\boldsymbol{m})$ runs from 1 to $N_e(N_o)$ and denotes the sites on the even(odd) sublattice. f has two indices; $\tau = 1, \ldots, N_\tau - 1$, and a site index $\boldsymbol{n}$ that takes values from 1 to N_e or N_o,

$$f_{\tau,\boldsymbol{n}} = \begin{pmatrix} z^{e}_{\tau,1} \\ \vdots \\ z^{e}_{\tau,N_e} \\ \hline z^{o*}_{\tau,1} \\ \vdots \\ z^{o*}_{\tau,N_o} \end{pmatrix}. \tag{B.2}$$

In this basis the inverse propagator G^{-1} is

$$G^{-1} = \left(\begin{array}{c|c} -\hat{\partial} + \lambda \hat{D} & Q \\ \hline Q^{\dagger} & -\hat{\partial}^{\dagger} + \lambda \hat{D}^{\dagger} \end{array}\right), \tag{B.3}$$

where the diagonal blocks have dimensions $N_e N_\tau$, and $N_o N_\tau$. The matrices $\hat{\partial}$, and $\hat{D}$ are

$$\hat{\partial}_{\tau,\tau'} = \delta_{\tau,\tau'-1} - \delta_{\tau,\tau'}, \qquad \hat{D}_{\tau,\tau'} = \delta_{\tau,\tau'-1}. \tag{B.4}$$

times the unity in the lattice indices. $\hat{Q}$ is a unit matrix in Euclidean time indices multiplied by an $N_e \times N_o$ matrix that describes the interactions between the two sublattices. Note that we do not take $N_e = N_o$, to account for systems with vacancies. In order to calculate the determinant of the propagator, it is convenient to work in Matsubara space. There we have

$$\hat{\partial}_{n,n'} = \delta_{n,n'}(-1 + e^{-i\omega_n \epsilon}), \qquad \hat{D}_{n,n'} = e^{-i\omega_n \epsilon}, \tag{B.5}$$

and the determinant of Eq. (B.3) becomes

$$\begin{aligned} \det G^{-1} &= \prod_{n=-\infty}^{\infty} \det \begin{pmatrix} c_n \mathbf{1}_{N_e} & \epsilon Q \\ \epsilon Q^{\dagger} & c_n^* \mathbf{1} \end{pmatrix} \\ &= \prod_n \det\left(c_n^* \mathbf{1}_{N_o}\right) \det\left(c_n \mathbf{1}_{N_e} - \epsilon^2 Q (c_n^*)^{-1} \mathbf{1} Q^{\dagger}\right) \\ &= \prod_n (c_n^*)^{N_o - N_e} \det\left(|c_n|^2 \mathbf{1}_{N_e} - \epsilon^2 Q Q^{\dagger}\right). \end{aligned} \tag{B.6}$$

Here $c_n = (1 - e^{-i\omega_n \epsilon}) + e^{-i\omega_n \epsilon}\epsilon\lambda$. Next we diagonalize the $N_e \times N_e$ matrix $QQ^{\dagger}$ and write the determinant as

$$\det G^{-1} = \prod_n |c_n|^{N_o - N_e} \prod_{\alpha=1}^{N_e} \left(|c_n|^2 - \epsilon^2 q_\alpha^2\right). \tag{B.7}$$

Here q_α^2 are the N_e eigenvalues of $QQ^{\dagger}$.

We now calculate the determinant for the continuum naive prescription, where the time derivative $\hat{\partial} \to -i\omega_n \epsilon \delta_{n,n'}$, and $\hat{D} \to \delta_{n,n'}$. In this case we have $c_n = \epsilon(i\omega_n + \lambda)$, and the products in Eq. (B.7) become

$$\prod_n |c_n| \propto \exp\left[\frac{1}{2}\sum_n \log\left(\omega_n^2 + \lambda^2\right)\right], \tag{B.8}$$

$$\prod_n \left(|c_n|^2 - \epsilon^2 q_\alpha^2\right) \propto \exp\left[\sum_n \log\left(\omega_n^2 + \omega_\alpha^2\right)\right]. \tag{B.9}$$

Using the following relation [87]

$$\sum_{n=-\infty}^{\infty} \log\left(\omega_n^2 + E^2\right) = -2\log 2\sinh \beta E/2 + \text{constant}, \tag{B.10}$$

where the constant depends only on β, we find

$$\det G^{-1}_{\text{continuum}} = \left(\frac{1}{2\sinh\left(\beta\lambda/2\right)}\right)^{N_o-N_e} \prod_\alpha \left(\frac{1}{2\sinh\left(\beta\omega_\alpha/2\right)}\right)^2 . \tag{B.11}$$

Returning to the exact prescription we see that the products in Eq. (B.7) become

$$\prod_n |c_n| \quad\propto\quad \exp\left[\frac{1}{2}\sum_n \log\left(4(1-\epsilon\lambda)\sin^2(\omega_n\epsilon/2) + \epsilon^2\lambda^2\right)\right], \tag{B.12}$$

$$\prod_n \left(|c_n|^2 - \epsilon^2 q_\alpha^2\right) \quad\propto\quad \exp\left[\sum_n \log\left(4(1-\epsilon\lambda)\sin^2(\omega_n\epsilon/2) + \epsilon^2\omega_\alpha^2\right)\right]. \tag{B.13}$$

We separate the sums of the form given above to

$$\sum_n \log\left(4(1-\epsilon\lambda)\sin^2(\omega_n\epsilon/2) + \epsilon^2 X^2\right) = -\beta\lambda + \sum_n \log\left(4\sin^2(\omega_n\epsilon/2) + \epsilon^2 Y^2\right). \tag{B.14}$$

Here $Y^2 = X^2/(1-\epsilon\lambda)$. We have verified numerically that the sum on the right hand side of Eq. (B.14) is given by the sum in Eq. (B.10), by replacing E with X. One can understand this point as follows. Divide the sum into two,

$$\sum_n \log\left(4\sin^2(\omega_n\epsilon/2) + \epsilon^2 Y^2\right) = \sum_{|n|\leq m} + \sum_{|n|>m}, \tag{B.15}$$

where $m \ll N_\tau$. In the first sum we replace $4\sin^2(\omega_n\epsilon/2)$ with ω_n^2, and Y with X. For $N_\tau \to \infty$, m becomes very large, and since this sum is convergent, one can replace m with ∞.

The second sum the $\sin^2(\omega_n\epsilon/2)$ term is no longer of $O(\epsilon^2)$, and Y^2 can be dropped. Collecting only the X dependent term we are left with a sum of the form of Eq. (B.10). This gives

$$\det G^{-1} = \left(\frac{1}{1-e^{-\beta\lambda}}\right)^{N_o-N_e} \prod_\alpha \left(\frac{e^{\beta\lambda/2}}{2\sinh\left(\beta\omega_\alpha/2\right)}\right)^2, \tag{B.16}$$

with $\omega_\alpha = \sqrt{\lambda^2 - q_\alpha^2}$.

As a result we see that the effective action received after integrating the bosons $S_{\text{eff}} \sim \beta^{-1} \log \det G^{-1}$ obeys

$$S_{\text{eff}}^{\text{exact}} = S_{\text{eff}}^{\text{continuum}} - (N_e + N_o)\lambda/2. \tag{B.17}$$

For practical reasons it is more convenient to perform calculations with the naive prescription of $\hat{\partial} \to -i\omega$, and in order to restore the correct result we use the rule of thumb given in Eq. (B.17).

Appendix C

Minimizing the next-nearest-neighbor term

The s^μ_η signs are defined only when the σ^η are written in the basis $M^\eta = \Gamma^A \otimes \lambda^a = \rho^\alpha \otimes \sigma^\beta \otimes \lambda^a$. We choose a chiral basis for the gamma matrices, so that $\gamma_5 = \rho^3$, $\alpha_i = \rho^3\sigma^i$, and $\beta = \rho^1$. The energy (4.76) is a sum of squares,

$$\epsilon' = \sum_\eta A_\eta \left(\sigma^\eta\right)^2 , \tag{C.1}$$

with the constraint $\sum_\eta (\sigma^\eta)^2 = N/2$. The coefficients $A_\eta = \sum_\mu s^\mu_\eta$ take on the values $\{-3, -1, 1, 3\}$. The minimum of ϵ' occurs when all σ^η are zero except those corresponding to $A_\eta = -3$, namely, those for $M^\eta = \beta \otimes \lambda^a = \rho^1 \otimes \lambda^a$ and $M^\eta = \beta\gamma_5 \otimes \lambda^a = \rho^2 \otimes \lambda^a$; the energy is independent of these σ^η, and will be equal to

$$\epsilon' = -3 \sum_\eta \left(\sigma^\eta\right)^2 = -3N/2. \tag{C.2}$$

Thus the set of solutions can be written in the form

$$\sigma_0 = \begin{pmatrix} 0 & 0 & U & 0 \\ 0 & 0 & 0 & U \\ U^\dagger & 0 & 0 & 0 \\ 0 & U^\dagger & 0 & 0 \end{pmatrix} = \frac{\rho^1 + i\rho^2}{2} \otimes U + \frac{\rho^1 - i\rho^2}{2} \otimes U^\dagger. \tag{C.3}$$

Recalling that $\sigma_0^2 = 1$, we have $UU^\dagger = \mathbf{1}$, so $U \in U(N_f)$. A chiral rotation $\sigma_0 \to V^\dagger \sigma_0 V$, with

$$V = \begin{pmatrix} U & 0 & 0 & 0 \\ 0 & U & 0 & 0 \\ 0 & 0 & \mathbf{1} & 0 \\ 0 & 0 & 0 & \mathbf{1} \end{pmatrix} = \frac{1}{2}(1+\rho^3) \otimes U + \frac{1}{2}(1+\rho^3) \otimes \mathbf{1}, \tag{C.4}$$

turns σ_0 into $\rho^1 = \gamma_0$, which is invariant only under vector transformations generated by $\mathbf{1} \otimes \lambda^a$.

Appendix D

The function Φ for mean field theory of the $U(3)$ toy model at non-zero density

In this section we give Φ for all configurations that appear in Table 4.1 with non-zero baryon number. The lower indices of the magnetizations correspond to the numbering in Table 4.1.

As for zero density, we reduce the number of independent variables in Φ by substituting for some of them with their corresponding MF equations. Also we assume that all magnetizations commute, and are therefore diagonal in some basis. This restriction is justified for all configurations except no. 2 where we have to assume this as an ansatz.

Configuration no. 2

In this case the form of the MF equations does not allow us to take the magnetizations as diagonal, and we make the ansatz that in this case

$$m_i \sim \begin{pmatrix} 1 & 0 & 0 \\ 0 & 1 & 0 \\ 0 & 0 & -2 \end{pmatrix}, \quad i = 1, 2, 3, 4, \tag{D.1}$$

which means that we allow $\mu_i^8 \neq 0$ only. This gives the following form for Φ as a function of μ_i^8.

$$\Phi/N_s \;=\; \sqrt{3}/4K(\mu_1 - 3\mu_3 - \mu_2 + \mu_4) - K/4(3\mu_1\mu_2 + 3\mu_3\mu_4 + 6\mu_1\mu_3) - \varphi(6K\sqrt{3}\mu_i),$$

$$\begin{aligned}\varphi(x_i) &= \frac{1}{8}\Bigg[\log\left(\frac{e^{-x_1}-1}{x_1^2}+\frac{1}{x_1}\right)+\log\left(\frac{e^{-x_3}-1}{x_3^2}+\frac{1}{x_3}\right) \\ &\quad +3\log\left(\frac{e^{-(\frac{2}{3}x_3+\frac{1}{3}x_2)}-1}{(\frac{2}{3}x_3+\frac{1}{3}x_2)^2}+\frac{1}{\frac{2}{3}x_3+\frac{1}{3}x_2}\right) \\ &\quad +3\log\left(\frac{e^{(\frac{2}{3}x_1+\frac{1}{3}x_4)}-1}{(\frac{2}{3}x_1+\frac{1}{3}x_4)^2}+\frac{1}{\frac{2}{3}x_1+\frac{1}{3}x_4}\right)\Bigg], \end{aligned} \tag{D.2}$$

$$\mu_2 = f(6K\sqrt{3}\mu_1), \tag{D.3}$$

$$\mu_3 = -f(-2K\sqrt{3}(2\mu_1+\mu_4)), \tag{D.4}$$

where we have dropped the "8" index from all μ's, and

$$f(x) = \frac{2}{\sqrt{3}} - \sqrt{3}\frac{e^x(1-2/x+2/x^2)-2/x^2}{e^x(1-1/x)+1/x}. \tag{D.5}$$

We find that there is a first order phase transition, similar to the zero density case, at $K_c = 0.94$.

Configurations no. 3, 5, 6

Here taking only diagonal magnetizations into account is justified and we obtain the following Φ's. (From here on we denote (μ^3, μ^8) by $\vec{\mu}$, for all magnetizations)

1. Configuration no. 3

   There are three independent magnetizations $\vec{\mu}_i$; $i = 1, 2, 3$ and we have

$$\Phi/N_s = \sqrt{3}/2K(3\mu_2^8 - 2\mu_1^8 - \mu_3^8) - 3K/4\,(2\vec{\mu}_1\cdot\vec{\mu}_2 + \vec{\mu}_2\cdot\vec{\mu}_3) - \varphi(6K\vec{\mu}_i), \tag{D.6}$$

$$\begin{aligned}\varphi(\vec{x}_i) &= \frac{1}{8}\Bigg[\log\left(\frac{e^{x_{+,2}}-1}{x_{+,2}x_2^3}-\frac{e^{x_{-,2}}-1}{x_{-,2}x_2^3}\right)+3\log\left(\frac{e^{\frac{2}{3}x_{+,2}}-1}{\frac{2}{3}x_{+,2}x_2^3}-\frac{e^{\frac{2}{3}x_{-,2}}-1}{\frac{2}{3}x_{-,2}x_2^3}\right) \\ &\quad +3\log\left(\frac{e^{-\frac{1}{3}(x_{+,3}+2x_{+,1})}-1}{\frac{1}{9}(x_{+,3}+2x_{+,1})(x_3^2+2x_4^3)}-\frac{e^{-\frac{1}{3}(x_{-,3}+2x_{-,1})}-1}{\frac{1}{9}(x_{-,3}+2x_{-,1})(x_3^2+2x_4^3)}\right)\Bigg]. \end{aligned} \tag{D.7}$$

$$\mu_1^3 = f_3(4K\mu_2^3, 4K\mu_2^8), \qquad \mu_1^8 = f_8(4K\mu_2^3, 4K\mu_2^8), \tag{D.8}$$

$$\mu_3^3 = f_3(6K\mu_2^3, 6K\mu_2^8), \qquad \mu_3^8 = f_8(6K\mu_2^3, 6K\mu_2^8), \tag{D.9}$$

   where $f_{3,8}$ are given in Eqs. (4.64)–(4.65). Also $x_{\pm,i} = \sqrt{3}x_i^8 \pm x_i^3$, and we use this definition in further cases as well.

2. Configuration no. 5

   There are three independent magnetizations $\vec{\mu}_i$; $i = 1, 2, 3$ and we have

$$\Phi/N_s = \sqrt{3}/2K(3\mu_2^8 + 2\mu_1^8 + \mu_3^8) - 3K/4\,(2\vec{\mu}_1 \cdot \vec{\mu}_2 + \vec{\mu}_2 \cdot \vec{\mu}_3) - \varphi(6K\vec{\mu}_i). \tag{D.10}$$

   Here φ, and $\vec{\mu}_{1,3}$ are given by Eqs. (D.8)–(D.9).

3. Configuration no. 6

   Here we have two magnetizations $\vec{\mu}_i$; $i = 1, 2$ and we have

$$\begin{aligned}
\Phi/N_s &= \sqrt{3}/2K(\mu_2^8 + \mu_1^8) - 3K/4\ \vec{\mu}_1 \cdot \vec{\mu}_2 - \varphi(6K\vec{\mu}_i), && \text{(D.11)}\\
\varphi(\vec{x}_i) &= \frac{1}{8}\left[\log\left(\frac{e^{x_{+,2}} - 1}{x_{+,2}x_2^3} - \frac{e^{x_{-,2}} - 1}{x_{-,2}x_2^3}\right) + 3\log\left(\frac{e^{\frac{1}{3}x_{+,1}} - 1}{\frac{2}{3}x_{+,1}x_1^3} - \frac{e^{\frac{1}{3}x_{-,1}} - 1}{\frac{2}{3}x_{-,1}x_1^3}\right)\right], && \text{(D.12)}\\
\mu_1^3 &= f_3(6K\mu_2^3, 6K\mu_2^8), \qquad \mu_1^8 = f_8(6K\mu_2^3, 6K\mu_2^8). && \text{(D.13)}
\end{aligned}$$

In these three configurations we find that Φ has three equivalent nontrivial minima on the lines Eqs. (4.32)–(4.34) in the μ^3–μ^8 plane. These become lower in energy than the symmetric solution for $K > K_c$. The phase transition is first order and K_c is 1.03, 1.14, and 1.72 for configurations 3, 5, and 6.

Configuration no. 4, 7, 8

Here we also find that one can take the two magnetizations to be diagonal. In all these configurations we have two magnetizations $\vec{\mu}_i$; $i = 1, 2$

1. Configuration no. 4

   Φ is given by

$$\begin{aligned}
\Phi(\vec{\mu}_i)/N_s &= -3K\ \vec{\mu}_1 \cdot \vec{\mu}_2 - 2K\sqrt{3}(\mu_1^8 + \mu_2^8) - \varphi(6K\vec{\mu}_i), && \text{(D.14)}\\
\varphi(\vec{x}_i) &= \frac{1}{2}\left[\log\left(\frac{e^{x_{+,1}} - 1}{x_{+,1}x_1^3} - \frac{e^{-x_{-,1}} - 1}{x_{-,1}x_1^3}\right) - \log\left(\frac{e^{x_{+,2}} - 1}{x_{+,2}x_2^3} - \frac{e^{x_{+,2}} - 1}{x_{+,2}x_2^3}\right)\right],\\
\mu_1^3 &= f_3(6K\mu_2^3, 6K\mu_2^8), \qquad \mu_1^8 = f_8(6K\mu_2^3, 6K\mu_2^8). && \text{(D.15)}
\end{aligned}$$

   In this case we find that the phase transition is of second order. Also, there are six nontrivial minima. All of them have the same Φ, and become preferable over the symmetric solution for $K > 1$. Four of these minima are invariant under $U(2) \times U(1)$, and two are invariant only under $U(1) \times U(1) \times U(1)$.

2. Configurations no. 7,8

   Since these configurations are the two and one dimensional counterparts of configuration 4 [see Table 4.1], the MF equations and Φ are given by replacing $6K$ in the MF equations and Φ of configuration no. 4 by $4K$ and $2K$, respectively. This replacement simply increases the value of K_c by factors 3/2 and 3.

Appendix E

The matrices C and D in the $O(1/N_c)$ calculations

To analyze the matrices C and $D_{\boldsymbol{n}}$, given by Eqs. (5.7) and (I.18), we begin with the $U(N)$ generators M^η that lie outside the subalgebra $H = U(m) \times U(N-m)$ that commutes with

$$\Lambda = \begin{pmatrix} \mathbf{1}_m & 0 \\ 0 & -\mathbf{1}_{N-m} \end{pmatrix}. \tag{E.1}$$

We choose for them a basis M^{pq1} and M^{pq2} with $p = 1, \ldots, m$ and $q = m+1, \ldots, N$, given by

$$\begin{aligned} (M^{pq1})_{\alpha\beta} &= \frac{1}{2}\left(\delta_{p\alpha}\delta_{q\beta} + \delta_{p\beta}\delta_{q\alpha}\right) && \text{(E.2)} \\ (M^{pq2})_{\alpha\beta} &= \frac{i}{2}\left(\delta_{p\alpha}\delta_{q\beta} - \delta_{p\beta}\delta_{q\alpha}\right). && \text{(E.3)} \end{aligned}$$

Since the coset space $U(N)/H$ is a symmetric space, the commutator $[M^{pqa}, M^{p'q'a'}]$ lies in H; in order for $\mathrm{Tr}\,(\Lambda[M^{pqa}, M^{p'q'a'}])$ to be nonzero, the commutator must have a nonzero component in the Cartan subalgebra of H. This is only possible if $a \neq a'$ and $(p,q) = (p',q')$. Thus in this basis C takes the form

$$C = i \begin{pmatrix} 0 & \mathbf{1}_{m(N-m)} \\ -\mathbf{1}_{m(N-m)} & 0 \end{pmatrix}. \tag{E.4}$$

Diagonalizing C gives eigenvalues ± 1. The generators corresponding to the basis that diagonalizes C are

$$(M^{pq+})_{\alpha\beta} = (M^{pq1} + iM^{pq2})_{\alpha\beta} = \delta_{p\beta}\delta_{q\alpha} \tag{E.5}$$

$$(M^{pq-})_{\alpha\beta} \;=\; (M^{pq1} - iM^{pq2})_{\alpha\beta} = \delta_{p\alpha}\delta_{q\beta}. \tag{E.6}$$

As for D: The only anticommutators among the $M^{pq\pm}$ that do not vanish [note the bounds on (p,q)] are between M^{pq+} and $M^{p'q'-}$, *viz.*,

$$\{M^{pq+}, M^{p'q'-}\}_{\alpha\beta} = \delta_{qq'}\delta_{p\alpha}\delta_{p'\beta} + \delta_{pp'}\delta_{q'\alpha}\delta_{q\beta}. \tag{E.7}$$

Noting that $M^{pq-} = (M^{pq+})^\dagger$, we find that $D_{\boldsymbol{n}}$ takes the block-diagonal form

$$\begin{aligned} D_{\boldsymbol{n}}^{pq\pm,p'q'\pm} &= -\sum_{\boldsymbol{m}(\boldsymbol{n})} \mathrm{Tr}\left[\{(M^{pq\pm})^\dagger, M^{p'q'\pm}\}\begin{pmatrix} \sigma_{\boldsymbol{m}}^{(m)} & 0 \\ 0 & -\mathbf{1}_{N-m} \end{pmatrix}\right] && \text{(E.8)} \\ &= \delta_{qq'} \sum_{\boldsymbol{m}(\boldsymbol{n})} (\mathbf{1}_m - \sigma_{\boldsymbol{m}}^{(m)})_{pp'}. && \text{(E.9)} \end{aligned}$$

We summarize this by writing

$$D = \begin{pmatrix} E_{\boldsymbol{n}} & 0 \\ 0 & E_{\boldsymbol{n}} \end{pmatrix} \otimes 1_{N-m}, \tag{E.10}$$

where $E_{\boldsymbol{n}}$ is an $m \times m$ matrix given by

$$E_{\boldsymbol{n}} = \sum_{\boldsymbol{m}(\boldsymbol{n})} \left(\mathbf{1}_m - \sigma_{\boldsymbol{m}}^{(m)}\right). \tag{E.11}$$

It is easy to prove that the eigenvalues of E range from 0 to $4d$. In particular, D is positive.

Appendix F

Feynman rules to $O(1/N_c)$ for the effective action of the nonlinear sigma model

The following are the Feynman rules extracted from Eqs. (5.28)–(5.31). $A = (\mathrm{e}, \mathrm{o})$ stands for even and odd respectively. Latin indices take values in the range $[1, N-m]$ while Greek indices take values in the range $[1, 2m-N]$. The propagators are given in Figs. F.1 and F.2. The vertices extracted from the cubic and quartic interactions [Eqs. (5.29)–(5.31)] are given in Figs. F.3–F.4.

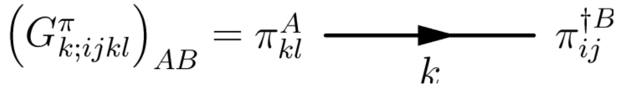

Figure F.1: Propagator of the π fields.

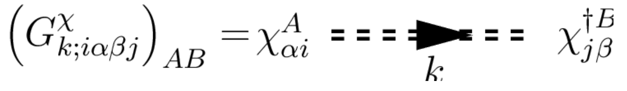
$\left(G^{\chi}_{k;i\alpha\beta j}\right)_{AB} = \chi^{A}_{\alpha i}$
k
$\chi^{\dagger B}_{j\beta}$

Figure F.2: Propagator of the χ fields.

(a)

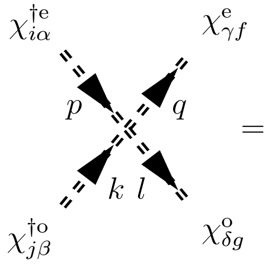
$\chi^{\dagger\mathrm{e}}_{i\alpha}$
$\chi^{\mathrm{e}}_{\gamma f}$
p
q
k
l
$\chi^{\dagger\mathrm{o}}_{j\beta}$
$\chi^{\mathrm{o}}_{\delta g}$

$$= -2Jd\tfrac{2}{N_sN_c\beta}\delta_{if}\delta_{jg}\delta_{\gamma\beta}\delta_{\alpha\delta}\gamma_{\boldsymbol{p}-\boldsymbol{q}}.$$

(b)

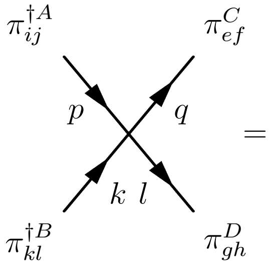

$$= 2Jd\tfrac{2}{N_sN_c\beta}\delta_{eh}\delta_{fi}\delta_{jk}\delta_{lg}\left[\delta_{A\mathrm{e}}\delta_{C\mathrm{e}}\delta_{B\mathrm{o}}\delta_{D\mathrm{o}} + (\mathrm{e}\leftrightarrow\mathrm{o})\right]\gamma_{\boldsymbol{p}-\boldsymbol{q}},$$

(c)

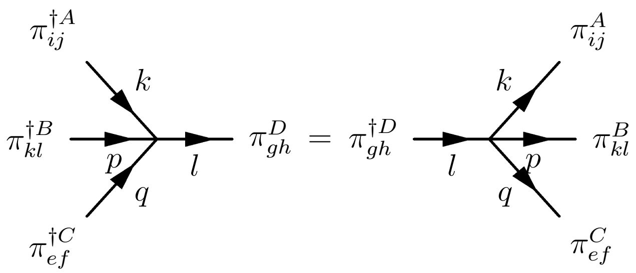

$$= -Jd\tfrac{2}{N_sN_c\beta}\delta_{ih}\delta_{jk}\delta_{le}\delta_{fg}\left[\delta_{D\mathrm{e}}\delta_{A\mathrm{e}}\delta_{B\mathrm{o}}\delta_{C\mathrm{e}} + (\mathrm{e}\leftrightarrow\mathrm{o})\right]\gamma_{\boldsymbol{p}}.$$

(d)

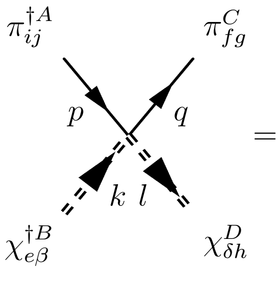

$$= 2Jd\tfrac{2}{N_sN_c\beta}\delta_{gi}\delta_{je}\delta_{\beta\delta}\delta_{hf}\left[\delta_{A\mathrm{e}}\delta_{C\mathrm{e}}\delta_{B\mathrm{o}}\delta_{D\mathrm{o}} + (\mathrm{e}\leftrightarrow\mathrm{o})\right]\gamma_{\boldsymbol{p}-\boldsymbol{q}},$$

(e)

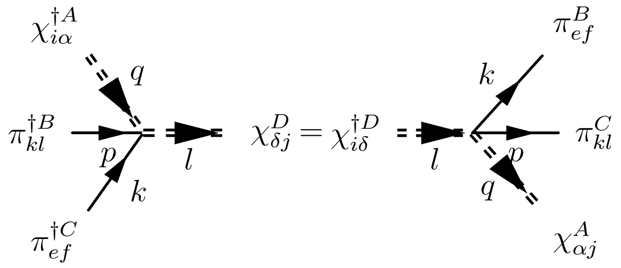

$$= -Jd\tfrac{2}{N_sN_c\beta}\delta_{\alpha\delta}\delta_{jk}\delta_{le}\delta_{if}\left[\delta_{A\mathrm{e}}\delta_{B\mathrm{e}}\delta_{C\mathrm{o}}\delta_{D\mathrm{e}} + (\mathrm{e}\leftrightarrow\mathrm{o})\right]\gamma_{\boldsymbol{p}}.$$

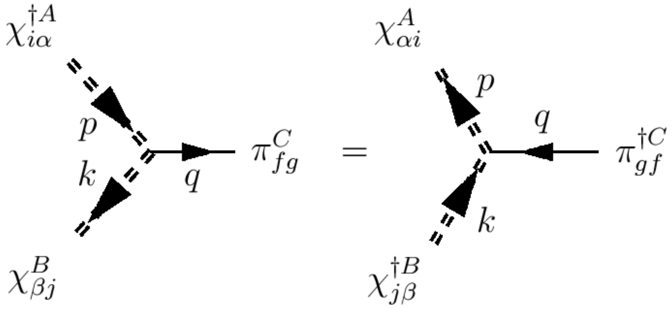

$$= -2Jd\sqrt{\frac{2}{N_s N_c \beta}}\delta_{\alpha\beta}\delta_{jf}\delta_{gi}\left[\delta_{A\mathrm{o}}\delta_{B\mathrm{e}}\delta_{C\mathrm{o}} - (\mathrm{e}\leftrightarrow\mathrm{o})\right]\gamma_{\boldsymbol{k}}$$

Figure F.4: Vertices corresponding to the cubic interaction.

Appendix G

Integral equations for the self energy of the zero modes

In this appendix we derive the integral equations represented by Fig. 5.3 and solve them approximately in order to obtain the dispersion relations of the χ bosons to $O(1/N_c)$. In analogy with the propagators of the antiferromagnetic spin waves we assume the following structure for $\Sigma_{1,k}$ and $\Sigma_{2,k}$ (we denote the frequency by Ω),

$$\begin{aligned} \Sigma_{1,k} &= A_1(\Omega^2;\boldsymbol{k}) + i\Omega B_1(\Omega^2;\boldsymbol{k}), && \text{(G.1)} \\ \Sigma_{2,k} &= A_2(\Omega^2;\boldsymbol{k}) + i\Omega B_2(\Omega^2;\boldsymbol{k}), && \text{(G.2)} \end{aligned}$$

where $A_{1,2}, B_{1,2}$ are real and $A_1^2 \geq A_2^2$ for stability. In order to perform the frequency integrals we make the following rational ansatz.

$$\begin{aligned} A_1 &= -\frac{2J_1 d}{N_c}\frac{P_1(\Omega^2;\boldsymbol{k})}{Q_1(\Omega^2;\boldsymbol{k})} < 0, && \text{(G.3)} \\ A_2 &= \frac{2J_1 d}{N_c}\frac{P_2(\Omega^2;\boldsymbol{k})}{Q_2(\Omega^2;\boldsymbol{k})}, && \text{(G.4)} \end{aligned}$$

Where $P_{1,2}(\Omega^2;\boldsymbol{k})$ and $Q_{1,2}(\Omega^2;\boldsymbol{k})$ are polynomials of the same order in ω^2. Thus we have

$$(G_k^\chi)_{AB} = \frac{1}{\Omega^2[(1+B_1)^2 - B_2^2] + A_1^2 - A_2^2}\begin{pmatrix} i\Omega(1+B_1) - A_1 & A_2 + i\Omega B_2 \\ A_2 - i\Omega B_2 & -i\Omega(1+B_1) - A_1 \end{pmatrix}_{AB}. \tag{G.5}$$

Since $B_{1,2} \sim O(1/N_c)$ we drop them in the denominator. The self-consistent equations for A and B then decouple, while only $A_{1,2}$ are needed to find the poles of the χ propagators to leading order.

G.1 Evaluation of diagrams

We begin with the diagrams that contribute to Σ_1. In this case we have contributions from all three diagrams in Fig. 5.3. Using the Feynman rules we evaluate each diagram and present the results for the self-energy matrix's upper left block with χ^e external legs in Fig. G.1. (The result for external legs of χ^o is the complex conjugate of that) [1]

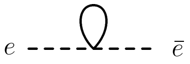

$$= \frac{2(N-m)J_1 d}{N_c}\int d^4q\left[\frac{-iq_0+2J_1d}{q_0^2+(2J_1dE_{\boldsymbol{q}})^2}-\frac{1}{2}\gamma_{\boldsymbol{q}}\left(\frac{2J_1d\gamma_{\boldsymbol{q}}}{q_0^2+(2J_1dE_{\boldsymbol{q}})^2}+c.c.\right)\right]$$

$$= \frac{N-m}{N_c}\int d^4q\,\frac{(2J_1dE_{\boldsymbol{q}})^2}{q_0^2+(2J_1dE_{\boldsymbol{q}})^2} = \frac{2(N-m)J_1d}{N_c}\int d^4q\,\frac{E_{\boldsymbol{q}}^2}{\bar{q}_0^2+E_{\boldsymbol{q}}^2}.$$

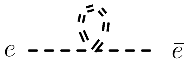

$$= -\frac{2(N-m)J_1d}{N_c}\int d^4q\,\frac{-iq_0-\Sigma_1(q)}{q_0^2+\Sigma_1^2(q)-\Sigma_2^2(q)}\gamma_0 = \frac{2(N-m)J_1d}{N_c}\int d^4q\,\frac{\bar{\Sigma}_1}{\bar{q}_0^2+\tilde{E}_{\boldsymbol{q}}^2}.$$

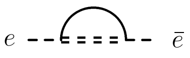

$$= \frac{4J_1^2d^2(N-m)}{N_c}\int d^4q\left[\gamma_k^2\frac{-iq_0-\Sigma_1(q)}{q_0^2+\Sigma_1^2(q)-\Sigma_2^2(q)}\times\frac{-i(q_0-k_0)+2J_1d}{(q_0-k_0)^2+(2J_1dE_{\boldsymbol{k}-\boldsymbol{q}})^2}\right.$$

$$+\gamma_{\boldsymbol{k}-\boldsymbol{q}}^2\frac{-i(q_0-k_0)-\Sigma_1(q-k)}{(q_0-k_0)^2+\Sigma_1^2(q-k)-\Sigma_2^2(q-k)}\times\frac{-iq_0+2J_1d}{q_0^2+(2J_1dE_{\boldsymbol{k}})^2}$$

$$\left.-\gamma_{\boldsymbol{k}}\gamma_{\boldsymbol{q}}\left(\frac{-iq_0-\Sigma_1(q)}{q_0^2+\Sigma_1^2(q)-\Sigma_2^2(q)}\times\frac{2J_1d\gamma_{\boldsymbol{k}-\boldsymbol{q}}}{(q_0-k_0)^2+(2J_1dE_{\boldsymbol{k}-\boldsymbol{q}})^2}+c.c.\right)\right].$$

Figure G.1: Schwinger-Dyson equation for Σ_1.

Here

$$E_{\boldsymbol{q}} = \sqrt{1-\gamma_{\boldsymbol{q}}^2}. \tag{G.6}$$

The factor of $(N-m)$ is the multiplicity of the diagram, and represents the number of particles that flow in the loop and have the same contribution. The diagrams that contribute to Σ_2 are only the second and third in Fig. 5.3. The result is given in Fig. G.2. Note that in this case there is no multiplicity to the diagrams. This is a result of the structure of the vertices. For example the first term in Eq. (5.31) that contributes to the

---

[1] Here we define $\int d^4q \equiv \int_{\mathrm{BZ}}\left(\frac{dq}{4\pi}\right)^d\int_{-\infty}^{\infty}\frac{dq_0}{2\pi}$.

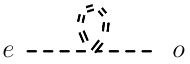

$$= -\frac{2J_1 d}{N_c}\int d^4q\, \frac{\Sigma_2(q)}{q_0^2+\Sigma_1^2(q)-\Sigma_2^2(q)}\gamma_{\boldsymbol{k}-\boldsymbol{q}}.$$

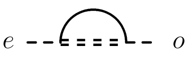

$$\begin{aligned}= \frac{4J_1^2 d^2}{N_c}\int d^4q \Bigg[&-\frac{\Sigma_2(q)}{q_0^2+\Sigma_1^2(q)-\Sigma_2^2(q)}\times\frac{2J_1 d\gamma_{\boldsymbol{k}-\boldsymbol{q}}}{(q_0-k_0)^2+(2J_1 dE_{\boldsymbol{k}-\boldsymbol{q}})^2}\times(\gamma_{\boldsymbol{q}}^2+\gamma_{\boldsymbol{k}}^2)\\ &+\frac{\Sigma_2(q)}{q_0^2+\Sigma_1^2(q)-\Sigma_2^2(q)}\times\frac{-i(k_0-q_0)+2J_1 d}{q_0^2+(2J_1 dE_{\boldsymbol{k}-\boldsymbol{q}})^2}\times\gamma_{\boldsymbol{k}}\gamma_{\boldsymbol{q}}\\ &-\frac{\Sigma_1(k-q)}{(q_0-k_0)^2+\Sigma_1^2(k-q)-\Sigma_2^2(k-q)}\times\frac{iq_0+2J_1 d}{q_0^2+(2J_1 dE_{\boldsymbol{k}})^2}\times\gamma_{\boldsymbol{k}}\gamma_{\boldsymbol{q}-\boldsymbol{k}}\Bigg].\end{aligned}$$

Figure G.2: Schwinger-Dyson equation for Σ_2.

second and first diagram in Fig. G.1, and Fig. G.2 has the following form.

$$\mathrm{Tr}\,\chi^e\chi^{\dagger e}\chi^o\chi^{\dagger o} = \sum_{\substack{\alpha\beta\in[1,2m-N]\\ ij\in[1,N-m]}}(\chi^e)_{\alpha i}(\chi^{*e})_{\beta i}(\chi^o)_{\beta j}(\chi^{*o})_{\alpha j}. \tag{G.7}$$

Its contribution to Σ_1 (of the even sites) comes from the contracting χ^o and χ^{*o}. Since this contraction is proportional to $\delta_{\alpha\beta}\delta_{jj}$, a sum over j gives a factor of $N-m$. The contribution to Σ_2 comes from contracting χ^{*o} to χ^{*e}. This gives $\delta_{\alpha\beta}\delta_{ij}$, and has multiplicity 1. The same reasoning applies to all the diagrams in the figures we present.

Using the parametrization (G.3)–(G.4) we get the following integral equations[2].

$$\begin{aligned}\frac{P_1(\Omega^2;\boldsymbol{k})}{Q_1(\Omega^2;\boldsymbol{k})} &= 2(N-m)\int_{\mathrm{BZ}}\left(\frac{dq}{4\pi}\right)^d\int_{-\infty}^{\infty}\frac{d\omega}{2\pi}\Bigg[-\frac{E_{\boldsymbol{q}}^2}{(\omega-\Omega)^2+E_{\boldsymbol{q}}^2}+\frac{\frac{1}{N_c}P_1(\omega^2;\boldsymbol{q})/Q_1(\omega^2;\boldsymbol{q})}{\omega^2+\tilde{E}^2(\omega^2;\boldsymbol{q})}\\ &-\frac{\omega(\omega-\Omega)\left(\gamma_{\boldsymbol{q}}^2-\gamma_{\boldsymbol{k}}^2\right)+\frac{1}{N_c}P_1(\omega^2;\boldsymbol{q})/Q_1(\omega^2;\boldsymbol{q})\left(2\gamma_{\boldsymbol{k}}\gamma_{\boldsymbol{q}}\gamma_{\boldsymbol{q}-\boldsymbol{k}}-\gamma_{\boldsymbol{q}}^2-\gamma_{\boldsymbol{k}}^2\right)}{\left[\omega^2+\tilde{E}^2(\omega^2;\boldsymbol{q})\right]\left[(\omega-\Omega)^2+E_{\boldsymbol{q}-\boldsymbol{k}}^2\right]}\Bigg],\end{aligned} \tag{G.8}$$

---

[2] We have defined $q_0 = 2J_1 d\omega$ and $k_O = 2J_1 d\Omega$.

where the three terms come from the three diagrams in Fig. G.1 and

$$\begin{aligned}\frac{P_2(\Omega^2;\boldsymbol{k})}{Q_2(\Omega^2;\boldsymbol{k})} &= 2\int_{\mathrm{BZ}}\left(\frac{dq}{4\pi}\right)^d\int_{-\infty}^{\infty}\frac{d\omega}{2\pi}\frac{\frac{1}{N_c}P_2(\omega^2;\boldsymbol{q})/Q_2(\omega^2;\boldsymbol{q})}{\omega^2+\tilde{E}^2(\omega^2;\boldsymbol{q})}\\ &\qquad\times\left[\frac{2\gamma_{\boldsymbol{k}}\gamma_{\boldsymbol{q}}-\gamma_{\boldsymbol{q}-\boldsymbol{k}}\left(\gamma_{\boldsymbol{q}}^2+\gamma_{\boldsymbol{k}}^2\right)}{(\omega-\Omega)^2+E_{\boldsymbol{q}-\boldsymbol{k}}^2}-\gamma_{\boldsymbol{q}-\boldsymbol{k}}\right],\end{aligned}\tag{G.9}$$

which comes from the second and third diagrams in Fig. G.2. Here

$$\tilde{E}(\omega^2;\boldsymbol{q})=\frac{1}{N_c}\sqrt{\frac{P_1^2}{Q_1^2}-\frac{P_2^2}{Q_2^2}}\equiv\frac{1}{N_c}\frac{P}{Q}.\tag{G.10}$$

G.2 Evaluation of frequency integrals

It remains to evaluate the $O(1/N_c)$ contribution of the following integrals

$$\begin{aligned}I_1^i &= \frac{1}{N_c}\int_{-\infty}^{\infty}\frac{d\omega}{2\pi}\frac{P_i/Q_i}{\omega^2+\tilde{E}^2}, &\text{(G.11)}\\ I_2^i &= \frac{1}{N_c}\int_{-\infty}^{\infty}\frac{d\omega}{2\pi}\frac{P_i/Q_i}{\left(\omega^2+\tilde{E}^2\right)[(\omega-\Omega)^2+E^2]}, &\text{(G.12)}\\ I_3 &= \int_{-\infty}^{\infty}\frac{d\omega}{2\pi}\frac{\omega(\omega-\Omega)}{\left(\omega^2+\tilde{E}^2\right)[(\omega-\Omega)^2+E^2]}. &\text{(G.13)}\end{aligned}$$

All these integrals are convergent at large ω and can be evaluated with residue calculus. Beginning with I_1^i,

$$I_1^i=\frac{1}{N_c}\int_{-\infty}^{\infty}\frac{d\omega}{2\pi}\frac{P_iQ_iQ_{j\neq i}^2}{\omega^2Q^2+\frac{1}{N_c^2}P^2}.\tag{G.14}$$

The poles of the integrands are given by

$$\omega^2Q^2(\omega^2)+\frac{1}{N_c^2}P^2(\omega^2)=0.\tag{G.15}$$

To leading order in $1/N_c$ the roots are determined by either

$$\omega^2=-\frac{1}{N_c^2}P^2(0)/Q^2(0)\equiv\omega_0^2\tag{G.16}$$

or by

$$Q^2(\omega^2) = 0. \tag{G.17}$$

Since the polynomials P_i and Q_i do not depend on N_c and $Q_i(0)$ can be chosen to be 1, the solutions of Eq. (G.17) are all $O(1)$. Moreover since $Q^2 > 0$, all these roots appear in complex conjugate pairs (ω, ω^*). For definiteness we choose $\mathrm{Im}\,\omega > 0$ and close the contours from above.

The result for I_1^i is [3]

$$\begin{aligned}
I_1^i &= \frac{1}{N_c}\frac{2\pi i}{2\pi}\sum_n \frac{P_i(\omega_n)Q_i(\omega_n)Q^2_{j\neq i}(\omega_n)}{2i\mathrm{Im}\,\omega_n \prod_{m\neq n}(\omega_n^2-\omega_m^2)(\omega_n^2-\omega_m^{*2})} \\
&= \frac{1}{2N_c}\left[\frac{P_i(\omega_0)Q_i(\omega_0)Q^2_{j\neq i}(\omega_0)}{\mathrm{Im}\,\omega_0 \prod_{\omega_m\neq\omega_0}(\omega_0^2-\omega_m^2)(\omega_0^2-\omega_m^{*2})} + \sum_{\omega_n\neq\omega_0}\frac{P_i(\omega_n)Q_i(\omega_n)Q^2_{j\neq i}(\omega_m)}{\mathrm{Im}\,\omega_n \prod_{m\neq n}(\omega_n^2-\omega_m^2)(\omega_n^2-\omega_m^{*2})}\right] \\
&\simeq \frac{1}{2N_c}\left[\frac{P_i(0)Q_i(0)Q^2_{j\neq i}(0)}{1/N_c P(0)/Q(0)\prod_{\omega_m\neq\omega_0}|\omega_m^{*2}|^2} + \sum_{\omega_n\neq\omega_0}\frac{P_i(\omega_n)Q_i(\omega_n)Q^2_{j\neq i}(\omega_0)}{\mathrm{Im}\,\omega_n \prod_{m\neq n}(\omega_n^2-\omega_m^2)(\omega_n^2-\omega_m^{*2})}\right] \\
&= \frac{1}{2N_c}\left[N_c\frac{P_i(0)Q_i(0)Q^2_{j\neq i}(0)}{P(0)/Q(0)\cdot Q^2(0)} + O(1)\right] = \frac{1}{2}\frac{P_i(0)}{P(0)}\frac{Q_i(0)Q_{i\neq j}(0)}{Q(0)} + O(1/N_c) \\
&= \frac{1}{2}\frac{P_i(0)}{Q_i(0)}\frac{1}{\sqrt{\left(\frac{P_1(0)}{Q_1(0)}\right)^2-\left(\frac{P_2(0)}{Q_2(0)}\right)^2}} + O(1/N_c).
\end{aligned} \tag{G.18}$$

The leading contribution to Eq. (G.11) comes from the poles given by Eq. (G.15). For the fourth row we used the fact that all other poles are of $O(1)$, and in the fact that $Q^2(0)$ can be written in terms of a product of its zeros. For the fifth row we used the definitions of $Q(0)$ and $P(0)$.

The calculation of I_2 and I_3 is similar, but one has two more poles to consider, at $\omega' = \Omega \pm iE$. In the case of I_2, the leading contribution is again due to the pole at ω_0 only.

$$\begin{aligned}
I_2^i &= \frac{1}{N_c}\int\frac{d\omega}{2\pi}\frac{P_iQ_iQ^2_{j\neq i}}{\left(\omega^2Q^2+\frac{1}{N_c^2}P^2\right)\left[(\omega-\Omega)^2+E^2\right]} \\
&= \frac{1}{N_c}\frac{2\pi i}{2\pi}\left\{\sum_n \frac{P_i(\omega_n)Q_i(\omega_n)Q^2_{j\neq i}(\omega_n)}{2i\mathrm{Im}\,\omega_n\prod_{m\neq n}(\omega_n^2-\omega_m^2)(\omega_n^2-\omega_m^{*2})}\times\frac{1}{(\omega_n-\Omega)^2+E^2}\right.
\end{aligned}$$

---

[3] Note that the denominator $Q^2\omega^2+1/N_c^2P^2 > 0$ is a polynomial in ω^2 and can be written as $\prod_m(\omega^2-\omega_m^2)(\omega^2-\omega_m^{2*})$, where $\pm\omega_m$ are the (complex) zeros of Eq. (G.15). We also have $Q^2 = \prod'_m(\omega^2-\omega_m^2)(\omega^2-\omega_m^{2*})$, where the product includes only the zeros of Eq. (G.17).

$$
\begin{aligned}
&\left.+\frac{P_i(\omega')Q_{j\neq i}(\omega')}{2iE\left[\omega'^2 Q^2(\omega')+1/N_c^2 P^2(\omega')\right]}\right\} \\
&= \frac{1}{2}\frac{P_i(0)}{Q_i(0)}\frac{1}{\sqrt{\left(\frac{P_1(0)}{Q_1(0)}\right)^2-\left(\frac{P_2(0)}{Q_2(0)}\right)^2}}\times\frac{1}{\Omega^2+E^2}+O(1/N_c). \qquad \text{(G.19)}
\end{aligned}
$$

The integral I_3 is written as

$$
\begin{aligned}
I_3 &= \int\frac{d\omega}{2\pi}\frac{\omega(\omega-\Omega)Q^2}{\left(\omega^2 Q^2+\frac{1}{N_c^2}P^2\right)\left[(\omega-\Omega)^2+E^2\right]} \\
&= \frac{2\pi i}{2\pi}\left\{\sum_n\frac{\omega_n(\omega_n-\Omega)Q^2(\omega_n)}{2i\mathrm{Im}\,\omega_n\prod_{m\neq n}(\omega_n^2-\omega_m^2)(\omega_n^2-\omega_m^{*2})}\times\frac{1}{(\omega_n-\Omega)^2+E^2}\right. \\
&\qquad\left.+\frac{iE\omega' Q^2(\omega')}{2iE\left[\omega'^2 Q^2(\omega')+1/N_c^2 P^2(\omega')\right]}\right\} \\
&\simeq \frac{1}{2}\left\{\frac{\omega_0(\omega_0-\Omega)Q^2(\omega_0)}{\mathrm{Im}\,\omega_0\prod_{\omega_m\neq\omega_0}(\omega_0^2-\omega_m^2)(\omega_0^2-\omega_m^{*2})}\times\frac{1}{(\omega_0-\Omega)^2+E^2}\right. \\
&\qquad\left.+\sum_{\omega_n\neq\omega_0}\frac{\omega_n(\omega_n-\Omega)Q^2(\omega_n)}{2i\mathrm{Im}\,\omega_n\prod_{m\neq n}(\omega_n^2-\omega_m^2)(\omega_n^2-\omega_m^{*2})}\times\frac{1}{(\omega_n-\Omega)^2+E^2}+\frac{i}{\Omega+iE}\right\} \\
&\simeq \frac{1}{2}\left[\frac{-i\Omega}{\Omega^2+E^2}+\frac{i}{\Omega+iE}\right]=\frac{1}{2}\frac{E}{\Omega^2+E^2}+O(1/N_c). \qquad \text{(G.20)}
\end{aligned}
$$

Here we used the the fact that $\omega_{n\neq 0}$ are the zeros of Q^2, which means that the residue of these poles is zero.

Using our freedom to normalize the polynomials $Q_{1,2}(0)>0$, we choose $Q_{1,2}(0)=1$ and write the integrals to leading order as

$$
I_1^i = \frac{1}{2}\frac{P_i(0)}{\sqrt{P_1^2(0)-P_2^2(0)}}, \qquad \text{(G.21)}
$$

$$
I_2^i = \frac{1}{2}\frac{P_i(0)}{\sqrt{P_1^2(0)-P_2^2(0)}}\frac{1}{\Omega^2+E^2}, \qquad \text{(G.22)}
$$

$$
I_3 = \frac{1}{2}\frac{E}{\Omega^2+E^2}. \qquad \text{(G.23)}
$$

Thus we find that to $O(1/N_c)$, all integrals depend only on the values of the polynomials at $\omega=0$. Finally, Eqs. (G.8)–(G.9) simplify to

$$
\frac{P_1(\Omega^2,\boldsymbol{k})}{Q_1(\Omega^2,\boldsymbol{k})} = (N-m)\int_{\mathrm{BZ}}\left(\frac{dq}{4\pi}\right)^d\left[\cosh\theta_{\boldsymbol{q}}\left(1+\frac{2\gamma_{\boldsymbol{k}}\gamma_{\boldsymbol{q}}\gamma_{\boldsymbol{q}-\boldsymbol{k}}-\gamma_{\boldsymbol{q}}^2-\gamma_{\boldsymbol{k}}^2}{E_{\boldsymbol{q}-\boldsymbol{k}}^2+\Omega^2}\right)\right.
$$

$$
\left. -\frac{E_{\boldsymbol{q}-\boldsymbol{k}}\left(\gamma_{\boldsymbol{q}}^2-\gamma_{\boldsymbol{k}}^2\right)}{E_{\boldsymbol{q}-\boldsymbol{k}}^2+\Omega^2} - E_{\boldsymbol{q}} \right], \tag{G.24}
$$

$$
\frac{P_2(\Omega^2,\boldsymbol{k})}{Q_2(\Omega^2,\boldsymbol{k})} = \int_{\mathrm{BZ}} \left(\frac{dq}{4\pi}\right)^d \left[\sinh\theta_{\boldsymbol{q}} \left(\frac{2\gamma_{\boldsymbol{q}}\gamma_{\boldsymbol{k}} - \gamma_{\boldsymbol{q}-\boldsymbol{k}}\left(\gamma_{\boldsymbol{q}}^2+\gamma_{\boldsymbol{k}}^2\right)}{E_{\boldsymbol{q}-\boldsymbol{k}}^2+\Omega^2} - \gamma_{\boldsymbol{q}-\boldsymbol{k}}\right)\right]. \tag{G.25}
$$

Where we have defined

$$
\tanh\theta_{\boldsymbol{q}} = \frac{P_2(0,\boldsymbol{q})}{P_1(0,\boldsymbol{q})}. \tag{G.26}
$$

Here we also point out that $\Sigma_{1,2}$ have zeros at $k=0$. For example the function multiplying the the cosh in Eq. (G.24) is exactly zero at $\Omega = 0$, and $\boldsymbol{q} = 0$. This is also the case for the rest of Eq. (G.24), and for the function multiplying the sinh in Eq. (G.25). This is a direct result of the Ward identities regarding the $U(N)$ generators that correspond to fluctuations in the χ directions.

Taking $\Omega = 0$, and dividing Eq. (G.25) by Eq. (G.24), we have

$$
(N-m)\tanh\theta_{\boldsymbol{k}} = \frac{\displaystyle\int_{\mathrm{BZ}} \left(\frac{dq}{4\pi}\right)^d I_2(\boldsymbol{q},\boldsymbol{k})\sinh\theta_{\boldsymbol{q}}}{\displaystyle\int_{\mathrm{BZ}} \left(\frac{dq}{4\pi}\right)^d I_1(\boldsymbol{q},\boldsymbol{k})\cosh\theta_{\boldsymbol{q}} - \eta(\boldsymbol{k})} \equiv \frac{\beta_{\boldsymbol{k}}}{\alpha_{\boldsymbol{k}}}. \tag{G.27}
$$

Here we have further defined

$$
\eta(\boldsymbol{k}) = \int_{\mathrm{BZ}} \left(\frac{dq}{4\pi}\right)^d \left[\frac{\gamma_{\boldsymbol{q}-\boldsymbol{k}}^2 - \gamma_{\boldsymbol{k}}^2}{E_{\boldsymbol{q}}} + E_{\boldsymbol{q}}\right], \tag{G.28}
$$

$$
I_1(\boldsymbol{q},\boldsymbol{k}) = \left(1 + \frac{2\gamma_{\boldsymbol{q}}\gamma_{\boldsymbol{k}}\gamma_{\boldsymbol{q}-\boldsymbol{k}} - \gamma_{\boldsymbol{q}}^2 - \gamma_{\boldsymbol{k}}^2}{E_{\boldsymbol{q}-\boldsymbol{k}}^2}\right), \tag{G.29}
$$

$$
I_2(\boldsymbol{q},\boldsymbol{k}) = \left(\frac{2\gamma_{\boldsymbol{q}}\gamma_{\boldsymbol{k}} - \gamma_{\boldsymbol{q}-\boldsymbol{k}}\left(\gamma_{\boldsymbol{q}}^2+\gamma_{\boldsymbol{k}}^2\right)}{E_{\boldsymbol{q}-\boldsymbol{k}}^2} - \gamma_{\boldsymbol{q}-\boldsymbol{k}}\right). \tag{G.30}
$$

A solution of this equation must obey

$$
\int_{\mathrm{BZ}} \left(\frac{dq}{4\pi}\right)^d I_1(\boldsymbol{q},\boldsymbol{k})\cosh\theta_{\boldsymbol{q}} - \eta(\boldsymbol{k}) \geq 0, \tag{G.31}
$$

so that the stability condition (5.49) will be satisfied.

After solving the integral equation (5.52) one can extract the spectrum of the χ bosons by calculating the poles of the propagator (5.48). These poles are given by equation (G.15). As seen there are two kinds of solutions. The $O(1/N_c)$ poles of the form (G.16) give rise to a low energy band [see Eq. (G.10)]

$$\pm i\omega = \frac{2J_1 d}{N_c}\sqrt{P_1^2(0,\boldsymbol{k}) - P_2^2(0,\boldsymbol{k})} \tag{G.32}$$

Using Eq. (G.26) and Eq. (5.52) we have

$$\pm i\omega = \frac{2J_1 d(N-m)}{N_c}\alpha_{\boldsymbol{k}}\sqrt{1-\tanh^2\theta_{\boldsymbol{k}}} \equiv \frac{2J_1 d(N-m)}{N_c}\epsilon_{\boldsymbol{k}}. \tag{G.33}$$

The $O(1)$ poles that solve Eq. (G.17) represent uninteresting massive excitations.

G.3 Solution of integral equations

In order to solve the integral equations we assumed that the function $\theta_{\boldsymbol{q}}$ is a function of the absolute value $q = |\boldsymbol{q}|$. Taking $\Omega = 0$, and dividing Eq. (G.25) by Eq. (G.24), we have (for $d = 3$)

$$(N-m)\tanh\theta_{\boldsymbol{k}} = \frac{\displaystyle\int_{\mathrm{BZ}} dq\, q^2 d\cos(\phi)\, d\varphi\, I_2(\boldsymbol{q},\boldsymbol{k})\sinh\theta_q}{\displaystyle\int_{\mathrm{BZ}} dq\, q^2\, d\cos(\phi)\, d\varphi I_1(\boldsymbol{q},\boldsymbol{k})\cosh\theta_q - \eta(\boldsymbol{k})}. \tag{G.34}$$

and $\boldsymbol{q} = q\,(\sin(\phi)\cos(\varphi), \sin(\phi)\sin(\varphi), \cos(\phi))$, where $0 < \varphi < 2\pi$, $0 < \phi < \pi$. The integration is over the first Brillouin zone of the fcc lattice. The BZ is presented in Fig. G.3. Since it is not spherically symmetric, the maximum value that $|\boldsymbol{q}|$ and $|\boldsymbol{k}|$ can take depend on the direction of the vectors. In direction $(1,0,0)$ it is 2π, whereas in direction $(1,1,1)$ it is $\sqrt{3}\pi$. The maximum allowed value is $\sqrt{5}\pi$, and is attained for example in direction $(0,1,2)$. In order to perform the momentum integrations we have generated a spherical mesh of the 6 coordinates $\boldsymbol{k}$ and $\boldsymbol{q}$ that has a radius of $\sqrt{5}\pi$ while restricting it to the BZ by multiplying all integrands by a step function that is 1 if a point in this six dimensional space obeys the following restrictions, and zero otherwise. We first restrict $|k_{x,y,z}| < 2\pi$ and $|q_{x,y,z}| < 2\pi$, and further

$$\begin{aligned} &|q_x + q_y + q_z| < 3\pi, \qquad && |-q_x + q_y + q_z| < 3\pi, \\ &|q_x - q_y + q_z| < 3\pi, \qquad && |q_x + q_y - q_z| < 3\pi, \end{aligned} \tag{G.35}$$

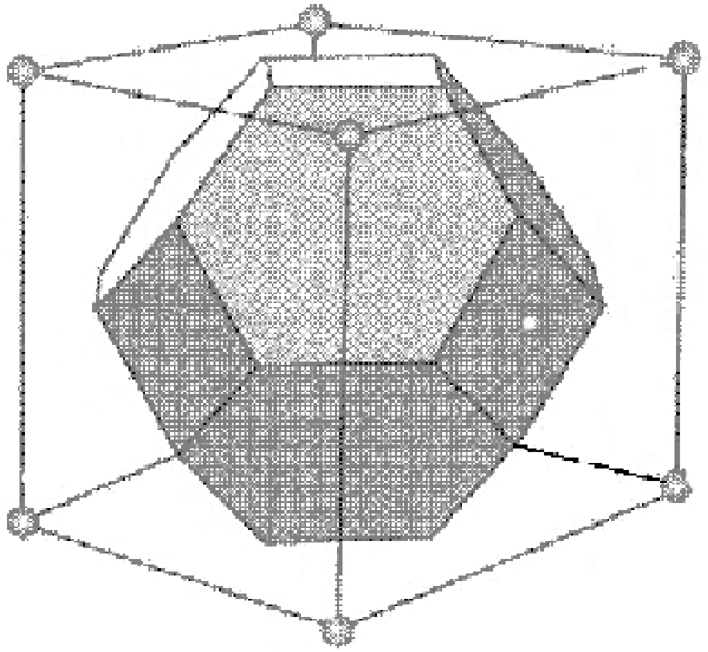

Figure G.3: The first Brillouin zone of the fcc lattice. The side of the outer cube is 4π. The BZ surface is composed out of six small and eight larger faces. The distance between the origin and the of the faces are $\sqrt{3}\pi$ and 2π. (Reproduced from http://140.114.18.41/micro/chap2/fig/fig0206.jpg)

and the same for $\boldsymbol{k}$. This forms the shape shown in Fig. G.3. Using the spherical assumption we reduce the integral equation to be one dimensional (with regard to the integration). We define

$$a_1(q,\boldsymbol{k}) = q^2 \int_{\mathrm{BZ}(q,\boldsymbol{k})} d\cos(\phi)\, d\varphi I_1(\boldsymbol{q},\boldsymbol{k}), \qquad a_2(q,\boldsymbol{k}) = q^2 \int_{\mathrm{BZ}(q,\boldsymbol{k})} d\cos(\phi)\, d\varphi I_2(\boldsymbol{q},\boldsymbol{k}), \tag{G.36}$$

where the boundaries of the integration depend on the value of q and $\boldsymbol{k}$, hence the notation $\mathrm{BZ}(q,\boldsymbol{k})$. Finally we have

$$(N-m)\tanh\theta_{\boldsymbol{k}} = \frac{\displaystyle\int_0^{\sqrt{5}\pi} dq\, a_2(q,\boldsymbol{k})\sinh\theta_q}{\displaystyle\int_0^{\sqrt{5}\pi} dq\, a_1(q,\boldsymbol{k})\cosh\theta_q - \eta(\boldsymbol{k})}. \tag{G.37}$$

Eq. (G.37) is only an approximation to Eq. (5.52). On the right hand side, there is an explicit dependence on the direction of $\boldsymbol{k}$ (via $a_{1,2}$ and η), while on the left hand side the dependence should vanish by assumption. We first examine the solution to Eq. (G.37) for $\boldsymbol{k}$ in the direction $(0,1,2)$, so that $|\boldsymbol{k}|$ can take all values up to $\sqrt{5}\pi$ like $|\boldsymbol{q}|$ on the left hand side. This solution is presented in Fig. 5.4. The next step is to see how this solution behaves in other directions. We do not expect the equation to be satisfied for all directions. More exactly we expect that the behavior away from the BZ boundary, near $\boldsymbol{k} = 0$, will indeed is spherical, so that the equation is approximately correct for this region. We give the results of this check in Fig. G.4. Here the solid line is the original

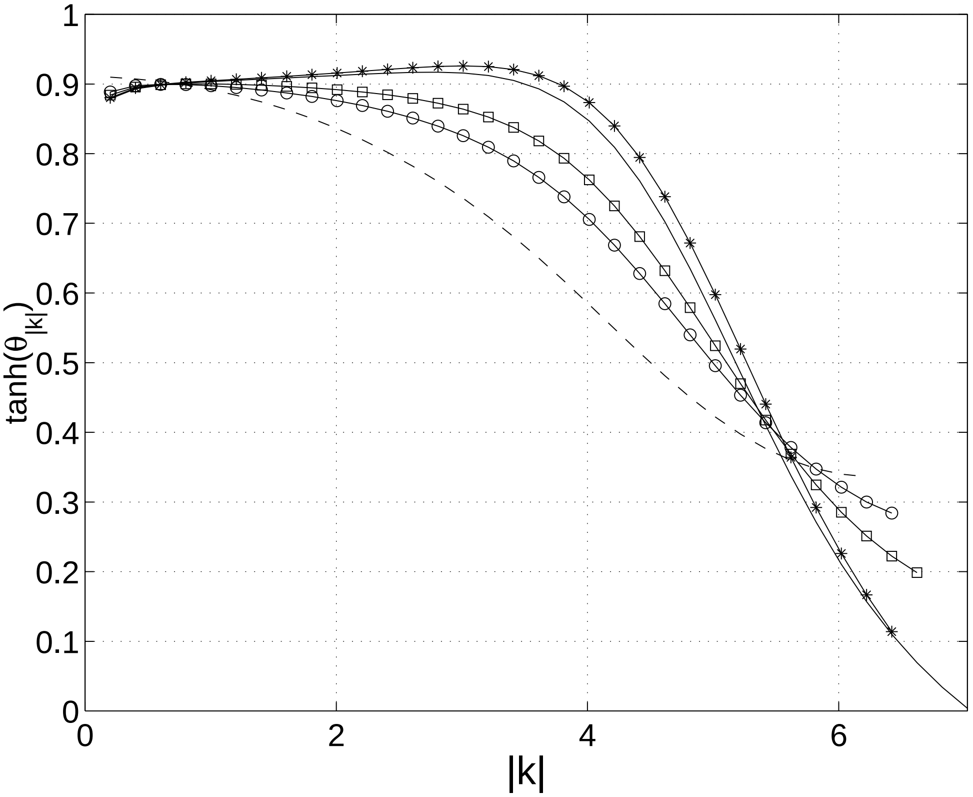

Figure G.4: Inspection of the integral equation with the spherical approximation in different directions. Here we show the case of $c = 5$.

solution of the integral equation, in direction $(0,1,2)$, with $(\theta,\phi) = (\tan^{-1}(0.5), 0)$. There $|\boldsymbol{k}|$ has a maximum value of $\sqrt{5}\pi$. The stars, boxes, and circles are for directions of $(\theta,\phi) = (\tan^{-1}(1/2), \pi/10), (\tan^{-1}(2/5), 0), (\pi/10, 0)$. The dashed line is for $(\theta,\phi) = 0$.

In all these cases, the solution deviates from the original one for high enough momenta. As we get further away from the original direction, the region in $|\boldsymbol{k}|$ space in which the solution is correct becomes smaller. Common to all directions is that near $\boldsymbol{k} = 0$ they agree, which was expected, and points to a spherical behavior there.

Appendix H

Hamiltonian approach to order from disorder for $N-m=1$

In this appendix we derive the self-consistent equations in a Hamiltonian formulation using a generalized Holstein-Primakoff transformation for $N-m=1$. The Hamiltonian is

$$H = J_1 \sum_{\boldsymbol{n}\hat{\boldsymbol{\mu}}\alpha\beta} Q_{\alpha\beta}(\boldsymbol{n}) Q_{\beta\alpha}(\boldsymbol{n}+\hat{\boldsymbol{\mu}}). \tag{H.1}$$

where the $U(N)$ generators $Q_{\alpha\beta}(\boldsymbol{n})$ obey

$$[Q_{\alpha\beta}(\boldsymbol{n}), Q_{\gamma\delta}(\boldsymbol{m})] = \left(Q_{\alpha\delta}(\boldsymbol{n})\delta_{\beta\gamma} - Q_{\gamma\beta}(\boldsymbol{n})\delta_{\alpha\delta}\right)\delta_{\boldsymbol{n}\boldsymbol{m}}. \tag{H.2}$$

For $N-m=1$ there is a simple representation of these operators in terms of $N-1$ boson operators boson operators [49],

$$Q(\boldsymbol{n})_{\alpha\beta} = \frac{N_c}{2}\begin{pmatrix} \mathbf{1}_{N-1} - 2\phi\phi^\dagger & 2\phi\sqrt{1-\phi^\dagger\phi} \\ 2\sqrt{1-\phi^\dagger\phi}\,\phi^\dagger & -1+2\phi^\dagger\phi \end{pmatrix}_{\alpha\beta} = Q^\dagger(\boldsymbol{n})_{\beta\alpha}. \tag{H.3}$$

Here ϕ is a $(N-1)$–component boson field defined on site $\boldsymbol{n}$ that obeys

$$\left[\phi(\boldsymbol{n})_i, \phi^\dagger(\boldsymbol{m})_j\right] = \frac{1}{N_c}\delta_{ij}\delta_{\boldsymbol{n}\boldsymbol{m}}, \qquad \forall i,j \in [1, N-1]. \tag{H.4}$$

The relation (H.4) has an important consequence. It means that at the large N_c limit the field operators ϕ_i are classical c-numbers, and the problem is not quantum. In the path integral formalism, Eq. (H.4) is equivalent to the fact that the Berry phase of the action is proportional to $S_B \sim N_c \int d\tau\, \phi_i^\dagger \partial_\tau \phi_i$. Indeed at large N_c, stationary phase arguments hold and the kinetic term is zero, making the system completely classical.

The Hilbert space is created by repeated applications of $\phi^\dagger$ on the no-quantum state $|0\rangle$, $\phi|0\rangle = 0$. It is restricted to be a $U(N)$ representation with N_c columns and $N-1$ rows, by restricting the eigenvalues of the number operator $\phi^\dagger\phi$ to be smaller than or equal to one. This representation is the generalized Holstein-Primakoff transformation. For $N-m>1$ the generalization is more complicated (see the Appendix in [21]).

We first verify that the relations Eq. (H.2) are satisfied by Eq. (H.3). We have four kinds of operator given by

$$\begin{aligned} Q_{ij} &= \frac{N_c}{2}\left(\delta_{ij} - 2\phi_i\phi_j^\dagger\right), && \text{(H.5)}\\ Q_{NN} &= \frac{N_c}{2}\left(-1+2\hat{n}\right), && \text{(H.6)}\\ Q_{iN} &= N_c\phi_i\sqrt{1-\hat{n}}, && \text{(H.7)}\\ Q_{Ni} &= N_c\sqrt{1-\hat{n}}\,\phi_i^\dagger = Q_{iN}^\dagger. && \text{(H.8)} \end{aligned}$$

Here we define the number operator $\hat{n} = \sum_i \phi_i^\dagger\phi_i$. We need to verify the following commutation relations. (All operators are on the same site.)

$$\begin{aligned} [Q_{ij}, Q_{kl}] &= Q_{il}\delta_{jk} - Q_{kj}\delta_{il}, && \text{(H.9)}\\ [Q_{ij}, Q_{NN}] &= Q_{iN}\delta_{jN} - Q_{Nj}\delta_{iN} = 0, && \text{(H.10)}\\ [Q_{ij}, Q_{kN}] &= Q_{iN}\delta_{jk} - Q_{kj}\delta_{iN} = Q_{iN}\delta_{jk}, && \text{(H.11)}\\ [Q_{NN}, Q_{iN}] &= Q_{NN}\delta_{iN} - Q_{iN}\delta_{NN} = -Q_{iN}, && \text{(H.12)}\\ [Q_{iN}, Q_{jN}] &= Q_{iN}\delta_{jN} - Q_{jN}\delta_{iN} = 0, && \text{(H.13)}\\ [Q_{iN}, Q_{Nj}] &= Q_{ij}\delta_{NN} - Q_{NN}\delta_{ij} = N_c(1-\hat{n}) - N_c\phi_i\phi_j^\dagger. && \text{(H.14)} \end{aligned}$$

All other commutators are automatically satisfied once the above list is satisfied. We first note that $\hat{n}$ (and therefore Q_{NN}) commutes with all operators that do not change the number of bosons. As a result the second commutator is zero, as expected from Eq. (H.10) (i cannot be equal to N). We now evaluate the rest of the commutators using Eq. (H.4).

$$\begin{aligned} [Q_{ij}, Q_{kl}] &= (-2\frac{N_c}{2})^2[\phi_i\phi_j^\dagger, \phi_k\phi_l^\dagger] = N_c^2\phi_i[\phi_j^\dagger,\phi_k]\phi_l^\dagger + N_c^2\phi_k[\phi_i,\phi_l^\dagger]\phi_j^\dagger \\ &\quad = Q_{il}\delta_{jk} - Q_{kj}\delta_{il}, && \text{(H.15)}\\ [Q_{ij}, Q_{kN}] &= -N_c^2[\phi_i\phi_j^\dagger, \phi_k]\sqrt{1-\hat{n}} = N_c\phi_i\delta_{jk}\sqrt{1-\hat{n}} = Q_{iN}\delta_{jk} - Q_{jk}\delta_{iN}, && \text{(H.16)} \end{aligned}$$

$$
\begin{aligned}
[Q_{NN}, Q_{iN}] &= N_c^2[\hat{n}, \phi_i]\sqrt{1-\hat{n}} = -N_c\phi_i\sqrt{1-\hat{n}} = Q_{NN}\delta_{iN} - Q_{iN}\delta_{NN}, && \text{(H.17)}\\
[Q_{iN}, Q_{jN}] &= N_c^2(1-\hat{n})[\phi_i, \phi_j] = 0, && \text{(H.18)}\\
[Q_{iN}, Q_{Nj}] &= N_c^2[\phi_i\sqrt{1-\hat{n}}, \sqrt{1-\hat{n}}\phi_j^\dagger] = N_c^2\left(\phi_i(1-\hat{n})\phi_j^\dagger - \sqrt{1-\hat{n}}\phi_j^\dagger\phi_i\sqrt{1-\hat{n}}\right) &&\\
&= N_c^2\left(\phi_i(1-\hat{n})\phi_j^\dagger - \phi_j^\dagger\phi_i\sqrt{1-\hat{n}}\right) = N_c^2[\phi_i(1-\hat{n}), \phi_j^\dagger] &&\\
&= N_c(1-\hat{n}) - N_c\phi_i\phi_j^\dagger. && \text{(H.19)}
\end{aligned}
$$

Q.E.D.

Next we write the operator ϕ as

$$\phi = \begin{pmatrix} \chi \\ \pi \end{pmatrix}. \tag{H.20}$$

The $(N-2)$–component field χ will represent the zero modes and the fields π will constitute the antiferromagnetic spin waves. We write the generators on the even sites by inserting Eq. (H.20) into Eq. (H.3). As in Section 5.2.1 we replace Q by

$$Q'(\phi) \equiv VQ(\phi)V^\dagger \tag{H.21}$$

on the odd sites. V is given in Eq. (5.21). It is easy to see that the algebra (H.2) on the odd sites is obeyed by Q' as well.

Now, we scale $\phi \to \phi/\sqrt{N_c}$, substitute Q and Q' into Eq. (H.1), and expand up to $O(1/N_c)$. We are left with the following normal ordered form of the Hamiltonian,

$$H_{\text{eff}} = N_c^2E_0 + N_cH_2 + \sqrt{N_c}H_3 + H_4, \tag{H.22}$$

where

$$
\begin{aligned}
H_2 &= J_1\sum_{\boldsymbol{n}\hat{\boldsymbol{\mu}}}\left(\pi_{\boldsymbol{n}}^\dagger\pi_{\boldsymbol{n}} + \pi_{\boldsymbol{n}+\hat{\boldsymbol{\mu}}}^\dagger\pi_{\boldsymbol{n}+\hat{\boldsymbol{\mu}}} - \pi_{\boldsymbol{n}}\pi_{\boldsymbol{n}+\hat{\boldsymbol{\mu}}} - \pi_{\boldsymbol{n}}^\dagger\pi_{\boldsymbol{n}+\hat{\boldsymbol{\mu}}}^\dagger\right), && \text{(H.23)}\\
H_3 &= J_1\sum_{\boldsymbol{n}\hat{\boldsymbol{\mu}},i}\left(\chi_{\boldsymbol{n}+\hat{\boldsymbol{\mu}},i}^\dagger\chi_{\boldsymbol{n}i}\pi_{\boldsymbol{n}+\hat{\boldsymbol{\mu}}} - \pi_{\boldsymbol{n}}^\dagger\chi_{\boldsymbol{n}+\hat{\boldsymbol{\mu}},i}^\dagger\chi_{\boldsymbol{n}i} + h.c.\right), && \text{(H.24)}\\
H_4 &= J_1\sum_{\boldsymbol{n}\hat{\boldsymbol{\mu}}}\Bigg\{\sum_{ij}\chi_{\boldsymbol{n}j}^\dagger\chi_{\boldsymbol{n}i}\chi_{\boldsymbol{n}+\hat{\boldsymbol{\mu}},i}^\dagger\chi_{\boldsymbol{n}+\hat{\boldsymbol{\mu}},j} &&\\
&\qquad \sum_i\Bigg[\frac{1}{2}\left(\chi_{\boldsymbol{n}i}^\dagger\chi_{\boldsymbol{n}i}\pi_{\boldsymbol{n}+\hat{\boldsymbol{\mu}}}\pi_{\boldsymbol{n}} + \chi_{\boldsymbol{n}+\hat{\boldsymbol{\mu}},i}^\dagger\chi_{\boldsymbol{n}+\hat{\boldsymbol{\mu}},i}\pi_{\boldsymbol{n}}\pi_{\boldsymbol{n}+\hat{\boldsymbol{\mu}}} + h.c.\right) &&\\
&\qquad\quad - \left(\chi_{\boldsymbol{n}i}^\dagger\chi_{\boldsymbol{n}i}\pi_{\boldsymbol{n}+\hat{\boldsymbol{\mu}}}^\dagger\pi_{\boldsymbol{n}+\hat{\boldsymbol{\mu}}} + (\boldsymbol{n}\leftrightarrow\boldsymbol{n}+\hat{\boldsymbol{\mu}})\right)\Bigg] && \text{(H.25)}\\
&\qquad +\frac{1}{2}\left[\left(\pi_{\boldsymbol{n}}^\dagger\pi_{\boldsymbol{n}}\pi_{\boldsymbol{n}}\pi_{\boldsymbol{n}+\hat{\boldsymbol{\mu}}} - \pi_{\boldsymbol{n}}^\dagger\pi_{\boldsymbol{n}+\hat{\boldsymbol{\mu}}}^\dagger\pi_{\boldsymbol{n}}\pi_{\boldsymbol{n}+\hat{\boldsymbol{\mu}}} + h.c.\right) + (\boldsymbol{n}\leftrightarrow\boldsymbol{n}+\hat{\boldsymbol{\mu}})\right]\Bigg\}
\end{aligned}
$$

H.1 The ground state at $O(1)$

At lowest order in $1/N_c$, the Hamiltonian is given by H_2, which does not depend on $\chi_{\boldsymbol{n}}$. Next we introduce the spatial Fourier transform

$$\phi^A_{\boldsymbol{N}} = \sqrt{\frac{2}{N_s}} \sum_{\boldsymbol{k}} \phi^A_{\boldsymbol{k}} e^{i\boldsymbol{k}\cdot\boldsymbol{N}} \times \left\{ \begin{array}{ll} 1 & A = \text{even} \\ e^{-ik_z/2} & A = \text{odd} \end{array} \right. , \tag{H.26}$$

where $\boldsymbol{N}$ is a site in the fcc lattice, and $\boldsymbol{k}$ belongs to its first Brillouin zone. In momentum space one diagonalizes H_2 with a Bogoliubov transformation to find

$$N_c H_2 = 2J_1 d N_c \sum_{\boldsymbol{q}} \sqrt{1-\gamma^2_{\boldsymbol{q}}} \left(a^\dagger_{\boldsymbol{q}} a_{\boldsymbol{q}} + b^\dagger_{\boldsymbol{q}} b_{\boldsymbol{q}} \right). \tag{H.27}$$

$\gamma_{\boldsymbol{q}}$ is given by Eq. (5.31) and

$$\begin{pmatrix} \pi^{\mathrm{e}}_{\boldsymbol{q}} \\ \pi^{\dagger\mathrm{o}}_{-\boldsymbol{q}} \end{pmatrix} = \begin{pmatrix} \cosh\varphi_{\boldsymbol{q}} & \sinh\varphi_{\boldsymbol{q}} \\ \sinh\varphi_{\boldsymbol{q}} & \cosh\varphi_{\boldsymbol{q}} \end{pmatrix} \begin{pmatrix} a_{\boldsymbol{q}} \\ b^\dagger_{-\boldsymbol{q}} \end{pmatrix}, \tag{H.28}$$

where the even function $\phi_{\boldsymbol{q}} = \phi_{-\boldsymbol{q}}$ is given by

$$\tanh 2\varphi_{\boldsymbol{q}} = \gamma_{\boldsymbol{q}}, \tag{H.29}$$

and the fields $a_{\boldsymbol{q}}$ and $b_{\boldsymbol{q}}$ obey the usual commutation relations of ladder operators. The $O(1)$ ground state $|\tilde{0}\rangle$ is thus given by

$$a_{\boldsymbol{q}}|\tilde{0}\rangle = b_{\boldsymbol{q}}|\tilde{0}\rangle = 0. \tag{H.30}$$

To $O(1)$ the excitations of $|\tilde{0}\rangle$ are antiferromagnetic spin waves with a linear dispersion relation. The ground state $|\tilde{0}\rangle$ has a local degeneracy, corresponding to creating an arbitrary number of χ bosons on any site (creation of a χ boson costs zero energy at this order). It is therefore more appropriate to write

$$|\tilde{0}\rangle = |\tilde{0}_\pi\rangle \otimes |\chi\rangle, \tag{H.31}$$

which emphasizes that the ground state projection to the χ Fock space is arbitrary. This is exactly the result of Section 5.2.1.

H.2 Self energy and $O(1/N_c)$ effective Hamiltonian

We now calculate an effective Hamiltonian that splits the spectrum of the degenerate subspace discussed above and removes the local degeneracy. We use Rayleigh-Schrödinger perturbation theory [67] where H_4 and H_3 are perturbations to H_2. In fact H_4 contributes at first order and H_3 at second order, and both give a contribution of $O(1/N_c)$. The effective Hamiltonian is therefore

$$\tilde{H}_{\text{eff}} = \boldsymbol{P} H_4 \boldsymbol{P} + \boldsymbol{P} H_3 \frac{\boldsymbol{1}-\boldsymbol{P}}{D} H_3 \boldsymbol{P} \equiv \tilde{H}^{(4)}_{\text{eff}} + \tilde{H}^{(3)}_{\text{eff}}. \tag{H.32}$$

Here $\boldsymbol{P}$ is a projection operator to the degenerate sector The projection operator is

$$\boldsymbol{P} = |\tilde{0}_\pi\rangle\langle\tilde{0}_\pi| \otimes \boldsymbol{1}_\chi, \tag{H.33}$$

and D is the energy denominator. H_{eff} is an effective Hamiltonian for the χ fields alone. Any bilinear of the π fields in $\tilde{H}^{(3,4)}_{\text{eff}}$ is replaced by the bilinear's vacuum expectations value (vev), which we calculate using (H.28) and (H.30),

$$\begin{aligned}
\langle\tilde{0}|\pi^{\dagger e}\pi^{e}|\tilde{0}\rangle_{\boldsymbol{N}} &= \frac{2}{N_s}\sum_{\boldsymbol{k},\boldsymbol{q}} e^{i\boldsymbol{N}(\boldsymbol{q}-\boldsymbol{k})}\langle\tilde{0}|\pi^{\dagger e}_{\boldsymbol{k}}\pi^{e}_{\boldsymbol{q}}|\tilde{0}\rangle \\
&= \frac{2}{N_s}\sum_{\boldsymbol{k},\boldsymbol{q}} e^{i\boldsymbol{N}(\boldsymbol{q}-\boldsymbol{k})}\sinh\varphi_{\boldsymbol{k}}\sinh\varphi_{\boldsymbol{q}}\langle\tilde{0}|b_{-\boldsymbol{k}}b^{\dagger}_{-\boldsymbol{q}}|\tilde{0}\rangle \\
&= \frac{2}{N_s}\sum_{\boldsymbol{q}}\sinh^2\varphi_{\boldsymbol{q}},
\end{aligned} \tag{H.34}$$

$$\begin{aligned}
\langle\tilde{0}|\pi^{\dagger o}\pi^{o}|\tilde{0}\rangle_{\boldsymbol{N}} &= \frac{2}{N_s}\sum_{\boldsymbol{k},\boldsymbol{q}} e^{i(\boldsymbol{N}-\hat{z}/2)(\boldsymbol{q}-\boldsymbol{k})}\langle\tilde{0}|\pi^{\dagger o}_{\boldsymbol{k}}\pi^{o}_{\boldsymbol{q}}|\tilde{0}\rangle \\
&= \frac{2}{N_s}\sum_{\boldsymbol{k},\boldsymbol{q}} e^{i(\boldsymbol{N}-\hat{z}/2)(\boldsymbol{q}-\boldsymbol{k})}\sinh\varphi_{-\boldsymbol{k}}\sinh\varphi_{-\boldsymbol{q}}\langle\tilde{0}|a_{-\boldsymbol{k}}a^{\dagger}_{-\boldsymbol{q}}|\tilde{0}\rangle \\
&= \frac{2}{N_s}\sum_{\boldsymbol{q}}\sinh^2\varphi_{\boldsymbol{q}},
\end{aligned} \tag{H.35}$$

$$\begin{aligned}
\langle\tilde{0}|\pi^{e}_{\boldsymbol{N}}\pi^{o}_{\boldsymbol{N}+\hat{\rho}}|\tilde{0}\rangle &= \frac{2}{N_s}\sum_{\boldsymbol{k},\boldsymbol{q}} e^{i\boldsymbol{N}(\boldsymbol{q}+\boldsymbol{k})+i\boldsymbol{q}(\hat{\rho}-\hat{z}/2)}\langle\tilde{0}|\pi^{e}_{\boldsymbol{k}}\pi^{o}_{\boldsymbol{q}}|\tilde{0}\rangle \\
&= \frac{2}{N_s}\sum_{\boldsymbol{k},\boldsymbol{q}} e^{i\boldsymbol{N}(\boldsymbol{q}+\boldsymbol{k})+i\boldsymbol{q}(\hat{\rho}-\hat{z}/2)}\cosh\varphi_{\boldsymbol{k}}\sinh\varphi_{-\boldsymbol{q}}\langle\tilde{0}|a_{\boldsymbol{k}}a^{\dagger}_{-\boldsymbol{q}}|\tilde{0}\rangle
\end{aligned}$$

$$
\begin{aligned}
&= \frac{2}{N_s}\sum_{\boldsymbol{q}} \sinh\varphi_{\boldsymbol{q}} \cosh\varphi_{\boldsymbol{q}} e^{i\boldsymbol{q}(\hat{\rho}-\hat{z}/2)}, && \text{(H.36)}\\
\langle\tilde{0}|\pi^{\dagger e}_{\boldsymbol{N}}\pi^{\dagger o}_{\boldsymbol{N}+\hat{\rho}}|\tilde{0}\rangle_{\boldsymbol{N}} &= \frac{2}{N_s}\sum_{\boldsymbol{k},\boldsymbol{q}} e^{-i\boldsymbol{N}(\boldsymbol{q}+\boldsymbol{k})-i\boldsymbol{q}(\hat{\rho}-\hat{z}/2)}\langle\tilde{0}|\pi^{e}_{\boldsymbol{k}}\pi^{o}_{\boldsymbol{q}}|\tilde{0}\rangle \\
&= \frac{2}{N_s}\sum_{\boldsymbol{k},\boldsymbol{q}} e^{-i\boldsymbol{N}(\boldsymbol{q}+\boldsymbol{k})-i\boldsymbol{q}(\hat{\rho}-\hat{z}/2)} \sinh\varphi_{\boldsymbol{k}}\cosh\varphi_{-\boldsymbol{q}}\langle\tilde{0}|b_{-\boldsymbol{k}}b^{\dagger}_{\boldsymbol{q}}|\tilde{0}\rangle \\
&= \frac{2}{N_s}\sum_{\boldsymbol{q}} \sinh\varphi_{\boldsymbol{q}} \cosh\varphi_{\boldsymbol{q}} e^{-i\boldsymbol{q}(\hat{\rho}-\hat{z}/2)}. && \text{(H.37)}
\end{aligned}
$$

Here we have used the following notation. $\boldsymbol{N}$ is a site on the fcc lattice of even sites. On each fcc site one has two degrees of freedom, π^e, and π^o. The neighboring sites of $\boldsymbol{N}$ are $\boldsymbol{N}+\hat{\rho}$, with

$$
\hat{\rho} = 0, \hat{z}, \hat{z}\pm\hat{x}/2, \hat{z}\pm\hat{y}/2. \tag{H.38}
$$

Inserting Eqs. (H.34)–(H.37) into $\boldsymbol{P}H_4\boldsymbol{P}$ we have

$$
\begin{aligned}
\boldsymbol{P}H_4\boldsymbol{P} &= |\tilde{0}_\pi\rangle\langle\tilde{0}_\pi|H_4|\tilde{0}_\pi\rangle\langle\tilde{0}_\pi| && \text{(H.39)}\\
\langle\tilde{0}_\pi|H_4|\tilde{0}_\pi\rangle &= J_1\sum_{\boldsymbol{N}\hat{\rho}}\Bigg\{\sum_{ij}\chi^{\dagger e}_{\boldsymbol{N}j}\chi^{e}_{\boldsymbol{N}i}\chi^{\dagger o}_{\boldsymbol{N}+\hat{\rho},i}\chi^{o}_{\boldsymbol{N}+\hat{\rho},j} \\
&\quad -\sum_i\left(\chi^{\dagger e}_{\boldsymbol{N}i}\chi^{e}_{\boldsymbol{N}i}+\chi^{\dagger o}_{\boldsymbol{N}+\hat{\rho},i}\chi^{o}_{\boldsymbol{N}+\hat{\rho},i}\right)\frac{2}{N_s}\sum_{\boldsymbol{q}}\sinh^2\varphi_{\boldsymbol{q}} \\
&\quad +\sum_i\frac{1}{2}\left[\left(\chi^{\dagger e}_{\boldsymbol{N}i}\chi^{e}_{\boldsymbol{N}i}+\chi^{\dagger o}_{\boldsymbol{N}+\hat{\rho},i}\chi^{o}_{\boldsymbol{N}+\hat{\rho},i}\right)\frac{2}{N_s}\sum_{\boldsymbol{q}}\sinh\varphi_{\boldsymbol{q}}\cosh\varphi_{\boldsymbol{q}}e^{i\boldsymbol{q}(\hat{\rho}-\hat{z}/2)}+h.c.\right]\Bigg\}. \\
&= J_1\frac{2}{N_s}\sum_{\boldsymbol{kq}i}\Bigg\{2\sum_{\boldsymbol{p}j}\chi^{\mathrm{e}\dagger}_{\boldsymbol{p}j}\chi^{\mathrm{e}}_{\boldsymbol{k}i}\chi^{\mathrm{o}\dagger}_{\boldsymbol{q}+\boldsymbol{k}-\boldsymbol{p},i}\chi^{\mathrm{o}}_{\boldsymbol{q}j}\cdot\gamma_{\boldsymbol{k}-\boldsymbol{p}} \\
&\quad -2d\left(\chi^{\dagger e}_{\boldsymbol{k}i}\chi^{e}_{\boldsymbol{k}i}+\chi^{\dagger o}_{\boldsymbol{k}i}\chi^{o}_{\boldsymbol{k}i}\right)\times\left(\sinh^2\varphi_{\boldsymbol{q}}-\gamma_{\boldsymbol{q}}\sinh\varphi_{\boldsymbol{q}}\cosh\varphi_{\boldsymbol{q}}\right)\Bigg\}. && \text{(H.40)}
\end{aligned}
$$

Here we have omitted an irrelevant constant that represents terms quartic in π. Finally we use Eq. (H.29) to write $\tilde{H}^{(4)}_{\text{eff}}$ as

$$
\begin{aligned}
\tilde{H}^{(4)}_{\text{eff}} &= J_1 d\frac{2}{N_s}\Bigg\{\sum_{\boldsymbol{qk},i}\begin{pmatrix}\chi^{\dagger \mathrm{e}}_{\boldsymbol{k}i} & \chi^{\mathrm{o}}_{-\boldsymbol{k}i}\end{pmatrix}\begin{pmatrix}1-\sqrt{1-\gamma^2_{\boldsymbol{q}}} & 0\\ 0 & 1-\sqrt{1-\gamma^2_{\boldsymbol{q}}}\end{pmatrix}\begin{pmatrix}\chi^{\mathrm{e}}_{\boldsymbol{k}i}\\ \chi^{\dagger \mathrm{o}}_{-\boldsymbol{k}i}\end{pmatrix}. \\
&\qquad +2\sum_{\substack{\boldsymbol{kpq}\\ ij}}\chi^{\mathrm{e}\dagger}_{\boldsymbol{p}j}\chi^{\mathrm{e}}_{\boldsymbol{k}i}\chi^{\mathrm{o}\dagger}_{\boldsymbol{q}+\boldsymbol{k}-\boldsymbol{p},i}\chi^{\mathrm{o}}_{\boldsymbol{q}j}\cdot\gamma_{\boldsymbol{k}-\boldsymbol{p}}\Bigg\} && \text{(H.41)}
\end{aligned}
$$

We see that $\tilde{H}^{(4)}_{\text{eff}}$ has harmonic and anharmonic terms. In order to evaluate $\tilde{H}^{(3)}_{\text{eff}}$ we write $(\mathbf{1}-\boldsymbol{P})$ as

$$\mathbf{1}-\boldsymbol{P} = \mathbf{1}_\chi \otimes \sum_{\boldsymbol{k}} |\boldsymbol{k}_a\rangle\langle\boldsymbol{k}_a| + |\boldsymbol{k}_b\rangle\langle\boldsymbol{k}_b|, \tag{H.42}$$

where, for example $|\boldsymbol{k}_a\rangle \equiv a^\dagger_{\boldsymbol{k}}|\tilde{0}_\pi\rangle \otimes |\chi\rangle$. Here $|\chi\rangle$ is $|\boldsymbol{k}_a\rangle$'s component in the χ Fock space. In general (H.42) is incorrect since it takes into account excitations of one spin wave only. Here it suffices since H_3 connects $|\tilde{0}_\pi\rangle$ with excitations of that sort only. Next we replace the energy denominator with

$$D = -2J_1 d N_c \sqrt{1-\gamma^2_{\boldsymbol{k}}}, \tag{H.43}$$

and obtain the following expression for $\tilde{H}^{(3)}_{\text{eff}}$,

$$\begin{aligned}\tilde{H}^{(3)}_{\text{eff}} \;=\; & -\frac{(J_1\sqrt{N_c})^2}{2dJ_1N_c}\sum_{\boldsymbol{k}}\frac{1}{\sqrt{1-\gamma^2_{\boldsymbol{k}}}}\boldsymbol{P}\sum_{\boldsymbol{N}\hat{\rho},i}\Big(\chi^{\dagger o}_{\boldsymbol{N}+\hat{\rho},i}\chi^{e}_{\boldsymbol{N}i}\pi^{o}_{\boldsymbol{N}+\hat{\rho}} - \pi^{\dagger e}_{\boldsymbol{N}}\chi^{\dagger o}_{\boldsymbol{N}+\hat{\rho},i}\chi^{e}_{\boldsymbol{N}i} + h.c.\Big)\times \\ & |\boldsymbol{k}_a\rangle\langle\boldsymbol{k}_a| + |\boldsymbol{k}_b\rangle\langle\boldsymbol{k}_b| \times \sum_{\boldsymbol{N}'\hat{\rho}'i'}\Big(\chi^{\dagger o}_{\boldsymbol{N}'+\hat{\rho}',i'}\chi^{e}_{\boldsymbol{N}'i'}\pi^{o}_{\boldsymbol{N}'+\hat{\rho}'} - \pi^{\dagger e}_{\boldsymbol{N}'}\chi^{\dagger o}_{\boldsymbol{N}'+\hat{\rho}',i'}\chi^{e}_{\boldsymbol{N}'i'} + h.c.\Big)\boldsymbol{P}.\end{aligned} \tag{H.44}$$

In order to calculate Eq. (H.44) we use Eq. (H.28) and note that

$$\langle\tilde{0}_\pi|\pi^{\dagger e}_{\boldsymbol{N}}|\boldsymbol{k}_a\rangle \sim \langle\tilde{0}_\pi|\Big(a^\dagger \quad \text{or} \quad \mathrm{b}\Big)a^\dagger_{\boldsymbol{k}}|\tilde{0}_\pi\rangle = 0. \tag{H.45}$$

On similar lines one can easily show that $\langle\tilde{0}_\pi|\pi^{o}_{\boldsymbol{N}}|\boldsymbol{k}_a\rangle = \langle\tilde{0}_\pi|\pi^{e}_{\boldsymbol{N}}|\boldsymbol{k}_b\rangle = \langle\tilde{0}_\pi|\pi^{\dagger o}_{\boldsymbol{N}}|\boldsymbol{k}_b\rangle = 0$. The only non-zero elements are

$$\langle\tilde{0}_\pi|\pi^{e}_{\boldsymbol{N}}|\boldsymbol{k}_a\rangle = \sqrt{\frac{2}{N_s}}\cosh\varphi_{\boldsymbol{k}}e^{i\boldsymbol{k}\boldsymbol{N}}, \tag{H.46}$$

$$\langle\tilde{0}_\pi|\pi^{\dagger o}_{\boldsymbol{N}}|\boldsymbol{k}_a\rangle = \sqrt{\frac{2}{N_s}}\sinh\varphi_{\boldsymbol{k}}e^{-i\boldsymbol{k}(\boldsymbol{N}-\hat{z}/2)}, \tag{H.47}$$

$$\langle\tilde{0}_\pi|\pi^{\dagger e}_{\boldsymbol{N}}|\boldsymbol{k}_b\rangle = \sqrt{\frac{2}{N_s}}\sinh\varphi_{\boldsymbol{k}}e^{i\boldsymbol{k}\boldsymbol{N}}, \tag{H.48}$$

$$\langle\tilde{0}_\pi|\pi^{o}_{\boldsymbol{N}}|\boldsymbol{k}_b\rangle = \sqrt{\frac{2}{N_s}}\cosh\varphi_{\boldsymbol{k}}e^{i\boldsymbol{k}(\boldsymbol{N}-\hat{z}/2)}. \tag{H.49}$$

Using these relations in Eq. (H.44) we see that $\tilde{H}_{\text{eff}}^{(3)}$ is a quartic interaction in the χ fields. For example the contribution of $|\boldsymbol{k}_b\rangle\langle\boldsymbol{k}_b|$ is

$$
\begin{aligned}
&-J_1\frac{1}{N_s}\sum_{\boldsymbol{k}}\frac{1}{\sqrt{1-\gamma_{\boldsymbol{k}}^2}}\sum_{\substack{\boldsymbol{N}\boldsymbol{N}'\\ \hat{\rho}\hat{\rho}'ii'}}\Big(\cosh\varphi_{\boldsymbol{k}}e^{i\boldsymbol{k}(\boldsymbol{N}+\hat{\rho}-\hat{z}/2)}\chi^{\dagger o}_{\boldsymbol{N}+\hat{\rho},i}\chi^{e}_{\boldsymbol{N}i}-\sinh\varphi_{\boldsymbol{k}}e^{i\boldsymbol{k}\boldsymbol{N}}\chi^{\dagger o}_{\boldsymbol{N}+\hat{\rho},i}\chi^{e}_{\boldsymbol{N}i}\Big)\times\\
&\qquad\qquad\Big(\cosh\varphi_{\boldsymbol{k}}e^{-i\boldsymbol{k}(\boldsymbol{N}'-\hat{z}/2+\hat{\rho}')}\chi^{\dagger e}_{\boldsymbol{N}'i'}\chi^{o}_{\boldsymbol{N}'+\hat{\rho}',i'}-\sinh\varphi_{\boldsymbol{k}}e^{-i\boldsymbol{k}\boldsymbol{N}'}\chi^{\dagger e}_{\boldsymbol{N}'i'}\chi^{o}_{\boldsymbol{N}'+\hat{\rho}',i'}\Big)\\
&=-J_1\frac{1}{N_s}\sum_{\boldsymbol{k}}\cosh 2\varphi_{\boldsymbol{k}}\sum_{\substack{\boldsymbol{N}\boldsymbol{N}'\\ \hat{\rho}\hat{\rho}'ii'}}\chi^{\dagger o}_{\boldsymbol{N}+\hat{\rho},i}\chi^{e}_{\boldsymbol{N}i}\chi^{\dagger e}_{\boldsymbol{N}'i'}\chi^{o}_{\boldsymbol{N}'+\hat{\rho}',i'}\times e^{i\boldsymbol{k}(\boldsymbol{N}-\boldsymbol{N}')}\times\\
&\qquad\qquad\qquad\Big(\cosh\varphi_{\boldsymbol{k}}e^{i\boldsymbol{k}(\hat{\rho}-\hat{z}/2)}-\sinh\varphi_{\boldsymbol{k}}\Big)\Big(\cosh\varphi_{\boldsymbol{k}}e^{-i\boldsymbol{k}(\hat{\rho}'-\hat{z}/2)}-\sinh\varphi_{\boldsymbol{k}}\Big)\\
&=-J_1\frac{1}{N_s}\sum_{\boldsymbol{k}}\cosh 2\varphi_{\boldsymbol{k}}\sum_{\substack{\boldsymbol{N}\boldsymbol{N}'\\ \hat{\rho}\hat{\rho}'ii'}}\chi^{\dagger o}_{\boldsymbol{N}+\hat{\rho},i}\chi^{o}_{\boldsymbol{N}'+\hat{\rho}',i'}\chi^{\dagger e}_{\boldsymbol{N}'i'}\chi^{e}_{\boldsymbol{N}i}\times e^{i\boldsymbol{k}(\boldsymbol{N}-\boldsymbol{N}')}\times\\
&\qquad\qquad\qquad\Big(\cosh\varphi_{\boldsymbol{k}}e^{i\boldsymbol{k}(\hat{\rho}-\hat{z}/2)}-\sinh\varphi_{\boldsymbol{k}}\Big)\Big(\cosh\varphi_{\boldsymbol{k}}e^{-i\boldsymbol{k}(\hat{\rho}'-\hat{z}/2)}-\sinh\varphi_{\boldsymbol{k}}\Big)\\
&-J_1\frac{1}{N_s}\sum_{\boldsymbol{k}}\cosh\varphi_{\boldsymbol{k}}\sum_{\boldsymbol{N}\hat{\rho}\hat{\rho}'i}\chi^{\dagger o}_{\boldsymbol{N}+\hat{\rho},i}\chi^{o}_{\boldsymbol{N}+\hat{\rho}',i}\times\Big(\cosh\varphi_{\boldsymbol{k}}e^{i\boldsymbol{k}(\hat{\rho}-\hat{z}/2)}-\sinh\varphi_{\boldsymbol{k}}\Big)\\
&\qquad\qquad\qquad\Big(\cosh\varphi_{\boldsymbol{k}}e^{-i\boldsymbol{k}(\hat{\rho}'-\hat{z}/2)}-\sinh\varphi_{\boldsymbol{k}}\Big).
\end{aligned}
\tag{H.50}
$$

We write the last (quadratic) term as

$$
\begin{aligned}
&-J_1\frac{1}{N_s}\sum_{\boldsymbol{q}\boldsymbol{k}i}\cosh 2\varphi_{\boldsymbol{k}}\sum_{\hat{\rho}\hat{\rho}'}\chi^{\dagger o}_{\boldsymbol{q}i}\chi^{o}_{\boldsymbol{q}i}\times\Big(\cosh^2\varphi_{\boldsymbol{k}}e^{i(\boldsymbol{k}+\boldsymbol{q})(\hat{\rho}-\hat{\rho}')}+\sinh^2\varphi_{\boldsymbol{k}}e^{(\boldsymbol{k}+\boldsymbol{q})(\hat{\rho}-\hat{\rho}')}\\
&\qquad-\cosh\varphi_{\boldsymbol{k}}\sinh\varphi_{\boldsymbol{k}}(e^{i(\boldsymbol{k}-\boldsymbol{q})(\hat{\rho}-\hat{z}/2)+i\boldsymbol{q}(\hat{\rho}'-\hat{z}/2)}+e^{i(\boldsymbol{q}-\boldsymbol{k})(\hat{\rho}'-\hat{z}/2)-i\boldsymbol{q}(\hat{\rho}-\hat{z}/2)})\Big)\\
&=-4d^2J_1\frac{1}{N_s}\sum_{\boldsymbol{q}\boldsymbol{k}i}\chi^{\dagger o}_{\boldsymbol{q}i}\chi^{o}_{\boldsymbol{q}i}\ \cosh 2\varphi_{\boldsymbol{k}}\Big(\gamma^2_{\boldsymbol{q}+\boldsymbol{k}}(\cosh^2\varphi_{\boldsymbol{k}}+\sinh^2\varphi_{\boldsymbol{k}})-2\gamma_{\boldsymbol{q}}\gamma_{\boldsymbol{q}+\boldsymbol{k}}\cosh\varphi_{\boldsymbol{k}}\sinh\varphi_{\boldsymbol{k}}\Big)\\
&=-4d^2J_1\frac{1}{N_s}\sum_{\boldsymbol{q}\boldsymbol{k}i}\chi^{\dagger o}_{\boldsymbol{q}i}\chi^{o}_{\boldsymbol{q}i}\ \cosh 2\varphi_{\boldsymbol{k}}\left(\gamma_{\boldsymbol{q}+\boldsymbol{k}}\cosh 2\varphi_{\boldsymbol{k}}-\gamma_{\boldsymbol{q}}\sinh 2\varphi_{\boldsymbol{k}}\right)\gamma_{\boldsymbol{q}+\boldsymbol{k}}
\end{aligned}
\tag{H.51}
$$

In order to treat the quartic interactions in $\tilde{H}_{\text{eff}}$ we make an ansatz for the ground state of the χ Fock space, and assume the following vacuum expectation values of the χ fields.

$$
\langle\tilde{0}|\chi^{\dagger e}_{\boldsymbol{k}j}\chi^{e}_{\boldsymbol{k}'i}|\tilde{0}\rangle \;=\; \langle\tilde{0}|\chi^{\dagger o}_{\boldsymbol{k}j}\chi^{o}_{\boldsymbol{k}'i}|\tilde{0}\rangle\equiv\frac{1}{2}\Delta_{1\boldsymbol{k}}\delta_{\boldsymbol{k}\boldsymbol{k}'}\delta_{ij},\tag{H.52}
$$

$$
\langle\tilde{0}|\chi^{e}_{\boldsymbol{k}i}\chi^{o}_{-\boldsymbol{k}',j}|\tilde{0}\rangle \;=\; \langle\tilde{0}|\chi^{\dagger e}_{\boldsymbol{k}i}\chi^{\dagger o}_{-\boldsymbol{k}',j}|\tilde{0}\rangle^*\equiv-\frac{1}{2}\Delta_{2\boldsymbol{k}}\delta_{\boldsymbol{k}\boldsymbol{k}'}\delta_{ij},\tag{H.53}
$$

or in real space

$$\begin{aligned}\langle\tilde{0}|\chi^{\dagger e}_{\boldsymbol{N}j}\chi^{e}_{\boldsymbol{N}'i}|\tilde{0}\rangle &= \langle\tilde{0}|\chi^{\dagger o}_{\boldsymbol{k}j}\chi^{o}_{\boldsymbol{k}'i}|\tilde{0}\rangle \equiv \frac{1}{N_s}\sum_{\boldsymbol{k}}\Delta_{1\boldsymbol{k}}e^{i\boldsymbol{k}(\boldsymbol{N}'-\boldsymbol{N})}\cdot\delta_{ij}, \qquad \text{(H.54)}\\ \langle\tilde{0}|\chi^{e}_{\boldsymbol{N}i}\chi^{o}_{\boldsymbol{N}',j}|\tilde{0}\rangle &= \langle\tilde{0}|\chi^{\dagger e}_{\boldsymbol{N}i}\chi^{\dagger o}_{\boldsymbol{N}',j}|\tilde{0}\rangle^{*} \equiv -\frac{1}{N_s}\sum_{\boldsymbol{q}}\Delta_{2\boldsymbol{k}}e^{i\boldsymbol{k}(\boldsymbol{N}-\boldsymbol{N}'+\hat{z}/2)}\delta_{\boldsymbol{k}\boldsymbol{k}'}\delta_{ij}. \qquad \text{(H.55)}\end{aligned}$$

Here $\Delta_{1,2}$ are assumed to be real and even in the momentum $\boldsymbol{k}$. Note that a non-zero value of Δ_2 breaks the stationary group of the condensates of Q_e and Q_o, $U(2m-N)\times U(N-m)\times U(N-m)$, to $O(2m-N)\times U(N-m)$.

As in the treatment of order from disorder in condensed matter (see for example [52]) we decouple all the quartic terms in $\tilde{H}_{\text{eff}}$ to be quadratic terms times a condensate in all possible ways. The quartic term in $\tilde{H}^{(4)}_{\text{eff}}$ becomes the following four quadratic terms. (We go back to real space.)

$$\begin{aligned}J_1\sum_{\substack{\boldsymbol{N}\hat{\rho}\\ ij}}\left(\chi^\dagger_j\chi_i\right)^e_{\boldsymbol{N}}\left(\chi^\dagger_i\chi_j\right)^o_{\boldsymbol{N}+\hat{\rho}} &\simeq J_1\sum_{\substack{\boldsymbol{N}\hat{\rho}\\ ij}}\Big[\langle\chi^\dagger_j\chi_i\rangle^e_{\boldsymbol{N}}\left(\chi^\dagger_i\chi_j\right)^o_{\boldsymbol{N}+\hat{\rho}}+\left(\chi^\dagger_j\chi_i\right)^e_{\boldsymbol{N}}\langle\chi^\dagger_i\chi_j\rangle^o_{\boldsymbol{N}+\hat{\rho}}\\ &\qquad +\chi^e_{\boldsymbol{N}i}\chi^o_{\boldsymbol{N}+\hat{\rho},j}\langle\chi^{\dagger e}_{\boldsymbol{N}j}\chi^{\dagger o}_{\boldsymbol{N}+\hat{\rho},i}\rangle+\langle\chi^e_{\boldsymbol{N}i}\chi^o_{\boldsymbol{N}+\hat{\rho},j}\rangle\chi^{\dagger e}_{\boldsymbol{N}j}\chi^{\dagger o}_{\boldsymbol{N}+\hat{\rho},i}\Big]\\ &= J_1\frac{1}{N_s}\sum_{\boldsymbol{q}\boldsymbol{N}\hat{\rho}i}\Big[\Delta_{1\boldsymbol{q}}\left(\chi^{\dagger o}_{\boldsymbol{N}+\hat{\rho},i}\chi^o_{\boldsymbol{N}+\hat{\rho},i}+\chi^{\dagger e}_{\boldsymbol{N}}\chi^e_{\boldsymbol{N}i}\right)-\Delta_{2\boldsymbol{q}}e^{i\boldsymbol{q}(\hat{\rho}-\hat{z}/2)}\left(\chi^e_{\boldsymbol{N}i}\chi^o_{\boldsymbol{N}+\hat{\rho},i}+\chi^{\dagger e}_{\boldsymbol{N}j}\chi^{\dagger o}_{\boldsymbol{N}+\hat{\rho},i}\right)\Big]\\ &= 2dJ_1\frac{1}{N_s}\sum_{\boldsymbol{q}\boldsymbol{k},i}\Big[\Delta_{1\boldsymbol{q}}\left(\chi^{\dagger e}_{\boldsymbol{k}i}\chi^e_{\boldsymbol{k}i}+\chi^{\dagger o}_{\boldsymbol{k}i}\chi^o_{\boldsymbol{k}i}\right)-\Delta_{2\boldsymbol{q}}\gamma_{\boldsymbol{q}-\boldsymbol{k}}\left(\chi^e_{\boldsymbol{k}i}\chi^o_{-\boldsymbol{k},i}+\chi^{\dagger e}_{\boldsymbol{k}i}\chi^{\dagger o}_{-\boldsymbol{k},i}\right)\Big]. \qquad \text{(H.56)}\end{aligned}$$

The next step is to use the ansatz (H.52)–(H.53) in Eq. (H.56). This gives

$$\tilde{H}^{(4)}_{\text{eff}} = J_1 d\frac{2}{N_s}\sum_{\boldsymbol{q}\boldsymbol{k},i}\begin{pmatrix}\chi^{\dagger\mathrm{e}}_{\boldsymbol{k}i} & \chi^{\mathrm{o}}_{-\boldsymbol{k}i}\end{pmatrix}\begin{pmatrix}\Delta_{1\boldsymbol{q}}+1-\sqrt{1-\gamma_q^2} & -\Delta_{2\boldsymbol{q}}\gamma_{\boldsymbol{q}-\boldsymbol{k}}\\ -\Delta_{2\boldsymbol{q}}\gamma_{\boldsymbol{q}-\boldsymbol{k}} & \Delta_{1\boldsymbol{q}}+1-\sqrt{1-\gamma_q^2}\end{pmatrix}\begin{pmatrix}\chi^{\mathrm{e}}_{\boldsymbol{k}i}\\ \chi^{\dagger\mathrm{o}}_{-\boldsymbol{k}i}\end{pmatrix}. \qquad \text{(H.57)}$$

The same procedure is performed to the quartic terms of $\tilde{H}^{(3)}_{\text{eff}}$. Here the procedure in much more cumbersome, and the four quartic terms of Eq. (H.50) alone give 4 × 4 = 16 different quadratic terms. The $|\boldsymbol{k}_a\rangle\langle\boldsymbol{k}_a|$ terms contribute 16 more. For example, in order to calculate the contribution of Eq. (H.50) we first decouple the quartic term,

$$\begin{aligned}\chi^{\dagger o}_{\boldsymbol{N}+\hat{\rho},i}\chi^{o}_{\boldsymbol{N}'+\hat{\rho}',i'}\chi^{\dagger e}_{\boldsymbol{N}'i'}\chi^{e}_{\boldsymbol{N}i} \;\rightarrow\; & \langle\chi^{\dagger o}_{\boldsymbol{N}+\hat{\rho},i}\chi^{o}_{\boldsymbol{N}'+\hat{\rho}',i'}\rangle\chi^{\dagger e}_{\boldsymbol{N}'i'}\chi^{e}_{\boldsymbol{N}i}+\chi^{\dagger o}_{\boldsymbol{N}+\hat{\rho},i}\chi^{o}_{\boldsymbol{N}'+\hat{\rho}',i'}\langle\chi^{\dagger e}_{\boldsymbol{N}'i'}\chi^{e}_{\boldsymbol{N}i}\rangle\\ &+\langle\chi^{\dagger o}_{\boldsymbol{N}+\hat{\rho},i}\chi^{\dagger e}_{\boldsymbol{N}'i'}\rangle\chi^{o}_{\boldsymbol{N}'+\hat{\rho}',i'}\chi^{e}_{\boldsymbol{N}i}+\chi^{\dagger o}_{\boldsymbol{N}+\hat{\rho},i}\chi^{\dagger e}_{\boldsymbol{N}'i'}\langle\chi^{o}_{\boldsymbol{N}'+\hat{\rho}',i'}\chi^{e}_{\boldsymbol{N}i}\rangle. \qquad \text{(H.58)}\end{aligned}$$

Next we substitute (H.54)–(H.55) into (H.58) and into its $|\boldsymbol{k}_a\rangle\langle\boldsymbol{k}_a|$ counterpart, and find (after a lot of algebra)

$$\tilde{H}_{\text{eff}} = J_1 d \sum_{\boldsymbol{k},i} \begin{pmatrix} \chi^{\dagger\text{e}}_{\boldsymbol{k}i} & \chi^{\text{o}}_{-\boldsymbol{k}i} \end{pmatrix} \begin{pmatrix} \mathcal{J}_{1\boldsymbol{k}} & \mathcal{J}_{2\boldsymbol{k}} \\ \mathcal{J}_{2\boldsymbol{k}} & \mathcal{J}_{1\boldsymbol{k}} \end{pmatrix} \begin{pmatrix} \chi^{\text{e}}_{\boldsymbol{k}i} \\ \chi^{\dagger\text{o}}_{-\boldsymbol{k}i} \end{pmatrix}, \tag{H.59}$$

with

$$\begin{aligned} \mathcal{J}_{1\boldsymbol{k}} &= \int_{\text{BZ}} \left(\frac{dq}{4\pi}\right)^d (\Delta_{1\boldsymbol{q}} + 1)\, I_1(\boldsymbol{q},\boldsymbol{k}) - \eta(\boldsymbol{k}), & \text{(H.60)} \\ \mathcal{J}_{2\boldsymbol{k}} &= \int_{\text{BZ}} \left(\frac{dq}{4\pi}\right)^d \Delta_{2\boldsymbol{q}} I_2(\boldsymbol{q},\boldsymbol{k}). & \text{(H.61)} \end{aligned}$$

$I_{1,2}(\boldsymbol{q},\boldsymbol{k})$ and $\eta(\boldsymbol{k})$ are as given in Eqs. (G.29)–(G.30). The Hamiltonian (H.59) can be diagonalized by a Bogoliubov transformation

$$\begin{pmatrix} \chi^{\text{e}}_{\boldsymbol{q}} \\ \chi^{\dagger\text{o}}_{-\boldsymbol{q}} \end{pmatrix} = \begin{pmatrix} \cosh\frac{1}{2}\theta_{\boldsymbol{q}} & \sinh\frac{1}{2}\theta_{\boldsymbol{q}} \\ \sinh\frac{1}{2}\theta_{\boldsymbol{q}} & \cosh\frac{1}{2}\theta_{\boldsymbol{q}} \end{pmatrix} \begin{pmatrix} c_{\boldsymbol{q}} \\ d^{\dagger}_{-\boldsymbol{q}} \end{pmatrix}, \tag{H.62}$$

with

$$\tanh(\theta_{\boldsymbol{k}}) = -\mathcal{J}_{2\boldsymbol{k}}/\mathcal{J}_{1\boldsymbol{k}}. \tag{H.63}$$

The result is

$$\tilde{H}_{\text{eff}} = J_1 d \sum_{\boldsymbol{k}i} \sqrt{\mathcal{J}^2_{1\boldsymbol{k}} - \mathcal{J}^2_{\boldsymbol{k}2}} \left(c^{\dagger}_{\boldsymbol{k}} c_{\boldsymbol{k}} + d^{\dagger}_{\boldsymbol{k}} d_{\boldsymbol{k}}\right), \tag{H.64}$$

which means that the energies of the χ bosons are smaller by a factor of N_c than the π fields' energies.

To obtain self-consistent equations we calculate the vevs (H.52)–(H.53) using (H.59) and as in the calculation of the π vevs (H.34)–(H.35) one has

$$\begin{aligned} \langle\tilde{0}|\chi^{\dagger e}_{\boldsymbol{q}}\chi^{e}_{\boldsymbol{q}}|\tilde{0}\rangle &= \langle\tilde{0}|\chi^{\dagger o}_{\boldsymbol{q}}\chi^{o}_{\boldsymbol{q}}|\tilde{0}\rangle = \sinh^2\frac{1}{2}\theta_{\boldsymbol{q}} = \frac{1}{2}(\cosh\theta_{\boldsymbol{q}} - 1), & \text{(H.65)} \\ \langle\tilde{0}|\chi^{\text{e}}_{\boldsymbol{q}}\chi^{\text{o}}_{-\boldsymbol{q}}|\tilde{0}\rangle &= \left(\langle\tilde{0}|\chi^{\dagger\text{e}}_{\boldsymbol{q}}\chi^{\dagger\text{o}}_{-\boldsymbol{q}}|\tilde{0}\rangle\right) = \sinh\frac{1}{2}\theta_{\boldsymbol{q}}\cosh\frac{1}{2}\theta_{\boldsymbol{q}} = \frac{1}{2}\sinh\theta_{\boldsymbol{q}}, & \text{(H.66)} \end{aligned}$$

which leads us to identify $\Delta_{1\boldsymbol{k}} = \cosh\theta_{\boldsymbol{k}} - 1$, and $\Delta_{2\boldsymbol{k}} = -\sinh\theta_{\boldsymbol{k}}$. Substituting this into Eqs. (H.60)–(H.61) we write Eq. (H.63) as

$$\tanh\theta_{\boldsymbol{k}} = \frac{\displaystyle\int_{\text{BZ}} \left(\frac{dq}{4\pi}\right)^d I_2(\boldsymbol{q},\boldsymbol{k})\sinh\theta_{\boldsymbol{q}}}{\displaystyle\int_{\text{BZ}} \left(\frac{dq}{4\pi}\right)^d I_1(\boldsymbol{q},\boldsymbol{k})\cosh\theta_{\boldsymbol{q}} - \eta(\boldsymbol{k})}, \tag{H.67}$$

which is exactly the integral equation Eq. (5.52) for $N - m = 1$.

This Hamiltonian calculation sheds light on the meaning of the function $\theta_{\boldsymbol{k}}$ that appears in Chapter 5 in terms of vevs of the χ operators. A stable solution that obeys (5.49) has non-zero vevs. Mathematically, the integral equation (5.52) has also a trivial solution with $\theta_{\boldsymbol{k}} = 0$ that leads to $\Delta_{1,2} = 0$. However, this solution does not obey (5.49) and is thus unphysical, giving $\mathcal{J}_1 < 0$ and making $\tilde{H}_{\text{eff}}$ not positive definite.

Finally, we note that the Holstein–Primakoff transformation for $N - m > 1$ is much more complicated [21], making the Hamiltonian approach unattractive for this case. The path integral approach is more general.

Appendix I

Effective ferromagnetic interaction at $O(1/N_c)$ between odd sites in the nonlinear sigma model with non-zero density

In this section we derive an effective interaction in $O(1/N_c)$ between the classical parts of the sigma fields on the odd sites, and show that this is a ferromagnetic interaction which prefers that these fields align to the same direction within the degenerate submanifold discussed in Chapter 4. The effective interaction comes from integrating over over fluctuations around the classical $N_c = \infty$ ground state and derive an effective action for the classical part (4.95) of the odd spins. We let the $\sigma_{\boldsymbol{n}}$ on the even sites fluctuate around Λ; we let the $\sigma_{\boldsymbol{n}}$ on odd sites roll freely around the $U(m)/[U(2m-N) \times U(N-m)]$ manifold covered by Eq. (4.95), and also execute small oscillations off the manifold into the $U(N)/[U(m) \times U(N-m)]$ coset space. The counterpart of the action (5.1) for our problem has an antiferromagnetic spin-spin interaction, with no $(-1)^{\boldsymbol{n}}$ factors. We separate it into odd, even, and coupled terms,

$$
\begin{aligned}
S &= \frac{N_c}{2}\left(S^{\text{odd}} + S^{\text{even}} + S^{AF}\right), \\
S^{\text{odd}} &= \int d\tau \sum_{\boldsymbol{n}\text{odd}} \operatorname{Tr} \Lambda U_{\boldsymbol{n}}^{\dagger} \partial_\tau U_{\boldsymbol{n}}, \\
S^{\text{even}} &= \int d\tau \sum_{\boldsymbol{n}\text{even}} \operatorname{Tr} \Lambda U_{\boldsymbol{n}}^{\dagger} \partial_\tau U_{\boldsymbol{n}},
\end{aligned}
$$

$$S^{AF} = \int d\tau \sum_{\boldsymbol{n}\text{even}} \frac{J_1}{2} \mathrm{Tr}\, \sigma_{\boldsymbol{n}} \sigma^o_{\boldsymbol{n}}. \tag{I.1}$$

Here $\sigma^o_{\boldsymbol{n}} = \sum_{\boldsymbol{m}(\boldsymbol{n})} \sigma_{\boldsymbol{m}}$, where $\boldsymbol{m}(\boldsymbol{n})$ are the nearest neighbors of the even site $\boldsymbol{n}$. We expand the field on the even sites around $\sigma_{\boldsymbol{n}} = \Lambda$ in the manner of Eq. (5.4),

$$\sigma_{\boldsymbol{n}} = \Lambda + L_{\boldsymbol{n}} - \frac{1}{2} L^2 \Lambda \qquad (\text{n} \quad \text{even}), \tag{I.2}$$

while for the odd sites we write (see Appendix J)

$$\sigma_{\boldsymbol{n}} = U_{\boldsymbol{n}} \begin{pmatrix} \mathbf{1}_{2m-N} & 0 \\ 0 & -\Lambda' - L' + \frac{1}{2} L'^2 \Lambda' \end{pmatrix} U^\dagger_{\boldsymbol{n}} \qquad (\text{n} \quad \text{odd}), \tag{I.3}$$

with

$$\Lambda' = \begin{pmatrix} \mathbf{1}_{N-m} & 0 \\ 0 & -\mathbf{1}_{N-m} \end{pmatrix} \tag{I.4}$$

and

$$U_{\boldsymbol{n}} = \begin{pmatrix} U^{(m)}_{\boldsymbol{n}} & 0 \\ 0 & \mathbf{1}_{N-m} \end{pmatrix}. \tag{I.5}$$

$L_{\boldsymbol{n}}$ describes the fluctuations of the even spins around their classical value Λ. $U_{\boldsymbol{n}}$ rotates the odd spins within the manifold of their classical values, while $L'_{\boldsymbol{n}}$ describes their fluctuations outside that manifold. We further define

$$\sigma^{\text{cl}}_{\boldsymbol{n}} = U_{\boldsymbol{n}} \begin{pmatrix} \mathbf{1}_{2m-N} & 0 \\ 0 & -\Lambda' \end{pmatrix} U^\dagger_{\boldsymbol{n}} = \begin{pmatrix} \sigma^{(m)}_{\boldsymbol{n}} & 0 \\ 0 & \mathbf{1}_{N-m} \end{pmatrix}, \tag{I.6}$$

the classical field on the odd sites.

We leave S^{odd} alone and expand S^{even} and S^{AF} around the classical values of the fields,

$$S^{\text{even}} = -\frac{1}{4} \int d\tau \sum_{\boldsymbol{n}\text{even}} \mathrm{Tr}\, \Lambda L_{\boldsymbol{n}} \partial_\tau L_{\boldsymbol{n}}, \tag{I.7}$$

$$\begin{aligned} S^{AF} &= S_0 + \frac{J_1}{2} \int d\tau \sum_{\boldsymbol{n}\text{even}} \left(\mathrm{Tr}\, L_{\boldsymbol{n}} \bar{\sigma}_{\boldsymbol{n}} - \frac{1}{2} \mathrm{Tr}\, L^2_{\boldsymbol{n}} \Lambda \bar{\sigma}_{\boldsymbol{n}} - \mathrm{Tr}\, L_{\boldsymbol{n}} \bar{L}_{\boldsymbol{n}} \right) \\ &\quad + d J_1 \int d\tau \sum_{\boldsymbol{n}\text{odd}} \left(-\mathrm{Tr}\, \Lambda \tilde{L}_{\boldsymbol{n}} + \frac{1}{2} \mathrm{Tr}\, \tilde{L}^2_{\boldsymbol{n}} \right). \end{aligned} \tag{I.8}$$

Here

$$\tilde{L}_{\boldsymbol{n}} = U_{\boldsymbol{n}} \begin{pmatrix} 0 & 0 \\ 0 & L'_{\boldsymbol{n}} \end{pmatrix} U^\dagger_{\boldsymbol{n}} \tag{I.9}$$

is the rotated fluctuation field on the odd sites, and the Hermitian matrices $\bar{\sigma}_{\boldsymbol{n}}$ and $\bar{L}_{\boldsymbol{n}}$ are sums over the odd neighbors of the even site $\boldsymbol{n}$,

$$\bar{\sigma}_{\boldsymbol{n}} = \sum_{\boldsymbol{m}(\boldsymbol{n})} \sigma^{\text{cl}}_{\boldsymbol{m}}, \tag{I.10}$$

$$\bar{L}_{\boldsymbol{n}} = \sum_{\boldsymbol{m}(\boldsymbol{n})} \tilde{L}_{\boldsymbol{m}}. \tag{I.11}$$

Since both $\bar{\sigma}_{\boldsymbol{n}}$ and Λ are block diagonal, the first trace in each integral in Eq. (I.8) is zero. Now we organize the partition function as follows:

$$Z = \int \left(\prod_{\boldsymbol{n}\text{odd}} d\sigma_{\boldsymbol{n}} \right) \exp\left[-\frac{N_c}{2} \left(S^{\text{odd}} + S_0 + \frac{dJ_1}{2} \int d\tau \sum_{\boldsymbol{n}\text{odd}} \operatorname{Tr} \tilde{L}^2_{\boldsymbol{n}} \right) \right] Z_{\text{even}}, \tag{I.12}$$

with

$$\begin{aligned} Z_{\text{even}} &= \int \left(\prod_{\boldsymbol{n}\text{even}} dL_{\boldsymbol{n}} \right) \exp\left[-\frac{N_c}{2} \int d\tau \right. \\ &\quad \left. \times \sum_{\boldsymbol{n}\text{even}} \left(-\frac{1}{4} \operatorname{Tr} \Lambda L_{\boldsymbol{n}} \partial_\tau L_{\boldsymbol{n}} - \frac{J_1}{4} \operatorname{Tr} L^2_{\boldsymbol{n}} \Lambda \bar{\sigma}_{\boldsymbol{n}} - \frac{J_1}{2} \operatorname{Tr} L_{\boldsymbol{n}} \bar{L}_{\boldsymbol{n}} \right) \right]. \end{aligned} \tag{I.13}$$

Z_{even} is a product of decoupled single-site integrals. Again we expand in the group algebra,

$$L_{\boldsymbol{n}} = l^\eta_{\boldsymbol{n}} M^\eta, \tag{I.14}$$

where the sum is over the $2m(N-m)$ generators of $U(N)$ that are not in $U(m) \times U(N-m)$. $\bar{L}_{\boldsymbol{n}}$ can be expanded similarly and we obtain the following form for the integral over the even fields:

$$Z_{\text{even}} = \int Dl_{\boldsymbol{n}} \exp\left[-\frac{N_c}{2} \int d\tau \sum_{\boldsymbol{n}} \left(l^\eta_{\boldsymbol{n}} \mathcal{M}^{\eta\eta'}_{\boldsymbol{n}} l^{\eta'}_{\boldsymbol{n}} + \frac{J_1}{4} l^\eta_{\boldsymbol{n}} \bar{l}^\eta_{\boldsymbol{n}} \right) \right], \tag{I.15}$$

where

$$\mathcal{M}^{\eta\eta'}_{\boldsymbol{n}} = -\frac{1}{8} C^{\eta\eta'} \partial_\tau + \frac{J_1}{8} D^{\eta\eta'}_{\boldsymbol{n}}. \tag{I.16}$$

The matrix C is the same as in Eq. (5.7),

$$C^{\eta\eta'} = \operatorname{Tr}(\Lambda [M^\eta, M^{\eta'}]), \tag{I.17}$$

while the new matrix D varies with the site $\boldsymbol{n}$ according to the average $\bar{\sigma}_{\boldsymbol{n}}$ of its neighboring spins,

$$D^{\eta\eta'}_{\boldsymbol{n}} = -\operatorname{Tr}(\{M^\eta, M^{\eta'}\} \Lambda \bar{\sigma}_{\boldsymbol{n}}). \tag{I.18}$$

We study the two matrices in Appendix E. Diagonalizing C as before, we arrive at

$$Z_{\text{even}} = \prod_{\boldsymbol{n}q} \left\{ \int Dl \, \exp - \frac{N_c}{2} \int d\tau \left[l^{q\dagger} \hat{\mathcal{M}}_{\boldsymbol{n}} l^q + \frac{J_1}{4} \left(l^{q\dagger} \bar{l}^q_{\boldsymbol{n}} + \bar{l}^{q\dagger}_{\boldsymbol{n}} l^q \right) \right] \right\}, \tag{I.19}$$

where $\hat{\mathcal{M}}_{\boldsymbol{n}}$ is the $m \times m$ matrix

$$\hat{\mathcal{M}}_{\boldsymbol{n}} = \frac{1}{4} \left(\partial_\tau + J_1 E_{\boldsymbol{n}} \right). \tag{I.20}$$

The quantities l^q (and $\bar{l}^q$) for each $q = 1, \ldots, N-m$ are complex m-component vectors; they are rotations of the $2m(N-m)$ real components l^η (and $\bar{l}^\eta$) into the basis that diagonalizes C. The matrix $E_{\boldsymbol{n}}$ is given by Eq. (6.11); it carries the dependence on $\bar{\sigma}_{\boldsymbol{n}}$. Performing the gaussian integration we have

$$Z_{\text{even}} = \prod_{\boldsymbol{n}q} \frac{1}{\operatorname{Det} \hat{\mathcal{M}}_{\boldsymbol{n}}} \exp \left[\frac{N_c}{2} \left(\frac{J_1}{4} \right)^2 \int d\tau \, \bar{l}^{q\dagger}_{\boldsymbol{n}} \hat{\mathcal{M}}^{-1}_{\boldsymbol{n}} \bar{l}^q_{\boldsymbol{n}} \right]. \tag{I.21}$$

Finally we separate the integral (I.12) over the odd spins into an integral over the classical field $\sigma^{\text{cl}}_{\boldsymbol{n}}$ and an integral over the fluctuations around it. We obtain

$$\begin{aligned} Z &= \int D\sigma^{\text{cl}}_{\boldsymbol{m}} \exp - \frac{N_c}{2} \left(S_0 + (N-m) \sum_{\boldsymbol{n}} \operatorname{Tr} \log \hat{\mathcal{M}}_{\boldsymbol{n}} \right) \\ &\quad \times \int D\tilde{l}_{\boldsymbol{m}} \exp - \frac{N_c}{2} \left\{ S^{\text{odd}} + \int d\tau \left[\frac{dJ_1}{2} \sum_{\boldsymbol{m}q} |\tilde{l}^q_{\boldsymbol{m}}|^2 - \left(\frac{J_1}{4} \right)^2 \sum_{\boldsymbol{n}q} \bar{l}^{q\dagger}_{\boldsymbol{n}} \hat{\mathcal{M}}^{-1}_{\boldsymbol{n}} \bar{l}^q_{\boldsymbol{n}} \right] \right\}. \end{aligned} \tag{I.22}$$

Here $\boldsymbol{m}$ stands for an odd site, $\boldsymbol{n}$ for an even one.

Equation (I.22) gives an effective action for the classical odd spins $\sigma^{\text{cl}}_{\boldsymbol{m}}$. These enter the exponents through $\hat{\mathcal{M}}$ [via Eqs. (6.11) and (I.20)] and through $\bar{l}^q_{\boldsymbol{n}}$ [via Eqs. (I.9) and (I.11)]. The action in the first exponent is minimized when each matrix $E_{\boldsymbol{n}}(\sigma^{\text{cl}}_{\boldsymbol{m}})$ has the largest number of zero eigenvalues, each of which makes $\operatorname{Tr} \log \hat{\mathcal{M}}_{\boldsymbol{n}}$ approach $-\infty$. It is easy to check that $E_{\boldsymbol{n}}$ has $2m - N$ zero eigenvalues (the maximal number) when the $\sigma^{\text{cl}}_{\boldsymbol{m}}$ on *all* the odd sites $\boldsymbol{m}(\boldsymbol{n})$ align, *i.e.,*

$$\sigma^{\text{cl}}_{\boldsymbol{m}} = \sigma_0 \in U(m)/[U(2m-N) \times U(N-m)]. \tag{I.23}$$

Moreover, when Eq. (I.23) holds, all the $\tilde{l}^q_{\boldsymbol{m}}$'s align parallel to each other and $\bar{l}^q_{\boldsymbol{n}}$ is maximized; also the eigenvalues of $\hat{\mathcal{M}}^{-1}_{\boldsymbol{n}}$ are maximized (to $+\infty$). Thus the action in the second exponent also has a minimum at this point in configuration space. These effects add up to an effective *ferromagnetic* interaction among the $2d$ nearest neighbors $\boldsymbol{m}$ of each even site $\boldsymbol{n}$. This effective interaction will align the classical spins on the odd sublattice to the same direction in their submanifold, $U(m)/[U(2m-N) \times U(N-m)]$.

The divergences in the effective action have their origin in the fact that the semiclassical corrections are calculated as gaussian integrals in the even fluctuation fields $L_{\boldsymbol{n}}$, and the coefficient matrix $\mathcal{M}_{\boldsymbol{n}}$ acquires zero eigenvalues. The correct range of integration over $L_{\boldsymbol{n}}$ is of course not infinite, but rather the volume of the $U(N)/[U(m) \times U(N-m)]$ manifold. This will regulate the divergences, but leave the effective action for the odd spins attractive.

Appendix J

Fluctuations on the odd sites at non-zero density

In this section we show how to separate the fluctuation outside the degenerate submanifold of the odd spin.

In the classical analysis, the fields on the odd sites take values in the sub-manifold $U(m)/[U(2m-N)\times U(N-m)]$ of the manifold $U(N)/[U(m)\times U(N-m)]$. We denote these values σ^{cl},

$$\sigma^{\mathrm{cl}} = \begin{pmatrix} \sigma^{(m)} & 0 \\ 0 & \mathbf{1}_{N-m} \end{pmatrix}. \tag{J.1}$$

Here

$$\sigma^{(m)} = U^{(m)}\Lambda^{(m)}U^{(m)\dagger}. \tag{J.2}$$

with $U^{(m)} \in U(m)$, and

$$\Lambda^{(m)} = \begin{pmatrix} \mathbf{1}_{2m-N} & \\ 0 & -\mathbf{1}_{N-m} \end{pmatrix}. \tag{J.3}$$

$\sigma^{(m)}$ contains $2(N-m)(2m-N)$ independent degrees of freedom. Any $\sigma \in U(N)/[U(m)\times U(N-m)]$ can be written as

$$\sigma = \begin{pmatrix} \cos\left(2\sqrt{aa^\dagger}\right) & -a\,\dfrac{\sin\left(2\sqrt{a^\dagger a}\right)}{\sqrt{a^\dagger a}} \\ -\dfrac{\sin\left(2\sqrt{a^\dagger a}\right)}{\sqrt{a^\dagger a}}\,a^\dagger & -\cos\left(2\sqrt{a^\dagger a}\right) \end{pmatrix} \tag{J.4}$$

[cf. Eq. (4.19)], which coincides with Eq. (J.1) if

$$a = U^{(m)} \begin{pmatrix} 0 \\ (\pi/2)\mathbf{1}_{N-m} \end{pmatrix}. \tag{J.5}$$

Recall that a is an $m \times (N-m)$ matrix, so the zero block has dimensions $(2m-N) \times (N-m)$.

We allow motion out of the sub-manifold by allowing a to vary further,

$$a = U^{(m)} \begin{pmatrix} 0 \\ \bar{a} \end{pmatrix}. \tag{J.6}$$

The $2(N-m)^2$ degrees of freedom in $\bar{a}$ complement the $2(N-m)(2m-N)$ degrees of freedom inherent in $U^{(m)}$ to give $2m(N-m)$, the dimensionality of the entire $U(N)/[U(m) \times U(N-m)]$ coset space.

Writing σ with the generalized a we have

$$\sigma = U \begin{pmatrix} \mathbf{1}_{2m-N} & 0 & 0 \\ 0 & \cos\left(2\sqrt{\bar{a}\bar{a}^\dagger}\right) & -\bar{a}\,\dfrac{\sin\left(2\sqrt{\bar{a}^\dagger\bar{a}}\right)}{\sqrt{\bar{a}^\dagger\bar{a}}} \\ 0 & -\dfrac{\sin\left(2\sqrt{\bar{a}^\dagger\bar{a}}\right)}{\sqrt{\bar{a}^\dagger\bar{a}}}\,\bar{a}^\dagger & -\cos\left(2\sqrt{\bar{a}^\dagger\bar{a}}\right) \end{pmatrix} U^\dagger, \tag{J.7}$$

with

$$U = \begin{pmatrix} U^{(m)} & 0 \\ 0 & \mathbf{1}_{N-m} \end{pmatrix}. \tag{J.8}$$

We can also write this as

$$\sigma = U \begin{pmatrix} \mathbf{1}_{2m-N} & 0 \\ 0 & \sigma^{[2(N-m)]}(\bar{a}, \bar{a}^\dagger) \end{pmatrix} U^\dagger. \tag{J.9}$$

$\sigma^{[2(N-m)]}$ is a matrix in the manifold $U(2(N-m))/[U(N-m) \times U(N-m)]$. Indeed for $\bar{a} = (\pi/2)\mathbf{1}_{N-m}$, we have

$$\sigma^{[2(N-m)]} = \begin{pmatrix} -\mathbf{1}_{N-m} & 0 \\ 0 & \mathbf{1}_{N-m} \end{pmatrix} \equiv -\bar{\Lambda}. \tag{J.10}$$

Since $U(2(N-m))/[U(N-m) \times U(N-m)]$ is a self-conjugate manifold, its structure near $\sigma^{[2(N-m)]} = -\bar{\Lambda}$ is the same as its structure near $\sigma^{[2(N-m)]} = \bar{\Lambda}$, which corresponds to $\bar{a} = 0$. Expanding $\sigma^{[2(N-m)]}$ around $-\bar{\Lambda}$ gives Eq. (I.3).

Appendix K

Coefficients in the dispersion relations of Goldstone bosons

Here we present the various coefficients that appear in the dispersion relations given by Eq. (6.62). These are c, c_1, a, and b found in Eqs. (6.63)–(6.68). These coefficients are extracted from the nearest-neighbor theory, and depend on the number $N-m$ only.

The constants c and c_1 are the zero momentum curvatures of the following functions,

$$c = \left(\frac{d\sqrt{\Sigma_1^2-\Sigma_2^2}}{d(\boldsymbol{k}^2)}\right)_{\boldsymbol{k}=0}, \tag{K.1}$$

$$c_1 = -\left(\frac{d\Sigma_1}{d(\boldsymbol{k}^2)}\right)_{\boldsymbol{k}=0}. \tag{K.2}$$

a and b are defined as

$$a = \frac{N_c}{6J_1}\frac{c_1^2-c^2}{2c_1c^2}, \tag{K.3}$$

$$b = \frac{N_c}{6J_1}\frac{2}{c_1}. \tag{K.4}$$

We present the constants in Table K.1.

Table K.1: The constants c, c_1, a, and b, for all values of $N-m$. Recall that for $N-m=1$, the solution of the integral equation is different from the other cases, and it is possible that the nearest-neighbor spectrum follows a power of momentum higher than 2. This is the source of the sizeable differences between this case and the other cases.

$N-m$	c	c_1	a	b
1	8.3×10^{-5}	0.12	8.4×10^{6}	17.1
2	0.002	0.01	1.2×10^{3}	187
3	0.003	0.009	490	220
4	0.003	0.008	350	240
5	0.003	0.008	280	250

Here we note that the case of $N-m=1$ has an exceptionally large value for a, with a very small curvature c. This is a result of the different behavior of the solution to the integral equation for this case [see Fig. 5.4]. This behavior should disappear if we take a better momentum mesh, especially near $\boldsymbol{k}=0$.

Appendix L

Classification of fields according to unbroken subgroups

In this section we consider the σ fields that represent Goldstone bosons of the effective theory. The σ multiplet contains fields called π that are type I Goldstone bosons in the nearest-neighbor theory, and fields called χ that are type II bosons there. Moreover, the antiferromagnetic nature of the theory leads us to consider separately the fields on the even and odd sites of the lattice.

The next-nearest-neighbor theory breaks its chiral $SU(N_f) \times SU(N_f)$ symmetry spontaneously as shown in Table 6.1. The following two tables show the classification of the various fields according to their representations and charges under the unbroken groups.

Table L.1: Classification of σ fields on the *even* sites under the unbroken symmetry for $3N/4 \leq m < N$. As indicated in Eq. (6.38), not all χ fields are present for a given combination of N_f and B. We neglect $U(1)_A$. All fields are complex.

N_f	B	Symmetry	Field	Matrix structure	Symmetry rep or $U(1)$ charge(s)
1	1	$\emptyset$	π, χ_1	1×1	-
2	2	$SU(2)$	π	2×2	$\mathbf{1} \oplus \mathbf{3}$
			χ_1	4×2	$\mathbf{1} \oplus \mathbf{1} \oplus \mathbf{3} \oplus \mathbf{3}$
2	3	$U(1)_{I_3}$	π	1×1	$+1$
			χ_{1e}	4×1	$\begin{pmatrix} +1 \\ 0 \\ +1 \\ 0 \end{pmatrix}$
			χ_{2e}	2×1	$\begin{pmatrix} +1 \\ 0 \end{pmatrix}$
3	3	$SU(3)$	π	3×3	$\mathbf{1} \oplus \mathbf{8}$
			χ_1	9×2	$\mathbf{1} \oplus \mathbf{1} \oplus \mathbf{8} \oplus \mathbf{8}$
3	4	$U(1)_{I_3} \times U(1)_Y$	π	2×2	$\begin{pmatrix} (+1/2,-3) & (0,0) \\ (+1,0) & (+1/2,+3) \end{pmatrix}$
			χ_{1e}	6×2	$\begin{pmatrix} (+1,0) & (+1/2,+3) \\ (0,0) & (-1/2,+3) \\ (+1/2,-3) & (0,0) \\ (+1,0) & (+1/2,+3) \\ (0,0) & (-1/2,+3) \\ (+1/2,-3) & (0,0) \end{pmatrix}$
			χ_{2e}	2×2	$\begin{pmatrix} (+1,0) & (+1/2,+3) \\ (0,0) & (-1/2,+3) \end{pmatrix}$
3	5	$U(1)_{I_3} \times U(1)_Y$	π	1×1	$(-1/2,+3)$
			χ_{1e}	6×1	$\begin{pmatrix} (+1/2,+3) \\ (-1/2,+3) \\ (0,0) \\ (+1/2,+3) \\ (-1/2,+3) \\ (0,0) \end{pmatrix}$
			χ	4×1	$(+1/2,+3)$ $(-1/2,+3)$

Table L.2: Classification of χ fields on the *odd* sites. The classification of the odd π fields is the same as of the even π fields for all values of N_f and B. For $N_f = B = 1, 2, 3$, the classification of the odd χ fields is the same as of the even χ fields. Here we present the classification of the odd χ's for the other cases. All fields are complex.

N_f	B	Symmetry	Field	Matrix structure	$U(1)$ charge(s)
2	3	$U(1)_{I_3}$	χ_{1o}	4×1	$\begin{pmatrix} 0 \\ -1 \\ 0 \\ -1 \end{pmatrix}$
			χ_{2o}	2×1	$\begin{pmatrix} 0 \\ -1 \end{pmatrix}$
3	4	$U(1)_{I_3} \times U(1)_Y$	χ_{1o}	6×2	$\begin{pmatrix} (+1/2, +3) & (0,0) \\ (-1/2, +3) & (-1,0) \\ (0,0) & (-1/2, -3) \\ (+1/2, +3) & (0,0) \\ (-1/2, +3) & (-1,0) \\ (0,0) & (-1/2, -3) \end{pmatrix}$
			χ_{2o}	2×2	$\begin{pmatrix} (+1/2, +3) & (0,0) \\ (-1/2, +3) & (-1,0) \end{pmatrix}$
3	5	$U(1)_{I_3} \times U(1)_Y$	χ_{1o}	6×1	$\begin{pmatrix} (+1,0) \\ (0,0) \\ (+1/2, -3) \\ (+1,0) \\ (0,0) \\ (+1/2, -3) \end{pmatrix}$
			χ_{2o}	4×1	$\begin{pmatrix} (+1,0) \\ (0,0) \\ (+1/2, -3) \\ (+1,0) \end{pmatrix}$

Bibliography

[1] D. J. Gross and F. Wilczek, "Ultraviolet behavior of non-abelian gauge theories," Phys. Rev. Lett. **30**, 1343 (1973).

[2] H. D. Politzer, "Reliable perturbative results for strong interactions?," Phys. Rev. Lett. **30**, 1346 (1973).

[3] J. C. Collins and M. J. Perry, "Superdense matter: Neutrons or asymptotically free quarks?" Phys. Rev. Lett. **34**, 1353 (1975).

[4] B. C. Barrois, "Superconducting quark matter," Nucl. Phys. B **129**, 390 (1977);

[5] B. C. Barrois, *Nonperturbative Effects In Dense Quark Matter.* Ph. D. thesis, California institute of technology, 1979, UMI 79-04847.

[6] D. Bailin and A. Love, "Superconductivity in quark matter," Nucl. Phys. B **205**, 119 (1982); "The color superconducting phase transition in quark matter," Phys. Lett. B **107**, 377 (1981); "Superfluidity and superconductivity in relativistic fermion systems" Phys. Rept. **107**, 325 (1984).

[7] M. Alford, K. Rajagopal, and F. Wilczek, "QCD at finite baryon density: Nucleon droplets and color superconductivity" Phys. Lett. B **422**, 247 (1998), `hep-ph/9711395`.

[8] R. Rapp, T. Schäfer, E. V. Shuryak, and M. Velkovsky, "Diquark Bose condensates in high density matter and instantons" Phys. Rev. Lett. **81**, 53 (1998), `hep-ph/9711396`.

[9] D. T. Son, "Superconductivity by long-range color magnetic interaction in high-density quark matter," Phys. Rev. D **59**, 094019 (1999), `hep-ph/9812287`.

[10] T. Schafer and F. Wilczek, "High density quark matter and the renormalization group in QCD with two and three flavors," Phys. Lett. B **450**, 325 (1999), `hep-ph/9810509`.

[11] M. Alford, K. Rajagopal and F. Wilczek, "Color-flavor locking and chiral symmetry breaking in high density QCD" Nucl. Phys. B **537**, 443 (1999), `hep-ph/9804403`.

[12] M. G. Alford, J. A. Bowers, and K. Rajagopal, "Crystalline color superconductivity," Phys. Rev. D **63**, 074016 (2001), `hep-ph/0008208`. J. A. Bowers and K. Rajagopal, "The crystallography of color superconductivity," Phys. Rev. D **66**, 065002 (2002), `hep-ph/0204079`.

[13] K. Rajagopal and F. Wilczek, in *At The Frontier of Particle Physics. Handbook of QCD,* eds. M. Shifman and B. Ioffe, (World Scientific, Singapore, 2001), Vol. 3, "The condensed matter physics of QCD," `hep-ph/0011333`.

[14] K. Rajagopal and E. Shuster, "On the applicability of weak-coupling results in high density QCD," Phys. Rev. D **62**, 085007 (2000), `hep-ph/0004074`.

[15] Z. Fodor and S. D. Katz, "Critical point of QCD at finite T and μ, lattice results for physical quark masses," JHEP **0404**, 050 (2004), `hep-lat/0402006`; "Lattice determination of the critical point of QCD at finite T and mu," JHEP **0203**, 014 (2002), `hep-lat/0106002`; Z. Fodor, S. D. Katz, and K. K. Szabo, "The QCD equation of state at nonzero densities: Lattice result," Phys. Lett. B **568**, 73 (2003) `hep-lat/0208078`.

[16] P. de Forcrand and O. Philipsen, "The phase diagram of $N_f = 3$ QCD for small baryon densities," Nucl. Phys. Proc. Suppl. **129-130**, 521 (2004), `hep-lat/0309109`. "The QCD phase diagram for small densities from imaginary chemical potential," Nucl. Phys. B **642**, 290 (2002), `hep-lat/0205016`.

[17] S. Ejiri, C. R. Allton, S. J. Hands, O. Kaczmarek, F. Karsch, E. Laermann and C. Schmidt, "Study of QCD thermodynamics at finite density by Taylor expansion," `hep-lat/0312006`.

[18] M. A. Stephanov, "QCD phase diagram and the critical point," `hep-ph/0402115`.

[19] T. Banks, L. Susskind, and J. Kogut, "Strong coupling calculations of lattice gauge theories: (1+1)-dimensional exercises," Phys. Rev. D **13**, 1043 (1976).

[20] B. Svetitsky, S. D. Drell, H. R. Quinn, and M. Weinstein, "Dynamical breaking of chiral symmetry in lattice gauge theories," Phys. Rev. D **22**, 490 (1980); M. Weinstein, S. D. Drell, H. R. Quinn, and B. Svetitsky, "Approximate dynamical symmetry in lattice quantum chromodynamics," *ibid.* **22**, 1190 (1980).

[21] J. Smit, "Chiral symmetry breaking in QCD: Mesons as spin waves," Nucl. Phys. B **175**, 307 (1980).

[22] R. C. Brower and B. Svetitsky, "Hamiltonian domain wall fermions at strong coupling," Phys. Rev. D **61** (2000) 114511, `hep-lat/9912019`.

[23] H. B. Nielsen and M. Ninomiya, "Absence of Neutrinos on a lattice. 1. Proof by homotopy theory," Nucl. Phys. B **185**, 20 (1981) [Erratum-*ibid.* **195**, 541 (1982)]; "Absence of Neutrinos on a lattice. 2. Intuitive topological proof," *ibid.* **193**, 173 (1981).

[24] K. G. Wilson, in *New phenomena in subnuclear physics*, (Erice 1975), ed. A. Zichichi (Plenum, New York, 1977), Part A.

[25] L. Susskind, "Lattice fermions," Phys. Rev. D **16**, 3031 (1977).

[26] R. Narayanan and H. Neuberger, "Infinitely many regulator fields for chiral fermions," Phys. Lett. B **302**, 62 (1993), `hep-lat/9212019`; "Chiral determinant as an overlap of two vacua," Nucl. Phys. B **412**, 574 (1994), `hep-lat/9307006`; "A construction of lattice chiral gauge theories," Nucl. Phys. B **443**, 305 (1995), `hep-th/9411108`; H. Neuberger, "Vector like gauge theories with almost massless fermions on the lattice," Phys. Rev. D **57**, 5417 (1998).

[27] M. Creutz, I. Horvath, and H. Neuberger, "A new fermion Hamiltonian for lattice gauge theory," Nucl. Phys. Proc. Suppl. **106**, 760 (2002), `hep-lat/0110009`.

[28] D. B. Kaplan, "A Method for simulating chiral fermions on the lattice," Phys. Lett. B **288**, 342 (1992), `hep-lat/9206013`.

[29] Y. Shamir, "Chiral fermions from lattice boundaries," Nucl. Phys. B **406**, 90 (1993), `hep-lat/9303005`.

[30] S. D. Drell, M. Weinstein, and S. Yankielowicz, "Strong coupling field theories: 2. Fermions and gauge fields on a lattice," Phys. Rev. D **14**, 1627 (1976).

[31] S. Myint and C. Rebbi, "Chiral perturbation theory on the lattice: Strong coupling expansion," Nucl. Phys. B **421**, 241 (1994), `hep-lat/9401009`.

[32] B. Svetitsky and Y. Shamir, Private communications (2002).

[33] G. 't Hooft, in *Recent developments in gauge theories* (Cargèse 1979), ed. G. 't Hooft *et al.* (Plenum, New York, 1980); E. H. Fradkin and S. H. Shenker, "Phase diagrams of lattice gauge theories iith Higgs fields," Phys. Rev. D **19**, 3682 (1979); L. F. Abbott and E. Farhi, "Are the weak interactions strong?," Phys. Lett. B **101**, 69 (1981); "A confining model of the weak interactions," Nucl. Phys. B **189**, 547 (1981).

[34] T. Schäfer, "Patterns of symmetry breaking in QCD at high baryon density," Nucl. Phys. B **575**, 269 (2000), `hep-ph/9909574`.

[35] V. Azcoiti, G. Di Carlo, A. Galante and V. Laliena, "Diquark condensation at strong coupling," JHEP **0309**, 014 (2003), `hep-lat/0307019`;

[36] A. Le Yaouanc, L. Oliver, O. Pene, J. C. Raynal, M. Jarfi and O. Lazrak, "Hamiltonian lattice QCD at finite temperature and chemical potential. 1. Minimum principle and Bogolyubov approximation," Phys. Rev. D **37**, 3691 (1988); "Hamiltonian lattice QCD at finite temperature and chemical potential. 2. Gauss law constraint on the thermal excitations," Phys. Rev. D **37**, 3702 (1988); "Hamiltonian lattice QCD at finite temperature and chemical potential. 3. Critical curve of symmetry restoration for arbitrary number Of colors And Flavors," Phys. Rev. D **38**, 3256 (1988).

[37] E. B. Gregory, S. H. Guo, H. Kroger and X. Q. Luo, "Hamiltonian lattice QCD at finite chemical potential," Phys. Rev. D **62**, 054508 (2000), `hep-lat/9912054`.

[38] Y. Umino, "QCD equation of state for cold and dense quark matter: The strong coupling limit," Phys. Rev. D **66**, 074501 (2002), `hep-ph/0101144`.

[39] F. Karsch and K. H. Mutter, "Strong coupling QCD at finite baryon number density," Nucl. Phys. B **313** (1989) 541.

[40] Y. Nishida, "Phase structures of strong coupling lattice QCD with finite baryon and isospin density," Phys. Rev. D **69**, 094501 (2004), `hep-ph/0312371`.

[41] Y. Z. Fang and X. Q. Luo, "Hamiltonian lattice quantum chromodynamics at finite density with Wilson fermions," `hep-lat/0210031`.

[42] F. D. M. Haldane, "Continuum dynamics of the 1-D Heisenberg antiferromagnetic identification with the $O(3)$ nonlinear sigma model," Phys. Lett. A **93**, 464 (1983); "Nonlinear field theory of large spin Heisenberg antiferromagnets. Semiclassically quantized Solitons of the one-dimensional easy axis Néel state," Phys. Rev. Lett. **50**, 1153 (1983); ""Theta physics" and quantum spin chains," J. Appl. Phys. **57**, 3359

(1985); "$O(3)$ nonlinear sigma-model and the topological distinction between integer-spin and half-integer-spin antiferromagnets in 2 dimensions," Phys. Rev. Lett. **61**, 1029 (1988).

[43] I. Affleck, "Large N limit of $SU(N)$ quantum 'spin' chains," Phys. Rev. Lett. **54**, 966 (1985); "The quantum Hall effect, sigma models at $\theta = \pi$ and quantum spin chains," Nucl. Phys. B **257**, 397 (1985); "Exact critical exponents for quantum spin chains, nonlinear sigma models at
$theta = \pi$ and the quantum Hall effect," Nucl. Phys. B **265**, 409 (1986).

[44] I. Affleck and J. B. Martson, "Large-n limit of the Heisenberg-Hubbard model: Imlications for high-T_c superconductors," Phys. Rev. B. **37**, 3774 (1988); J. B. Martson, I. Affleck, "Large-n limit of the Hubbard-Heisenberg model," Phys. Rev. B. **39**, 11538 (1989).

[45] D. P. Arovas and A. Auerbach, "Functional integral theories of low-dimensional quantum Heisenberg models," Phys. Rev. B **38**, 316 (1988).

[46] N. Read and S. Sachdev, "Some features of the phase diagram of the square lattice $SU(N)$ antiferromagnet," Nucl. Phys. B **316** (1989) 609.

[47] N. Read and S. Sachdev, "Valence-bond and spin-Peierls ground state of low-dimensional quantum antiferromagnets," Phys. Rev. Lett. **62**, 1694 (1989); "Spin-Peierls, valence-bond solid, and Néel ground state of low-dimensional quantum antiferromagnets," Phys. Rev. B. **42**, 4568 (1990).

[48] D. P. Arovas, "Mean field theories of the quantum Heisenberg Model," Helvetica Physica Acta **63**, 323 (1990).

[49] S. Randjbar-Daemi, A. Salam and J. Strathdee, "Generalized spin systems and sigma models," Phys. Rev. B **48**, 3190 (1993), `hep-th/9210145`.

[50] A. Auerbach, *Interacting electrons and quantum magnetism* (Springer-Verlag, Berlin, 1994).

[51] J. R. Klauder and B. Skagerstam, *Coherent States: Applications in Physics and Mathematical Physics* (World Scientific, Singapore, 1985).

[52] A. B. Harris, A. Aharony, O. Entin-Wohlman, I. Ya. Korenblit, R. J. Birgeneau, Y. J. Kim, "Quantum fluctuations in frustrated antiferromagnet $Sr_2Cu_3O_4Cl_2$," Phys. Rev. B **64** 024436 (2001), `cond-mat/0009315`.

[53] A. V. Chubukov and T. Jolicoeur, "Order-from-disorder phenomena in Heisenberg antiferromagnet on a triangular lattice," Phys. Rev. B **46** 11137 (1992);

[54] N. Shannon and A. V. Chubukov, "Spin-wave expansion, finite temperature corrections, and order from disorder effects in the double exchange model," Phys. Rev. B **65** 104418 (2002).

[55] A. B. Harris, C. Kallin, A. J. Berlinsky, "Possible Néel ordering of the Kagomé antiferromagnet," Phys. Rev. B **45**, 2899 (1992); A. Chubukov, "Order from Disorder in a Kagomé antiferromagnet," Phys. Rev. Lett. **69**, 832 (1992).

[56] S. Sachdev, "Kagomé-acute- and triangular-lattice Heisenberg antiferromagnets: Ordering from quantum fluctuations and quantum-disordered ground states with unconfined bosonic spinons," Phys. Rev. B **45**, 12377 (1992).

[57] J. vonDelft and C. L. Henley, "Spin tunneling in the Kagoé antiferromagnet," Phys. Rev. B **48** 965 (1993).

[58] B. Bringoltz and B. Svetitsky, "Towards a strong-coupling theory of QCD at finite density," Nucl. Phys. Proc. Suppl. **119**, 565 (2003), `hep-lat/0209005`.

[59] B. Bringoltz and B. Svetitsky, "Lattice gauge theory with baryons at strong coupling," Phys. Rev. D **68** 034501 (2003), `hep-lat/0211018`.

[60] B. Bringoltz, "Order from disorder in lattice QCD at high density," Phys. Rev. D **69**, 014508 (2004), `hep-lat/0308018`.

[61] B. Bringoltz and B. Svetitsky, "Spontaneous symmetry breaking in strong-coupling lattice QCD at high density," Phys. Rev. D **69**, 014502 (2004), `hep-lat/0310032`.

[62] B. Bringoltz and B. Svetitsky, "Anisotropic Goldstone bosons of strong-coupling lattice QCD at high density,", `hep-lat/0405013`.

[63] J. B. Kogut and L. Susskind, "Hamiltonian formulation of Wilson's lattice gauge theories," Phys. Rev. D **11**, 395 (1975).

[64] K. G. Wilson, "Confinement of quarks," Phys. Rev. D **10**, 2445 (1974).

[65] S. L. Adler, "Axial vector vertex in spinor electrodynamics," Phys. Rev. **177**, 2426 (1969); J. S. Bell and R. Jackiw, "A PCAC puzzle: $pi_0 \to \Gamma\Gamma$ in the sigma model," Nuovo Cim. A **60**, 47 (1969).

[66] L. H. Karsten and J. Smit, "Lattice fermions: species doubling, chiral invariance, and the triangle anomaly," Nucl. Phys. B **183**, 103 (1981).

[67] T. Kato, Prog. Theor. Phys. **4**, 154 (1949); A. Messiah, *Quantum Mechanics* (North-Holland, Amsterdam, 1961), Ch. 16.

[68] S. Pittel, J. M. Arias, J. Dukelsky and A. Frank, "Consistent baryon mapping of quark systems," Phys. Rev. C **50**, 423 (1994).

[69] J. Meyer, "Boson fermion and baryon mapping of multi - quark states," J. Math. Phys. **32**, 2142 (1991).

[70] D. Hadjimichef, G. Krein, S. Szpigel and J. S. da Veiga, "Second quantization approach to composite hadron interactions in quark models," Phys. Lett. B **367**, 317 (1996), `hep-ph/9511423`.

[71] M. Sambataro, "Baryon mapping of quark systems," Phys. Rev. C **52**, 3378 (1995), `nucl-th/9510038`.

[72] D. Hadjimichef, G. Krein, S. Szpigel and J. S. da Veiga, "Mapping of composite hadrons into elementary hadrons and effective hadronic Hamiltonians," Annals Phys. **268**, 105 (1998), `hep-ph/9805459`.

[73] M. D. Girardeau, G. Krein and D. Hadjimichef, "Field-theoretic approach for systems of composite hadrons," Mod. Phys. Lett. A **11**, 1121 (1996).

[74] W. Brenig and A. P. Kampf, "Spin excitations in a quantum antiferromagnet with magnetic impurities and vacancies," Phys. Rev. B **43**, 12914 (1991).

[75] K. J. B. Lee and P. Schlottmann, "Isolated ferromagnetic bonds in the two-dimmensional spin-1/2 Heisenberg antiferromagnet," Phys. Rev. B **42**, 4426 (1990).

[76] V. N. Kotov, J. Oitmaa and O. Sushkov, "Local magnetic impurity in the two dimensional heisenberg antiferromagnet," Phys. Rev. B **58**, 8495 (1998).

[77] B. Schlittgen and U.-J. Wiese, "Quantum spin formulation of the principal chiral model," Nucl. Phys. Proc. Suppl. **83**, 718 (2000), `hep-lat/0005020`; "Low-energy effective theories of quantum spin and quantum link models," Phys. Rev. D **63**, 085007 (2001), `hep-lat/0012014`.

[78] B. Schlittgen and T. Wettig, "Color-flavor transformation for the special unitary group," Nucl. Phys. B **632**, 155 (2002), `hep-lat/0111039`.

[79] A. N. Berker and L. P. Kadanoff, J. Phys. A **13**, L259 (1980); J. R. Banavar, G. S. Grest, and D. Jasnow, Phys. Rev. B **25**, 4639 (1982).

[80] H. B. Nielsen and S. Chadha, "On how to count Goldstone bosons," Nucl. Phys. B **105**, 445 (1976).

[81] H. Leutwyler, "Nonrelativistic effective Lagrangians," Phys. Rev. D **49**, 3033 (1994), `hep-ph/9311264`.

[82] T. Schafer, D. T. Son, M. A. Stephanov, D. Toublan and J. J. Verbaarschot, "Kaon condensation and Goldstone's theorem," Phys. Lett. B **522**, 67 (2001), `hep-ph/0108210`; F. Sannino, "Locking internal and space-symmetries: Relativistic vector condensation," `hep-ph/0303168`.

[83] M. E. Peskin, "The alignment of the vacuum in theories of technicolor," Nucl. Phys. B **175**, 197 (1980).

[84] F. Sannino, "General structure of relativistic vector condensation," Phys. Rev. D **67**, 054006 (2003), `hep-ph/0211367`.

[85] D. V. Deryagin, D. Y. Grigoriev and V. A. Rubakov, "Standing wave ground state in high density, zero temperature QCD at large N_c," Int. J. Mod. Phys. A **7**, 659 (1992).

[86] E. Shuster and D. T. Son, "On finite-density QCD at large N_c," Nucl. Phys. B **573**, 434 (2000), `hep-ph/9905448`.

[87] J. I. Kapusta, *Finite-temperature field theory* (Cambridge University Press, 1989).

Acknowledgments

It is my pleasure to thank my advisor Prof. Benjamin Svetitsky, who suggested the idea for this work, supported and guided me continuously during the research, and proofread this manuscript. Ben, with his wide knowledge of physics and deep understanding of quantum field theory, made this research an inspiring experience. He dedicated a lot of time in countless enlightening discussions, in which he shared his ideas. For that I am grateful.

I have benefited greatly from fruitful discussions with Dr. Yigal Shamir who was always willing to teach me more about lattice gauge theory.

At different stages of the work I had useful discussions with Prof. A. Aharony, Prof. A. Auerbach, Prof. O. Entin-Wohlman, Prof. L. Frankfurt, Prof. S. Nussinov, Prof. K. Rajagopal, Prof. S. Sachdev, and Dan Gluck.

Finally I would like to thank all my colleagues and friends at Tel Aviv University for the enjoyable working and social atmosphere.

This work was supported by the Israel Science Foundation under grant no. 222/02-1 and by the Tel Aviv University Research Fund.